Standard Model Vacuum Decay with Gravity

Stephen Stopyra

Imperial College London, Department of Physics

Blackett Laboratory, Imperial College, London SW7 2AZ

Thesis submitted for the degree of Doctor of Philosophy, Physics Research

November 2, 2018

Abstract

I present a study of the vacuum instability problem in the Standard Model, with particular emphasis on the effect of gravitational corrections on this process. This covers four main effects: (1) gravitational back-reaction of nucleating bubbles and their associated bounce solutions, which alters the decay rate; (2) the nucleation of true vacuum bubbles in an inflationary background; (3) the effect of non-flat backgrounds on the running of the Standard Model couplings; and (4) the effect of non-minimal Higgs-curvature coupling on decay rates in the Standard Model. The key result presented is the discovery of previously unseen bounce solutions contributing to Standard Model vacuum decay during inflation.

Declaration

I certify that the material here presented is my own work, except where otherwise referenced.

Most of the material here presented has also been published in three collaborative papers, [1, 2, 3]. The majority of this new material is discussed in chapters 4 to 6, with chapters 2 and 3 covering background material.

In [1] and [2], my specific contribution to the collaboration included writing and developing the numerical code that produced the results, producing the graphs, developing the method for finding the new type of bounce solutions described in chapter 6. The ideas were developed collaboratively between myself and my co-author, Arttu Rajantie.

My main contribution to [3] was implementing the numerics for the various plots, double checking the expression derived for the effective potential, and developing the approach for dealing with the multiple possible scale choices.

Acknowledgements

Contents

List of Figures

List of Tables

Acronyms

A list of acronyms and their definitions used throughout the thesis is as follows:

1. CdL - Coleman-de Luccia (instanton).

2. HM - Hawking-Moss (instanton)

3. dS - de Sitter

4. AdS - Anti de Sitter

5. FLRW - Friedman-Lemaître-Robertson-Walker (metric)

6. LHS/RHS - Left hand side/Right hand side

7. GUT - Grand Unified Theory

8. WKB - Wentzel-Kramers-Brillouin (approximation)

9. LW - Lee Weinberg (bounce)

Symbols and Conventions

A list of symbols used and their meanings (unless otherwise stated) is as follows:

1. ξ - non-minimal Scalar curvature couplings, i.e. $\frac{1}{2}\xi\phi^2 R$.

2. χ - radial parameter in 4D Euclidean space.

3. ϕ - generic scalar field.

4. h - the Higgs field.

5. H - The Hubble rate, which unless otherwise stated, should be assumed to be when the scalar (Higgs) field is in the *false vacuum* state, ie, $H^2 = \frac{V(\phi_{\text{fv}})}{3M_{\text{P}}^2}$.

6. ϕ_{fv} - the false vacuum value of a scalar field.

7. ϕ_{tv} - the true vacuum value of a scalar field.

8. ϕ_{bar} - the position of the top of the barrier of a scalar field potential.

9. G_N - Newton's gravitational constant.

10. M_{P} - the reduced Planck mass, $M_{\text{P}} = 1/\sqrt{8\pi G_N}$.

11. g_1, g_2, g_3 - the $U(1)$, $SU(2)$, and $SU(3)$ couplings of the Standard Model respectively, using $SU(5)$ normalisation for g_1, so that $g_2 = g$ and $g_1 = \sqrt{\frac{5}{3}}g'$. This means that the Higgs sector of the Standard Model is given by $\mathcal{L}_h = D_\mu^\dagger \Phi D^\mu \Phi + \mu^2 \Phi^\dagger \Phi - \lambda(\Phi^\dagger \Phi)^2$ where $D_\mu \Phi = (\partial_\mu - -ig_2 W_\mu^a t^a - i\sqrt{\frac{3}{5}}g_1 Y_\Phi B_\mu)\Phi$.

12. V_0 - potential of a scalar field in the false vacuum, $V_0 = V(\phi_{\text{fv}})$. Effectively the cosmological constant energy density.

13. $\Delta V(\phi)$ - scalar potential relative to false vacuum value, i.e. $\Delta V(\phi) = V(\phi) - V(\phi_{\text{fv}})$.

14. $\mathrm{d}\Omega_n^2$ - n dimensional sphere metric. E.g. $\mathrm{d}\Omega_2^2 = \mathrm{d}\theta^2 + \sin^2\theta \mathrm{d}\varphi^2$.

15. $a(\chi)$ - metric component in 4D Euclidean metric $\mathrm{d}s^2 = \mathrm{d}\chi^2 + a^2(\chi)\mathrm{d}\Omega_3^2$.

16. $\mathcal{D}\phi$ denotes the path integral measure of ϕ.

17. M_t - top quark pole mass.

18. M_h - Higgs boson pole mass.

19. M_W, M_Z - W and Z boson pole masses, respectively.

20. $\alpha_S = \frac{g_3^2}{4\pi}$ is the strong force coupling parameter, measured at energy scale M_Z unless otherwise specified.

Conventions used throughout:

- The metric signature is the $-+++$ convention.

- Riemmann tensor is defined as $R^\rho{}_{\sigma\mu\nu} = \partial_\mu \Gamma^\rho_{\nu\sigma} - \partial_\nu \Gamma^\rho_{\mu\sigma} + \Gamma^\rho_{\mu\lambda}\Gamma^\lambda_{\nu\sigma} - \Gamma^\rho_{\nu\lambda}\Gamma^\lambda_{\mu\sigma}$.

- The sign of ξ is such that $\xi = 1/6$ is the conformally symmetric value.

- The anomalous dimension, γ_φ, for field φ is related to the field renormalisation, Z_φ, by $\gamma_\varphi = \frac{1}{Z_\varphi^{1/2}}\frac{\mathrm{d}Z_\varphi^{1/2}}{\mathrm{d}\varphi}$.

- Beta functions for coupling g_i are defined by $\beta_{g_i} = M\frac{\mathrm{d}g_i}{\mathrm{d}M}$.

- Natural units are used throughout, where $\hbar = c = 1$, but M_{P} is retained.

Chapter 1

Introduction

1.1 The Decay of Nothing - a Non-technical Introduction to Vacuum Instability

The Standard Model is one of the crowning achievements of twentieth century physics. This theory describes all matter known to modern science, from the familiar electrons and photons that we deal with in the everyday world, to more exotic, fleeting particles such as the top quark. Tests of the Standard Model have shown time and time again that it accurately reproduces the world as we see it, and not just approximately. An example of this stunning success is the gyromagnetic ratio of the electron, which tells us the magnetic field produced by an electron as a result of its spin (and rotating charged object generates a magnetic field - in fact, that is what a magnetic field is: the effect of rotating charged objects). The theory of Quantum Electrodynamics, a subset of the Standard Model, predicts that electron's gyromagnetic ratio should be [8]:

$$g_e = 2.00231930436356 \pm (1.28 \times 10^{-14}), \tag{1.1}$$

while the measured value[1] is [9]:

$$g_e = 2.002319304361715 \pm (1.52 \times 10^{-14}). \tag{1.2}$$

This is agreement to within twelve significant figures. The accuracy of the Standard Model demonstrates that is is a resounding success at describing the world we live in, at least at low energies. This cannot be the end of the story, however. There are many things the Standard Model does not explain: the unnatural smallness of the cosmological constant ('dark energy'), dark matter, and the question of why the early universe contained more matter than anti-matter. Each of these is a subtle problem, that we will not discuss in detail here. The subject of this thesis is not so much something that the Standard Model cannot explain, but something that it predicts: vacuum decay.

1.1.1 Fields and Particles: What is the Vacuum?

The vacuum, or what a layperson might term 'empty space' has a long and peculiar history. Right back to the discovery of electromagnetism physicists have wondered whether empty space is truly empty: before the discovery of special relativity by Einstein, it was believed that the universe must be filled with an invisible substance called 'luminiferous aether'. The idea is not as crazy as it sounds at first - light was shown to be a wave, and this poses the obvious question of 'what is waving'. Einstein showed that in fact the aether was unnecessary - it was unobservable, and nothing would change in the observed behaviour of light and matter if it simply weren't there. Occam's razor demanded, therefore, that its existence be abandoned. The modern interpretation is that light is a wave in the electromagnetic field.

The basis of modern particle physics is the notion of the quantum field. Electric and magnetic fields are at least somewhat intuitive: at every point in space there is an arrow (a vector) which tells us the direction an object at that point will be pushed by a force, and it's length (magnitude) tells us how much. Objects in these fields move if they have the appropriate charge,

---

[1]The astute reader will notice that since QED has a free parameter, it is more correct to say that the 'measured' and 'predicted' values of g_e is really comparing two independent measurements of g_e by different methods, and checking that they agree to within a given precision - that is to say, the predictions of the theory are consistent.

and fundamentally all a field is is an time-varying object at each point in space. This object could be a number (a 'scalar field'), a vector (like electric fields - they tell us the magnitude and direction of a force that will be exerted on an object at a given point), or something more exotic (such as the 'spinor' fields that describe electrons). This is of course physically unsatisfying, because it only tells us how a field is described mathematically, not what it *is*. In fact, we don't actually need to know what a field is to understand its behaviour. Consider a bar magnet, for example. It is made up of huge numbers of atoms, each of which contains electrons with 'spin magnetic moments' that contribute to the total magnetic field of the bar magnet. We could attempt to describe a bar magnet using the aggregate of 10^{23} or more atoms, but this would be a fools errand. A description that averages over the individual atoms is much more convenient (and actually tractable).

In fact, the modern ('Effective field theory') view of fields is that they should always be regarded as averages like this over unseen degrees of freedom. The crucial observation is that we don't even need to know what these degrees of freedom *are*. Bar magnets were fairly well understood long before atoms were widely accepted as the building blocks of matter. We should view other fields in physics - like magnetic fields and Higgs fields - the same way. They are to be understood as aggregate descriptions of underlying degrees of freedom whose nature may not may not be understood. We can be agnostic as to their precise nature, because on large scales, it doesn't affect what we observe.

1.1.2   Vacuum Instability - The Dam Analogy

So what then, should be understand by empty space, or the vacuum? The intuitive definition is 'that which remains when you remove all the matter'. But what is matter? According to the Standard Model (which in the spirit of the previous discussion, we should regard as a large-scale description of underlying degrees of freedom obeying laws we may know little-to-nothing about), all matter in the universe consists of particles that are excitations of a set of fundamental fields. By 'excitation', we mean a small, localised clump of energy that has non-zero energy, and can move about in space.

To explain what this means, let us introduce an analogy that will also illuminate what it means for a vacuum to decay. Consider a lake - the field is like the surface of the lake, and particles are like waves on the surface of the water. It is in this sense that a particle and a field are inseparable concepts - without the lake, there can be no waves, and thus, without a field, there can be no particles. Individual particles of the same type are really just different waves on the lake's surface. So what is the 'vacuum state' of a lake? If we believe a vacuum is what remains when you remove all the particles, and particles are waves on the lake's surface, the answer is obvious - the vacuum state of a lake is when it is perfectly still, with no waves on it's surface.

But what about a more complicated set-up? Imagine a lake split in two by a dam, into an upper and lower section. See figure 1.1. The water level in each half of the lake is different. One half might even be empty. In a sense there are two different vacuum states the lake could be in: everything in the upper lake, or everything in the lower lake (or both halves partially filled, but for reasons we will discuss shortly, that situation isn't stable for particles in our universe). If we are in the lower half, everything is perfectly stable - opening the dam would do nothing,
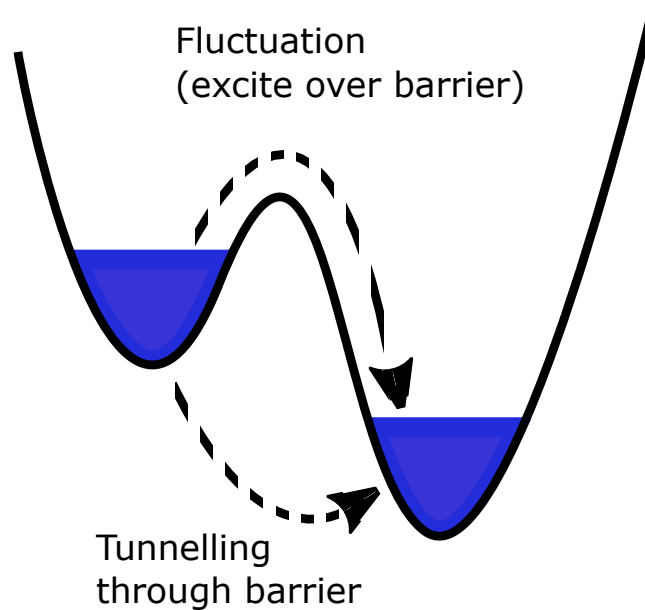
Figure 1.1: Two lakes separated by a dam, an analogue for the vacuum of the Standard Model.

as water does not flow up hill. We might call this a 'true vacuum' state.

But if we are in the situation where the upper half is filled, things get more interesting. Now, opening the dam will cause the entire lake to empty into the lower half. We call the upper half of the lake a 'false vacuum' state because although it may appear stable, given the right conditions it can collapse into the 'true vacuum' state. This state of affairs is in fact an analogy for the situation we appear to find ourselves in in our universe, at least according to the Standard Model. There are two different vacuum states that our universe can possess; a true and a false. Observations indicate that we are in the false vacuum.

This of course begs the question, is it possible for circumstances to arise in which the 'dam' bursts? In short: classical physics states that objects cannot pass through a potential barrier (such as the dam, in this analogy) unless it is given sufficient energy to pass over the top. In quantum mechanics, however, this isn't true: it is also possible for a particle to spontaneous appear on the opposite side of a barrier without being given sufficient energy to pass over it. This process is called 'quantum tunnelling', and is also responsible for radioactive decay (hence the name 'vacuum decay'). A radioactive atomic nucleus consists of a bunch of protons and neutrons held together by the strong nuclear force, which overcomes the electro-static repulsion between protons. If the universe were classical, this would be enough[2], and the nucleus would not decay. However, quantum mechanics gives a small probability for the nucleus to disintegrate, tunnelling through this classical barrier. This process is entirely random, and gets less likely if the barrier is high and thick. There is a predictable probability per unit time that this disintegration of the nucleus will occur, and this information is often characterised by the 'half-life' of the nucleus, ie, the time it takes, on average, before half of a large sample of the nuclei will have decayed (one cannot say when a given nucleus will decay, only that after a certain amount of time, on average half the nuclei will have decayed).
Vacuum decay is entirely analogous to this disintegration of a nucleus by quantum tunnelling.

---

[2]Though a 'classical' atom would behave very differently to a quantum atom - electrons would spiral into the nucleus, which doesn't happen in reality - this is why quantum mechanics was devised in the first place.

Although the universe may appear to be in the false vacuum state, there is a tiny probability that in any given second, some part of the universe will tunnel through the barrier and appear in the true vacuum. This gives the vacuum a 'half-life', albeit a very, very long one.

It doesn't require much imagination to conclude that such an event would be catastrophic. If it were to occur, it would manifest itself as an expanding 'bubble' of true vacuum that moves outwards at near the speed of light, annihilating everything in its path. The good news is we would never see it coming, since it moves almost as fast as the light that heralds it, and destruction would be virtually instantaneous: we would never know what hit us. The even better news is that this nightmare vacuum decay scenario is most probably not a true prediction, but a spurious one, indicating not that we should be worried empty space is about to collapse on us, but that the Standard Model has begun to go awry at distance scales much smaller than those we are able to study in particle collider experiments. This is actually a good thing, as it would mean the Standard Model contains the seeds of its own destruction (quite literally in this case), and points the way to a better theory, and a better understanding of the universe.

1.1.3   Summary of Results

The subject of this thesis is the formation of true vacuum bubbles when gravitational effects are included. The principal result is a new calculation that demonstrates the existence of additional types of vacuum bubbles that can form during the early universe. The early universe is believed to have been very different to the present day: it is believed that the universe underwent a process of extremely rapid (exponential) expansion called inflation. This involves a strong gravitational field, which changes the way vacuum bubbles form. Without gravitational effects, the bubbles form via a process called quantum tunnelling, which as discussed, is similar to the process that causes radioactive atoms (like Uranium 235 nuclei) to decay. However, gravity can also add a thermal component to the decay of the vacuum. This is a classical process - disturbing the water (say by getting it to boil over, or dropping a large stone into it) in a lake might give it sufficient energy to pass over the top of a barrier, and the same is true of the vacuum. The combination of these thermal and quantum tunnelling effects means that there are several ways for a decay to occur: entirely thermal effects, entirely quantum tunnelling, or a combination of the two.

Ordinarily, the expansion of the universe gives the vacuum a temperature: this is because the universe's expansion exceeds the speed of light for space sufficiently far away from any observer. The distance beyond which this happens is called the 'de Sitter (dS) radius'. Since no object can move through space faster than light, information cannot pass between regions further away than the de Sitter radius. This means that the sphere with a de Sitter radius behaves much like the event horizon of a black hole (in fact, this is much more like the more familiar horizon in the sky, since it is centred on the observer). It is well known that black hole event horizons radiate Hawking-radiation, and the same is true of the de Sitter horizon. This radiation means that the vacuum becomes thermal, and has a temperature that depends on how rapidly the universe expands.

Usually, when this expansion rate is increased, quantum tunnelling becomes increasingly irrelevant, and thermal fluctuations over the barrier dominate. However, the conclusion of this thesis is that this picture is overly simplistic for the Standard Model. While the general picture

remains true, as the expansion rate is raised, new routes for quantum tunnelling appear, instead of disappearing. This significantly complicates the process of vacuum decay.

1.2   Technical Introduction

1.2.1   Destabilisation of the Electroweak Vacuum - Loop Corrections in the Standard Model

The reason that vacuum decay can potentially occur in the Standard Model is ultimately due to the running of the Higgs self-coupling, λ, which receives positive corrections from the bosons, and negative corrections from the fermions which couple to it. The effect of this is summarised by the beta function for λ, which at one loop is [10]:

$$\frac{\mathrm{d}\lambda}{\mathrm{d}\log M} = \frac{1}{16\pi^2}\left(24\lambda^2 - 3\lambda(g'^2 + 3g^2) + \frac{3}{4}\left(\frac{g'^2}{2} + g'^2 g^2 + \frac{3g^4}{2}\right) + 4Y_2\lambda - 2Y_4\right), \quad (1.3)$$

where:

$$Y_2 = 3(y_u^2 + y_c^2 + y_t^2) + 3(y_d^2 + y_s^2 + y_b^2) + (y_e^2 + y_\mu^2 + y_\tau^2), \quad (1.4)$$

$$Y_4 = 3(y_u^4 + y_c^4 + y_t^4) + 3(y_d^4 + y_s^4 + y_b^4) + (y_e^4 + y_\mu^4 + y_\tau^4). \quad (1.5)$$

Notice that there is a negative term in the fourth powers of the Yukawa couplings - essentially proportional to the fourth power of the fermion masses. This tends to drive λ towards negative values, an effect which is dominated by the heaviest fermion - in this case the top quark. With a heavy enough top quark, and insufficiently heavy Higgs mass, this can result in λ running to negative values at large scales, M. We plot this in figure 1.2 for the most recent values of the top quark and Higgs boson masses, $M_t = 173.1 \pm 0.9\,\mathrm{GeV}$, $M_h = 125.18 \pm 0.16\,\mathrm{GeV}$ [4]. This result shows clearly, that at at the 2σ level, vacuum metastability is expected for the Standard Model, although an exceptionally light top quark could change this with future measurements. The result of $\lambda(\mu)$ turning negative at large μ is that the (flat space) effective potential of the Standard Model, which can be approximated as:

$$V(h) \approx \frac{\lambda(h)}{4}h^4, \quad (1.6)$$

turns negative at a scale of around $\mu \sim 10^{10}\,\mathrm{GeV}$, developing a deep true minimum at trans-planckian field values. If no new physics exists to change this between the electroweak and Planck scales, then this implies that the Standard Model vacuum is not the most stable, and can decay via quantum, tunnelling.

This particular problem has been known for a long time [11, 12, 13, 14, 15, 16, 17, 18, 19, 20], especially in the context of attempts prior to the discovery of the Higgs boson to put constraints on its possible mass [21, 22, 23, 24, 25, 26], and for constraining various alternatives to the Higgs mechanism such as multiple Higgs doublets [27, 26]. Among the first to consider gravitational corrections to this process was [28], and even before the Higgs boson's discovery, the was much interest in the possible cosmological implications [29]. Since the discovery of the Higgs boson [30, 31], however, there has been an explosion of interest in the subject, which is no longer a purely theoretical endeavour, as it appears to be the most likely scenario. Many authors have since studied the vacuum stability problem and its implications for the Standard
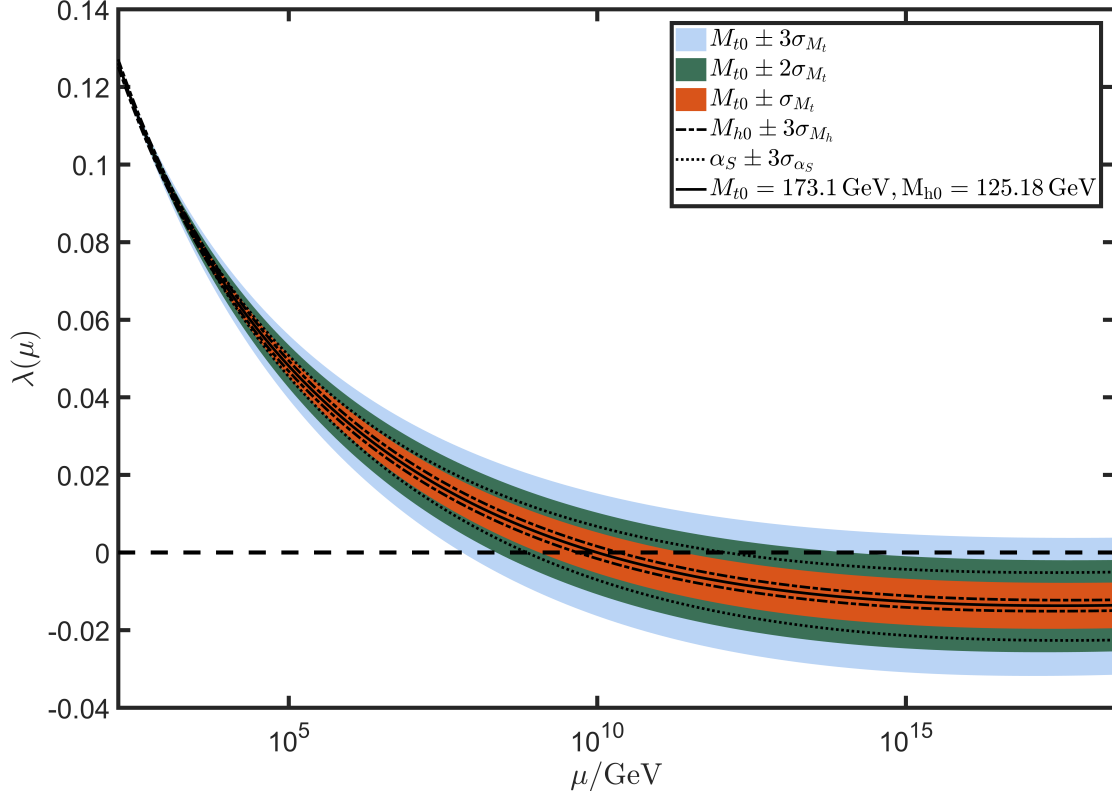
Figure 1.2: Three loop running of the Higgs self coupling with 1,2, and 3 σ errors bars on M_t drawn from [4]. 3 sigma error bars for M_h and the strong coupling, $\alpha_s(M_Z)$ are also plotted as dotted lines. $M_h = 125.18 \pm 0.16\,\mathrm{GeV}$, $M_t = 173.1 \pm 0.9\,\mathrm{GeV}$, $\alpha_S(M_Z) = 0.1181 \pm 0.0011$ are used as inputs, as given in [4].

Model [32, 33, 34, 35, 36, 37, 38, 39, 40, 41], as well as for the constraints it places on beyond the Standard Model physics [42, 43, 44, 45, 46, 47, 48, 49, 50, 51, 52, 53, 54, 55]. The fact that the electroweak vacuum appears to be unstable can be regarded as one of the first evident 'chinks in the armour' of the Standard Model, as it represents a possible inconsistency in the theory with the observational fact that we are still here today, apparently in the 'false' vacuum. This has led to numerous proposals as to how the Standard Model could be fixed to avoid vacuum instability [56, 57, 58, 59]. Equally interesting as the implications for new physics, are the implications that an unstable Higgs vacuum might have for cosmology, for example, constraining high-scale inflation [60, 61, 62, 63, 64, 65, 66, 67, 68, 7, 69, 70, 71, 2, 3, 71, 72, 73, 74, 75]. Many authors have also looked at the implications that Higgs-inflaton couplings might have on the vacuum stability problem [76, 77], and the behaviour of the Higgs field towards the end of inflation, particularly during re-heating [77, 78, 79], and the effect that finite temperature might have [80]. Authors have also considered other effects of vacuum stability relating to gravity, including vacuum decay triggered by black holes [81, 82, 83, 84], the possibility that non-minimal Higgs curvature coupling could stabilise the effective potential [57, 85, 86, 1, 3, 87, 88, 89, 90, 91], and the effect of Planck-suppressed operators [58]. Many issues arising in the study of Standard Model vacuum instability have been explored in depth, including whether the fact that the effective potential is gauge dependent affects the result [92, 93, 94, 95, 3], and the interpretation of vacuum decay in a theory which only becomes metastable due to quantum corrections, despite being stable at the classical level [96].

1.2.2   Instantons and Bubble Nucleation

The main mechanism for vacuum decay, both with and without gravity, is quantum tunnelling. Classically, a false vacuum state such as that which seems to appear in the Standard Model is perfectly stable, so long as the system, does not have sufficient energy to pass over the barrier. Since the barrier in the Standard Model is at huge energy scales - 10^{10} GeV or more, no natural process present in the universe is likely to be able to destabilise it. However, in quantum mechanics, the vacuum state does not describe the Higgs field lying purely in the false vacuum for all time, i.e. $\phi = \phi_{\mathrm{fv}}$. This is because the false vacuum state is not an energy eigenstate, but a superposition of different energy eigenstates, which evolve in time independently. Indeed - it is precisely because the false vacuum is *not* an energy eigenstate that decay can occur: there is a small chance that the field will be observed to be in the true vacuum state at any place and time.

One can therefore calculate the exact rate of this decay in exactly the same way as the decay rate of a decaying alpha-particle. The main complication is that a quantum field such as the Higgs field has an essentially infinite number of degrees of freedom, and thus slightly different techniques are generally needed to treat the system.

The main technique is the Instanton approach, described by Coleman [97, 98, 99]. The idea here is to exploit the fact that the energy of a metastable state can be regarded as complex (we will describe what this means in more detail in chapter 2). The rate at which the vacuum decays can then be estimated from the imaginary part of this energy, since the amplitude squared of the wave function for such a complex-valued energy state evolves as:

$$|\psi(x,t)|^2 = |\psi(x,0)|^2 e^{-2\mathrm{Im}(-\mathrm{E})\mathrm{t}}. \tag{1.7}$$

If the false vacuum state were describing the decay of an ensemble of radioactive particles, the decay rate would be defined by $|\psi(x,t)|^2 = |\psi(0,t)|^2 e^{-\Gamma t}$, thus, $\Gamma = -2\mathrm{Im}(\mathrm{E})$ is the decay rate of a state with complex energy, where Im denotes the imaginary part. Now, the energy can be extracted by Wick rotating time to imaginary values, since the imaginary time evolution of the vacuum state becomes:

$$|\psi_{\mathrm{fv}}(t)\rangle = \sum_n \langle n|\psi_{\mathrm{fv}}(0)\rangle e^{-E_n t}|n\rangle \to_{t\to\infty} \langle 0|\psi_{\mathrm{fv}}(0)\rangle e^{-t E_0}|0\rangle. \tag{1.8}$$

This tells us that by taking imaginary time, t, to infinity, we can extract the lowest-lying energy state, E_0, which for distributions starting around the false vacuum, is the false vacuum state[3]. However, we can also evaluate the vacuum to vacuum transition amplitude using a Euclidean path integral:

$$|\psi_{\mathrm{fv}}(t)|^2 = \langle \psi_{\mathrm{fv}}(0)|e^{-\hat{H}t}|\psi_{\mathrm{fv}}(0)\rangle = \int_{\phi_{\mathrm{fv}}}^{\phi_{\mathrm{fv}}} \mathcal{D}\phi \, e^{-S_{\mathrm{E}}[\phi]}, \tag{1.9}$$

where ϕ_{fv} in the integral limits denote that we integrate over all configurations for ϕ with $\phi = \phi_{\mathrm{fv}}$ at the boundaries, ie, the configurations much touch the false vacuum somewhere[4].

---

[3]This somewhat hand-waving argument is obviously suspect since, necessarily, for decay to the true vacuum to occur, we would have to have mixtures of the true vacuum state in the initial superposition, which would be expected to dominate at large t. This will be addressed with a more formal derivation in chapter 2

[4]This restriction is relaxed in de Sitter space due to its inherently thermal nature - see [100, 101] for a discussion.

$S_\mathrm{E}[\phi]$ is the *Euclidean* action, that is, the action for the scalar field with time Wick rotated to imaginary values. One can therefore extract the energy of the false vacuum by evaluating the Euclidean path integral semi-classically, that is, finding the stationary points of $S_\mathrm{E}[\phi]$, then approximating:

$$\int_{\phi_\mathrm{fv}}^{\phi_\mathrm{fv}} \mathcal{D}\phi\, e^{-S_\mathrm{E}[\phi]} \approx \sum_i \det[S''[\phi_i]]^{-1/2} e^{-S_\mathrm{E}[\phi_i]}, \tag{1.10}$$

which is essentially summing up Gaussian fluctuations around each stationary point ϕ_i, described by the functional determinants. This is essentially performing a 1-loop approximation of the path integral. Coleman and Callan showed that this gives the decay rate per unit four volume [99]:

$$\frac{\Gamma}{V_4} \approx \left(\frac{B}{2\pi}\right)^2 \left|\frac{\det'(S''_\mathrm{E}[\phi_B])}{\det S''_\mathrm{E}[\phi_\mathrm{fv}]}\right|^{-1/2} e^{-B}, \tag{1.11}$$

where $B = (S_\mathrm{E}[\phi_B] - S_\mathrm{E}[\phi_\mathrm{fv}])$, and ϕ_B is the *dominant* (lowest action) stationary point, referred to as a bounce-solution of the Euclidean equations of motion. The primed determinant, $\det'(S''_\mathrm{E}[\phi_\mathrm{B}])$ is a functional determinant around the bounce, with a number of zero modes extracted. These correspond to translations of the bounce solution around the 4D Euclidean space, which are obviously symmetries of the action and thus lead to zero-eigenvalues in the spectrum of fluctuations around ϕ_B which the functional determinant encapsulates. These would at face value lead to a divergence, however, dividing by the four-volume removes this. Note that there is also a negative mode, which is responsible for the energy of the vacuum being imaginary.

Now, the instanton approach doesn't only describe the rate at which spontaneous decay of the false vacuum occurs. It also describes what this process looks like. One way to look at this is to note that there are infinitely many ways to tunnel through a barrier when there are more than one (or infinitely many) degrees of freedom. See for example fig. 1.3. The path integral explores all the possible tunnelling routes, but the dominant solution is the most likely, ie, the shortest route through the barrier. As we will discuss in chapter 2, the bounce solution can be cut half-way through and used to give initial conditions for the evolution of the field after decay occurs. This tells us that the 'point' on the other side of the barrier where the field emerges is not a point, but an entire *field configuration*, $\phi_\mathrm{Bubble}(x)$. This configuration is called a *true vacuum bubble*, and is distinct from, but related to, the bounce solution. It can be regarded as the analytic continuation of the bounce solution back to Lorentzian space, and describes the behaviour of the nucleated bubble after vacuum decay occurs. As we will see, the result is that the bubble expands outwards at near the speed of light, converting space around it to the true vacuum. This is a result manifestly incompatible with the observation of the Higgs vacuum expectation value from collider experiments, and as we will discuss in chapter 3, would also lead to gravitational collapse, effectively ending the universe.

Such an event has obviously never (yet) occurred. This brings us to the main interesting fact about vacuum decay - it's non-observation puts a constraint on high energy replacements of the Standard Model, such as GUT theories or theories of the early universe, such as Inflation. Of particular interest is that the apparent scale of vacuum decay - $10^{10}\,\mathrm{GeV}$ where the effective potential first goes negative - appears to be well below the proposed GUT scale of $10^{15}\,\mathrm{GeV}$. Thus, if we believe that the vacuum is absolutely stable, then we *must* have new physics between the electroweak scale and the Planck scale if the vacuum decay problem is to be fixed.
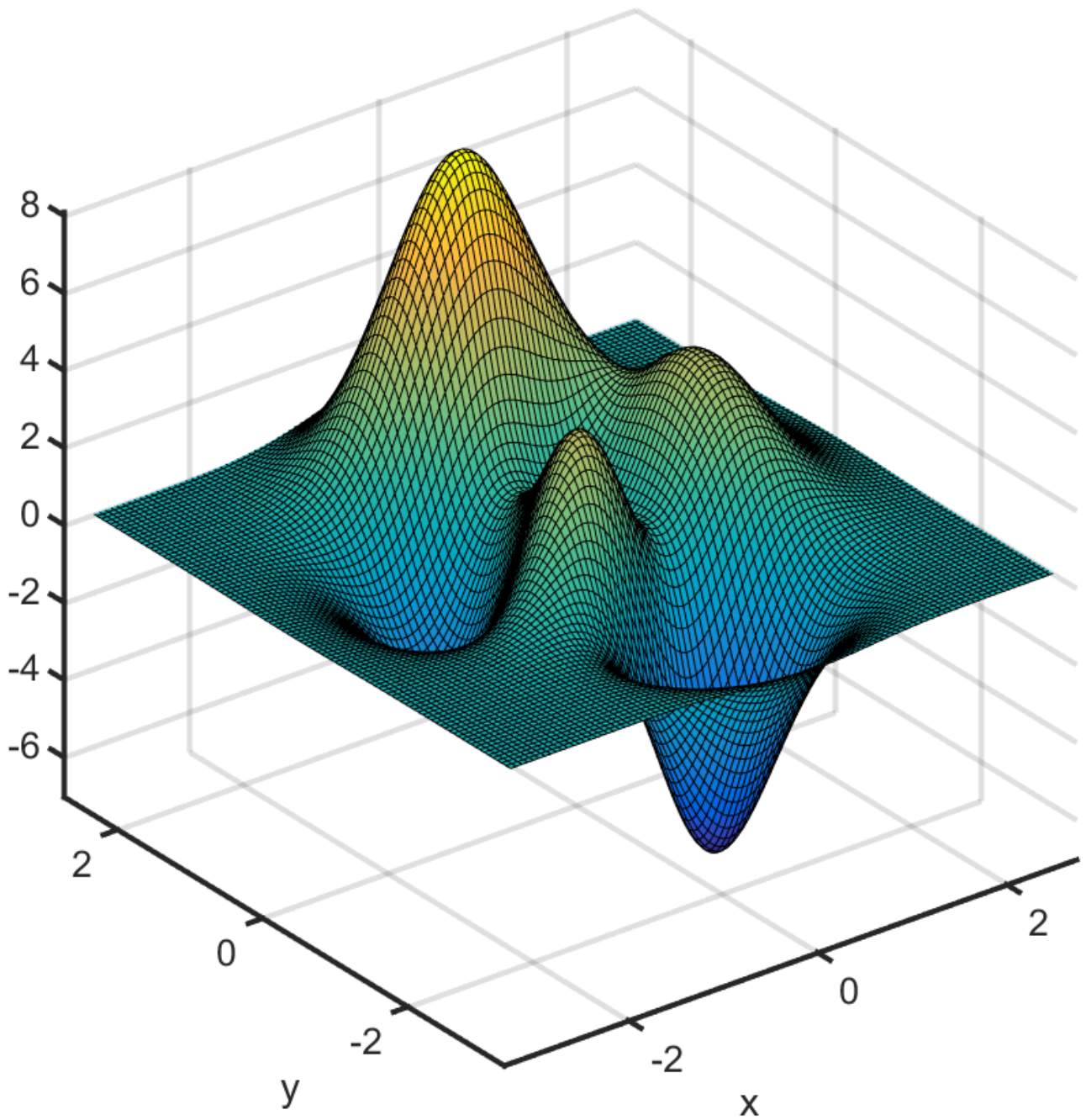
Figure 1.3: Example potential in 2D. There are several stationary points, and a false vacuum between the three peaks: infinitely many routes are possible for a particle to tunnel through the barrier.
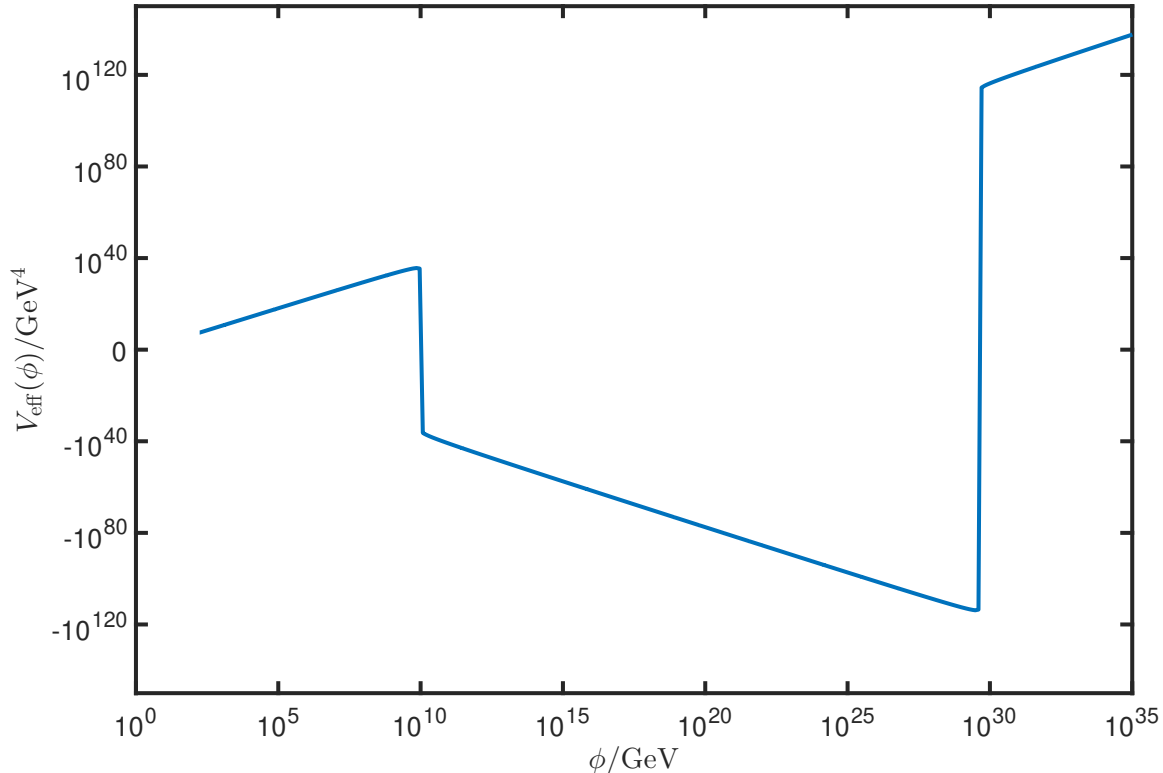
Figure 1.4: Plot of the effective potential for the Standard Model with $M_t = 173.1\,\text{GeV}$, $M_h = 125.18\,\text{GeV}$, extrapolated up to trans-planckian values. Although this cannot be taken seriously at such large ϕ, it illustrates the depth of the potential's true minimum.

1.2.3 The Effective Potential and Gravitational Corrections

One of the key features of the effective potential that is noticeable in the central value of the top and Higgs mass, is that the minimum is extremely deep. For example, with $M_t = 173.1\,\text{GeV}$, $M_h = 125.18\,\text{GeV}$, λ becomes positive again at $\mu = 4.2 \times 10^{29}\,\text{GeV}$, far beyond the Planck scale (λ will always ultimately become positive in the Standard Model due to the Landau-pole in the $U(1)$ coupling). The resulting potential, extrapolated far beyond the regime in which it can be expected to give realistic results, is plotted in fig. 1.4, which illustrates just how deep the True vacuum is in this case.

This begs the question, at what point do gravitational effects start to become important? One could argue that they will never matter, since Planck suppressed operators will change the result completely - an effect which some authors have investigated [58]. Although this is almost certainly the case, since we cannot know what those corrections will be (and they could even make the situation worse), it is still worthwhile to ask what the effect of a deep potential well is under the agnostic (but likely unrealistic) assumption that there is no new physics between here and the Planck scale, and that cut-off suppressed operators are negligible (note that from an effective field theory point of view, while cut-off suppressed operators are part of the Standard Model, they encapsulate an approximation to the more complete description above the cut-off that gets increasingly inaccurate as we approach it).

The reason that gravity may be important is that most calculations of the vacuum decay rate assume a 'fixed back-ground approximation', namely, that the bounce solution has no

back-reaction on the underlying geometry [100]. Note, however, that in the Standard Model, the size of a typical nucleated bubble is controlled by the scale at which $|\lambda(\mu)|$ takes on it's largest value over the region for which is it negative - in otherwords, the *minimum* of $\lambda(\mu)$ [18]. For $M_t = 173.1\,\text{GeV}$, $M_h = 125.18\text{GeV}$, this is at $\mu_{\min} = 3.12 \times 10^{17}\,\text{GeV}$, which is little more than an order of magnitude below the Planck scale. This means that the nucleated bubbles probe deep into the negative region of the potential, while tells us that whatever happens between the electroweak and the Planck scales, the vacuum decay rate *is sensitive to gravitational corrections*, and would also be substantially changed by Planck suppressed operators if they are present. Thus, it is worthwhile understanding what these gravitational corrections are, even if we expect that ultimately new physics will change the situation.

There are two reasons this can matter. The first is non-minimal coupling between the Higgs field and Ricci curvature. A term like $\xi\phi^2 R/2$ is required to be present in the scalar field theories in curved space-time for renormalisability [102]. In the Standard Model, ξ can be shown to run with energy, and at one loop its beta function is [3, 103, 104]:

$$\frac{\mathrm{d}\xi}{\mathrm{d}\log\mu} = \beta_\xi = \left(\xi - \frac{1}{6}\right)\left[12\lambda + 2Y_2 - \frac{3g'^2}{2} - \frac{9g^2}{2}\right]. \tag{1.12}$$

Here, Y_2 is defined as in Eq. (1.4). The best available bounds on ξ in the Standard Model from colliders are extremely weak [105], and so the parameter is essentially unset. We plot the running of ξ in the Standard Model at 1-loop in all couplings in figure 1.5, assuming $\xi_{\text{EW}} = \xi(M_t) = 0$. One way that a non-zero ξ can effect vacuum stability is related to the observations previously noted that (1) the Higgs potential is very deep, and (2) the scale of nucleated bubbles is controlled by large field values, around $10^{17}\,\text{GeV}$. Taken together, these imply that the Ricci curvature at the centre of a nucleated bubble is not negligible, and thus any non-minimal coupling between the Higgs field and gravity can potentially affect both the form and nucleation rate of Standard Model true vacuum bubbles. We investigate this effect further, in the case of zero cosmological constant, in chapter 5. Note that this would not happen if we assume a fixed background approximation, since then there would be no Ricci curvature to couple to in the flat-false vacuum limit - the effect of non-minimal coupling in this case is inherently a non-fixed background effect (although the same is not necessarily true in de Sitter space).

The second way that gravity can matter for vacuum stability is in a de Sitter background. This is particularly relevant for inflation, which is approximately de Sitter. Throughout this thesis, we will not assume a particular model of inflation, but instead consider vacuum decay with a non-zero cosmological constant as an approximation.

In most cases, the depth of the Standard Model vacuum, at least that reached by vacuum bubbles in flat space, is far larger than the cosmological constant during inflation, even if inflation were to take place at the GUT scale, $H \sim 10^{15}\,\text{GeV}$. This means that back-reaction is potentially relevant here too. The mechanism for vacuum decay in de Sitter space - the Coleman de Luccia mechanism - will be discussed in more detail in chapter 6. However, let us first note the big difference between bubble nucleation in de Sitter, and bubble nucleation in flat space. This is that there two main routes for (spontaneous) vacuum decay to occur:

1. Quantum tunnelling through the barrier, as in flat space.

2. 'Thermal' excitation over the barrier, due to fluctuations in the Higgs field induced by quantum effects.
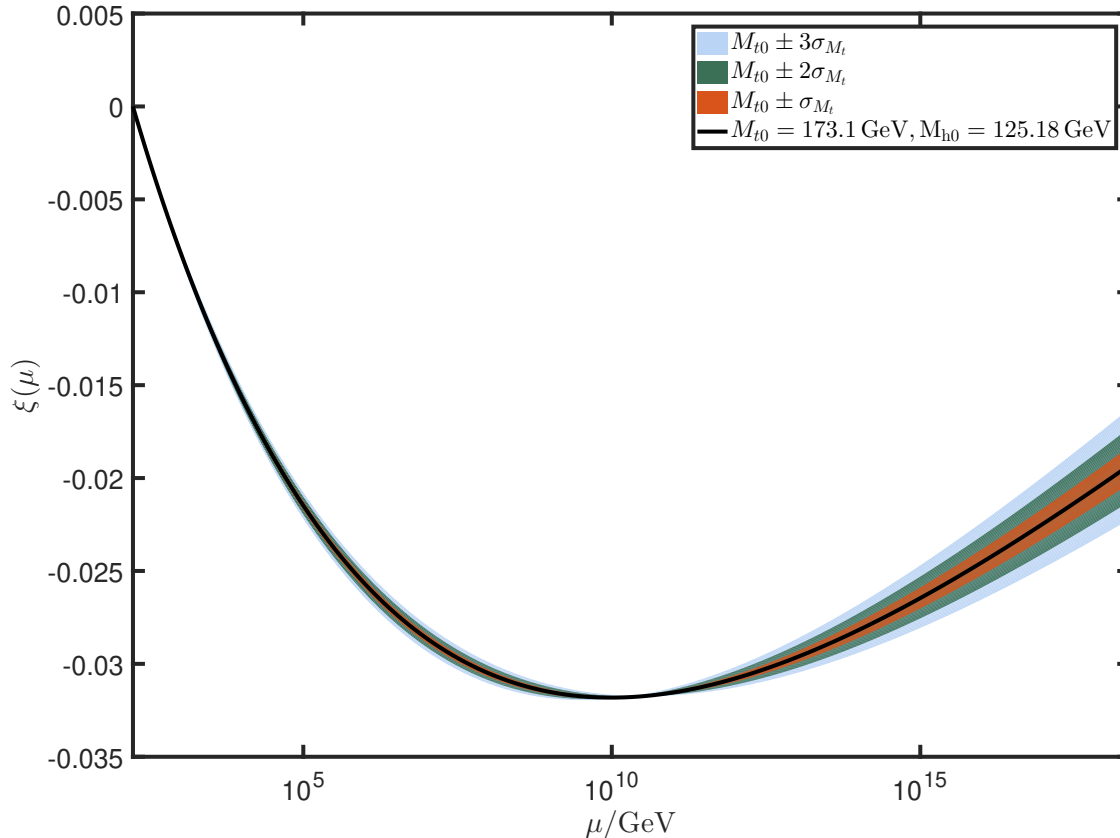
Figure 1.5: One loop running of ξ in the Standard Model at 1-loop in all couplings, with initial value $\xi_{\mathrm{EW}} = \xi(M_t) = 0$. This results in ξ being effectively negative at most energy scales, an effect which can potentially destabilise the electroweak vacuum. 1,2, and 3 sigma uncertainty bounds of $M_t = 173.1 \pm 0.9\,\mathrm{GeV}$ from [4] are plotted.

The first effect is broadly similar to its flat space equivalent. As we will see, however, it is not quite the same, since it describes the field being partially excited up the barrier by fluctuations, and then tunnelling the rest of the way through, rather than tunnelling directly from the false vacuum. This is why bounce solutions in de Sitter have the slightly peculiar feature of *not* touching the false vacuum [101].

The second process is described by the so called Hawking-Moss instanton [106], and can be thought of as describing thermally assisted tunnelling over the barrier [101]. This process is related to the stochastic fluctuations of light scalar fields during inflation [107], which is another approach that can be taken to computing vacuum decay rates during inflation [65, 60]. We will not focus on the stochastic approach and the Fokker-Planck equation describing it here - instead we will focus on the properties of Coleman de Luccia (CdL) instantons. However, the Hawking-Moss solution will be shown to play a key role.

1.2.4 The Critical Threshold

One feature of vacuum decay in de Sitter space that will prove central to this thesis is the critical Hubble rate, (or critical cosmological constant, related by $H_{\text{crit}}^2 = \frac{V_{0\text{crit}}}{3M_{\text{P}}^2}$) defined by:

$$H_{\text{crit}} = \sqrt{-\frac{V^{(2)}(\phi_{\text{bar}})}{4} - \frac{[V(\phi_{\text{bar}}) - V(\phi_{\text{fv}})]}{3M_{\text{P}}^2}}, \qquad (1.13)$$

where ϕ_{bar} is the top of the barrier in potential V, and ϕ_{fv} is the false vacuum. Note that Hubble rates here are defined by V in the false vacuum, i.e. $H^2 = V(\phi_{\text{fv}})/3M_{\text{P}}^2$. This threshold has long been known to hold importance in the subject of vacuum decay in de Sitter space, since it is the point at which the number of negative eigenvalues in the spectrum of fluctuations about the Hawking-Moss instanton changes from many to 1 as H crosses H_{crit} from below [108, 109, 110]. The number of negative modes is important, since it can be shown that having more than one negative mode means that the stationary point does not contribute to tunnelling, as there is always a bounce with lower action [111, 101]. It was shown by Balek and Demetrian that in any potential, a CdL solution always exists if $H < H_{\text{crit}}$, and *may* not exist if $H > H_{\text{crit}}$. Note that the non-existence argument is not strong - what is shown, as we will discuss in chapter 6, is that a sufficient, *but not necessary* condition for the existence of CdL solutions ceases to hold for $H > H_{\text{crit}}$. In many potentials, as we will discuss in chapter 6, it appears that for $H > H_{\text{crit}}$ no CdL solutions exist, and the action smoothly merges with the Hawking-Moss. This is justified on the basis of a perturbative calculation of bounces for $H \sim H_{\text{crit}}$ which shows a solution that smoothly merges with the Hawking-Moss solution and has lower action than it as $H \to H_{\text{crit}}^-$ [112]. Based on this, it would seem that H_{crit} divides Hubble rates into two domains:

1. For $H < H_{\text{crit}}$, CdL tunnelling dominates. The Hawking-Moss solution has too many negative eigenvalues to contribute to vacuum decay.

2. For $H > H_{\text{crit}}$, CdL solutions disappear and the Hawking-Moss solution loses enough negative eigenvalues to contribute to vacuum decay. Hence, Hawking-Moss solutions dominate.

However, this is not the end of the story. It has been known for some time that peculiar potentials existed which did not satisfy this, and still have CdL solutions for $H > H_{\text{crit}}$. It was proposed that some sort of average over V'' might replace H_{crit} [110]. Indeed, a criteria for such potentials based on perturbative analysis of solutions for $H \sim H_{\text{crit}}$ has long been known [112, 113], though it has not always been appreciated that this always implies multiple CdL solutions, and in particular, the solution that exists for $H < H_{\text{crit}}$ in this case is *not* the same as the perturbative solution. This result is central to the main argument of chapter 6, where we present evidence that this behaviour does not just happen in peculiar, perhaps 'unphysical' potentials, but in potentials such as the Standard Model.

1.2.5 Overview

The first half of this thesis will cover in detail some necessary background, developing the bounce and CdL formalism for computing vacuum decay rates. Results in flat space will be reviewed in chapter 2, in which we also review the interpretation of complex vacuum energies in terms of the WKB approximation and wave-function picture of tunnelling.

Chapter 3 will discuss the CdL prescription for including gravity, mostly reviewing the details of the procedure, and also providing some more formal proofs of statements often taken for granted while applying it. We will also prove some lemmas here that will go on to support the main conclusions of the thesis, most importantly lemma 4 which reveals important information about bounce solutions around the critical threshold at which thermally dominated (Hawking-Moss) fluctuations start to become more important than tunnelling dominated (CdL) solutions.

Chapter 4 will discuss the effective potential of the Standard Model in detail, using Yukawa theory as a toy model to understand how loop corrections can destabilise the vacuum, and then go on to discuss the computation of the effective potential in curved space. This covers much of the material presented in our recent paper [3], which also includes an analysis of vacuum stability in the presence of non-minimal coupling during Inflation, using the Hawking-Moss solution in the new effective potential derived in [3]. Chapter 5 will discuss non-minimal coupling as it relates to back-reaction of bubbles nucleating in a flat false vacuum. This was the subject of [1], for which the key results were the discovery that ξ tends to suppress vacuum bubbles in the absence of a positive cosmological constant, and how the effect of ξ is closely linked to the breaking of conformal symmetry by quantum corrections to the running of the Higgs self coupling.

In chapter 6, we present one of the most important results: the discovery that the Standard Model effective potential allows for *multiple* CdL solutions contributing to vacuum decay, in addition to the CdL solution that resembles that present in flat space. This proves that the Standard Model is an exception to the idea that there is a smooth transition between CdL dominated tunnelling at low Hubble rates, and Hawking-Moss dominated tunnelling at high Hubble rates. Instead of disappearing at $H \geq H_{\text{crit}}$, new CdL solutions appear, significantly complicating the question of the vacuum decay rate during de Sitter space, since without a complete understanding of how and why CdL solutions exist, it is never possible to be certain that all solutions have been found, and thus that the computed decay rate is correct. To support this claim, we present a proof that potentials satisfying:

$$\Delta \equiv -\frac{1}{14}\left(V^{(4)}(\phi_{\text{bar}}) - \frac{(V^{(3)}(\phi_{\text{bar}}))^2}{3V^{(2)}(\phi_{\text{bar}})} - \frac{8V^{(2)}(\phi_{\text{bar}})}{3M_{\text{P}}^2}\right) > 0, \tag{1.14}$$

of which *the Standard Model is one example*, always have multiple solutions when $H > H_{\text{crit}}$. We present the derivation of a perturbative expression for one of the new solutions that arises at H_{crit}, showing that it always has higher action than the Hawking-Moss, and also proving that potentials satisfying $\Delta < 0$ *do* have CdL solutions that merge continuously with the Hawking-Moss solution. We consider examples of this in two different model potentials, and then the Standard Model itself, showing that it is not only the perturbative solution that arises.

We discuss some of the consequences that this might have for vacuum decay during inflation, and summarise our results in chapter 7.

Chapter 2

Basics I - Vacuum Decay without Gravity

2.1 Vacuum Decay Rates and Bounce Solutions

The process of nucleating true vacuum bubbles in the Standard Model and other theories is essentially a quantum tunnelling process. There is a certain probability per unit time that a vacuum bubble will be nucleated at any point in space, and this bubble then proceeds to expand, filling the universe if it is flat (the case of an expanding bubble in a non-flat universe is more complicated, and will be addressed in chapters 3 and 6). Fundamental to addressing the question of vacuum instability in the Standard Model is answering the question: "How likely is it that the electroweak vacuum survived to the present day, given that it is metastable". Since in flat space an expanding bubble will eventually fill all of space, one way of addressing this question is to ask for the probability per unit time that a bubble will nucleate in some fixed three-volume, usually the volume of the visible universe (a more careful analysis would consider the probability of nucleation per unit four-volume integrated over the past light cone). This can then be used to compute the expected life-time of our vacuum (which is very much analogous to the radioactive decay of a particle - another quantum tunnelling process). If the life-time is less than the age of the observable universe, then we have a problem, as the fact that we observe our universe to be in the electroweak universe is not compatible with the Standard Model in its current form.

There are two ways we can calculate it. One way, which directly shows the link to other tunnelling calculations, is to use a WKB approximation of the wave function. For tunnelling in ordinary quantum mechanics, this predicts the transition rate through a barrier in potential $U(x)$ with turning points $x_1(E), x_2(E)$ when the total energy is E to be:

$$T \propto \exp\left(-2\int_{x_1}^{x_2} \mathrm{d}x \sqrt{2(U(x) - E)}\right). \tag{2.1}$$

Note that for this system, the equation of motion is:

$$\frac{\mathrm{d}^2 x}{\mathrm{d}t^2} + U'(x) = 0. \tag{2.2}$$

Equation (2.2) can be re-written in terms of energy by multiplying by $\mathrm{d}x/\mathrm{d}t$ and integrating:

$$\frac{1}{2}\left(\frac{\mathrm{d}x}{\mathrm{d}t}\right)^2 + U(x) = E. \tag{2.3}$$

Notice that in the barrier, $U(x) - E > 0$. which is why the region (x_1, x_2) is *classically forbidden*. However, if we change variables from time to an imaginary time co-ordinate: $\tau = it$. then it is possible to re-write the exponent of Eq. (2.1) as:

$$
\begin{aligned}
2\int_{x_1}^{x_2} \mathrm{d}x \sqrt{2(U(x) - E)} =& 2\int_{x_1}^{x_2} \mathrm{d}x \sqrt{\left(\frac{\mathrm{d}x}{\mathrm{d}\tau}\right)^2} \\
=& 2\int_{\tau_1}^{\tau_2} \mathrm{d}\tau \left[\frac{\mathrm{d}x}{\mathrm{d}\tau}\right]^2 \\
=& 2\int_{\tau_1}^{\tau_2} \mathrm{d}\tau \left[\frac{1}{2}\frac{\mathrm{d}x}{\mathrm{d}\tau} + U(x) - E\right] = \quad [S_E(x_B) - S_E(x_{\mathrm{fv}})],
\end{aligned}
$$

where S_E is the action:

$$S_E[x] = \int \mathrm{d}\tau \left[\frac{1}{2}\left(\frac{\mathrm{d}x}{\mathrm{d}\tau}\right)^2 + U(x)\right]. \tag{2.4}$$

27

Here, x_B and x_{fv} are solutions of the associated Euler-Lagrange equation:

$$\frac{\mathrm{d}^2 x}{\mathrm{d}\tau^2} - U'(x) = 0, \tag{2.5}$$

which is also obtained by setting $\tau = it$ in Eq. (2.2). The solution x_B is periodic, starting at $x(\tau_1) = x_1$, and rolling down the inverted potential $-U(x)$, eventually bouncing off the equal-energy point $x(\tau_2) = x_2$ and returning to x_1. For this reason, it is called a *bounce solution* and its period if $2(\tau_2 - \tau_1)$ (due to the bouncing back). The other solution, x_{fv}, is called the 'false-vacuum solution': it is constant, and sits in the false vacuum for a period $2(\tau_2 - \tau_1)$ (for energy E, the action is thus $2(\tau_2 - \tau_1)E$). In the case of vacuum tunnelling, $E = 0$ and the false vacuum solution is irrelevant. In general, however:

$$T = \exp(-\left[S_E(x_B) - S_E(x_{\mathrm{fv}}) \right]). \tag{2.6}$$

This approach can be generalised to quantum mechanics with N degrees of freedom, q_i. In this case, however, there are generally many possible routes through the barrier, instead of a single path (see for example figure 1.3. The WKB approximation for a particular route $\mathbf{q}(s)$ through the barrier gives:

$$T = \exp\left(-2 \int_{\mathbf{q_1}}^{\mathbf{q_2}} \sqrt{\sum_i^N \left(\frac{\mathrm{d}q_i}{\mathrm{d}s} \right)^2} \mathrm{d}s \sqrt{2 \left(U(\mathbf{q}(s)) - E \right)} \right). \tag{2.7}$$

It can then be said that the dominant route for tunnelling is the route that produces the largest T, that is, has the smallest Euclidean action, $S_E[\mathbf{q}(\tau)]$. The action that determines tunnelling in this case is:

$$S_E = \int_\tau \mathrm{d}\tau \left[\sum_i^N \frac{1}{2} \left(\frac{\mathrm{d}q_i}{\mathrm{d}\tau} \right)^2 + U(\mathbf{q}(\tau)) \right]. \tag{2.8}$$

This formulation makes it clear how to generalise the results to a field theory. The simplest case is a relativistic scalar field, $\phi(x)$, which can be thought of as the large N limit of the field theory. The usual action for a scalar field is:

$$S[\phi] = \int \mathrm{d}^4 x \left[-\frac{1}{2} \partial_\mu \phi \partial^\mu \phi - V(\phi) \right]. \tag{2.9}$$

To obtain the Euclidean action that will dominate tunnelling, we first set $t = -i\tau$, and then extract an overall $+i$ factor from the action. We also perform an appropriate analytic continuation of the metric from $(-, +, +, +)$ to $(+, +, +, +)$, which is to say, R^4 (had we extracted $-i$ instead of $+i$, the metric signature would have been the peculiar $(-, -, -, -)$):

$$S_E(\phi) = \int \mathrm{d}^4 x_E \left[\frac{1}{2} \partial_\mu \phi \partial^\mu \phi + V(\phi) \right], \tag{2.10}$$

where $x_E = (\tau, \mathbf{x})$. Throughout the rest of this thesis, we will refer to this as x.

The action in Eq. (2.10) is not in the right form to directly compare it with Eq. (2.8), however. We need to re-write it as:

$$S_E[\phi] = \int \mathrm{d}\tau \left[\left\{ \int \mathrm{d}^3\mathbf{x} \frac{1}{2} \left(\frac{\mathrm{d}\phi}{\mathrm{d}t} \right)^2 \right\} + \left\{ \int \mathrm{d}^3\mathbf{x} \left(\frac{1}{2} (\nabla\phi)^2 \right) + V(\phi) \right\} \right]. \tag{2.11}$$

In particular, note that the potential we tunnel through in a field theory is *not* $V(\phi)$, but:

$$U[\phi] = \int \mathrm{d}^3\mathbf{x} \left(\frac{1}{2} (\nabla \phi)^2 + V(\phi) \right), \tag{2.12}$$

which includes the gradient terms as well as the potential energy density $V(\phi)$ (which is frequently called 'the potential', but in fact it is Eq. (2.12) that we tunnel through). The fact that is is $U[\phi]$ that controls tunnelling, not $V(\phi)$, can have seemingly peculiar consequences; for example, it is possible to have tunnelling with no barriers at all in $V(\phi)$ [114]. In such cases, the potential does not immediately roll down the hill because to do so as a local fluctuation (the whole field can't roll homogeneously as this would be acausal) requires overcoming a gradient barrier, which is always positive. In fact, as we will see, it is the gradient barrier that provides most of the stability of the electroweak vacuum in the absence of gravity: somewhat surprisingly, erasing the barrier altogether would have almost no effect on the stability of the vacuum, at least as far as tunnelling in flat space is concerned (the observations of the electroweak vacuum, namely that $\lambda > 0$ and the Higgs field has a mass, rule this scenario out, however).

An less obvious conclusion of this analysis is that it tells us what happens when the false vacuum decays: In ordinary quantum mechanics, a tunnelling particle will emerge on the other side of the barrier at x_2, and the process conserves energy. The same is true in a field theory, however, the point x_2 is not a point in space, but a field configuration over the spatial degrees of freedom, $\phi(\mathbf{x})$, given by the value of the bounce solution at its half way point. This field configuration is the nucleated bubble of true vacuum, and after forming it will begin to expand.

2.1.1 The Semi-classical Approximation

The discussion up to now leads us to believe that the decay rate per unit four-volume should be of the form:

$$\Gamma = A e^{-B}, \tag{2.13}$$

where B is given by the difference in action between a bounce solution and the false vacuum solution of the Euclidean action:

$$B = S[\phi_{\mathrm{B}}] - S[\phi_{\mathrm{fv}}]. \tag{2.14}$$

However, this analysis doesn't tell us what the pre-factor A should be. Furthermore, it does not include the effect of quantum corrections. This last point is potentially relevant, because as discussed, for the Standard Model the second minimum only appears when radiative corrections are taken into account. Callan, Curtis and Coleman put this discussion on firmer grounds by deriving Eq. (2.13) using a path integral approach [98, 99]. The basic idea is that the evolution of the false vacuum can be described using the Schroedinger equation. The amplitude for the false vacuum state, $|\phi_{\mathrm{fv}}\rangle$ to survive after some long-time T is given by a path integral:

$$\langle \phi_{\mathrm{fv}} | e^{-\frac{i}{\hbar} \hat{H} T} | \phi_{\mathrm{fv}} \rangle = \int \mathcal{D}\phi \, e^{iS[\phi]}. \tag{2.15}$$

The decay rate of the vacuum is encapsulated in the energy of the false vacuum state, E_{fv}. This state is unstable because E_{fv} can be regarded as *complex*. This is possible because the false vacuum state is not an eigenstate of the Hamiltonian of the meta-stable theory, but of an analytically related, stable theory, similar to how the excited states of an atom are

exact eigenstates of Hamiltonian with an unquantised electromagnetic field, but when the electromagnetic field is quantised, they cease to be eigenstates of the Hamiltonian and instead become long-lived states which eventually decay to the ground state. We discuss and define this state and its complex energy precisely in appendix A.1. With a complex energy then, the probability of finding the particle in the vacuum at some large time t is:

$$\langle \phi_{\text{fv}}(t)|\phi_{\text{fv}}(t)\rangle = \langle \phi_{\text{fv}}(0)|\phi_{\text{fv}}(0)\rangle \exp(2\mathbb{I}\text{m}(E_{\text{fv}})T). \tag{2.16}$$

If $-2\mathbb{I}\mathbb{M}(E_{\text{fv}}) > 0$, this means that the particle decays and its decay rate can be extracted from the imaginary part of the false vacuum energy. This of course raises an obvious question - how is it that the energy of the false vacuum can be complex if the Hamiltonian is Hermitian? The discussion of section A.1 answers this: low lying states around the false vacuum are a Breit-Wigner distribution sum of the energy eigenstates in a band around certain resonance energies, E_n, and the time evolution of this sum produces an exponential decay. The complex energy is a shortcut to this result. It can be defined by starting from an absolutely stable potential, and deforming it in such a way that it becomes metastable. We know from the discussion of section A.1 that the bound states will deform into resonance states when we do this, and thus to obtain the 'energy' of a resonance states, we should analytically continue the energy of the corresponding bound state energies as a function of the deformation parameter, $E_n(\alpha)$. Precisely what α is depends on how the potential is deformed, but as long as the deformation does not significantly distort the false vacuum part of the potential, then the analytically continued (complex) energy will be unique.

As an example, we could consider the potential of Eq. (A.1). In that case, the potential can be deformed by varying λ' from positive to negative values. Expanding the initial state in terms of energy eigenstates, we find that for a general potential:

$$|\phi_{\text{fv}}\rangle = \sum_n \langle n|\phi_{\text{fv}}\rangle |n\rangle. \tag{2.17}$$

We can now extract the overlap with the lowest lying energy state, E_0, by performing a Wick rotation, $t = -i\tau$:

$$\lim_{T\to\infty} \langle \phi_{\text{fv}}| e^{-\hat{H}T} |\phi_{\text{fv}}\rangle \sim |\langle \phi_{\text{fv}}|0\rangle|^2 e^{-E_0 T}. \tag{2.18}$$

We can evaluate the LHS of this equation using a Euclidean path integral:

$$\lim_{T\to\infty} \langle \phi_{\text{fv}}| e^{-\hat{H}T} |\phi_{\text{fv}}\rangle \sim \lim_{T\to\infty} \int_{\phi_{\text{fv}}}^{\phi_{\text{fv}}} \mathcal{D}\phi e^{-S_E[\phi]}, \tag{2.19}$$

where the boundary conditions of this path integral require that we integrate over all configurations that reach the false vacuum. This path integral can be estimated using the semi-classical approximation, which assumes that the path integral is dominated by classical solutions called instantons, or bounces, which are stationary points of the Euclidean action. Consider expanding the action such a solution, $\phi = \phi_B + \eta$:

$$\int \mathcal{D}\phi e^{-S[\phi]} \approx \int \mathcal{D}\eta \exp\left(-S[\phi_B] - \frac{1}{2}\int \mathrm{d}^4 x \int \mathrm{d}^4 y \eta(x)\frac{\delta^2 S[\phi_B]}{\delta\phi(x)\delta\phi(y)}\eta(y) + \ldots\right). \tag{2.20}$$

Neglecting the higher order terms as giving small corrections (equivalent to a one-loop expansion around the bounce solution) we find we can expand $\eta(x)$ in terms of the eigenfunctions of

$S''[\phi_B] = \frac{\delta S[\phi_B]}{\delta\phi(x)\delta\phi(y)}$ to give:

$$\int \mathcal{D}\eta \exp\left(-\frac{1}{2}\int \mathrm{d}^4x \int \mathrm{d}^4y \, \eta(x)\frac{\delta^2 S[\phi_B]}{\delta\phi(x)\delta\phi(y)}\eta(y).\right)$$

$$= \int \mathcal{D}\eta \exp\left(-\frac{1}{2}\int \mathrm{d}^4x \int \mathrm{d}^4y \sum_{n,m} c_n c_m \delta\phi_n(x)\delta^{(4)}(x-y)\delta\phi_m(y)\right)$$

$$= N \prod_n \left(\int \mathrm{d}c_n e^{-\frac{\lambda_n c_n^2}{2}}\right), \tag{2.21}$$

where the factor N accounts for the difference in measure between $\mathcal{D}\eta$ and $\prod_n \mathrm{d}c_n$, both of which integrate over all possible fluctuations, $\eta(x)$. We also used the eigenvalue equation:

$$\frac{\delta^2 S[\phi_B]}{\delta\phi(x)\delta\phi(y)}\delta\phi_m(y) = \delta^{(4)}(x-y)\lambda_n \delta\phi_m(y), \tag{2.22}$$

and the orthogonality of the eigenfunctions. This makes it clear that the result of the path integral in the semi-classical approximation is a functional determinant, since:

$$\int_{-\infty}^{\infty} \mathrm{d}c_n e^{-\frac{c_n^2 \lambda_n}{2}} = \sqrt{\frac{2\pi}{\lambda_n}} \tag{2.23}$$

$$\implies \int \mathcal{D}\phi e^{-S[\phi]} \approx N e^{-S[\phi_B]} \prod_n \left(\frac{2\pi}{\lambda_n}\right)^{\frac{1}{2}} = N \det\left(\frac{S''[\phi_B]}{2\pi}\right)^{-\frac{1}{2}} e^{-S[\phi_B]}. \tag{2.24}$$

Note that this expression is formally infinite, which is not surprising, since the path integral diverges and only has meaning if we consider ratios of functional determinants. A careful treatment by Callan, Coleman, and Curtis finds that the resulting decay rate per unit four-volume, Γ, is to one-loop order [98, 99]:

$$\Gamma = \frac{B^2}{4\pi^2 \hbar^2}\left|\frac{\det'(S''[\phi_B])}{S''[\phi_{\mathrm{fv}}]}\right|^{-\frac{1}{2}}[1 + O(\hbar)]\exp\left(-\frac{B}{\hbar}\right), \tag{2.25}$$

where V is the volume of space under consideration and

$$B = S[\phi_B] - S[\phi_{\mathrm{fv}}], \tag{2.26}$$

is the difference in action between ϕ_B, the bounce solution, and ϕ_{fv}, the false vacuum solution (which sits in the false vacuum for all time). S'' indicates the second functional derivative of the Euclidean action, and $\det'$ indicates a determinant subtracting off four of the zero eigenvalues, which correspond to spatial translations of the bounce solution through Minkowski space. This subtraction is equivalent to summing over the possible locations that the bounce can nucleate, and is responsible for the otherwise infinite volume factor in Eq. (2.25): this is dealt with by computing the decay rate per unit volume. Note that there may well be other zero eigenvalues if the theory contains some symmetry. Indeed, neglecting quantum corrections, the Standard Model has this property and requires careful treatment [28]. This happens because at tree level, the Standard Model has an approximate conformal symmetry in the potential, $V(\phi) = \frac{\lambda\phi^4}{4}$, which is in fact broken by quantum corrections to the running of λ. It can be dealt with using the method of constrained instantons [115, 28], or by considering bounce solutions in the effective potential, rather than the classical potential -see [116, 96] for a discussion. The issue

is related to the fact that the false vacuum in the Standard Model only arises when radiative corrections are taken into account.

It should be noted that in deriving Eq. (2.25), one encounters the problem that the bounce always has a negative eigenvalue. In fact, this negative eigenvalues if responsible for making the energy of the false vacuum appear to be complex, but at first glance, it appears to be problematic, because the semi-classical contribution to the path integral diverges (consider what happens to the integral in Eq. (2.23)). This simply reflects the fact that the bounce solution we have considered is not a minimum of the action, but a saddle point, and there will be larger contributions (namely $\phi_{\rm fv}$) that dominate the integral. However, since only the imaginary part of the energy contributes to the decay rate, the bounce can still be included.

One might object to this analysis, however, for two reasons: (1), we have neglected the possible contribution of a true vacuum solution, $\phi_{\rm tv}$, that sits in the true vacuum for all time, and (2), the full Euclidean path integral should give a real result. In fact these two problems are related. It can be shown that the the true vacuum solution gives a contribution that cancels out the imaginary contribution from the bounce [117], which means the actual result of the calculation should be real. What then are we to make of this complex energy?

The answer is that if we deform the potential as per the discussion of section A.1, such that the false vacuum becomes absolutely stable, the true vacuum disappears and we have true bound states once more. In the deformed, absolutely stable potential, the eigenvalue is positive and we have no problem defining the semi-classical approximation. As the potential is deformed back to the metastable case, the result varies analytically with λ_0 until it becomes negative, since we know from the previous discussion that the bound states of the deformed potential are analytically related to the resonance states of the metastable one. Consequently, the path integral contribution, $\int \mathrm{d}c_0 e^{-\frac{c_0^2 \lambda_0}{2}}$ should also be an analytic continuation of the result when λ_0 goes negative. This corresponds to deforming the c_n integration contour into the complex plane, and integrating out to infinity along a Stokes wedge (see [118] for a discussion) such that the integral converges, and will deform back to the real line when the potential is deformed back to stability. Since the precise contour chosen doesn't matter, by analyticity and the residue theorem, we can choose the path of steepest descent that allows us to evaluate the integral along the contour most accurately in the semi-classical approximation. This leads to a unique complex energy, and corresponds to the result of Eq. (A.41).

2.2 $O(4)$ Symmetric Bounces

To compute the decay rate, it is necessary to find stationary points of the Euclidean action. Let us restrict ourselves to the case of a single scalar field in flat space-time, which has Euclidean action:

$$S_E[\phi] = \int \mathrm{d}^4x \left[\frac{1}{2} \partial_\mu \phi \partial^\mu \phi + V(\phi) \right]. \tag{2.27}$$

The equation of motion that minimise this is:

$$\nabla_\mu \nabla^\mu \phi - V'(\phi) = 0. \tag{2.28}$$

In general, there can be many solutions of this equation, and we can evaluate the corresponding contribution to the path integral by summing up the contributions from each bounce. However,

in general only the solution with the smallest action will contribute significantly, with other solutions giving exponentially small contributions relative to this.

It turns out that in flat space, Eq. (2.28) is minimised by solutions that have $O(4)$ symmetry (to be more precise, within any class of solutions, there is always an $O(4)$ symmetric solution that has the lowest action of that class). This was proven by Coleman, Glazer, and Martin [119]. This affords a great simplification to the equation of motion, since in an $O(4)$ symmetric polar-co-ordinate system, it becomes:

$$\ddot{\phi} + \frac{3}{\chi}\dot{\phi} - V'(\phi) = 0, \tag{2.29}$$

where dots denote differentiation with respect to the radial parameter, χ. Note that this equation appears to behave much like the motion of an object rolling down an inverted potential, $-V(\phi)$ (since due to the Wick rotation, the potential appears in the equation with the opposite sign to the Minkowski case). In this mechanical analogy, the second term behaves much like a time dependent friction term. The action of these solutions is:

$$S = 2\pi^2 \int_0^\infty r^3 \left[\frac{1}{2}\dot{\phi}^2 + V(\phi) \right] \mathrm{d}r. \tag{2.30}$$

In order to give a finite contribution to the action (and thus a non-zero contribution to the decay rate), it is necessary to impose the boundary conditions:

$$\dot{\phi}(0) = 0, \tag{2.31}$$

$$\phi(r \to \infty) \to \phi_{\mathrm{fv}}. \tag{2.32}$$

The first condition ensures that the bounce is smooth in the centre, while the second ensures that it resembles the false vacuum at infinity, which is necessary so that the action integral Eq. (2.30) converges (recall also that only contributions that touch the false vacuum are included in the path integral expression for the energy, Eq. (2.19)). Although these boundary conditions allow us to solve for $\phi(r)$, they do not give rise to a unique solution, in keeping with the general notion that two-point boundary value problems do not generally have unique solutions. One solution is $\phi = \phi_{\mathrm{fv}}$, the false vacuum solution. Another sometimes relevant solution of these equations, but not satisfying the boundary conditions Eq. (2.31) and (2.32) is $\phi = \phi_{\mathrm{tv}}$, the analogous solution sitting in the true vacuum.

There is also a non-trivial solution, which we will generally refer to as 'the bounce', since it is easy to prove (in flat space) that it is the unique non-trivial solution. The proof of this was originally given by Coleman [98], but we repeat it here because the fact that it fails to hold in curved space is crucial to the findings of this thesis.

Consider some initial $\phi_0 = \phi(0)$, and attempt to solve Eq. (2.29) by the shooting method. The $\frac{1}{r}$ term behaves like a monotonically decreasing friction term, and the potential appearing is inverted compared to the usual Lorentzian field equation (this is a consequence of the Wick rotation). Let ϕ_{fv}, ϕ_{bar} and ϕ_{tv} denote the locations of the false vacuum, top of the barrier, and true vacuum respectively. Any ϕ_0 starting on the range $(\phi_{\mathrm{fv}}, \phi_{\mathrm{tv}})$ will start rolling towards the top of the barrier, and eventually cross it. Evidently to match the boundary condition Eq. (2.32), it will be necessary to start on the range $(\phi_{\mathrm{bar}}, \phi_{\mathrm{tv}})$, since solutions starting on the false vacuum side of the barrier will eventually fall back, but due to the friction removing 'energy' from the system, they can never reach closer to ϕ_{fv} than their starting point, ϕ_0. For solutions on the true-vacuum side of the barrier, $\phi \in (\phi_{\mathrm{bar}}, \phi_{\mathrm{tv}})$, there are two possibilities:
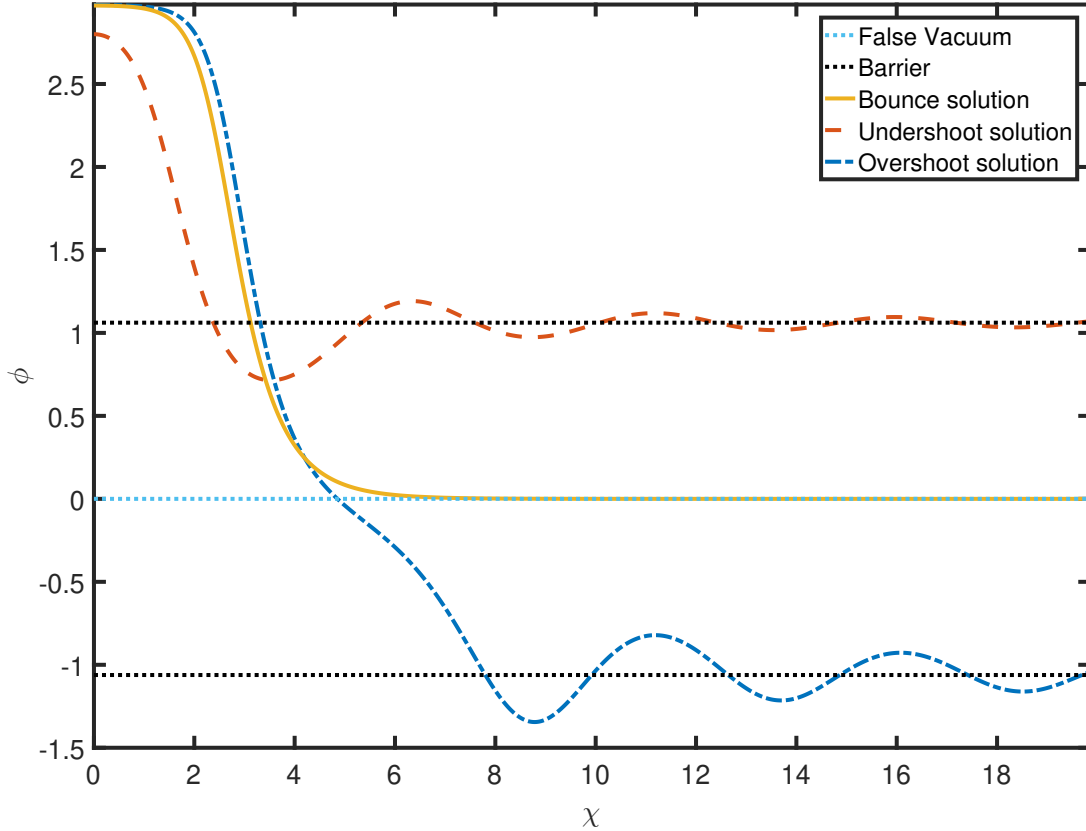
Figure 2.1: Example overshoot and undershoot solutions. The undershoot solutions lacks the energy to reach the false vacuum, and falls back to the barrier, oscillating. The overshoot solution, conversely, overshoots the false vacuum and (in this case) eventually oscillates about the other barrier. Note that in general the defining feature of an overshoot is that it overshoot the false vacuum - the potential may or may not have another barrier to oscillate about, and may either escape to infinity, or reflect backwards depending on the potential: all these scenarios count as overshoots. Between the overshoot and undershoot solution there lies a bounce solution - it is this that dominates vacuum decay.

- Solutions too close to ϕ_{bar} initially will lack the energy to climb to ϕ_{fv}: such solutions will reach $\dot{\phi} = 0$ at some finite r and then fall back, oscillating forever and giving and infinite contribution to the action. Such solutions are called 'undershoot' solutions.

- Solutions starting too close to ϕ_{tv} will stay there for a long time (since $V'(\phi_0)$ can be made arbitrarily small if ϕ_0 is sufficiently close to ϕ_{fv}), until the friction term has fallen to near zero: when they finally do fall down, since the true vacuum has higher $-V(\phi)$ than the false vacuum, they will have too much energy and will overshoot the false vacuum: these solutions are known as 'overshoot' solutions for this reason.

These two types of solutions are illustrated in figure 2.1.

2.3 Uniqueness of Flat Space Bounces

By continuity, it can be argued that between any undershoot and overshoot, there must lie a bounce solution. Furthermore, this solution is unique by a simple energy argument first given by Coleman [98]: the friction term in Eq. 2.29 is always positive, and thus the 'energy' of the system is monotonically decreasing. This can be seen explicitly by recasting Eq. 2.29 as:

$$\frac{\mathrm{d}}{\mathrm{d}\chi}\left(\frac{\dot{\phi}^2}{2} - V(\phi)\right) = -\frac{3\dot{\phi}^2}{\chi}. \tag{2.33}$$

Note that 'energy' here is defined with V having the opposite sign to the usual definition: this is due to the Wick rotation, but in any case its physical interpretation does not affect the result, which is that the 'energy' is monotonically decreasing. Consequently, if a particle doesn't have enough energy to reach the false vacuum for some initial ϕ_1 (since $\dot{\phi}(0) = 0$, the initial energy is $-V(\phi_1)$), then for any $\phi_0 \in (\phi_{\mathrm{bar}}, \phi_1)$, the initial energy is also too small to reach the false vacuum. This implies that if ϕ_0 leads to an undershoot solution, then all ϕ between ϕ_0 and the barrier also lead to undershoots. Now assume that there are multiple bounce solutions, starting at ϕ_1 and ϕ_2, with ϕ_1 closest to the barrier. Since a solution lies between a range of undershoots and a range of overshoots, then any ϕ_0 between ϕ_1 and ϕ_{bar} is also an undershoot. This contradicts the assumption that there is a second solution, which requires overshoots on one side of it, hence the bounce solution is unique.

This argument, as we will see, is modified in curved space, which will be crucial to the main results of this thesis.

2.4 Application to the Standard Model

The Standard Model is a theory with a scalar doublet, the Higgs field, whose behaviour is governed by the Higgs potential:

$$V_{\mathrm{Higgs}}(\Phi) = \lambda(\Phi^\dagger\Phi - \nu^2)^2. \tag{2.34}$$

After spontaneous symmetry breaking, three of the components of this doublet correspond to Goldstone bosons, and in unitary gauge these are absorbed into the W and Z bosons, giving a single Higgs scalar, h, satisfying:

$$V(h) = -\frac{1}{2}m^2h^2 + \frac{\lambda}{4}h^4, \tag{2.35}$$

where $m^2 = 2\nu^2\lambda$, and the tree level Higgs mass is $M_h^2 = 2m^2$. As discussed in the introduction the Higgs self-coupling, λ, runs with the energy scale, μ, and the correct description requires the use of the Higgs effective potential (action). Let $S[h] = S_0[h] + S_1[h]$ where $S_0[h]$ is the tree level action and $S_1[h]$ the 1 loop correction. Now let $h = h^{(0)} + h^{(1)}$ be the bounce solution, with $h^{(0)}$ the tree level bounce, and $h^{(1)}$ the 1-loop correction to it. Expanding about $h^{(0)}$ gives:

$$S[h] \approx S_0[h^{(0)}] + S_0'[h^{(0)}]h^{(1)} + S_1[h^{(0)}] + S_1'[h_0]h^{(1)} + O(h^{(1)})^2 \tag{2.36}$$

$$= S_0[h^{(0)}] + S_1[h^{(0)}] + O(h^{(1)})^2. \tag{2.37}$$

This follows since, by definition, $S_0'[h^{(0)}] = 0$ and because $S_1'[h^0] = S_1'[h^0] + S_0'[h^{(0)}] = S'[h^0] = S'[h] + O(h^{(1)})$. Since $S'[h] = 0$ by definition, then $S_1'[h^{(0)}]h^{(1)}$ is a second order correction and

can be ignored. This means that to 1-loop order, the bounce action is given by the 1-loop action of the tree-level bounce solution: the corrections to this solution from loops contribute only at second order.

Of course, in the Standard Model, we run into the obvious snag that there *is* no bounce solution at tree level, nominally. However, we know the problem is caused by the running of λ, and for constant negative values of λ, it is possible to find a tree level solution, the so called Fubini or Lee-Weinberg bounce [120, 114]:

$$
h_{LW}(\chi) = \sqrt{\frac{2}{|\lambda|}} \frac{2R}{R^2 + \chi^2}, \tag{2.38}
$$

which is easily verified to solve Eq. (2.29) in the case of a negative λ potential: $V(h) = -\frac{|\lambda|}{4}h^4$. This satisfies both of the boundary conditions Eqs. (2.31)-(2.32) for *arbitrary* R. The reason that this happens is that the equation:

$$
\ddot{h} + \frac{3}{\chi}\dot{h} + |\lambda|h^3 = 0, \tag{2.39}
$$

has conformal symmetry: it is invariant under the scale transformation $\chi \to a\tilde{\chi}, h \to \frac{\tilde{h}}{a}$. Consequently, if some scale R solves the equations, then all other scales must solve it too. The tree level action of this solution is:

$$
B_0[h_{LW}] = \frac{8\pi^2}{3|\lambda|}, \tag{2.40}
$$

which is independent of R, as we would expect for a conformally symmetric system. Note that this is only in fact true for large h, and the Standard Model has $-\frac{1}{2}m^2h^2$ terms that break this conformal symmetry. However, it is precisely large h which control the behaviour of tunnelling. In general, the loop corrections to this are complicated in the Standard Model - they are considered by [18] for example. Two things are of note from this calculation: the running of the couplings spoils the conformal symmetry of the tree level action, which means different scales μ will describe bounces with different action. Specifically, inspection of Eq. (2.40) shows that decay will be dominated by the scale μ at which $|\lambda|$ is maximised (which is the *minimum* value of $\lambda < 0$). Also, the loop corrections will in general come out with logarithmic terms such as $\log(\alpha\mu^2R^2)$ where α is some $O(1)$ constant. This implies that we should choose:

$$
\mu \approx \frac{1}{R}, \tag{2.41}
$$

in order to minimise quantum corrections to the bounce - essential for the accuracy of the calculation to avoid the problem of large logarithms. This essentially fixes the decay rate result as:

$$
h^{(0)}(\chi) = \sqrt{\frac{2}{|\lambda(\mu_{\min})|}} \frac{2\mu_{\min}}{1 + \mu_{\min}^2\chi^2}, \tag{2.42}
$$

$$
B_0 = \frac{8\pi^2}{3|\lambda(\mu_{\min})|}, \tag{2.43}
$$

where $\mu_{\min}$ is the renormalisation scale at which λ is minimised (conversely, $|\lambda(\mu)|$ is maximised on the set $\{\mu : \lambda(\mu) < 0\}$). The three loop running of λ, using the top mass $M_t = 173.34\text{GeV}$

and Higgs mass $M_h = 125.15\text{GeV}$ gives this scale as $\mu_{\text{min}} = 2.79 \times 10^{17}\text{GeV}$, and $\lambda(\mu_{\text{min}}) = -0.01459$. This corresponds to $B_0 \approx 1804$.

To get an idea of how this affects the life-time, we would need to compute the pre-factor, A, of the $\Gamma \sim Ae^{-B}$ formula, since this contains the dimension-full parameters that determine Γ/V, the decay rate per unit volume. However, we know that the bounce is dominated by the scale μ_{min}, so the dimensions of A should be dominated by this. Thus, a good approximation of the decay rate per unit four-volume is:

$$\frac{\Gamma}{V} = \mu_{\text{min}}^4 e^{-B_0}. \tag{2.44}$$

We now ask the question: what is the probability that a bubble formed within our past light cone? This corresponds to a Hubble volume of roughly $V \approx H_0^{-3}$, where H_0 is the present day Hubble rate[1]. This means that the expected life-time of the vacuum (after which the probability that a bubble was present in our past light cone exceeds $1/e$) is:

$$\tau_{\text{Univ}} = \frac{1}{\Gamma} = \frac{1}{H_0}\left(\frac{H_0}{\mu_{\text{min}}}\right)^4 e^{+B_0} = \frac{1}{H_0} \times 10^{B_0 \log_{10}(e) - 4\log_{10}\left(\frac{H_0}{\mu_{\text{min}}}\right)} \approx \frac{10^{550}}{H_0}. \tag{2.45}$$

Consequently, the decay rate of the electroweak vacuum in the present day leads to a life-time 550 orders of magnitude longer than the age of the visible universe. It is safe to say that this is compatible with observations: we know that the present day vacuum is *not* the true vacuum, but decay events are so overwhelmingly unlikely that even if the electroweak vacuum is metastable, it would be expected to remain in its present state today, as we observe. One might naively think that this should be the end of the issue - whatever the instability implies about high energy physics, it evidently puts us in no danger of spontaneous vacuum decay. However, there are other effects that must be taken into account: one of these is gravity, and that will form the discussion of the rest of this thesis.

---

[1]Actually, the volume is larger than this because the age of the universe is not precisely $\frac{1}{H_0}$, and depends on the precise cosmological model, and also because the visible universe has radius somewhat larger than $\frac{1}{H_0}$, due to the expansion of the universe stretching the distance that observed light can have travelled since the Big Bang to (apparently) superluminal distances.

Chapter 3

Basics II - Vacuum Decay with Gravity

Gravitational corrections to the decay rate of a false vacuum state in field theories have been considered since the idea's inception. There are three main potential influences of gravity that we wish to consider:

1. Gravitational back-reaction of the nucleated bubble on the metric, and how this affects nucleation.

2. The effect of non-minimal couplings between the Higgs field and gravity.

3. The nucleation of vacuum bubbles during inflation.

Gravitational back-reaction at first glance may seem irrelevant, however, it should be noted that the true vacuum of the Standard Model appears to be very deep - it is unclear exactly how deep. Certainly this matters for the subsequent evolution of true vacuum bubbles, but as we have seen in the flat space discussion, nucleated bubbles tunnel through the barrier to a scale $\mu_{\min} \sim 10^{17}\,\text{GeV}$, which is not far off the Planck scale. It is not unreasonable therefore to ask what effect back-reaction might have. This is ultimately tied up with the fact that the Standard Model true vacuum is not shallow compared with the false vacuum, and thus the thin wall approximation is not valid there.

Non-minimal coupling is related to gravitational back-reaction. It is well known that if a term such as $\frac{\xi}{2}\phi^2 R$ is included in the action, then ξ will run with the energy scale [57]. Current bounds on ξ are extremely weak, showing only that $|\xi| < 2.6 \times 10^{15}$ [105]. At one loop level, this running is given in the Standard Model by [57, 3]:

$$\mu^2 \frac{\mathrm{d}\xi}{\mathrm{d}\mu^2} = \frac{1}{16\pi^2}\left(\xi - \frac{1}{6}\right)\left[6\lambda + Y_2(S) - \frac{9}{10}g_1^2 - \frac{9}{2}g_2^2\right], \tag{3.1}$$
$$Y_2(S) \equiv 3(y_u^2 + y_c^2 + y_t^2 + y_d^2 + y_s^2 + y_b^2) + y_e^2 + y_\mu^2 + y_\tau^2,$$

where y_X are the fermion Yukawa couplings to the Higgs. $\xi = \frac{1}{6}$ attracts special attention, since if the potential of the theory is conformally invariant, then the the Lagrangian is also conformally invariant. It is notable that this value is a fixed point of the renormalisation flow at one loop - a manifestation of the conformal symmetry. However, what is important about this equation is that $\xi = 0$ is *not* a fixed point. Thus, the Standard Model cannot have $\xi = 0$ at all energy scales. Consequently, it is never correct to ignore it. This becomes doubly important when one considers the depth of the Standard Model effective potential, since this means that the heart of a nucleated bubble can potentially have a large (negative) Ricci scalar, to which the Higgs field can couple. This can significantly distort the shape of nucleated true vacuum bubbles, or even suppress them. Other order-6 operators such as ϕ^6/M_{P}^2 and $\phi^2\partial_\mu\phi\partial^\mu\phi/M_{\mathrm{P}}^2$ can also affect vacuum stability - see section 5.1 for further discussion.

Finally, inflation is one of the main reasons that the vacuum instability problem is a potential problem. Light scalar fields such as the Higgs receive fluctuations of order H from inflation [107], and this could potentially destabilise the electroweak vacuum by pushing the field over the barrier and into the true vacuum [65, 66, 68, 60]. As we saw in chapter 2, the flat space decay rate of the vacuum is sufficiently slow that it is overwhelmingly likely that a true vacuum bubble would not have nucleated during the life-time of the visible universe. However, if the decay rate is enhanced during Inflation, this scenario could change drastically.

One of the first works on this was produced by Coleman and de Luccia [97]. Coleman and de Luccia considered thin wall bounce solutions, asking what happens when the energy density

of the true vacuum is such that the critical nucleated bubble has a size comparable to its own Schwarzschild radius.

They proceeded by analogy to the flat space case, which is to consider the Euclidean action for the theory of a scalar field in a gravitational background:

$$S[\phi, g_{\mu\nu}] = \int \mathrm{d}^4x \sqrt{\det g} \left[\frac{1}{2} \nabla_\mu \phi \nabla^\mu \phi + V(\phi) - \frac{M_{\mathrm{P}}^2}{2} R \right]. \tag{3.2}$$

It is of course worth noting that Wick rotating a metric is by no means a straightforward matter, and it remains unclear if the procedure can even by done for arbitrary metrics [121]. One obvious problem is that the prescription $t \to i\tau$ obviously cannot be interpreted literally. Consider the de Sitter metric, for example:

$$\mathrm{d}s^2 = -\mathrm{d}t^2 + e^{2Ht}\tilde{g}_{ij}\mathrm{d}x^i\mathrm{d}x^j \to \mathrm{d}\tau^2 + e^{2iH\tau}\tilde{g}_{ij}\mathrm{d}x^i\mathrm{d}x^j. \tag{3.3}$$

Taken at face value, this procedure would make the metric complex. However, the procedure is well defined in flat space, and this can be extended to de Sitter-like spaces of the form[1]:

$$\mathrm{d}s^2 = \mathrm{d}\chi^2 + a^2(\rho)[-\mathrm{d}\psi^2 + \cosh^2\psi\mathrm{d}\Omega_2^2]. \tag{3.4}$$

Following [84], we can then transform via:

$$t = f(\chi)\sinh(\psi), \tag{3.5}$$
$$r = f(\chi)\cosh(\psi), \tag{3.6}$$

with $f(\chi)$ defined by $f'(\chi) = f(\chi)/a(\chi)$ giving:

$$\mathrm{d}s^2 = \frac{a^2(\chi)}{f^2(\chi)}(-\mathrm{d}t^2 + \mathrm{d}r^2 + r^2\mathrm{d}\Omega_2^2), \tag{3.7}$$

which shows that this metric is conformally flat. The Wick rotation $t = -i\tau$, which is equivalent to $\psi = -i(\frac{\pi}{2} - \varphi)$ then gives an unambiguously real metric:

$$\mathrm{d}s_{\mathrm{Euc}}^2 = \frac{a^2(\chi)}{f^2(\chi)}(\mathrm{d}\tau^2 + \mathrm{d}r^2 + r^2\mathrm{d}\Omega^2) = \mathrm{d}\chi^2 + a^2(\chi)\mathrm{d}\Omega_3^2. \tag{3.8}$$

This also makes clear in what sense de Sitter space can be regarded as an analytic continuation of the 4-sphere metric to Lorentzian space. Inverting the procedure can also be used to obtain the subsequent evolution of the bubble after nucleation.

3.1 Equations of Motion

Accepting for the moment that the action Eq. (3.2) is the correct generalisation to describe tunnelling when gravity is present, we move to describe the equations of motion that the bounce solutions must satisfy:

$$\nabla_\mu \nabla^\mu \phi - V'(\phi) = 0, \tag{3.9}$$
$$R_{\mu\nu} - \frac{1}{2}Rg_{\mu\nu} = \frac{1}{M_{\mathrm{P}}^2}\left(-\nabla_\mu\phi\nabla_\nu\phi + \frac{1}{2}g_{\mu\nu}\left[\frac{1}{2}\nabla_\rho\phi\nabla^\rho\phi + V(\phi)\right]\right). \tag{3.10}$$

---

[1]By de Sitter like, it is meant that this metric reduces to de Sitter space when $a(\rho) = \frac{1}{H}\sin(\rho)$, in which case, Eq. (3.4) is just the dS-slicing co-ordinates form of de Sitter spacing, where the dS_n is divided into slices of unit dS_{n-1} metrics each expressed in closed-slicing co-ordinates.

Solving the coupled Einstein-scalar field equations in full generality, however, is no straightforward task. As discussed in chapter 2, the flat space results are dominated by $O(4)$ symmetric bounces. In curved space, no such theorem exists that would imply this [97], but it seems plausible that the same would apply, with caveats. It seems unreasonable, for example, to expect that the dominant solution for a decay triggered by a black hole [82, 122, 83, 84] or by a cosmic string, would respect an $O(4)$ symmetry if the background does not. A more reasonable conjecture might be that the dominant contribution to the decay rate is always the solution which respects the symmetry of the initial metastable state. In the cases that we are interested in, namely the electroweak vacuum in empty space, possibly undergoing (homogeneous) inflation, it seems reasonable to assume $O(4)$ symmetry.

Assuming that the bounce solutions are $O(4)$ symmetric, the Euclidean metric can be placed in the form:

$$ds^2_{\text{Eucl}} = d\chi^2 + a(\chi)^2 d\Omega^2_3, \tag{3.11}$$

where χ is a radial co-ordinate, and $d\Omega^2_3$ describes the unit 3-sphere metric. The equations of motion reduce to:

$$\ddot{\phi} + \frac{3\dot{a}}{a}\dot{\phi} - V'(\phi) = 0, \tag{3.12}$$

$$\dot{a}^2 = 1 - \frac{a^2}{3M_{\text{P}}^2}\left(-\frac{\dot{\phi}^2}{2} + V(\phi)\right), \tag{3.13}$$

$$\ddot{a} = -\frac{a}{3M_{\text{P}}^2}\left(\dot{\phi}^2 + V(\phi)\right). \tag{3.14}$$

Dots here denote differentiation with respect to χ. Note that Eq. (3.13) resembles the Friedmann equation of cosmology, but it's interpretation is different. To begin with, this equation appears to always have positive 'spatial curvature' in the form of the first term, which is always 1. Physically, $a(\chi)$ describes the radius of curvature of a surface of constant χ. Since $O(4)$ symmetry implies that such surfaces are always 3-spheres, they necessarily have constant (positive) curvature. However, this does *not* imply that the curvature of this four-dimensional Euclidean space is always positive. In fact, the Ricci scalar is given by:

$$R = \frac{6(1 - \dot{a}^2)}{a^2} - \frac{6\ddot{a}}{a} = \frac{6(1 - \dot{a}^2)}{a^2} - \frac{6\ddot{a}}{a}. \tag{3.15}$$

This can be negative, if the potential is negative, which can happen in the interior of a bounce solution as it lies deep in the true vacuum. An analogue of what this geometry would look like is plotted in figures 3.1 and 3.2. Note that these are not exact representations of the geometry, since representing a surface with negative curvature isometrically is not possible in three dimensions. This can easily be seen by considering the distance along an embedded surface described by $z = f(r)$ where $r = \sqrt{x^2 + y^2}$. The arc length out to r is:

$$l(r) = \int_0^r dr\sqrt{1 + f'(r)^2} \geq r. \tag{3.16}$$

But in two dimensions, the Gaussian curvature is given by [123]

$$K = 3\lim_{l \to 0}\frac{2\pi l - C(l)}{\pi l^3}, \tag{3.17}$$

where $C(l)$ is the circumference of a circle at constant l, in this case $2\pi r$. But since $l \geq r$, we will always have positive Gaussian curvature for such an embedded surface. This is related to

Hilbert's Theorem [124], which states that a surface of constant negative curvature cannot be isometrically embedded in $\mathbb{R}^3$. For this reason, figures 3.1 and 3.2 use model embeddings that are positively curved (or discontinuous) at the origin, and negatively curved elsewhere, in order to represent the geometry of the bounce solution[2] Note additionally, that when the equations
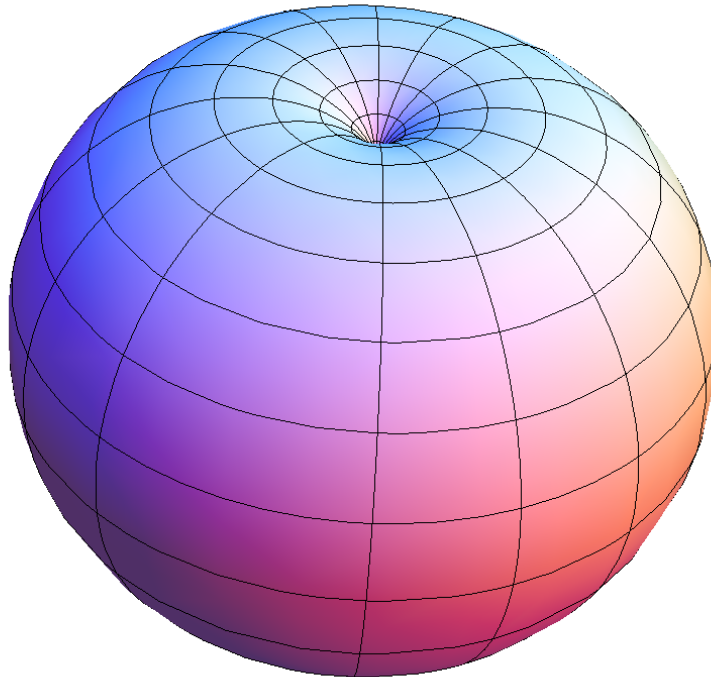
Figure 3.1: 2D analogue of a bounce geometry for the four sphere (actual plot here is a cardioid shape, because the bounce cannot be embedded in 3D, but the curvature of this surface matches that which might be found in a bounce geometry, except for a singular point at the pole - the bounce is smooth).

of motion hold, the action is:

$$S[\phi, a] = -2\pi^2 \int_0^{\chi_{\mathrm{max}}} \mathrm{d}\chi a^3(\chi) V(\phi(\chi)). \tag{3.18}$$

In particular, the kinetic terms of the action cancel after substituting the expression for R:

$$R = \frac{\dot{\phi}^2 + 4V(\phi)}{M_{\mathrm{P}}^2}. \tag{3.19}$$

---

[2]Consequently, these representations are not valid at the origin.
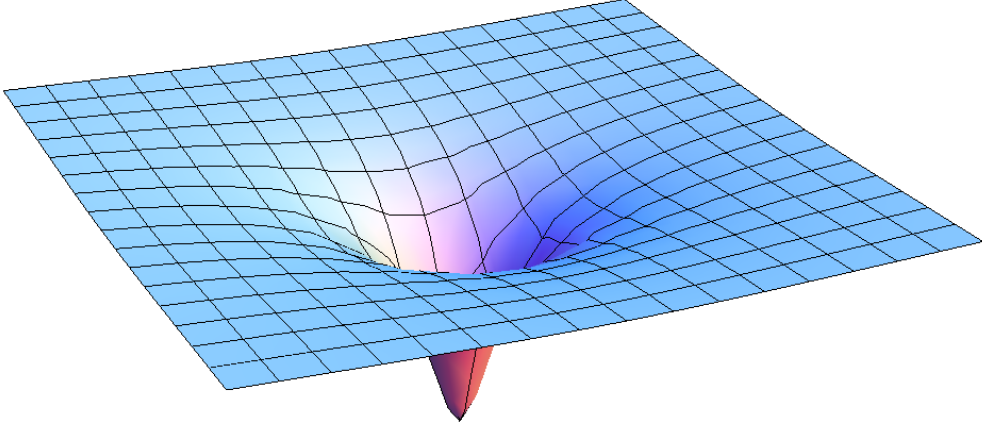
Figure 3.2: 2D analogue of a bounce geometry in an asymptotically flat space. Curvature is negative in the interior of the bounce, and zero far outside it (note that the origin here is singular).

3.2 Boundary Conditions

The boundary conditions in when including gravity depend on the sign of the potential in the false vacuum, $V(\phi_{\mathrm{fv}})$.

1. If $V(\phi_{\mathrm{fv}}) > 0$, then the solution is compact and there necessarily exists $\chi_{\max} > 0$ for which $a(\chi_{\max}) = 0$ (this is proven in section 3.4). In this case, $\dot{\phi}(0) = \dot{\phi}(\chi_{\max}) = 0$ is necessary to avoid divergence at the co-ordinate singularities.

2. If $V(\phi_{\mathrm{fv}}) \leq 0$, then the solution is non-compact and we require $\dot{\phi}(0) = 0$ and $\phi(\chi \to \infty) \to \phi_{\mathrm{fv}}$.

These conditions and the reasons they are required are discussed further in section 3.4.

3.3 Types of Gravitational Bounces

The array of possible bounce solution is much richer with gravity than without. Here we will consider only bounces with $V(\phi_{\mathrm{fv}}) = 0$, the 'flat false vacuum' bounces, and $V(\phi_{\mathrm{fv}}) > 0$, which describes bounces in a de Sitter background.

3.3.1 Flat False Vacuum Bounces

If $V(\phi_{\mathrm{fv}}) = 0$, then the bounce solutions will be non-compact, and thus satisfy the second of the two cases, namely $\dot{\phi}(0) = 0$ and $\phi(\chi \to \infty) \to \phi_{\mathrm{fv}}$. Finding these bounces proceeds much the same way as in flat space, and they have similar properties. As we will show in section 3.4.2,

there is never any χ for which $\dot{a}(\chi) = 0$, and thus $a(\chi)$ grows without bound. Since the solution approaches the (flat) false vacuum, as $\chi \to \infty$, this means that it also approaches $a(\chi) \sim \chi$ at large χ, that is, the exterior of the bounce resembles the flat space case. This means that the effect of gravity is largely confined to the interior of the bounce, where the scalar potential is deepest, as thus we expect more significant gravitational corrections.

Since $\phi(0)$ is always in the $V(\phi(0)) < 0$ region (this is necessary to conserve energy, since the gradient in the scalar field gives a positive energy contribution), then the interior resembles an anti-de-Sitter space, and can potentially undergo gravitational collapse when a bubble nucleates. It always has a strong negative Ricci curvature.

3.3.2 Coleman-De Luccia Bounces

When $V(\phi_{\mathrm{fv}}) > 0$, bounce solutions are necessarily complicated. The most general non-trivial tunnelling solution is called the Coleman de Luccia (CdL) solution, first proposed in [97]. These solutions satisfy $\dot{\phi}(0) = \dot{\phi}(\chi_{\max}) = 0$, and interpolate between two points on opposite sides of the barriers, $\phi(0) = \phi_0, \phi(\chi_{\max}) = \phi_1$. Generically, neither of ϕ_1, ϕ_0 is the false vacuum, so the exterior of the bounce does not touch the false vacuum (this is because reaching the false vacuum can only be done in infinite time, while the bounce must be compact).

This presents a difficulty in interpreting the bounce solution, which is supposed to describe tunnelling from a false vacuum state. At first it appears contradictory - the energy of the false vacuum state in flat space is determined from the vacuum survival amplitude:

$$\langle \phi_{\mathrm{fv}} | e^{-\hat{H}T} | \phi_{\mathrm{fv}} \rangle = \int_{\phi_{\mathrm{fv}}}^{\phi_{\mathrm{fv}}} \mathcal{D}\phi \, e^{-S[\phi]}, \tag{3.20}$$

which describes an integral over states which all touch the false vacuum as a boundary condition. How then, can a CdL solution possibly describe tunnelling from a metastable vacuum? It would seem to be excluded.

The answer comes from considering the quantum properties of gravitational backgrounds such as de Sitter space. De Sitter space has a horizon, which results from the exponential expansion of space-time:. Much like a black hole horizon, it can be shown that this horizon has an associated temperature, the Gibbons-Hawking temperature [125]:

$$T_{\mathrm{GH}} = \frac{H}{2\pi}, \tag{3.21}$$

where $H^2 = \frac{V(\phi_{\mathrm{fv}})}{3M_{\mathrm{P}}^2}$ is the Hubble rate. The horizon itself can be visualised by considering the structure of de Sitter space, which is defined by embedding a hyperboloid, $-x_0^2 + x_1^2 + x_2^2 + \ldots + x_N^2 = \frac{1}{H^2}$, in $N + 1$ dimensional Minkowski space. Figure 3.3a shows an example of this. As can be seen from figure 3.3b, observers sitting at one point on the surface can never see some null rays, even after an infinite amount of time.

The thermal fluctuations that result from this mean that vacuum decay in a de Sitter background cannot be considered a purely tunnelling process - there is also a process of thermal excitation that can lift states in the false vacuum up the barrier.

44
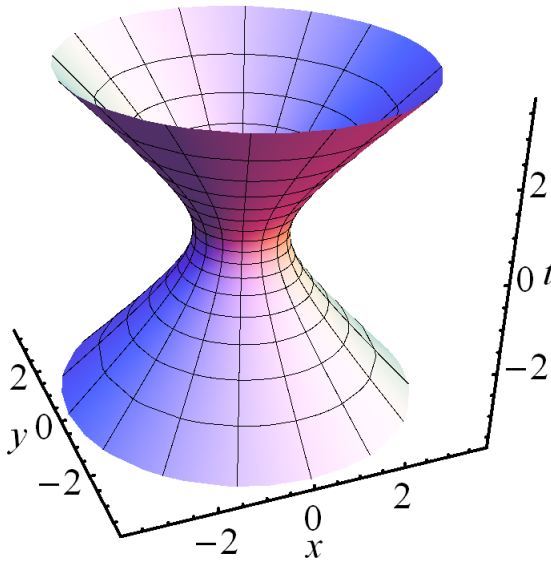
(a) De Sitter space, dS_2, as a hyperboloid in $\mathbb{R}_{1,2}$.
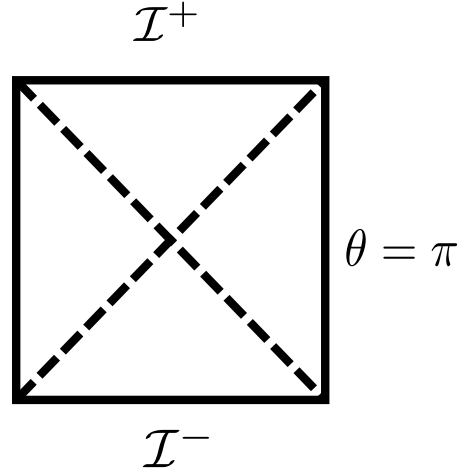
(b) Penrose diagram for de Sitter space. Dashed lines indicate the horizon for points at $\theta = 0, \theta = \pi$ respectively, and $\mathcal{I}^{\pm}$ represent past and future infinity.

This idea was explored in [101], where they showed that by considering tunnelling at the de Sitter temperature in a space with de Sitter curvature, one arrives at precisely the CdL prescription for computing tunnelling rates. In this context then, the CdL solution should be interpreted as states in the false vacuum being lifted from ϕ_{fv} to some higher value, ϕ_1, by thermal excitations, and then tunnelling through the barrier to emerge at ϕ_0. This explains why these solutions do not appear to touch the false vacuum.

Note that it is possible in many potentials to solve the bounce boundary conditions $\dot{\phi}(0) = \dot{\phi}(\chi_{\text{max}}) = 0$ in multiple ways, and some solutions may satisfy $\dot{\phi} = 0$ at points in the interval $(0, \chi_{\text{max}})$, in addition to the boundaries. For reasons to be discussed in section 3.3.4, we will reserve the term 'CdL solution' for those solutions that only satisfy $\dot{\phi} = 0$ at the boundaries and nowhere else. Solutions with one of more turning points in the interval $(0, \chi_{\text{max}})$ will be denotes 'oscillating solutions' and discussed in section 3.3.4.

3.3.3 Hawking-Moss Bounces

There is a simpler type of solution that can always exist, first discussed by [106] and called the Hawking-Moss solution. This consists of the field sitting as a constant at the top of the barrier, $\phi = \phi_{\text{bar}}$. The solution to Eq. (3.13) is thus:

$$a(\chi) = \frac{1}{H_{HM}} \sin(H_{HM}\chi), \tag{3.22}$$

where $H_{HM}^2 = \frac{V(\phi_{\text{bar}})}{3M_{\text{P}}^2}$ (note that this is different to $H^2 = \frac{V(\phi_{fv})}{3M_{\text{P}}^2}$). This solution has trivial action and thus decay exponent:

$$B = S[\phi_{HM}] - S[\phi_{\text{fv}}] = 24\pi^2 M_{\text{P}}^4 \left(\frac{1}{V(\phi_{\text{fv}})} - \frac{1}{V(\phi_{\text{bar}})} \right). \tag{3.23}$$

45

For special cases where $\Delta V(\phi_{\text{bar}}) = V(\phi_{\text{bar}}) - V(\phi_{\text{fv}}) \ll V(\phi_{\text{fv}})$, then this can be approximated as:

$$B \approx \frac{8\pi^2 \Delta V(\phi_{\text{bar}})}{3H^4} = \frac{4\pi}{3}\left(\frac{1}{H}\right)^3 \frac{\Delta V(\phi_{\text{bar}})}{T_{\text{GH}}}. \tag{3.24}$$

This can be interpreted as the ratio of the energy required to excite a Hubble volume (radius $1/H$) to the top of the barrier, to the temperature T_{GH}. Since the decay rate goes as $\Gamma \propto e^{-B}$, this implies a thermal interpretation of the Hawking-Moss solution. In the context of the thermal description of CdL bounces discussed in section 3.3.2, the Hawking-Moss solution is simply the case when the field is excited completely up to the top of the barrier, without tunnelling through (while CdL solutions describe partial excitation followed by tunnelling through the rest of the way). This gives these solutions an entirely thermal character.

3.3.4 Oscillating Bounces

As mentioned in section 3.3.2, it is possible to find solutions that satisfy $\dot{\phi}(0) = \dot{\phi}(\chi_{\text{max}}) = 0$ while having additional turning points in the interval $(0, \chi_{\text{max}})$. These solutions are called 'oscillating bounces' because they cross the barrier more than once.

Ostensibly, it seems as if such solutions, if they exist, should be included in any computation of the decay rate. However, this is not the case - these solutions have more than one negative eigenvalue in the space of fluctuations about them [126, 127, 110], and thus do not contribute to vacuum decay [101, 111]. This will be discussed in more detail in section 3.5.2.

3.4 Boundary Conditions

The boundary conditions for tunnelling in the presence of gravity require special attention. First we consider the gravitational field: since $a(\chi)$ describes the radius of curvature of a surface of constant χ, then necessarily $a(0) = 0$, since a surface at $\chi = 0$ is just a single point - the origin (in effect, this choice of boundary condition is just defining $\chi = 0$ to be the origin).

However, the $a = 0$ condition means that non-singular solutions must satisfy $\dot{\phi}(0) = 0$, for much the same reason that this is required in flat space. One more boundary condition is required for the scalar field in order to make the problem fully specified. There are, however, two possible behaviours:

1. If there exists some point χ_{max} such that $a(\chi_{\text{max}}) = 0$, then we will require $\dot{\phi}(\chi_{\text{max}}) = 0$. This will result in a *compact* solution, like figure 3.1, where χ_{max} represents the second pole.

2. Otherwise, the solution is non-compact, and in order to ensure finite $S[\phi, a] - S[\phi_{\text{fv}}, a_{\text{fv}}]$, the solution must satisfy $\phi(\chi \to \infty) \to \phi_{\text{fv}}$ so that the solution matches the false vacuum at infinity.

Which boundary condition applies depends on false vacuum solution. This is a constant solution, $\phi = \phi_{\text{fv}}$, which can only take place consistently at $V'(\phi_{\text{fv}}) = 0$. We will consider the three possible signs for the potential in the false vacuum in turn:

3.4.1 $V(\phi_{\mathrm{fv}}) > 0$

In this case, the solution to the gravitational equation is especially simple if $V(\phi_{\mathrm{fv}}) > 0$:

$$\ddot{a} = -\frac{V(\phi_{\mathrm{fv}})}{3M_{\mathrm{P}}^2} a \implies a(\chi) = \frac{1}{H_0}\sin(H_0\chi), \tag{3.25}$$

where $H_0 = \sqrt{V(\phi_{\mathrm{fv}})/3M_{\mathrm{P}}^2}$, and we solve the acceleration equation subject to $a(0) = 0$, and $\dot{a}(1) = 1$. This second boundary condition is required for consistency with Eq. (3.13), which is first order. Note that this solution is clearly compact, since $a(\pi/H_0) = 0$. The action of the false vacuum solution in this case is:

$$S_{\mathrm{fv}} = -\frac{24\pi^2 M_{\mathrm{P}}^4}{V(\phi_{\mathrm{fv}})}. \tag{3.26}$$

This means that any bounce solution that contributes to vacuum decay must be finite, otherwise the decay exponent will be infinite. In fact, we can prove a stronger statement: the bounce solution in this case must be *compact*.

Statement 1. *No non-trivial finite-action non-compact solution to the bounce equations of motion exists for simple tunnelling potentials if $V(\phi_{\mathrm{fv}}) > 0$.*

By simple tunnelling potential, we mean that the potential only has at most three stationary points, the false vacuum, ϕ_{fv}, the top of the barrier, ϕ_{bar}, and the true vacuum, ϕ_{tv}. Note that ϕ_{bar} and ϕ_{tv} could be absent from the potential, and this lemma will still apply (though there is no guarantee that any bounce solution necessarily exists if the potential has no barrier).

Proof. Assume that such a bounce solution *does* exists. In this case, the upper limit of the action integral is infinite since the solution is assumed to be non-compact:

$$S = -2\pi^2 \int_0^\infty \mathrm{d}\chi\, a(\chi)^3 V(\phi(\chi)). \tag{3.27}$$

Thus, for the action to be finite, we require that $a^3(\chi)V(\phi(\chi))$ vanishes faster than $\frac{1}{\chi}$ in the $\chi \to 0$ limit. Note that $a(\chi)$ cannot vanish asymptotically, or over any extended range of χ, since by Eq. (3.13), if $a = 0$ at some point, $\dot{a}^2 = 1$ there, and the solution will rapidly move away from $a = 0$. Also, non-compactness requires $a > 0$, since if there exists some finite point at which $a(\chi_{\mathrm{max}}) = 0$, then we have arrived precisely at a compact solution. Thus, we require $V(\phi(\chi)) \to 0$.

However, if ϕ asymptotically approaches some point ϕ_z such that $V(\phi_z) = 0$, then this point must also satisfy $V'(\phi_z) = 0$, otherwise the solution to Eq. (3.12) will not stay there for any extended period of χ.

It is here that the assumption that the potential is a simple tunnelling potential becomes important. For such potentials, there are at most three stationary points that ϕ could approach. However, since $V(\phi_{\mathrm{bar}}) > V(\phi_{\mathrm{fv}}) > 0$, the only point that could possibly be suitable is ϕ_{tv}. If $V(\phi_{\mathrm{tv}}) \neq 0$, then the proof is immediate - no suitable stationary point exists, so no finite action non-compact bounce solution exists.

There is, however, the possible loop-hole of $V(\phi_{\mathrm{tv}}) = 0$. This is not an unphysical loophole, however, since it would describe tunnelling from a de-Sitter space to a flat space, which is

potentially of physical interest. Thus, we consider this special case. Assume that a bounce solution exists that asymptotically approaches ϕ_{tv}. At this point, $\dot{\phi} \to 0$, $V(\phi) \to 0$, and so by Eq. (3.13), $\dot{a} \to \pm 1$. The $\dot{a} = -1$ case can be ruled out, since if $\dot{a} \to -1$, $\dot{a}$ is bounded above and negative, and we will necessarily encounter $a = 0$ at finite χ, resulting in a compact solution.

For the $\dot{a} = 1$ case, because $V(\phi_{\mathrm{tv}}) = 0$, then $V(\phi) > 0$ everywhere, since the true vacuum is the lowest point of the potential. Thus, by Eq. (3.14), $\ddot{a} \leq 0$, with equality only at $\dot{\phi} = 0, \phi = \phi_{\mathrm{fv}}$. Thus, with the exception of the true vacuum solution itself, which is a trivial solution, the bounce solution will have $\ddot{a} < 0$ somewhere, and thus $\exists \chi$ such that $\dot{a}(\chi) < 1$. But since $\ddot{a} \leq 0$, $\dot{a}$ is monotonically decreasing, which contradicts the fact that $\dot{a} \to 1$, which requires $\dot{a}$ to increase. This is a contradiction, so the bounce solution in question cannot exist.   □

Since we have just ruled out the non-compact case, we know that the bounce solution for $V(\phi_{\mathrm{fv}}) > 0$ must be compact, that is, there exists finite $\chi_{\max} > 0$ such that $a(\chi_{\max}) = 0$. Necessarily, therefore, we must impose the $\dot{\phi}(\chi_{\max}) = 0$ boundary condition.

3.4.2 $V(\phi_{\mathrm{fv}}) = 0$

In this case, the false vacuum is flat and the false vacuum solution is $\phi(\chi) = \phi_{\mathrm{fv}}, a_{\mathrm{fv}}(\chi) = \chi$, but since $V(\phi_{\mathrm{fv}}) = 0$ everywhere, $S_{\mathrm{fv}} = 0$. Lemma 1 does not apply in this case, and so non-compact solutions terminating at ϕ_{fv} are allowed. Indeed they are expected, since they would correspond to the flat space case with back-reaction corrections. It is also easy to argue that there can only be one such non-compact solution. To see this, we first we establish that non-compact solutions have $\dot{a} > 0$ throughout:

Statement 2. *A non-compact bounce solution satisfies $\dot{a} \geq 1$ everywhere, and $\dot{a}$ approaches 1 from above.*

Proof. First note that $\dot{a}(0) = 1$, so $\dot{a}$ starts out positive. In order to cross to $\dot{a} < 1$, Eq. (3.13) implies that we need $V(\phi) > 0$, that is, we must be in the positive region of the potential. Since the bounce solution is monotonic[3], then after ϕ has entered the positive region of the potential, it will stay there for all subsequent χ. However, if we are in the positive region, then Eq. (3.14) implies:

$$\ddot{a} = -\frac{a}{3M_{\mathrm{P}}^2}(\dot{\phi}^2 + V(\phi)) < 0, \tag{3.28}$$

which is to say, $\dot{a}$ can only decrease. Now, if the solution approaches the false vacuum at $\chi \to \infty$, both $\dot{\phi} \to 0$ and $V(\phi) \to 0$, and thus by Eq. (3.13), $\dot{a} \to \pm 1$. But if $\dot{a} < 1$ in the positive potential region, then it is bounded above by 1 and monotonically decreasing. Consequently, it will never approach 1. It also cannot approach $\dot{a} = -1$ asymptotically, since $\dot{a} < 0$ implies that a is decreasing, and we know the gradient is bounded above by a negative value: this means it will cross zero, resulting in a singularity (or a compact solution) at finite χ. Since this is incompatible with a non-compact solution, we know that it must never cross zero, so we require $\dot{a} \to +1^+$ as $\chi \to \infty$. We thus conclude that $\dot{a}$ is never less than 1 anywhere and approaches 1 from above.   □.

It is also possible to argue that such a solution must exist, although this will require a discussion of the non-instanton, divergent solutions which we leave to section 3.4.4. With this in mind, it is reasonable to ask if any compact solutions exist for $V(\phi_{\mathrm{fv}}) = 0$. If they do, then

---

[3]Non-monotonic solutions cannot contribute to vacuum decay - see section 3.9

they present a potential problem: the false vacuum action in the $V(\phi_\text{fv}) > 0$ case diverges in the $V(\phi_\text{fv}) \to 0$ limit (see Eq. (3.26)), which opens up the possibility that solutions which exist for $V(\phi_\text{fv}) > 0$ might be discontinuous across the $V(\phi_\text{fv}) \to 0$ transition. Two things might happen to such solutions in this limit:

1. A solution which exists for $V(\phi_\text{fv}) > 0$ might change so that $\phi \to \phi_\text{fv}$ as $V(\phi_\text{fv}) \to 0$, that is, it becomes non-compact. In this case, the action of the solution will diverge in such a way that it cancels the divergence in Eq. (3.26), and the decay exponent will smoothly transition to some flat-false-vacuum, finite value.

2. A solution might not approach ϕ_fv smoothly, in which case, the decay exponent diverges when $V(\phi_\text{fv}) \to 0+$, but at $V(\phi_\text{fv}) = 0$, it appears to exist, with (possibly) finite decay exponent since $S_\text{fv} = 0$.

However, the second case presents a problem: if such a solution exists in the $V(\phi_\text{fv}) \to 0$ limit, then we have a discontinuity across the $V(\phi_\text{fv}) = 0$ point. One could eliminate this by arguing that such solutions do not exist, but at present, there does not appear to be any way of ruling them out.

We conclude, therefore, that the boundary condition of interest is:

1. $\phi(\chi \to \infty) \to \phi_\text{fv}$ for the non-compact solution, analogous to the flat space case.

2. If compact solutions are expected, they will satisfy $\dot{(\phi)}(0) = \dot{\phi}(\chi_\text{max}) = 0$ for some finite χ_max, just as in the $V(\phi_\text{fv}) > 0$ case.

3.4.3 $V(\phi_\text{fv}) < 0$

This scenario is of less physical interest, because it would correspond to an anti-de-Sitter false vacuum, which would be unstable to perturbations [97, 65], and would rapidly lead to gravitational collapse to a singularity. Furthermore, the cosmological constant of the present vacuum is observed to be positive. The false vacuum solution to Eq. (3.13) in this case is:

$$a(\chi) = \frac{1}{H_0} \sinh(H_0\chi), \tag{3.29}$$

where in this case, $H_0^2 = |V(\phi_\text{fv})|/3M_\text{P}^2$. The action integral Eq. (3.27) is then obviously divergent. This immediately rules out any compact solutions, as they will have finite action, and thus divergent decay exponent. Non-compact solutions are possible, however, because the late time behaviour as $\phi \to \phi_\text{fv}$ is $a \to \frac{1}{H_0} \sinh(H_0\chi)$. This has the effect of possibly cancelling out the divergent false vacuum action, giving a finite decay exponent, if such solution exist. Eitherway, the relevant boundary condition is $\phi(\chi \to \infty) \to \phi_\text{fv}$.

3.4.4   The Overshoot/Undershoot Method in Curved Space

The boundary conditions considered here lead us to a two-point boundary value problem to solve for the bounce configuration. To actually find bounce solutions, one can use the overshoot/undershoot method. In flat space, this is motivated by the observation, due to Coleman [98], that there are two types of non-instanton solutions that start at some $\phi(0) = \phi_0$ with $\dot{\phi}(0) = 0$: those that overshoot the false vacuum as $\chi \to \infty$, and those that come to rest before

reaching it, fall back and oscillate. These were illustrated in figure 2.1.

In curved space, this discussion has to be modified somewhat. The main complication is that the 'friction' term, $\dot{a}/a$, can now be negative for compact solutions. Originally, it was argued in flat space [97], that solutions starting close to the top of the barrier are necessarily undershoots because they lack the energy to reach the false vacuum, and can only lose it since the friction term is always positive. In curved space this no-longer holds, because 'anti-friction ' when $\dot{a} < 0$ can add energy to the system:

$$\frac{\mathrm{d}}{\mathrm{d}\chi}\left(\frac{\dot{\phi}^2}{2} - V(\phi)\right) = -\frac{3\dot{a}}{a}\dot{\phi}^2. \tag{3.30}$$

To deal with this, Balek and Demetrian [109] discuss a modified notion of overshoot and undershoot solutions, which we will use here. First, we categorise non-instanton solutions by the number of nodes they possess in their derivative, $\dot{\phi}$. Then:

1. Undershoot solutions are those for which there is at least one node.

2. Overshoot solutions have zero nodes.

Balek and Demetrian argue that between an L-node solution and an $(L+1)$-node solution, continuity demands that a bounce solution which crosses the barrier L times. This is because such solutions always diverge, but depend continuously on the initial value, $\phi(0) = \phi_0$. ϕ diverges to positive or negative infinity according to the number of nodes (whether it diverges to $\pm\infty$ depends on which side of the barrier it starts, and how the potential is arranged). Thus, in order for a change in ϕ_0 to change the number of nodes in the derivative, the divergent part of the solution must pass from $+\infty \to -\infty$ or vice-versa. As it does so, a node appears at the singularity $a(\chi_{\max}) = 0$ for some ϕ_0, and this corresponds to a solution of the boundary value problem which crosses the barrier L times.

It is believed, however, that solutions crossing the barrier more than once - so called 'oscillating bounces', do not contribute to vacuum decay. This is because the spectrum of fluctuations about such solutions contains more than one negative eigenvalue [126, 127, 110]. Solutions with more than one negative eigenvalue are known not to contribute to vacuum decay, because despite being stationary points of the Euclidean action, they are *not* stationary points of the barrier penetration integral [111]. Note that the argument of [111] does not directly apply in the case of curved space, but it can be modified to do so [101]. Thus, if we are only interested in monotonic bounce solutions that cross the barrier once, then undershoots are those with 1 node, and overshoots with 0 nodes (not counting $\chi = 0$). The argument of [109] then implies that between any undershoot and overshoot, there *must* lie a bounce solution. This will become crucial when we discuss the extra bounce solutions that arise in the Standard Model.

In flat space, the existence of a bounce solution is established by arguing that solutions sufficiently close to the barrier lead to undershoots (because they have insufficient energy to reach the false vacuum), and that solutions starting sufficiently close to the true vacuum stay there for long enough that the friction falls to zero and they eventually overshoot. In curved space this argument must be modified.

The analogous argument in curved space is as follows, which we have also made in [2].

Statement 3. *Solutions starting infinitesimally close to the false vacuum are always overshoot solutions.*

Proof. Consider first a solution starting infinitesimally close to the false vacuum (or the true vacuum - the argument is essentially identical). It satisfies the linearised equation:

$$\Delta\ddot{\phi} + 3H\cot(H\chi)\Delta\dot{\phi} - V''(\phi_{\rm fv})\Delta\phi = 0, \tag{3.31}$$

where $H^2 = \frac{V(\phi_{\rm fv})}{3M_{\rm P}^2}$. The solution to this can be expressed in closed form with the Hypergeometric function:

$$\Delta\phi(\chi) = \Delta\phi_0 \, {}_2F_1\left(\frac{3}{2}+\alpha, \frac{3}{2}-\alpha, 2, \sin^2(\frac{H\chi}{2})\right), \tag{3.32}$$

where:

$$\alpha = \sqrt{\frac{9}{4} - \frac{V''(\phi_{\rm fv})}{H^2}}. \tag{3.33}$$

The question becomes, what happens to this solution in the limit as χ approaches the $a = 0$ singularity, since this will determine whether the solution is an overshoot or an undershoot. In this case, it can be deduced from the Hypergeometric function transformation formula [128]:

$$ {}_2F_1(a, b, c, z) = (1-z)^{c-a-b} \, {}_2F_1(c-a, c-b, c, z), \tag{3.34}$$

that the asymptotic behaviour of $\Delta\phi$ in the limit $\chi \to \frac{\pi}{H}$ is:

$$\Delta\phi(\chi) \approx \frac{\Delta\phi_0 \, {}_2F_1(\frac{1}{2}-\alpha, \frac{1}{2}+\alpha, 2, \sin(\frac{H\chi}{2}))}{\cos^2(\frac{H\chi}{2})}. \tag{3.35}$$

Using the identity [128]:

$$ {}_2F_1(a, b, c, 1) \equiv \frac{\Gamma(c)\Gamma(c-a-b)}{\Gamma(c-a)\Gamma(c-b)}, \tag{3.36}$$

we find:

$$
\begin{aligned}
{}_2F_1\left(\frac{1}{2}-\alpha, \frac{1}{2}+\alpha, 2, 1\right) &= \frac{1}{\Gamma\left(\frac{3}{2}+\alpha\right)\Gamma\left(\frac{3}{2}-\alpha\right)} \\
&= \frac{1}{(\frac{1}{4}-\alpha^2)\Gamma\left(\frac{1}{2}-\alpha\right)\Gamma\left(1-[\frac{1}{2}-\alpha]\right)} \\
&= -\frac{\cos(\pi\alpha)}{\left(2 - \frac{V''(\phi_{\rm fv})}{H^2}\right)\pi},
\end{aligned} \tag{3.37}
$$

where in the second line we have used the gamma function reflection identity, $\Gamma(z)\Gamma(1-z) = \frac{\pi}{\sin(\pi z)}$, and $\sin\left(\frac{\pi}{2} - \alpha\pi\right) = \cos(\alpha\pi)$. Consequently:

$$\Delta\phi(\chi) \sim \frac{-4\Delta\phi_0 \cos\left(\pi\sqrt{\frac{9}{4} - \frac{V''(\phi_{\rm fv})}{H^2}}\right)}{\left(2 - \frac{V''(\phi_{\rm fv})}{H^2}\right)\pi(H\chi - \pi)^2}. \tag{3.38}$$

Now, writing the Hypergeometric differential equation as:

$$z(1-z)\frac{{\rm d}^2y}{{\rm d}z^2} + (2-4z)\frac{{\rm d}y}{{\rm d}z} - \left(\frac{9}{4}-\alpha^2\right)y = 0, \tag{3.39}$$

51

we can demonstrate that the solution diverges as $z \to 1$ without encountering any turning points. Consider what happens at a turning point of the solution $\frac{\mathrm{d}y}{\mathrm{d}z} = 0$:

$$\frac{\mathrm{d}^2 y}{\mathrm{d}z^2} = \frac{\frac{9}{4} - \alpha^2}{z(1-z)} y. \tag{3.40}$$

Since $\frac{9}{4} - \alpha^2 = \frac{V''(\phi_{\mathrm{fv}})}{H^2} > 0$, then the character of the turning point is determined solely by the sign of y: if $y > 0$, it is a minimum, and if $y < 0$ it is a maximum. For sufficiently small z, the expansion of the hypergeometric function shows that:

$$\lim_{z \to 0^+} \frac{\mathrm{d}\,_2F_1(3/2 + \alpha, 3/2 - \alpha, 2, z)}{\mathrm{d}z} = \frac{\left(\frac{9}{4} - \alpha^2\right)}{2}, \tag{3.41}$$

since $\alpha^2 < \frac{9}{4}$ the derivative is initially positive. If we encounter a stationary point at some $0 < z_s < 1$, this means that for $z < z_s$ there exists points with negative derivative. By continuity, therefore, there must exist a maximum for some $z < z_s$, which contradicts Eq. (3.40). Thus, no stationary points can be encountered, the the solution must diverge to positive infinity without encountering a stationary point. This means $\Delta\phi(\chi)$ is an overshoot.

For completeness, we can conclude that the solution definitely diverges because the coefficient of $1/(1-z)$ in the $z \to 1^-$ limit is:

$$y(z \to 1^-) \sim \frac{\cos(\pi\alpha)}{\left(\frac{1}{4} - \alpha^2\right)\pi(1-z)}. \tag{3.42}$$

Since $V''(\phi_{\mathrm{fv}}) > 0$, then $\alpha^2 < \frac{9}{4}$. For $0 \le \alpha^2 < \frac{9}{4}$, this coefficient is always positive (the only possible exception is $\alpha^2 = \frac{1}{4}$, for which $\cos(\pi\alpha) = 0$, but since $\left(\frac{1}{4} - \alpha^2\right)$ appears in the denominator, L'Hopital's rule implies that the coefficient approaches 1 there). For $\alpha^2 < 0$, $\cos(\alpha\pi) = \cosh(|\alpha|\pi) > 0$, and so the coefficient is also positive, and never zero.

The only possible exception to this is if $\alpha = \frac{9}{4}$, or in other words, if the false vacuum is massless, $V''(\phi_{\mathrm{fv}}) = 0$ (a quartic potential is an example of how this might occur in practice). In this case, the linearisation breaks down since there is no quadratic term, but one can consider linearising about some small ϕ_1 close to ϕ_{fv}. If the potential has a barrier, then there must be some point ϕ_0 sufficiently close to ϕ_{fv} for which $V'(\phi_0) > 0$, and consequently there exists some point ϕ_1 between $(\phi_{\mathrm{fv}}, \phi_0)$ for which $V''(\phi_1) > 0$, by the mean value theorem. One can then linearise about this point, with a shift $\Delta\phi = \phi - \phi_1 = -\frac{V'(\phi_1)}{V''(\phi_1)} + y$, for which y satisfies Eq. (3.39) (replacing $V''(\phi_{\mathrm{fv}})$ with $V''(\phi_1)$ in the definition of α). The results above then apply to y, which therefore also diverges as an overshoot. $\qquad\square$

Statement 4. *Solutions starting infinitesimally close to the barrier are undershoots if*

$$\frac{V(\phi_{\mathrm{bar}})}{3M_{\mathrm{P}}^2} + \frac{V''(\phi_{\mathrm{bar}})}{4} < 0, \tag{3.43}$$

and overshoots otherwise.

Proof. This proceeds much as in lemma 3, but replacing $V''(\phi_{\mathrm{fv}}) \to V''(\phi_{\mathrm{bar}})$, so that α is defined by:

$$\alpha = \sqrt{\frac{9}{4} - \frac{V''(\phi_{\mathrm{bar}})}{H_{\mathrm{bar}}^2}}, \tag{3.44}$$

and the linearised equation of motion is:

$$\Delta\ddot{\phi} + 3H_{\text{bar}}\cot(H_{\text{bar}}\chi)\Delta\dot{\phi} - V''(\phi_{\text{bar}})\Delta\phi = 0, \tag{3.45}$$

where $H_{\text{bar}}^2 = \frac{V(\phi_{\text{bar}})}{3M_{\text{P}}^2}$. The asymptotic solution is:

$$\Delta\phi(\chi) = \Delta\phi_0 \, {}_2F_1\left(\frac{3}{2}+\alpha, \frac{3}{2}-\alpha, 2, \sin^2\left(\frac{H_{\text{bar}}\chi}{2}\right)\right). \tag{3.46}$$

This time, since $V''(\phi_{\text{bar}}) < 0$ for the top of the barrier generically, we must have $\alpha^2 > \frac{9}{4}$. The asymptotic form of the hypergeometric solution is Eq. (3.42) as $z \to 1^-$. The denominator is obviously negative.

On the range $\frac{9}{4} < \alpha^2 < \frac{25}{4}$, $\cos(\phi\alpha)$ is positive, and this implies that $y \to -\infty$. By Eq. (3.41), the initial derivative is positive, and since the initial value is $y = 1$, this must cross zero somewhere by the intermediate value theorem. On the region where $y > 0$, there can be no stationary points, since by Eq. (3.40), these must be maxima, which is impossible if y is initially decreasing. But for the $y < 0$ region, only minima are allowed. If a stationary point existed here, the solution would diverge to $+\infty$ unless it re-crosses zero and encounters a maximum. This cannot happen, however, as a direct corollary of the Sturm Comparison Theorem. To see this, transform Eq. (3.45) with $x = H_{\text{bar}}\chi$ and $\Delta\phi(\chi) = u(x)v(x)$ with:

$$v(x) = \exp\left(-\frac{3}{2}\int_\epsilon^x \cot(t)\mathrm{d}t\right). \tag{3.47}$$

The ϵ lower limit here is to deal with the fact that this is a singular Sturm-Liouville equation - it poses no problem as we can propagate forward the boundary conditions to some small value ϵ. Under this transformation, the equation becomes:

$$u'' + \left[\alpha^2 - \frac{15}{4} - \frac{3}{4}\cot^2(x)\right]u = 0. \tag{3.48}$$

We can now apply the Sturm Comparison Theorem to the equation in this form. We know that there is a solution with $\alpha^2 = \frac{25}{4}$ which has a single zero. The Sturm Comparison theorem states that if $u_1'' + r_1(x)u_1 = 0$ and $u_2'' + r_2(x)u_2 = 0$, and $r_1(x) \geq r_2(x)$ for all x in the interval (a,b) on which both Sturm-Liouville problems are defined, then there must be at least one zero of u_1 between every consecutive pair of zeros of u_2. If we assume that there is more than one zero for $\alpha^2 < \frac{25}{4}$, then we end up with a contradiction, because $r_{\alpha^2}(x) = \alpha^2 - \frac{15}{4} - \frac{3}{4}\cot^2(x) \leq r_{\frac{25}{4}}$, which implies the $\alpha^2 = \frac{25}{4}$ solution has multiple zeros, contradicting the Sturm-Liouville theorem. Consequently, such zeros cannot exist. More generally, this just means that if a Sturm-Liouville equation has eigenvalues λ_n, then the singular solutions with $\lambda < \lambda_n$ cannot have more zeros than the non-singular eigen-solution with eigenvalue λ_n. Intuitively, this means that zeros can only arise when λ passes through an eigenvalue, and the sign of the divergence changes.

This proves that for $\frac{9}{4} < \alpha^2 < \frac{25}{4}$, the solution is monotonically decreasing and diverges to $-\infty$, as possessing stationary points would require in multiple zeros, contradicting the Sturm-Comparison theorem. Consider now the case $\alpha^2 > \frac{25}{4}$. Re-applying the Sturm-Comparison theorem, we conclude that this solution must have at least two zeros, and consequently has a stationary point. Thus, it is an undershoot. We conclude therefore that $\alpha^2 > \frac{25}{4}$ leads to

undershoots, and $\alpha^2 < \frac{25}{4}$ leads to overshoots. In terms of the potential, the condition for undershoots can be expressed as:

$$\frac{V(\phi_{\text{bar}})}{3M_{\text{P}}^2} + \frac{V''(\phi_{\text{bar}})}{4} < 0, \tag{3.49}$$

and the > 0 case implies overshoots. $\qquad\qquad\qquad\qquad\qquad\qquad\qquad\qquad\qquad$ $\square$

The message of lemma 4 is that is the condition Eq. (3.49) is satisfied, then solutions with $\phi(0) = \phi_0$ sufficiently close to the barrier are undershoots, and solutions with ϕ_0 sufficiently close to the false vacuum are overshoots. Thus, by continuity, there must lie some $\phi_0 \in (\phi_{\text{fv}}, \phi_{\text{bar}})$ such that the solution satisfies the bounce boundary conditions. This proves that a CdL solution exists.

The interesting question is what happens when this criteria is *not* satisfied:

$$\frac{V(\phi_{\text{bar}})}{3M_{\text{P}}^2} + \frac{V''(\phi_{\text{bar}})}{4} > 0. \tag{3.50}$$

In this case, both ϕ_0 close to ϕ_{bar} and to ϕ_{fv} lead to overshoots, and thus we cannot conclude that a CdL solution necessarily exists. Balek and Demetrian showed ([109]) that a necessary condition for the existence of such a solution is that there exists ϕ somewhere on the interval $(\phi_{\text{fv}}), \phi_{\text{tv}})$ such that:

$$\frac{V(\phi)}{3M_{\text{P}}^2} + \frac{V''(\phi)}{4} < 0, \tag{3.51}$$

however, this does not guarantee their existence: it can only rule them out if it fails to be satisfied.

3.5 Eigen-spectrum of Gravitational Bounces

It was discussed in section 2 that a bounce solution can contribute to vacuum decay if and only if it has a single negative eigenvalue in the spectrum of fluctuations about it. This is crucial: if there are no negative eigenvalues, then the bounce provides no imaginary contribution to the energy, and hence does not contribute to vacuum decay. If there is more than one negative eigenvalue, then the bounce, while a stationary point of the Euclidean action, is *not* an stationary point of the barrier penetration integral [111]. Here we will consider the eigen-spectrum of compact bounces, which are the bounces relevant in de Sitter tunnelling.

3.5.1 Negative Eigenvalues in Flat Space

This was first derived in [99]. Because the bounces are $O(4)$ symmetric, it is possible to decompose the fluctuation equation:

$$-\nabla^2 y + V''(\phi_B(\chi))y = \lambda y, \tag{3.52}$$

into 3-sphere spherical harmonics and associated radial functions: $y = R(\chi)\Phi(\theta, \varphi, \psi)$. Applying standard techniques, the spherical harmonics satisfy [129]:

$$-\tilde{\nabla}^2\Phi = -l(l+2)\Phi, \tag{3.53}$$

54

with degeneracy $D_l(3,0) = (l+1)^2$, $l = 0, 1, 2 \ldots$. If there is to be at most one negative eigenvalue, therefore, it must be in the $l = 0$ sector, since eigenvalues with $l \geq 1$ are degenerate. The radial equation is:

$$\frac{\mathrm{d}}{\mathrm{d}\chi}\left(\chi^3 \frac{\mathrm{d}R_l}{\mathrm{d}\chi}\right) + \chi^3 \left[\lambda - V''(\phi_B(\chi)) - \frac{l(l+2)}{\chi^2}\right] R_l = 0. \tag{3.54}$$

This equation is of Sturm-Liouville form, so has distinct ordered eigenvalues $\lambda_1 < \lambda_2 < \ldots$, and λ_{nl} is associated to an eigenfunction with exactly $n-1$ nodes on the interval $(0, \infty)$. To proceed, we need to make use of the Sturm-Picone Comparison theorem [130]:

Theorem 1 (Sturm-Picone Comparison Theorem). *For non-trivial solutions u_1, u_2 of the equations:*

$$\ddot{u}_1 + p_1(x)u_1 = 0, \tag{3.55}$$
$$\ddot{u}_2 + p_2(x)u_2 = 0, \tag{3.56}$$

with $p_2(x) \geq p_1(x) \forall x \in [a, b]$, then if $p_1 \neq p_2$, $\forall x_1, x_2 \in [a, b]$ such that $p_1(x_1) = p_1(x_2) = 0$, $\exists x \in (x_1, x_2)$ such that $p_2(x) = 0$. If $p_1 = p_2$ then $u_1 \propto u_2$.

Essentially, this theorem states that if $p_2(x) \geq p_1(x)$ everywhere, then between every pair of zeros of u_1, there must lie a zero of u_2. This theorem is essential in deriving key properties of Sturm-Liouville equations. To apply it here, we need to simplify the radial equation, Eq. (3.54), with the substitution $R_l = \left(\frac{\varepsilon}{\chi}\right)^{\frac{3}{2}} u(\chi)$, which yields:

$$\ddot{u} + \left[\lambda - V''(\phi_B(\chi)) - \frac{\{l(l+2) + \frac{3}{4}\}}{\chi^2}\right] u = 0. \tag{3.57}$$

Now consider solutions of the radial equation, with boundary conditions $R_l(0) = R_l(\infty) = 0$. As usual, only discrete λ will satisfy the $R_l(\infty) = 0$ equation - these are the eigenvalues, $\lambda_1, \lambda_2, \ldots$ and the rest diverge as $\chi \to \infty$. Although we might worry about the singular nature of $p(x)$ in Eq. (3.57), this is not a problem as the proof of the Sturm-Picone Comparison theorem only requires that the Wronskian of the two solutions and it's derivative is finite everywhere on the interval under consideration. Because of the choice of boundary condition $R_l(0) = 0$, this only fails to be true for non-eigen solutions at $\chi \to \infty$. We write $u^\lambda(\chi)$ as the solution with eigenvalue λ, and:

$$p^\lambda(\chi) = \lambda - V''(\phi_B(\chi)) - \frac{\{l(l+2) + \frac{3}{4}\}}{\chi^2}. \tag{3.58}$$

Then if u^{λ_1} has no zeros on the interval $(0, \infty)$, it follows that for all $\lambda < \lambda_1$, $u^\lambda(\chi)$ is positive for all $\chi > 0$ (since if it had a zero at χ_0, $p^{\lambda_1} > p^\lambda$ so the Sturm-Picone Comparison theorem would imply that u^{λ_1} has a zero on the interval $(0, \chi_0)$, which is a contradiction), so diverges to positive infinity if at all. While for $\lambda > \lambda_1$, u^λ must have at least one zero, since $p^\lambda > p^{\lambda_1}$, but u^{λ_1} has zeros at 0 and ∞, so u^λ must have one in between these. Repeating this reasoning as we increase λ ultimately leads to the familiar Sturm-Lioville result that the eigenvalues are ordered. $\lambda_1 < \lambda_2 < \ldots$, and that λ_n has $n-1$ zeros, since all $\lambda < \lambda_1$ have no zeros, all $\lambda_1 < \lambda < \lambda_2$ have one zero, etc.... We can now prove the following:

Statement 5. *There are no negative eigenvalues of $l \geq 1$.*

Proof. We denote the n-th eigenvalue with angular momentum number l as λ_{nl}, and by the Sturm-Liouville theorem, $\lambda_{1l} < \lambda_{2l} < \lambda_{3l} < \ldots$, but there is no necessary ordering between eigenvalues with different l, since these correspond to different Sturm-Liouville equations. First note that there is a zero eigenvalue with $l = 1$, namely $R_1 = \dot{\phi}_B$, which is easily verified to satisfy:

$$\frac{1}{\chi^4}\frac{\mathrm{d}}{\mathrm{d}\chi}\left(\chi^3\frac{\mathrm{d}\dot{\phi}_B}{\mathrm{d}\chi}\right) - V''(\phi_B)\dot{\phi}_B - \frac{3}{\chi^2}\dot{\phi}_B. \tag{3.59}$$

This is the same as Eq. (3.54) with $l = 1$ and $\lambda = 0$, indicating that this fluctuation corresponds to a zero eigenvalue with degeneracy 4. This is not surprising - it corresponds to translations of the centre of the bounce about the space-time and is accounted for in the derivation by Callan and Coleman [99]. Now, note that this fluctuation does not have *any* nodes, since $\dot{\phi}_B = 0$ only at $\chi = 0, \infty$. Hence, it is the lowest eigen-solution for $l = 1$, and all other eigenvalues λ_{n1} are higher, so there cannot be any negative eigenvalues for $l = 1$.

Now consider fixed λ, but change l. The form of the radial equation for the Sturm-Picone comparison theorem is:

$$u_l'' + \left[\lambda - V''(\phi_B(\chi)) - \frac{\{l(l+2) + \frac{3}{4}\}}{\chi^2}\right]u_l = 0, \tag{3.60}$$

$$u_{l'}'' + \left[\lambda - V''(\phi_B(\chi)) - \frac{\{l'(l'+2) + \frac{3}{4}\}}{\chi^2}\right]u_{l'} = 0. \tag{3.61}$$

Consequently, if $l' > l$, then $p_{l'} < p_l$, and thus between every pair of zeros of $u_{l'}$ there must lie a zero of u_l. Now assume that for some $l' > 1$, there is a negative eigenvalue. This means that the $\lambda = 0$ solution (which generically diverges) must have a zero at some finite $\chi = \chi_0$ (since if $\lambda_{0l'}$ corresponds to a node-less eigenfunction, all $\lambda > \lambda_{0l'}$ lead to solutions with at least one zero). However, since it also has a zero for $\chi = 0$, then the Sturm-Picone comparison theorem implies that u_1 for $\lambda = 0$ must have a zero on the interval $(0, \chi_0)$. This is not the case, and so by contradiction we are forced to conclude that no such negative eigenvalue can exist. $\qquad\square$

As for whether there are negative eigenvalues in the $l = 0$ sector, this is less clear. At the very least, lemma 5 implies that they can *only* exist here. In the case of thin wall bubbles, it can be shown that there is only one negative eigenvalue [99, 131]. If bounces do exist with more than one, however, then they can be shown not to contribute significantly to tunnelling, because a linear combination of fluctuations with different negative eigenvalues can be chosen that both lowers the action, and also corresponds to a possible tunnelling path through the barrier. Note that the main reason that a single negative eigenvalue does not allow one to lower the action is that fluctuations about the bounce do not necessarily map into fluctuations that correspond to tunnelling paths through the barrier. This is because they generically move the end-point of the barrier penetration path away from the other side of the barrier (specifically the 'escape surface', that is, the points on the far side of the barrier at which the field can emerge within the constraint of energy conservation); adding a second negative eigenvalue fluctuation direction allows one to construct a linear sum of fluctuations which still decreases the action, but with the correct end-point (sitting on the escape surface) to describe a possible tunnelling path, meaning that such solutions with more than one negative eigenvalue always correspond to saddle points of the action [111], while those with a single negative eigenvalue do not.

3.5.2 Negative Eigenvalues of Compact Bounces in Curved Space

The situation in curved space is considerably more complicated, due to the presence of metric fluctuations in the spectrum of fluctuations about a given bounce. This is more difficult than the scalar case, not only due to the increased number of degrees of freedom, but the gauge symmetry inherent when dealing with a metric.

Several authors have considered the problem of fluctuations around an $O(4)$ symmetric bounce solution [131, 132, 126]. One way to approach this is to decompose the fluctuations into 3-sphere spherical harmonics, $Y_l(\theta, \varphi, \psi)$, related to the three angular variables, θ, φ, ψ (note that we are suppressing the other angular momentum quantum numbers here, since the radial parts of the fluctuations which were are most interested in do not depend on them; formally we should write $Y_{lm_1m_2}(\theta, \varphi, \psi)$ however). This exploits the residual $O(3)$ symmetry around a nucleated bounce, and gives [131]:

$$
\begin{aligned}
\mathrm{d}s^2 =& [1 + 2A_l(\chi)Y_l(\theta, \varphi, \psi)]\mathrm{d}\chi^2 + B_l(\chi)\nabla_a Y_l(\theta, \varphi, \psi)\mathrm{d}\chi\mathrm{d}z^a \\
&+ a^2(\chi)\left[\tilde{g}_{ab}\{1 + 2\Psi_l(\chi)Y_l(\theta, \varphi, \psi)\} + \frac{2C_l(\chi)}{l(l+2)}\left(\nabla_a\nabla_b + \frac{l(l+2)}{3}\tilde{g}_{ab}Y_l(\theta, \varphi, \psi)\right)\right]\mathrm{d}z^a\mathrm{d}z^b,
\end{aligned}
\tag{3.62}
$$

where A_l, B_l, C_l, Ψ_l are the radial metric fluctuations, which depend on l, χ is as usual the radial parameter, and z^a represent the angular co-ordinates. Note that there is a gauge symmetry here [131]: $\chi \to \chi + \alpha_l(\chi)Y_l(\theta, \varphi, \psi)$, $z_a \to z_a + \beta_l(\chi)\partial_a Y_l(\theta, \varphi, \psi)$, and this can be used to remove two of the fluctuations (for example A_l and B_l), leaving only two remaining, as expected for a massless graviton. Together with the scalar field fluctuation, $\phi \to \phi + \Phi_l Y_l(\theta, \varphi, \psi)$, and the gauge invariant combination $\zeta_l = \dot{a}\Phi_l - a\dot{\phi}\Psi_l - a\dot{\phi}\frac{C_l}{3}$, this gives a quadratic Lagrangian for fluctuations [131]:

$$
\mathcal{L}^{(2)}(\zeta_l, \dot{\zeta}_l) = \frac{a^3(\chi)\left(1 - \frac{l(l+2)}{3}\right)}{2\left(Q - \frac{\dot{a}^2 l(l+2)}{3}\right)}\left[\dot{\zeta}_l^2(\chi) + f(a, \phi)\zeta_l^2(\chi)\right],
\tag{3.63}
$$

where:

$$
Q = 1 - \frac{a^2(\chi)V(\phi)}{3M_\mathrm{P}^2},
\tag{3.64}
$$

$$
\begin{aligned}
f(a, \phi) =& V''(\phi) + \frac{l(l+2)}{a^2} \\
&+ \frac{1}{3M_\mathrm{P}^2\left(Q - \frac{\dot{a}^2 l(l+2)}{3}\right)}\left[a\dot{\phi}V'(\phi) + a^2\dot{a}V'(\phi)^2 - l(l+2)\left(2a\dot{a}^2\dot{\phi}V'(\phi) - 3\dot{a}\dot{\phi}^2 Q + \dot{a}\dot{\phi}^2\right)\right] \\
&+ \frac{1}{3M_\mathrm{P}^2}\left[2\dot{\phi}^2 - 3\frac{a\dot{\phi}V'(\phi)}{\dot{a}} - 4V(\phi)\right] - \frac{\ddot{a}}{a}\left(\frac{\dot{Q} - \frac{2\dot{a}\ddot{a}l(l+2)}{3}}{Q - \frac{\dot{a}^2 l(l+2)}{3}}\right).
\end{aligned}
\tag{3.65}
$$

From this expression, in principle, one can derive the eigenvalues for fluctuations about an $O(4)$ symmetric gravitational bounce. This was done, for example, by [131], who found the interesting result that CdL bounces *always* have more than one negative eigenvalue in the metric fluctuation sector. This can be seen by noting that CdL bounces always have a value χ_peak for which $\dot{a}(\chi_\mathrm{peak}) = 0$. Using Eq. (3.13), one sees that Q can be re-written as:

$$
Q = \dot{a}^2 - \frac{a^2\dot{\phi}^2}{6M_\mathrm{P}^2},
\tag{3.66}
$$

which is negative when $\dot{a} = 0$. This means that the kinetic term for $l = 0$ fluctuations in Eq. (3.63) is negative in this region. Thus, negative eigenvalue fluctuations (an infinite number, in fact) can always be created by considering sufficiently high frequency fluctuations of the field in the vicinity of $\dot{a} = 0$. Lee and Weinberg termed these negative modes 'rapidly oscillating modes' to distinguish them from the 'slowly varying modes' characteristic of flat space bounces. Their role in not well understood. On the face of it, it would appear to suggest that all CdL bounces do not contribute to vacuum decay.

However, it should be noted that these high frequency modes come into play precisely when quantum gravity corrections would be expected to be important. Since it will ultimately be necessary to renormalise the theory to compute the prefactor of the bounce, it is far from clear whether these rapidly oscillating modes actually rule CdL bounces out from contributing to vacuum decay or not - a correct quantum description of gravity will likely affect them. We will assume that the CdL bounces do contribute and the rapidly oscillating modes should be ignored, but it is worth keeping their existence in mind.

As for the slowly varying negative modes, it seems reasonable to think that these should satisfy the same rules as in flat space - namely that there should only be one.

3.6 Eigen-spectrum of the Hawking-Moss Solution

We introduced the Hawking-Moss solution in section 3.3.3. This solution is unique, however, in that it is possible to compute the eigen-spectrum exactly, and thus easily find the total number of eigenvalues.

Starting with the quadratic action of Eq. (3.63), we substitute in the expressions for the Hawking-Moss solution to find:

$$
\begin{aligned}
\mathcal{L}^{(2)} = &\frac{\sin^3(H_{HM}\chi)}{H_{HM}^3 \cos^2(H_{HM}\chi)} \left[\frac{1}{2} \frac{\mathrm{d}}{\mathrm{d}\chi} \left(\cos(H_{HM}\chi)\Phi \right)^2 \right. \\
&\left. + \left\{ V''(\phi_{\mathrm{bar}}) + \frac{H_{HM}^2 l(l+2)}{\sin^2(H_{HM}\chi)} - 4H_{HM}^2 - 2H_{HM}^2 \tan^2(H\chi) \right\} \frac{1}{2}(\cos(H_{HM}\chi)\Phi)^2 \right]. \quad (3.67)
\end{aligned}
$$

The metric fluctuations have clearly dropped out altogether for this gauge choice, so only Φ, the scalar field fluctuation, determines the eigenvalue spectrum. The Euler-Lagrange equation for Φ gives an eigenvalue equation:

$$
\frac{1}{\sin^3(H_{HM}\chi)} \frac{\mathrm{d}}{\mathrm{d}\chi} \left(\sin^3(H_{HM}\chi) \frac{\mathrm{d}\Phi}{\mathrm{d}\chi} \right) - V''(\phi_{\mathrm{bar}})\Phi - \frac{H_{HM}^2 l(l+2)}{\sin^2(H_{HM}\chi)}\Phi = -\lambda\Phi. \quad (3.68)
$$

Note that in this case, the $l = 1$ modes do *not* vanish identically. The eigenvalue on the RHS is defined with a minus sign because this ensures that negative λ corresponds to *decreasing* action. The substitutions $u = \cos(H_{HM}\chi)$ and $\Phi = (1 - u^2)^r z$ gives:

$$
(1 - u^2)\frac{\mathrm{d}^2 z}{\mathrm{d}u^2} - 4u(r+1)\frac{\mathrm{d}z}{\mathrm{d}u} + \left(\lambda - \frac{V''(\phi_{\mathrm{bar}}) - 2r}{H_{HM}^2} \right) + \frac{1}{1-u^2} \left[4r(r+1)u^2 - l(l+2) \right] z = 0. \quad (3.69)
$$

Thus, by choosing $4r^2 + 4r - l(l+2) = 0$, we can eliminate the $(1-u^2)^{-1}$ term (this is completely analogous to solving the associated Legendre equation in quantum mechanics). This has two

58

possible solutions, $r = l/2$ and $r = -1 - l/2$, but the negative solution cannot be made to satisfy the boundary conditions for eigen-solutions, and so we discard it. The result is:

$$(1 - u^2)\frac{\mathrm{d}^2 z}{\mathrm{d}u^2} - 4u(r+1)\frac{\mathrm{d}z}{\mathrm{d}u} + \left(\lambda - l(l+2) - \frac{V''(\phi_{\mathrm{bar}})}{H_{HM}^2} - 2r\right)z = 0. \tag{3.70}$$

This equation is of known form - the eigenvalues can be found in terms of the Gegenbauer polynomials, which satisfy [128]:

$$(1 - x^2)\frac{\mathrm{d}^2 C_n^{(\alpha)}(x)}{\mathrm{d}x^2} - (2\alpha + 1)x\frac{\mathrm{d}C_n^{(\alpha)}(x)}{\mathrm{d}x} + n(n + 2\alpha)C_n^{(\alpha)}(x) = 0. \tag{3.71}$$

Comparing these, we see that $\alpha = 2r + \frac{3}{2} = l + \frac{3}{2}$. Hence the eigenvalues are:

$$\lambda_{n,l} = n(n + 2l + 3) + l(l+2) + \frac{V''(\phi_{\mathrm{bar}})}{H_{HM}^2} + l = (n+l)(n+l+3) + \frac{V''(\phi_{\mathrm{bar}})}{H_{HM}^2}. \tag{3.72}$$

Setting $N = n + l$, we can summarise the eigenvalues as:

$$\lambda_N = N(N+3) + \frac{V''(\phi_{\mathrm{bar}})}{H_{HM}^2}, \tag{3.73}$$

for $N = 0, 1, 2, \ldots$. Since the degeneracy over l is $(l+1)^2$ (see [129]), the degeneracy of states with eigenvalue λ_N is $1^2 + 2^2 + \ldots + (N+1)^2$, which is simply:

$$D_N(3, 0) = \frac{1}{6}(N+1)(N+2)(2N+3). \tag{3.74}$$

This is unsurprising; in fact, these states are simply the 4-sphere spherical harmonics [129], as we would expect, since the geometry here is just that of a 4-sphere. Note that the $N = 0$ mode is always negative, with degeneracy 1 - it is this that is responsible for the Hawking-Moss describing tunnelling. Furthermore. It follows then that the Hawking-Moss solution only has a single negative eigenvalue when:

$$\frac{V''(\phi_{\mathrm{bar}})}{H_{HM}^2} + 4 \geq 0. \tag{3.75}$$

3.7 Potentials with no Barrier and De Sitter Space

Statement 6. *There are no curved space bounce solutions in potentials lacking a barrier.*

Proof. First consider that a solution must have some point where $\dot{a} = 0$ if it exists and $V_0 > 0$. To see this, compare the curved space and flat space equations for the friction:

$$\frac{\mathrm{d}}{\mathrm{d}\chi}\left(\frac{\dot{a}}{a}\right) = -\frac{1}{a^2} - \frac{\dot{\phi}^2}{6M_{\mathrm{P}}^2}, \tag{3.76}$$

$$\frac{\mathrm{d}}{\mathrm{d}\chi}\left(\frac{1}{\chi}\right) = -\frac{1}{\chi^2}. \tag{3.77}$$

This tells us that the curved space friction term decreases faster, and so when plotted on the same graph, the curves will never cross (if they did, the curved-space friction curve would have a steeper gradient, which would indicate it crossing $1/\chi$ from above, which cannot happen if

it is initially smaller). Consequently, if there is no place where $\dot{a} = 0$ then $\dot{a}/a$ is bounded by $0 < \dot{a}/a < 1/\chi$, proving that $\dot{a}/a \to 0$ as $\chi \to \infty$. This means that the energy, $E = \dot{\phi}^2/2 - V$, approaches a constant. In order for there to be a solution, this constant *must* be $-V_0$, since that is the energy at the false vacuum, which the solution must approach. However, this cannot be the case because:

$$E = \frac{\dot{\phi}^2}{2} - \Delta V(\phi) - V_0 > -V_0, \tag{3.78}$$

since $\Delta V(\phi) > 0$. Hence, the solution will always overshoot, due to having too much energy, implying that no solution exists if $\dot{a}$ is never zero *somewhere*.

However, assuming that there is some region where $\dot{a} = 0$ is also problematic. After this point, $\dot{a} < 0$ and thus the friction term becomes negative. This means that the field accelerates, and in the absence of a barrier, the gradient of the potential is also causing the field to accelerate. Thus, nothing can slow the field down, and it will also overshoot the false vacuum. Hence, no solution exists. $\qquad\square$

One way of interpreting this result was pointed out by Lee [133], who pointed out that solutions exist in flat space only because fluctuations away from the nominally unstable false vacuum the false vacuum are suppressed by the gradient terms in the potential of the field:

$$U[\phi(x)] = \int \mathrm{d}^3 x \sqrt{\det h} \left[\frac{1}{2}(\nabla\phi)^2 + V(\phi) \right]. \tag{3.79}$$

It is worth stressing that it is $U[\phi]$, which includes gradient terms, and *not* $V(\phi)$ that the field tunnels through: thus even if $V(\phi)$ may *appear* to have no barrier, from a tunnelling point of view there is still a barrier against the nucleation of localised bubbles, since these necessarily have gradients. In de Sitter space, however, the Hamiltonian is not well defined beyond the horizon, and causal interactions (such as gradient terms) cannot influence the behaviour of the field. This means that long-wavelength, super-horizon modes are unimpeded by the gradient terms and there is nothing to stop them rolling down the barrier, which is the reason their amplitude tends to grow with time [134]. This gives the scalar field an unstable direction to roll down, making the false vacuum unstable, rather than meta-stable. In some cases, it is possible to constrain the system to try and remove these rolling modes [133, 135, 136, 108], however, this situation can also be dealt with using the stochastic approach, which directly takes into account the behaviour of long wavelength modes [107].

3.8 Vacuum Instability and Bubble Nucleation During Inflation

One of the simplest examples of a situation in which gravity comes into play for vacuum stability calculations is during inflation. An inflationary background can be modelled with $V(\phi_\mathrm{fv}) > 0$, and this background respects $O(4)$ symmetry. Note that in flat space, $O(4)$ symmetric solutions can be proven to be the dominant solutions [119]. The situation is less clear in curved space, where this proof does not directly apply.

However, it seems reasonable to conclude that this does hold true, at least in backgrounds that respect $O(4)$ symmetry, as flat space does (it would be surprising if the dominant solution for vacuum decay was the nucleation of an asymmetric bubble, particularly as this is

not true in the flat limit). There is some evidence that this is the case [137, 138]. Possible exceptions to this would be space-times that do not respect $O(4)$ symmetry, such as around a black hole [82, 83, 84] or cosmic string.

If we accept, however, that $O(4)$ symmetric solutions are dominant, then this implies that vacuum decay should be controlled either by Hawking-Moss solutions, CdL solutions, or some combination thereof - whichever solution has the lowest action will dominate the decay rate.

This is, however, not in itself sufficient to answer the question of what happens when a bubble nucleates during inflation. In flat space, one computes the decay rate per unit volume, Γ/V_3, and then uses this to find the expected life-time. We then compare to the age of the universe to decide if decay is expected. The dynamics are more complicated in an inflationary background, however, as not only must true vacuum bubbles nucleate, but they must do so frequently enough that the exponential expansion does not push them all beyond the horizon of the visible universe.

One can phrase this question as requiring that there must not be *any* bubble within out past light-cone. In section 3.9, we concluded that bubbles nucleated during inflation expand to fill a full Hubble volume, but no further. After inflation these regions can expand, and any bubbles in them will presumably grow to envelop the entire universe. This means that we can address this question by counting the number of Hubble volumes at the end of inflation that we are today in causal contact with (since nucleated bubbles expand at near the speed of light).

In to obtain a decay rate from a bubble, it is necessary to compute the exponential pre-factor, A, in the decay rate: $\Gamma = Ae^{-B}$. This factor contains the dimensional dependence which gives the decay rate per unit *volume*. However, this pre-factor is generically difficult to compute, since it depends on fluctuations about the bounce solution:

$$A = \frac{B^2}{4\pi^2} \left| \frac{\det'(S''[\phi_{\text{HM}}])}{\det(S''[\phi_{\text{fv}}])} \right|^{-\frac{1}{2}}. \tag{3.80}$$

Recall that the prime denotes the determinant with the four zero eigenvalues removed, which is what makes this a density. In principle, this can be calculated, using the Gel'fand-Yaglom theorem [139, 140, 141]:

$$\frac{\det(-\frac{\text{d}^2}{\text{d}r^2} + M^{(1)}(r) - \lambda)}{\det(-\frac{\text{d}^2}{\text{d}r^2} + M^{(2)}(r) - \lambda)} = \frac{\psi_\lambda^{(1)}(b_1)}{\psi_\lambda^{(2)}(b_2)}, \tag{3.81}$$

where the boundary conditions for the eigenfunctions are $\psi_\lambda^{(i)}(a_i) = \psi_\lambda^{(i)}(b_i) = 0$, and we normalise the solutions with the condition $\phi_\lambda^{(i)'}(a_i) = 1$. This result follows from the fact that, regarded as a function of λ, both sides of Eq. (3.81) have the same poles and zeros, and thus by the Liouville theorem, are the same function up to a constant, which in this case is 1. This result can be generalised to d-dimensional partial differential operators of the form $-\nabla^2 + M(r)$ as well, by decomposing the eigen-solutions into (d-1)-sphere spherical harmonics [140]:

$$\log\left(\frac{\det(-\nabla^2 + M^{(1)}(r))}{\det(-\nabla^2 + M^{(2)}(r))}\right) = \sum_{l=0}^{\infty} D_l(d-1,0) \log\left(\frac{-\frac{1}{a^3(r)}\frac{\text{d}}{\text{d}r}\left(a^3(r)\frac{\text{d}}{\text{d}r}\right) + \frac{l(l+d-1)}{a^2(r)} + M^{(1)}}{-\frac{1}{a^3(r)}\frac{\text{d}}{\text{d}r}\left(a^3(r)\frac{\text{d}}{\text{d}r}\right) + \frac{l(l+d-1)}{a^2(r)} + M^{(2)}}\right), \tag{3.82}$$

where we have assumed a radially symmetric metric of the form $ds^2 = dr^2 + a^2(r)d\Omega_{d-1}^2$ and the degeneracy is given by [129]:

$$D_l(d-1,0) = \frac{(l+d-3)!(2l+d-2)}{l!(d-2)!}. \tag{3.83}$$

Additionally, if the result involves a vector, it may be necessary to generalise Eq. (3.81) using determinants of the Wronskian of a set of independent solutions, since these will have the correct poles and zeros. See [18] for an example of this done with the Standard Model in flat space.

However, although these functional determinants can in principle be evaluated, this alone is not sufficient - Eq. (3.82) consists of a divergent sum, to begin with. This is because these functional determinants need to be renormalised before they give finite, sensible results [99, 140]. This is doubly problematic in the case of gravitational bounces because, as we have seen, these include gravitational *fluctuations*. Lacking a proper theory of quantum gravity, the calculation cannot easily be performed.

However, one can get around this by assuming that, regardless of what the final theory of quantum gravity is, it should presumably give a finite result, and that the pre-factor A will be fixed, on dimensional grounds to be the same order of magnitude of some characteristic scale for the bounce. During Inflation, for example, this might be the Hubble rate, H. In the flat space Standard Model, it is the scale $\mu_{\min}$ at which $\lambda(\mu)$ is minimised [18].

From a phenomenological point of view, the relevant question we ask about vacuum decay is: what is the probability that a bubble nucleated within out past light-cone? If we know (possibly space-time dependent) decay rate per unit space-time volume, Γ, then the expected number of bubbles nucleating in the past light-cone of the present day is:

$$\langle n \rangle = \int_{\text{Past lightcone}} d^4x \sqrt{-\det g}\, \Gamma(x). \tag{3.84}$$

In an Friedmann-Lemaître-Robertson-Walker (FLRW) space-time, the comoving radius $R(t)$ of the past light cone follows a radial null trajectory:

$$ds^2 = -dt^2 + \frac{a^2(t)dR^2}{1 - kR^2} = 0, \tag{3.85}$$

and thus:

$$R(t) = \frac{1}{\sqrt{k}} \sin^{-1}\left(\sqrt{k} \int_t^{t_0} \frac{dt'}{a(t')}\right). \tag{3.86}$$

Assuming that the decay rate depends only on time, and is homogeneous, then:

$$
\begin{aligned}
\langle n \rangle &= 4\pi \int_{t_{\text{start}}}^{t_0} dt a^3(t)\Gamma(t) \int_0^{R(t)} \frac{R^2}{\sqrt{1-kR^2}} \\
&= 4\pi \int_{t_{\text{start}}}^{t_0} dt a^3(t)\Gamma(t) \frac{1}{2k}\left(\frac{\sin^{-1}(\sqrt{k}R(t))}{\sqrt{k}} - R(t)\sqrt{1-kR^2(t)}\right).
\end{aligned} \tag{3.87}
$$

The $k = 0$ case is especially simple:

$$\langle n \rangle = 4\pi \int_{t_{\text{start}}}^{t_0} dt a^3(t)\Gamma(t)\frac{R^3(t)}{3}. \tag{3.88}$$

62

If $k = 0$ and inflation ends at some time t_{rad} (the beginning of the radiation era) and has approximately constant Hubble rate, H, then:

$$R(t) = \int_{t_{\text{rad}}}^{t_0} \frac{dt'}{a(t')} + \int_{a(t)}^{a(t_{\text{rad}})} \frac{da}{Ha^2} = \int_{t_{\text{rad}}}^{t_0} \frac{dt'}{a(t')} + \frac{1}{H}\left[\frac{1}{a(t)} - \frac{1}{a(t_{\text{rad}})}\right]. \tag{3.89}$$

If we let $R_0 = R(t_{\text{rad}})$ be the contribution from the hot-big-bang evolution post-inflation, then (for $t < t_{\text{rad}}$):

$$
\begin{aligned}
\langle n \rangle =& \frac{4\pi}{H} \int_{a(t_{\text{start}})}^{a(t_{\text{rad}})} da\, a^2(t) \frac{\Gamma(t)}{3} \left(R_0^3 + \frac{3R_0^2}{H}\left[\frac{1}{a(t)} - \frac{1}{a_{t_{\text{rad}}}}\right] + \frac{3R_0}{H^2}\left[\frac{1}{a^2(t)} - \frac{2}{a(t)a(t_{\text{rad}})} + \frac{1}{a^2(t_{\text{rad}})}\right] \right. \\
&\left. + \frac{1}{H^3}\left[\frac{1}{a^3(t)} - \frac{3}{a^2(t)a(t_{\text{rad}})} + \frac{3}{a(t)a^2(t_{\text{rad}})} - \frac{1}{a^3(t_{\text{rad}})}\right] \right) + \frac{4\pi}{3}\int_{t_{\text{rad}}}^{t_0} dt\, a^3(t)\Gamma(t)R^3(t).
\end{aligned}
\tag{3.90}
$$

If we are only interested in the bubbles that nucleate during inflation, then we neglect the last term, but it is generally used to compute the expected number of flat space bubbles during the cosmological history of the universe. The contribution of inflationary bubbles is:

$$
\begin{aligned}
\langle n \rangle =& \frac{4\pi}{3H} \int_{a_{\text{start}}}^{a_{\text{rad}}} da\, \Gamma(a) \left(\left[R_0^3 - \frac{3R_0^2}{Ha_{\text{rad}}} + \frac{3R_0}{H^2 a_{\text{rad}}^2} - \frac{1}{H^3 a_{\text{rad}}^3}\right] a^2 + \left[\frac{3R_0^2}{H} - \frac{6R_0}{H^2 a_{\text{rad}}} + \frac{3}{H^3 a_{\text{rad}}^2}\right] a \right. \\
&\left. + \left[\frac{3R_0}{H^2} - \frac{3}{H^3 a_{\text{rad}}}\right] + \frac{1}{H^3 a} \right).
\end{aligned}
\tag{3.91}
$$

For a *constant* decay rate, $\Gamma(a) = \Gamma$, this gives:

$$
\begin{aligned}
\langle n \rangle =& \frac{4\pi\Gamma}{3H^4} \left[\left(\frac{(HR_{0\text{rad}})^3}{3} - (HR_{0\text{rad}})^2 + HR_{0\text{rad}} - \frac{1}{3}\right)(1 - e^{-3N}) \right. \\
&+ \left(\frac{3}{2}(HR_{0\text{rad}})^2 - 3HR_{0\text{rad}} + \frac{3}{2}\right)(1 - e^{-2N}) \\
&\left. + (3HR_{0\text{rad}} - 3)(1 - e^{-N}) + N \right],
\end{aligned}
\tag{3.92}
$$

where $R_{0\text{rad}} = R_0 a_{\text{rad}}$ is the physical radius of the past-light-cone at the end of inflation, and $N = \log(a_{\text{rad}}/a_{\text{start}})$ is the number of e-folds since the start of inflation. At large N, this takes the form:

$$\langle n \rangle \approx \frac{4\pi\Gamma}{3H^4}\left(\frac{(HR_{0\text{rad}})^3}{3} + \frac{(HR_{0\text{rad}})^2}{2} + HR_{0\text{rad}} - \frac{11}{6} + N\right). \tag{3.93}$$

Notice that this is *divergent* in the $N \to \infty$ limit, which corresponds to $t \to -\infty$, $a_{\text{start}} \to 0$. This indicates that if inflation lasts infinitely far into the past, then the expected number of bubbles in the past light cone is logarithmically divergent! Most models of inflation, however, would assume some boundary condition for the field that makes this untrue, but the details will depend on the model of inflation, and likely quantum gravity effects which set the initial conditions for inflation. Regardless, it is interesting that the nucleation rate of bubbles is sensitive to how long inflation went on for. This further highlights the potential benefits of vacuum decay as an indirect probe of high energy phenomena.

3.9 Expansion of Vacuum Bubbles after Nucleation

A key assumption in the discussion so far is that any vacuum bubble that nucleates is necessarily threatening. In flat space, this is justified because bubbles expand at near the speed of light after nucleation [98, 99]. The reason for this is their $O(4)$ symmetry, which corresponds to $O(3,1)$ symmetry when analytically continuing back to real space. We can show this by transforming (r,t) to the $O(3,1)$ symmetric co-ordinates (ρ, ψ), valid for $r > t$:

$$r = \rho \cosh(\psi), \tag{3.94}$$
$$t = \rho \sinh(\psi), \tag{3.95}$$

in which the (flat) metric takes the form:

$$ds^2 = d\rho^2 - \rho^2 d\psi^2 + \rho^2 \cosh^2 \psi d\Omega_2^2. \tag{3.96}$$

In these co-ordinates, the (Lorentzian) scalar field equation is:

$$\frac{\partial^2 \phi}{\partial \rho^2} + \frac{3}{\rho} \frac{\partial \phi}{\partial \rho} - \frac{1}{\rho^2 \cosh^2 \psi} \frac{\partial}{\partial \psi} \left(\cosh^2 \psi \frac{\partial \phi}{\partial \psi} \right) + \frac{\hat{L}_{\varphi\theta}^2}{\rho^2 \cosh^2 \psi} - V'(\phi) = 0, \tag{3.97}$$

where $\hat{L}_{\varphi\theta}^2$ is the usual angular momentum operator for the angular terms φ, θ. The initial conditions are $\phi(0, t, \theta, \varphi) = \phi_B(r), \frac{\partial \phi}{\partial t} = 0$ in the (r,t) co-ordinates, at $t = 0$, which translates to $\psi = 0$ in the new-co-ordinates, with the initial conditions translating to $\phi(\rho, 0, \theta, \varphi) = \phi_B(\rho)$, $\frac{\partial \phi}{\partial \psi} = 0$. From the equation for the bounce solution, we know that:

$$\frac{d^2 \phi_B}{d\rho^2} + \frac{3}{\rho} \frac{d\phi_B}{d\rho} - V'(\phi) = 0. \tag{3.98}$$

Hence, the unique solution of Eq. (3.97) satisfying these boundary conditions if $\phi(\rho, \psi, \theta, \varphi) = \phi_B(\rho)$, ie, independent of ψ, θ, φ. This translates back to the (r,t) co-ordinates as:

$$\phi(t, r, \theta, \varphi) = \phi_B(\sqrt{r^2 - t^2}). \tag{3.99}$$

Thus, for $r > t$, we can read off the evolution of the bubble immediately. The $r < t$ portion is not covered by this solution, and must be dealt with separately. However, we will show later that it describes gravitational collapse of the bubble, and so defer discussion for now. Eq. (3.99) allows us to extract information about the expansion of the bubble, since a point of constant $\phi = \phi_0$ will correspond to $r^2 - t^2 = R_0^2$ where $R_0 = \phi_B^{-1}(\phi_0)$ (ϕ_B is one-to-one and thus invertible for ϕ on the range $[\phi_{\text{fv}}, \phi_B(0)]$). This describes the bubble expanding:

$$r(t) = \sqrt{R_0^2 + t^2}. \tag{3.100}$$

The velocity of this point is:

$$\dot{r}(t) = \frac{t}{\sqrt{R_0^2 + t^2}}, \tag{3.101}$$

which approaches the speed of light in the $t \to \infty$ limit. For any ϕ significantly different to vacuum, R_0 is around the characteristic scale of the bubble (such as it's width, R, the point where $\phi(R) = \phi(0)/2$). This is typically very small - in the Standard Model $R \sim 1/(10^{17} \text{ GeV})$. Consequently, $\dot{r} \sim c$ within a few R/c periods, and thus the bubble wall expands at essentially the speed of light, eventually filling the entire universe and converting it to a true vacuum. As

this disagrees with observations, this cannot have happened.

In curved spaces, such as de Sitter, the situation is somewhat more complicated. First of all, we have to be careful to define how to analytically continue the bounce solution back to Lorentzian space. A particularly useful way to do this was discussed by [84]. The idea is to transform the $O(4)$ symmetric co-ordinates where the metric looks like:

$$\mathrm{d}s^2 = \mathrm{d}\chi^2 + a^2(\chi)\left[\mathrm{d}\psi^2 + \sin^2\psi\mathrm{d}\Omega_2^2\right], \tag{3.102}$$

to a conformally flat metric, which can then by analytically continued in the same way as flat space:

$$\mathrm{d}s^2 = \frac{a^2(\chi)}{f^2(\chi)}\left(\mathrm{d}\tilde{\tau}^2 + \mathrm{d}\tilde{r}^2 + \tilde{r}^2\mathrm{d}\Omega_2^2\right), \tag{3.103}$$

where:

$$\tilde{\tau} = f(\chi)\cos\psi, \tag{3.104}$$
$$\tilde{r} = f(\chi)\sin\psi. \tag{3.105}$$

The function f must be chosen such that $f'(\chi) = f/a, f(0) = 0, f'(\chi) > 0$ to implement this transformation. There is then a natural way to analytically continue back to Lorentzian space, via the transformation $\tilde{t} = -i\tilde{\tau}$, or equivalently:

$$\tilde{r} = f(\chi)\cosh(\psi_+), \tag{3.106}$$
$$\tilde{t} = f(\chi)\sinh(\psi_+), \tag{3.107}$$

where $\psi_+ = i(\psi - \pi/2)$. Note that while (t, r) covers a patch twice as large as the (χ, ψ_+) system, since in the latter one clearly has $\tilde{r}^2 - \tilde{t}^2 = f^2(\chi) > 0$, that is, it covers only the outside of the light-cone, $\tilde{r} > \tilde{t}$. On this region, for exactly the same reason as in flat space, the bounce solution is $\phi(\tilde{r}, \tilde{t}) = \phi_B(\chi(\tilde{r}, \tilde{t}))$, only this time χ is related to $\tilde{r}$ and $\tilde{t}$ by:

$$\chi = f^{-1}(\sqrt{\tilde{r}^2 - \tilde{t}^2}), \tag{3.108}$$

a function which exists because $f' > 0$ and thus f is monotonic. Hence the solution evolves much like in flat space, with the effect of the metric being accounted for by the $f(\chi)$ function:

$$\phi(\tilde{r}, \tilde{t}) = \phi_B(f^{-1}(\sqrt{\tilde{r}^2 - \tilde{t}^2})). \tag{3.109}$$

Burda et al. also show how to deal with the interior of the light-cone, $r < t$, by use of the co-ordinates [84]:

$$\tilde{r} = f(\tilde{\chi})\sinh(\psi_-), \tag{3.110}$$
$$\tilde{t} = f(\tilde{\chi})\cosh(\psi_-), \tag{3.111}$$

in which the metric takes the form:

$$\mathrm{d}s^2 = -\mathrm{d}\tilde{\chi}^2 + a^2(\tilde{\chi})\left[\mathrm{d}\psi_-^2 + \sinh^2(\psi_-)\mathrm{d}\Omega_2^2\right]. \tag{3.112}$$

Note that although their role is similar, $\tilde{\chi}$ and χ are different co-ordinates defined on different patches of space-time. Thus, we cannot simply carry over the Euclidean solution to the $\tilde{r} < \tilde{t}$

region covered by this patch. We have to solve the scalar field and metric equations of motion directly:

$$-\frac{\partial^2 \phi}{\partial \tilde{\chi}^2} - \frac{3\dot{a}}{a}\frac{\partial \phi}{\partial \tilde{\chi}} + \frac{1}{a^2 \sinh^2 \psi_-} \frac{\partial}{\partial \psi_-}\left(\sinh^2 \psi_- \frac{\partial \phi}{\partial \psi_-}\right) + \frac{\hat{L}_{\theta\varphi}^2}{a^2 \sinh^2 \psi_-} - V'(\phi) = 0. \qquad (3.113)$$

The initial conditions are defined on the $\tilde{\chi} = 0$ hypersurface, corresponding to the light-cone, $\tilde{r} = \tilde{t}$, namely, $\phi(0, \psi_-, \theta, \varphi) = \phi_B(0), \frac{\partial \phi}{\partial \tilde{\chi}} = 0$. These initial conditions are independent of the angular variables, and thus if a solution satisfying the boundary conditions that is independent of ψ_-, θ, φ exists, then by uniqueness of Cauchy problems, it must be the solution of this ode and the relevant analytic continuation of the bounce to the $\tilde{r} < \tilde{t}$ region. Such a solution corresponds to the ode system:

$$\frac{\mathrm{d}^2 \phi}{\mathrm{d}\tilde{\chi}^2} + \frac{3\dot{a}}{a}\frac{\mathrm{d}\phi}{\mathrm{d}\tilde{\chi}} + V'(\phi) = 0, \qquad (3.114)$$

$$\dot{a}^2 = 1 - \frac{a^2}{3M_{\mathrm{P}}^2}\left(\frac{\dot{\phi}^2}{2} + V(\phi)\right), \qquad (3.115)$$

subject to initial conditions $\dot{\phi}(0) = 0, \phi(0) = \phi_B(0), a(0) = 0$, where dots denote differentiation with respect to $\tilde{\chi}$. Since this solution exists, then the solution of the system on the $\tilde{r} < \tilde{t}$ patch is well defined and respects $O(3,1)$ symmetry. To understand the behaviour of this solution, it is instructive to analyse the second derivative of the 'Friedmann' equation:

$$\ddot{a} = -\frac{a}{3M_{\mathrm{P}}^2}\left(\dot{\phi}^2 - V(\phi)\right). \qquad (3.116)$$

When the solution starts at $\phi_B(0)$, the sign of Eq. (3.114) is now Lorentzian, so it rolls down the potential towards the true vacuum. Inevitably, if $V(\phi_{\mathrm{tv}}) < 0$, then it rolls into a negative curvature, Anti de Sitter (AdS), region with the RHS of Eq. (3.116) negative. As [84] pointed out, this means that $a(\tilde{\chi})$ inevitable hits a 'big-crunch' singularity at finite $\tilde{\chi}$, supporting the conclusions of [97] which was based on a thin-wall analysis.

How are we to interpret this? If the true vacuum is anti-de-Sitter, then it appears that the vacuum bubble will undergo gravitational collapse, which to observers inside the bubble, $\tilde{r} < \tilde{t}$, looks like a Big Crunch singularity. Note, however, that this doesn't happen until $\tilde{r} < \tilde{t}$: for $\tilde{r} > \tilde{t}$, the solution of Eq. (3.109) applies, which describes the expansion of the bubble. This is crucial to understanding the behaviour of such bubbles. To summarise:

1. The $\tilde{r} > \tilde{t}$ patch describes the bubble wall expanding outwards.

2. The $\tilde{r} < \tilde{t}$ patch describes the bubble undergoing gravitational collapse.

Note that, on its own, the gravitational collapse for $\tilde{r} < \tilde{t}$ has no way of preventing the expansion in the $\tilde{r} > \tilde{t}$ region, so the fact that a singularity forms does not imply that the bubble always collapses into a black hole rather than expand. The $\tilde{r} > \tilde{t}$ region however, shows that the bubble will continue to follow a null trajectory. Depending on the back-reaction of the bubble, encapsulated by $f(\chi)$ and $a(\chi)$, this could conceivable describe a bubble collapsing to a black hole if the null trajectories were to become trapped behind a horizon somehow.

Of particular importance is de Sitter space. To get an idea about the behaviour of the bubble in a de Sitter background, consider the fixed background approximation, for which we find, in Euclidean space, the metric to be:

$$a(\chi) = \frac{1}{H} \sin(H\chi). \tag{3.117}$$

Integrating $f' = f/a$ with this metric, we find:

$$f(\chi) = C \tan\left(\frac{H\chi}{2}\right). \tag{3.118}$$

Taking $C = 1$ without loss of generality, the analytic continuation then gives a Lorentzian metric of:

$$ds^2 = \frac{4}{H^2(1 + \tilde{r}^2 - \tilde{t}^2)^2} \left[-d\tilde{t}^2 + d\tilde{r}^2 + \tilde{r}^2 d\Omega_2^2\right]. \tag{3.119}$$

Although this co-ordinate system is unfamiliar, this is actually pure de Sitter space, as we might expect from analytically continuing a 4-sphere back to Lorentzian space. The transformation:

$$t = \frac{1}{2H} \log \left|\frac{1 - \tilde{r}^2 + 2\tilde{t} + \tilde{t}^2}{1 - \tilde{r}^2 - 2\tilde{t} + \tilde{t}^2}\right|, \tag{3.120}$$

$$r = \frac{2\tilde{r}}{H(1 + \tilde{r}^2 - \tilde{t}^2)}, \tag{3.121}$$

can be shown to put this in the more familiar static patch, used to define tunnelling in de Sitter space [101]:

$$ds^2 = -dt^2(1 - H^2 r^2) + dr^2(1 - H^2 r^2)^{-1} + r^2 d\Omega_2^2. \tag{3.122}$$

Tracking the evolution of a point with constant ϕ_0, as we did for flat space, is then as simple as writing:

$$\tilde{r}(\tilde{t}) = \sqrt{\tilde{t}^2 + f^2(\chi_0(\phi_0))}, \tag{3.123}$$

where χ_0 is the value of χ corresponding to a given ϕ_0, found by inverting the bounce ($\chi_0 = \phi_B^{-1}(\phi_0)$). Plugging in the appropriate $f(\chi)$ and the transformations Eq. (3.120) and (3.121) gives the evolution in the static co-ordinates, (r, t):

$$r(t) = \frac{2}{H^2(1 + \tilde{r}_0^2)} \sqrt{\tilde{r}_0^2 + \frac{1}{4}(1 - \tilde{r}_0^2)^2 \tanh^2(Ht)}, \tag{3.124}$$

where $\tilde{r}_0 = f(\chi_0(\phi_0))$. As $t \to \infty$, notice that $r \to 1/H$, that is, it approaches the Horizon. In the static patch, r is a physical radius, so this tells us that while the bubble continues to expand at close to the speed of light, the space around it is exponentially expanding and thus it is unable to reach regions beyond the horizon. The bubble never stops expanding, it simply fills an entire Hubble volume, after which, that Hubble volume continues to expand exponentially like all others. Crucially, because the bubble wall never quite reaches $r = 1/H$, the Hubble volume itself does not collapse and disappear. Another way of looking at this is that Eq. (3.124) increases with $\tilde{r}_0$ at constant t, for $\tilde{r}_0 < 1/H$, since:

$$\frac{\partial r(t)}{\partial \tilde{r}_0} = \frac{2\tilde{r}_0(1 - \tilde{r}_0^2)(1 - \tanh^2(Ht))}{H(1 + \tilde{r}_0^2)^2 \sqrt{\tilde{r}_0^2 + (1 - \frac{1}{4}\tilde{r}_0^2)^2 \tanh^2 Ht}}. \tag{3.125}$$

Consequently, the leading edge of the bubble is always a region with positive Ricci curvature, due to the bubble walls. The AdS region in the centre never quite 'catches up'.

Previously, it has been claimed in the literature that vacuum bubbles forming during inflation will necessarily collapse and vanish, because their centre is anti de Sitter, which describes a collapsing space-time, while the exterior is exponentially expanding de Sitter [142, 67, 66]. More recent analyses have concluded, however, that this is not correct [68, 65]. [65] for example show explicitly, for a thin wall bubble, that although it does not occupy the entire global de Sitter space-time, it does not collapse. The analytic continuation approach of [84] as we have discussed here, however, appears to back this up, and also gives a hint as to why: the gravitationally collapsing region is constrained to lie at $\tilde{r} < \tilde{t}$, which always lies within the interior of the Hubble-volume, never reaching its edge, since the point $\tilde{r}_0 = 0$ takes infinite time to reach the Horizon. This demonstrates that the ultimate fate of a region of space in which a bubble nucleates: it will be hit by a bubble wall, likely destroying any matter present, and then collapse to an AdS big-crunch like singularity. Similar conclusions were reached by [65, 68, 84] regarding the ultimate fate of vacuum bubbles during inflation.

Chapter 4

Effective Potential in De Sitter Space

4.1 The Effective Action, Energy Functional, and False Vacuum Decay

To make precise predictions about the Standard Model, it is necessary to accurately describe the effective potential of the Higgs field. As we will discuss, there is a difference between the effective potential in curved and flat space. First, let us describe what the effective potential means. When describing the evolution of a quantum field, one cannot ask about the evolution of the field itself, ϕ, which is an operator, but only the evolution of observable quantities, such as the expectation value, $\langle \phi \rangle$. This is done using the effective action. Following [143], one can define the energy functional $E[J]$ in terms of the vacuum-to-vacuum transition amplitude:

$$Z[J] \equiv e^{-iE[J]} \equiv \lim_{T \to \infty} \langle 0 | e^{-i\hat{H}T} | 0 \rangle = \int_{\phi(0,x)=\phi_{\mathrm{fv}}}^{\phi(T,x)=\phi_{\mathrm{fv}}} \mathcal{D}\phi \exp \left(iS[\phi] + i \int \mathrm{d}^4 x J\phi \right), \qquad (4.1)$$

where $|0\rangle$ represents the vacuum state, where $\phi = \phi_{\mathrm{fv}}$ everywhere and J is an external current. Note that one purpose of the exponential here is to simplify the expansion of the path integral expression into Feynman diagrams, since if D_n is the nth possible connected Feynman diagram, then:

$$Z[J] = \sum_m \frac{1}{m!} \left(\sum_n D_n \right)^m, \qquad (4.2)$$

since Z includes the sum over all possible products of connected Feynman diagrams of any number, and the factorial here accounts for the symmetry factor of having multiple copies of the same diagram in a given product. With some thought, it is also possible to see that this factorial combined with the binomial coefficients from raising the sum to the power m reproduces the symmetry factors of all possible products. This form makes it clear that the energy functional is just the sum over all *connected* diagrams:

$$E[J] = i \sum_n D_n. \qquad (4.3)$$

In this case, because we included the external field, J, this reproduces the sum of all diagrams with any number of external legs, where each external leg is attached to a "vertex", $J(x)$, and we integrate over all possible positions of these vertices. In particular, for $J = 0$, we will find that only diagrams with no external legs are included, that is, the so called 'bubble diagrams' (not to be confused with vacuum bubbles that describe false vacuum decay). See fig. 4.1 for example. Notice, however, that if $|0\rangle$ is an eigenstate of the Hamiltonian, then $E[0]$ also has a
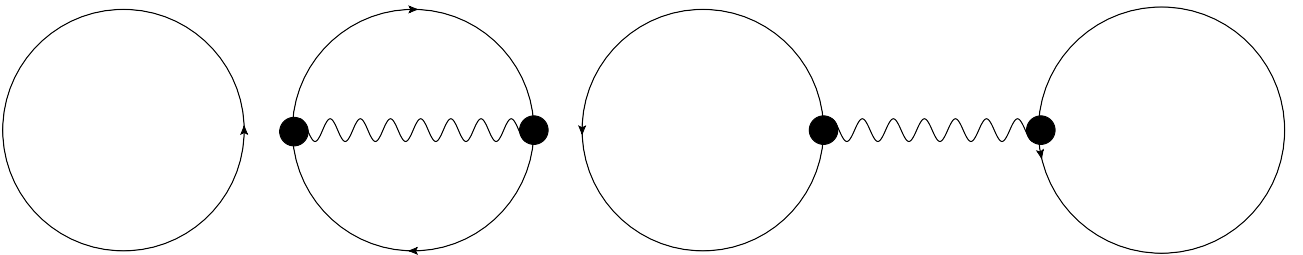
Figure 4.1: Examples of diagrams with no external legs contributing to $E[J]$, in QED.

natural interpretation in terms of the energy of the vacuum. This tells us that loop diagrams contribute to the vacuum energy. In the case of a false vacuum, the same is true, but the

energy is now complex and we have to be somewhat more careful to define what we mean by (1) a complex energy, and (2) the energy of a state which is not an exact eigenstate of the Hamiltonian. This was discussed in more detail in section A.1.

As is standard in quantum and classical field theory, it is useful not only to define the Hamiltonian (energy), but the action of a theory. If we can interpret $E[J]$ as being related to the energy of the theory, after including all quantum loop corrections, then it makes sense to ask how we might interpret the Legendre transform (see appendix A.2.1) of $E[J]$, which should be an action of some sorts. This is the effective action,

$$\Gamma[\phi_{\text{cl}}] = \sup_J \left(-E[J] - \int \mathrm{d}^4 \mathrm{x} J \phi_{\text{cl}} \right), \tag{4.4}$$

where $\sup_J$ denotes taking the supremum (maximum) over the set J of the quantity on the right hand side. Consider the first functional derivative:

$$\frac{\delta \Gamma}{\delta \phi_{\text{cl}}} = - \int \mathrm{d}^4 x \frac{\delta E}{\delta J(x)} \frac{\delta J(x)}{\delta \phi_{\text{cl}}} - J - \int \mathrm{d}^4 x \phi_{\text{cl}} \frac{\delta J(x)}{\delta \phi_{\text{cl}}}. \tag{4.5}$$

Note that:

$$\frac{\delta E}{\delta J} = \frac{i}{Z} \frac{\delta Z}{\delta J} = -\langle \phi \rangle_J, \tag{4.6}$$

and that maximising over J at constant ϕ_{cl} requires:

$$-\frac{\delta E}{\delta J} - \phi_{\text{cl}} = 0. \tag{4.7}$$

This means that $\phi_{\text{cl}} = \langle \phi \rangle_J$, and thus:

$$\frac{\delta \Gamma[\phi_{\text{cl}}]}{\delta \phi_{\text{cl}}} + J = 0. \tag{4.8}$$

This tells us that ϕ_{cl} the conjugate variable to J, can be interpreted as the expectation value of ϕ at external field J. Furthermore, $\Gamma[\phi_{\text{cl}}]$ is a functional that describes the full evolution of the expectation value of the field, including all quantum effects. In particular, it is Γ, the effective action, not S, the classical action, that tells us where the vacuum of the theory lies, and whether it is stable or not.

One way to express Γ is the so called 'gradient expansion' or local potential approximation:

$$\Gamma[\phi] = \int \mathrm{d}^4 x \sqrt{|\det g|} \left[-V_{\text{eff}}(\phi) + Z(\phi) \frac{1}{2} (\partial_\mu \phi \partial^\mu \phi) + Z_1(\phi)(\partial_\mu \phi \partial^\mu \phi)^2 + \dots \right]. \tag{4.9}$$

Here, we have essentially written down all terms that are compatible with Lorentz symmetry (which is preserved by quantum corrections). However, for low energies, the higher order gradient terms are suppressed (this can be seen from renormalisation, since these terms will have negative mass term couplings and are thus suppressed by powers of the cut-off scale). Furthermore, we can always re-define ϕ so that $Z(\phi) = 1$ (unless there is more than one field, in which case we end up with a field space metric which can have observable consequences). Assuming this is valid, then we can write:

$$\Gamma[\phi] \approx \int \mathrm{d}^4 x \sqrt{|\det g|} \left[\frac{1}{2} \partial_\mu \phi \partial^\mu \phi - V_{\text{eff}}(\phi) \right]. \tag{4.10}$$

This then defines V_{eff}, the 'effective potential'. It is this potential which appears in tunnelling calculations, and is the one we now seek to compute. The simplest way to do this, following standard texts such as [143], is to compute the effective action, and evaluate it at a constant field configuration. This will suppress all the gradient terms, leaving us with an (infinite) factor of the space-time volume and a minus sign. The one loop calculation is well known to yield a Gaussian integral. We can show this by noting that J is chosen so that Eq. (4.7) holds, which means that ϕ_{cl} is a stationary point of $S[\phi] + J\phi$. Hence, we can perform a steepest descent approximation of the path integral around ϕ_{cl}:

$$
\begin{aligned}
E[J(\phi_{\text{cl}})] &= i \log \left[\int \mathcal{D}\phi e^{iS[\phi] + i \int \mathrm{d}^4 x J\phi} \right] \\
&= i \log \left[\int \mathcal{D}\eta \exp \left(iS[\phi_{\text{cl}}] + i \int \mathrm{d}^4 x \left\{ J\phi_{\text{cl}} + J\eta \right\} + i \int \mathrm{d}^4 x \eta \frac{\delta S[\phi_{\text{cl}}]}{\delta \phi} \right. \right. \\
&\qquad \left. \left. + \frac{i}{2} \int \mathrm{d}^4 x \mathrm{d}^4 y \eta(x) \frac{\delta^2 S[\phi_{\text{cl}}]}{\delta \phi(x) \delta \phi(y)} \eta(y) + O(\eta^3) \right) \right] \\
&= i \log \left[e^{iS[\phi_{\text{cl}}] + i \int \mathrm{d}^4 x J\phi_{\text{cl}}} \int \mathcal{D}\eta \exp \left(\frac{i}{2} \int \mathrm{d}^4 x \mathrm{d}^4 y \eta(x) \frac{\delta^2 S[\phi_{\text{cl}}]}{\delta \phi(x) \delta \phi(y)} \eta(y) + O(\eta^3) \right) \right].
\end{aligned}
$$
$$(4.11)$$

In the last line, we used the highly non-trivial trick of introducing a counter-term for J, namely $J = J_0 + \Delta J$, and arguing that this counter term is chosen on renormalisation to preserve the relationship $\phi_{\text{cl}} = \langle \phi \rangle_J$ to all loop orders. This is equivalent to stating that all tadpole diagrams vanish because their role is to renormalise the expectation value of the field. This gets rid of the linear terms in η, leaving us with a Gaussian integral (to one loop order, ignoring the $O(\eta^3)$ terms):

$$
E[J(\phi_{\text{cl}})] \approx -S[\phi_{\text{cl}}] - \int \mathrm{d}^4 x J\phi_{\text{cl}} + i \log \left(\det \left[\frac{-i}{2\pi} \frac{\delta^2 S[\phi_{\text{cl}}]}{\delta \phi(x) \delta \phi(y)} \right]^{-1/2} \right). \tag{4.12}
$$

Ultimately, this expression will have to be renormalised since the functional determinant as written is divergent. On doing this, the $-i/2\pi$ factor will become irrelevant as it is merely absorbed into the renormalisation scale. The standard way to approach this is to go to momentum space, and regularised the integrals via MS-bar. Generically we have the effective action:

$$
\Gamma[\phi_{\text{cl}}] = S[\phi_{\text{cl}}] + \frac{i}{2} \operatorname{Tr} \log \left[\frac{-i}{2\pi} \frac{\delta^2 S[\phi_{\text{cl}}]}{\delta \phi(x) \delta \phi(y)} \right]. \tag{4.13}
$$

This must be modified in the case of fermions, because the Gaussian integrals are of a different nature and involve anti-commuting Grassmann variables. Specifically:

$$
\int \mathcal{D}\eta \mathcal{D}\bar{\eta} e^{-\bar{\eta} M \eta} = \det M. \tag{4.14}
$$

This differs from the scalar, bosonic integral by a factor of 2 and a sign (the factor fo 2 is because we are integrating over extra degrees of freedom, and the sign because fermions anti-commute past each other). So for example, in a theory with classical action:

$$
\mathcal{L} = \frac{1}{2} \partial_\mu \phi \partial^\mu \phi + \bar{\Psi}(i\gamma^\mu \partial_\mu - m_\Psi)\Psi - ig\phi \bar{\Psi}\gamma^5 \Psi - \frac{1}{2} m_\phi^2 \phi^2 + \frac{\lambda}{4} \phi^4, \tag{4.15}
$$

we find the effective potential to be, at one loop:

$$V_{1\text{loop}}(\phi) = \frac{1}{2}m_\phi^2\phi^2 + \frac{\lambda}{4}\phi^4 + \frac{M_\phi^4}{64\pi^2}\left(\log\left(\frac{M_\phi^2}{\mu^2}\right) - \frac{3}{2}\right) - \frac{4M_\Psi^4}{64\pi^2}\left(\log\left(\frac{M_\Psi^2}{\mu^2}\right) - \frac{3}{2}\right), \quad (4.16)$$

where $M_\phi^2 = m_\phi^2 + 3\lambda\phi^2$, $M_\Psi = m_\Psi + g\phi$. As expected, the fermions loops give a negative sign compared to their bosonic equivalent, and also come with an extra factor of 4, in this case because the Dirac fermion has four degrees of freedom. Eq. (4.16) gives a hint of how metastable vacua can arise due to quantum corrections, and was first considered by [144]. If the fermion mass, M_Ψ, becomes much larger than the scalar mass, M_ϕ, then we will eventually find that the effective potential goes negative. To see this, we can re-arrange Eq. (4.16) as:

$$\begin{aligned} V_{1\text{loop}}(\phi) = &\frac{m_\phi^4}{64\pi^2}\left[\log\frac{M_\phi^2}{\mu^2} - \frac{3}{2}\right] - \frac{m_\Psi^4}{16\pi^2}\left[\log\frac{M_\Psi^2}{\mu^2} - \frac{3}{2}\right] - \frac{gm_\Psi^3}{\pi^2}\left[\log\frac{M_\Psi^2}{\mu^2} - \frac{3}{2}\right]\phi \\ &- \frac{g^3 m_\Psi}{\pi^2}\left[\log\frac{M_\Psi^2}{\mu^2} - \frac{3}{2}\right]\phi^3 + \frac{1}{2}\phi^2\left\{m_\phi^2 + \frac{3\lambda m_\phi^2}{16\pi^2}\left[\log\frac{M_\phi^2}{\mu^2} - \frac{3}{2}\right] - \frac{3g^2 m_\Psi^2}{4\pi^2}\left[\log\frac{M_\Psi^2}{\mu^2} - \frac{3}{2}\right]\right\} \\ &+ \frac{1}{4}\phi^4\left\{\lambda + \frac{9\lambda^2}{16\pi^2}\left[\log\frac{M_\phi^2}{\mu^2} - \frac{3}{2}\right] - \frac{g^4}{4\pi^2}\left[\log\frac{M_\Psi^2}{\mu^2} - \frac{3}{2}\right]\right\}. \end{aligned} \quad (4.17)$$

This means we can interpret the effective potential as saying that the effective quartic coupling goes negative at some ϕ.

However, there is a problem with this interpretation. There is an explicit dependence on the renormalisation scale, μ here, which seems odd, as this should not affect the physics. Furthermore, it seems that the potential will experience problems if M_ϕ^2 ever goes negative, as might happen in the Standard Model, since negative λ is precisely what precipitates vacuum decay. The potential would appear to be complex there, however, which seems nonsensical. Furthermore, we will also run into the 'large logarithms' problem, namely that if μ is greatly different to M_ϕ or M_Ψ, the logarithmic terms become large, and perturbation theory breaks down. An explicit way to see this is just by asking at what point the effective quartic coupling, λ_{eff}, goes negative. By definition this happens when:

$$-\frac{9\lambda^2}{16\pi^2}\left[\log\frac{M_\phi^2}{\mu^2} - \frac{3}{2}\right] + \frac{g^4}{4\pi^2}\left[\log\frac{M_\Psi^2}{\mu^2} - \frac{3}{2}\right] = \lambda. \quad (4.18)$$

However, this means that the first order loop correction to the effective potential is the same size as the zeroth-order term, which signals the breakdown of perturbation theory. Thus, it seems we cannot reliably use the Coleman-Weinberg potential in precisely the region it is most interesting.

The resolution to these problems is the well known renormalisation group improvement of the effective potential [145, 146, 144, 147]. The idea here is that the true effective potential should be renormalisation group invariant, and thus we can apply the Callan-Symanzik equation [143, 148]:

$$\left(\frac{\partial}{\partial\mu} + \sum_i \beta_i \frac{\partial}{\partial g_i} + \gamma_\phi \phi \frac{\partial}{\partial\phi}\right) V_{\text{eff}}(\phi, g, \mu) = 0. \quad (4.19)$$

To solve this we require an initial condition, which the loop expansion can give as at some ϕ_0 by choosing μ_0 such that the logarithms are as small as possible (for this particular ϕ_0 only -

it is not possible to choose one μ that does this for all ϕ). This gives the boundary condition $V_{\text{eff}}(\phi_0) = V_{\text{1loop}}(\phi_0, g_{i0}, \mu_0)$, which is accurate up to a two-loop error. The solution of the Callan-Symanzik equation with this boundary condition is then:

$$V_{\text{eff}}(\phi, \mu) = V_{\text{1loop}}(\phi(\mu), g_i(\mu), \mu), \qquad (4.20)$$

where:

$$\frac{\mathrm{d}g_i(\mu)}{\mathrm{d}\log\mu} = \beta_i(g_i(\mu)), \qquad (4.21)$$

$$\frac{\mathrm{d}\phi(\mu)}{\mathrm{d}\log\mu} = \gamma_\phi \phi(\mu), \qquad (4.22)$$

subject to boundary conditions $g_i(\mu_0) = g_0, \phi(\mu_0) = \phi_0$. The accuracy here is as good as the accuracy in the beta functions and initial conditions, ie, up to one loop in this case (although the procedure can be repeated at higher loops if required).

4.2   Example - Yukawa Theory

An example model that resembles the behaviour of the Standard Model is Yukawa theory. There are two main variants of this theory, according to whether ϕ is interpreted as a scalar or pseudo-scalar field:

$$\mathcal{L}_{\text{Yuk pseudoscalar}} = \frac{1}{2}\partial_\mu\phi\partial^\mu\phi + \bar{\Psi}(i\gamma^\mu\partial_\mu - m_\Psi)\Psi - \frac{1}{2}m_\phi^2\phi^2 - \frac{\lambda}{4}\phi^4 - ig\bar{\Psi}\gamma^5\Psi\phi, \qquad (4.23)$$

$$\mathcal{L}_{\text{Yuk scalar}} = \frac{1}{2}\partial_\mu\phi\partial^\mu\phi + \bar{\Psi}(i\gamma^\mu\partial_\mu - m_\Psi)\Psi - \frac{1}{2}m_\phi^2\phi^2 - \frac{\lambda}{4}\phi^4 - g\bar{\Psi}\Psi\phi. \qquad (4.24)$$

We will first consider the pseudo-scalar theory, since this lacks linear and cubic terms by parity symmetry. The Feynman rules for this theory are shown in figure 4.2. The purpose of the $i\gamma^5$ term here is to preserve parity symmetry for the pseudo-scalar field ϕ. Another way to see this is that the three-point ϕ^3 interaction does not receive any loop correction (see fig. 4.3) because is vanishes identically. The loop correction in that case is:

$$\Gamma_{\phi^3} = -g^3 \int \frac{\mathrm{d}^4 p}{(2\pi)^4} \frac{\mathrm{Tr}(i[(\not{p} + m_\Psi)\gamma^5 i((\not{p} + \not{k}_2) + m_\Psi)\gamma^5 i((\not{p} - \not{k}_1) + m_\Psi)\gamma^5])}{(p^2 - m_\Psi^2)((p + k_2)^2 - m_\Psi^2)((p - k_1)^2 - m_\Psi^2)} = 0, \qquad (4.25)$$

which vanishes identically because the trace of γ^5 multiplied by any number of gamma matrices fewer than four is zero: $\mathrm{Tr}(\gamma^5) = \mathrm{Tr}(\gamma^5\gamma^\mu) = \mathrm{Tr}(\gamma^5\gamma^\mu\gamma^\nu) = \mathrm{Tr}(\gamma^5\gamma^\mu\gamma^\nu\gamma^\rho) = 0$. The way that fermions affect the self-coupling λ can be understood by computing the beta functions of the theory, which we do now. First, we split the theory into renormalised and counter terms:

$$\mathcal{L}_{\text{Yuk}} = \frac{1}{2}\partial_\mu\phi_R\partial^\mu\phi_R + \bar{\Psi}_R(i\gamma^\mu\partial_\mu - m_{\Psi R})\Psi_R - \frac{1}{2}m_{\phi R}^2\phi_R^2 - \frac{\lambda}{4}\phi_R^4 - ig_R\bar{\Psi}_R\gamma^5\Psi_R$$
$$+ \frac{1}{2}\delta Z_\phi\partial_\mu\phi_R\partial^\mu\phi_R + \delta Z_\Psi\bar{\Psi}_R i\gamma^\mu\partial_\mu\Psi_R - \delta m_\Psi\bar{\Psi}_R\Psi_R - \frac{1}{2}\delta m_\phi^2\phi_R^2 - \frac{\delta\lambda}{4}\phi_R^4 - i\delta g\bar{\Psi}_R\gamma^5\Psi_R, \qquad (4.26)$$

74

$$= -6i\lambda$$

$$= \frac{i}{k^2 - m_\phi^2}$$

$$= -6i\delta\lambda$$

$$\bar{\Psi}_\beta \longrightarrow \Psi_\alpha \qquad = \frac{i(\gamma^\mu k_\mu + m_\Psi)_{\alpha\beta}}{k^2 - m_\Psi^2}$$

$$= g\gamma^5_{\alpha\beta}$$

$$= i(k^2\delta Z_\phi - \delta m_\phi^2)$$

$$= \delta g\gamma^5_{\alpha\beta}$$

$$= i(\gamma^\mu_{\alpha\beta}k_\mu\delta Z_\Psi - \delta m_\Psi)$$
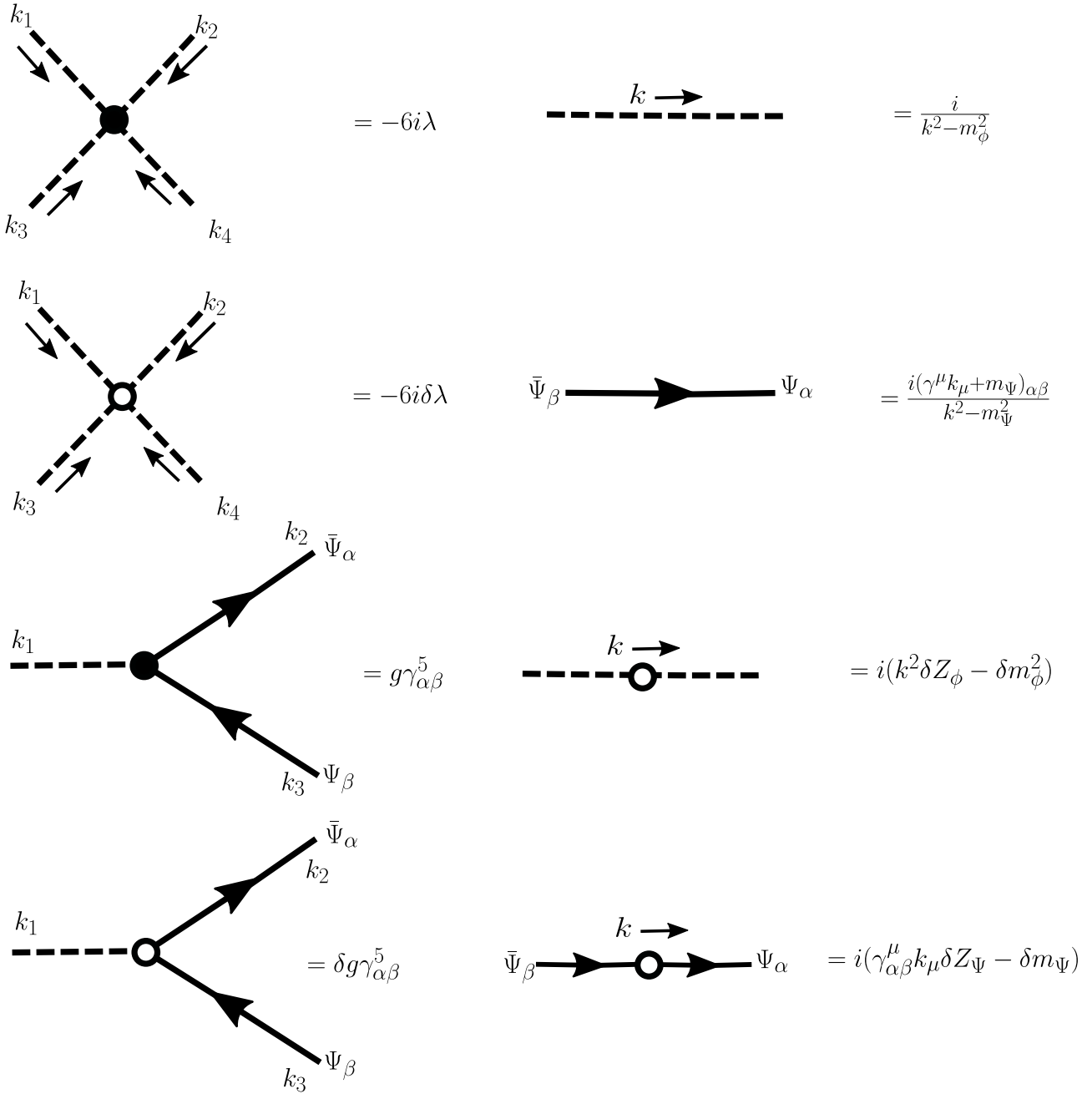
Figure 4.2: Feynman rules for the Yukawa theory of Eq. (4.23), including counter terms (hollow circular vertices).
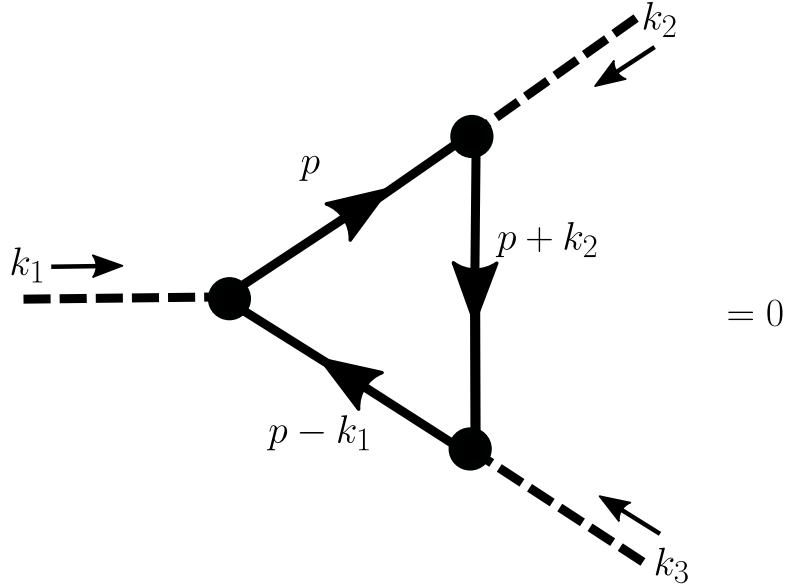
Figure 4.3: Loop correction to the point correlation function in a Yukawa theory with a $-ig\bar{\Psi}\Gamma^5\Psi$ type interaction. This vanishes identically due to parity symmetry, protecting the ϕ^3 and ϕ terms from receiving quantum corrections. However, this is not the case with a $-g\bar{\Psi}\Psi$ type interaction, which does not respect parity invariance.

where the counter terms and renormalised couplings are defined by:

$$Z_\phi m_{\phi B}^2 = m_{\phi R}^2 + \delta m_\phi^2, \tag{4.27}$$

$$Z_\phi^2 \lambda_B = \lambda_R + \delta\lambda, \tag{4.28}$$

$$Z_\Psi Z_\phi^{1/2} g_B = g_R + \delta g, \tag{4.29}$$

$$Z_\Psi m_{\Psi B} = m_{\Psi R} + \delta m_\Psi, \tag{4.30}$$

$$Z_\phi = 1 + \delta Z_\phi, \phi_B = Z_\phi^{1/2}\phi_R, \tag{4.31}$$

$$Z_\Psi = 1 + \delta Z_\Psi, \Psi_B = Z_\Psi^{1/2}\Psi_R. \tag{4.32}$$

A generic expression for the beta function of coupling g_i associated to operator $\phi_1^{n_1}\phi_2^{n_2}\ldots\phi_m^{n_m}$ where ϕ_i are independent fields and the counter terms are defined by $g_{iB}Z_1^{n_1/2}Z_2^{n_2/2}\ldots Z_m^{n_m/2} = g_{iR} + \delta G_i$ is:

$$\beta_{g_i} = \frac{\partial g_{iR}}{\partial \log M} = \sum_{a=1}^{m}\left[g_{iB}Z_1^{n_1/2}Z_2^{n_2/2}\ldots Z_m^{n_m/2}n_a\frac{1}{2Z_a}\frac{\partial Z_a}{\partial \log M}\right] - \frac{\partial \delta g_i}{\partial \log M}. \tag{4.33}$$

Thus, to compute the beta functions, we need to evaluate the relevant counter term and the field renormalisation factors, Z. To do this, we compute the 1PI correlation functions $\Gamma_{\phi^2}, \Gamma_{\bar{\Psi}\Psi}, \Gamma_{\phi^4}, \Gamma_{\phi\bar{\Psi}\Psi}$ respectively and regularise them using $\overline{\text{MS}}$.
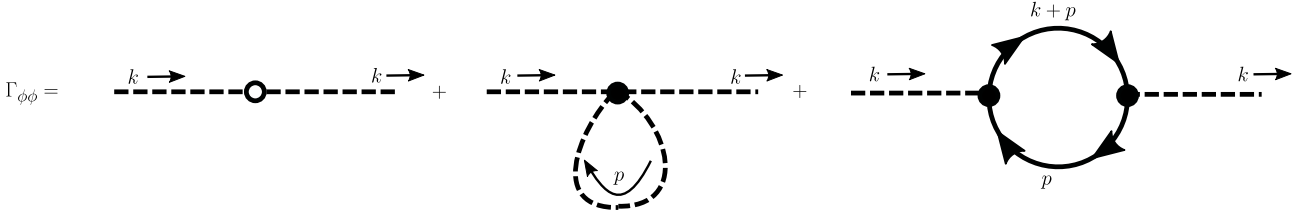
Figure 4.4: 1-loop diagrams contributing to the scalar propagator, $\Gamma_{\phi\phi}(k^2)$.

The 2-point 1PI function for scalar fields is given by (see fig. 4.4):

$$\Gamma_{\phi\phi}(k^2) = i(k^2\delta Z_\phi - \delta m_\phi^2) + \frac{3\lambda_R i m_{\phi R}^2}{16\pi^2}\left(\frac{2}{\epsilon} + \log\frac{4\pi\mu^2}{m_{\phi R}^2} + 1 - \gamma_E\right) +$$

$$-\frac{4g_R^2 i m_{\Psi R}^2}{16\pi^2}\left(\frac{2}{\epsilon} + \log\frac{4\pi\mu^2}{m_{\Psi R}^2} + 1 - \gamma_E\right)$$

$$+\frac{2g_R^2 i k^2}{16\pi^2}\left(\frac{2}{\epsilon} + \log\frac{4\pi\mu^2}{m_{\Psi R}^2} + 1 - \gamma_E\right) + f_{\phi\phi}(k, m_{\Psi R}, m_{\phi R}^2, g_R, \lambda_R), \qquad (4.34)$$

where $\gamma_E \approx 0.5772\ldots$ is the Euler-Mascheroni constant and $f_{\phi\phi}$ is a complicated, finite contribution depending on the precise kinematics. Such terms do not interest us here, as we are only interested in the divergent pieces which determine the beta functions. From this we determine the δZ_ϕ and δm_ϕ^2 counter terms:

$$\delta Z_\phi = -\frac{2g_R^2}{16\pi^2}\left(\frac{2}{\epsilon} + \log\frac{4\pi\mu^2}{M^2} - \gamma_E\right), \qquad (4.35)$$

$$\delta m_\phi^2 = \frac{3\lambda_R m_{\phi R}^2 - 4g_R^2 m_{\Psi R}^2}{16\pi^2}\left(\frac{2}{\epsilon} + \log\frac{4\pi\mu^2}{M^2} - \gamma_E\right). \qquad (4.36)$$

Note that this is different to the pure scalar theory, in which $\delta Z_\phi = 0$ at the one loop level.

Next we compute the 2-point function for fermions, $\Gamma_{\bar\Psi\Psi}$ (fig. 4.5):
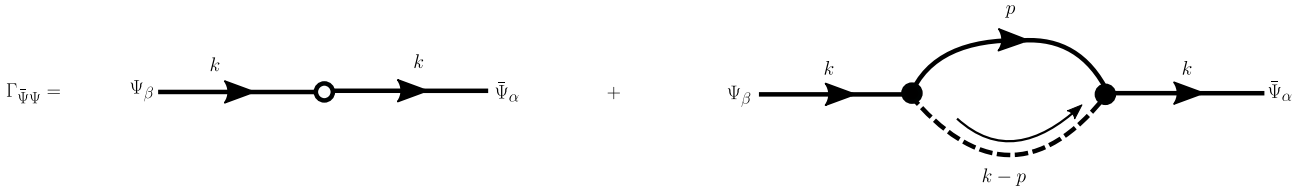
Figure 4.5: Diagrams contributing at one loop to the 1PI two-point function for the fermion in Yukawa theory, including counter terms.

$$\Gamma_{\bar\Psi\Psi} = i(\slashed{k}_{\alpha\beta}\delta Z_\Psi - \delta m_\Psi) - \frac{ig_R^2}{16\pi^2}\left(-\frac{\slashed{k}_{\alpha\beta}}{2} + m_{\Psi R}\right)\left(\frac{2}{\epsilon} + \log\frac{4\pi\mu^2}{m_{\Psi R}^2} - \gamma_E\right) + f_{\Psi\Psi}(k, m_{\Psi R}, m_{\phi R}^2, g_R, \lambda_R),$$
$$(4.37)$$

where $f_{\Psi\Psi}$ is another finite kinematic function. From this we deduce:

$$\delta Z_\Psi = -\frac{g_R^2}{32\pi^2}\left(\frac{2}{\epsilon} + \log\frac{4\pi\mu^2}{M^2} - \gamma_E\right), \qquad (4.38)$$

$$\delta m_\Psi = -\frac{g_R^2 m_{\Psi R}}{16\pi^2}\left(\frac{2}{\epsilon} + \log\frac{4\pi\mu^2}{M^2} - \gamma_E\right). \qquad (4.39)$$
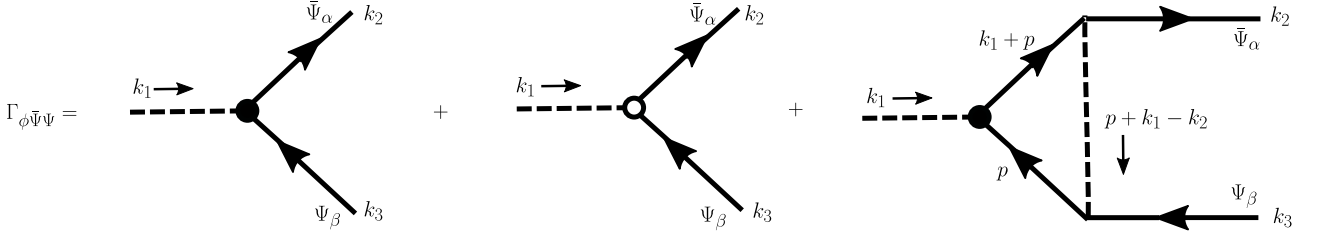
Figure 4.6: Diagrams contributing at one loop to the 1PI three-point ($\phi\bar{\Psi}\gamma^5\Psi$) in Yukawa theory, including counter terms.

The three-point Yukawa interaction function is given by (fig. 4.6):

$$\Gamma_{\phi\bar{\Psi}\Psi} = g_R\gamma^5_{\alpha\beta} + \delta g\gamma^5_{\alpha\beta} - \frac{g_R^3\gamma^5_{\alpha\beta}}{16\pi^2}\left(\frac{2}{\epsilon} + \log\frac{4\pi\mu^2}{m_{\Psi R}^2} - \gamma_E\right) + f_{\phi\bar{\Psi}\Psi}(k_1, k_2, k_3, m_{\Psi R}, m_{\phi r}^2, g_R, \lambda_R), \tag{4.40}$$

giving a counter term:

$$\delta g = \frac{g_R^3}{16\pi^2}\left(\frac{2}{\epsilon} + \log\frac{4\pi\mu^2}{M^2} - \gamma_E\right). \tag{4.41}$$

Finally the four-point function for the scalar field, Γ_{ϕ^4} (fig. 4.7) is given by:
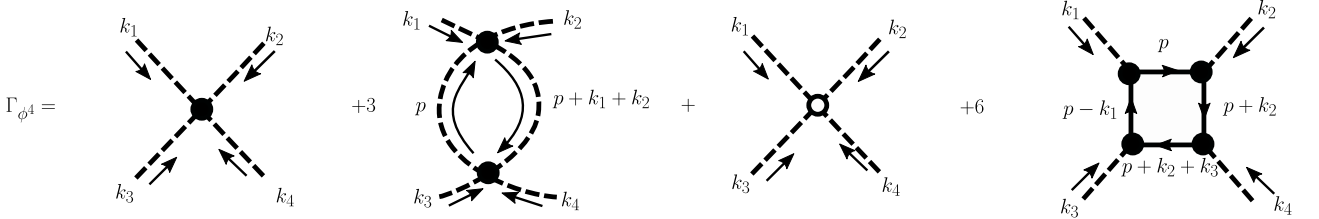
Figure 4.7: Diagrams contributing at one loop to the 1PI four-point function for ϕ in Yukawa theory, including counter terms. Note that the scalar loop diagram has 3 possible configurations tying up the external momenta, while the fermion box diagram has 6. Each of these configurations have different kinematic factors, but the same divergence, which multiplies the overall divergence.

$$\Gamma_{\phi^4} = -6i\lambda_R - 6i\delta\lambda + \frac{54\lambda_R^2 i - 24g_R^4 i}{i16\pi^2}\left(\frac{2}{\epsilon} + \log\frac{4\pi\mu^2}{m_{\phi R}^2} - \gamma_E\right) + f_{\phi^4}(k_1, k_2, k_3, k_4, m_{\Psi R}, m_{\phi R}^2, g_R, \lambda_R). \tag{4.42}$$

Hence the final counter term is:

$$\delta\lambda = \frac{9\lambda_R^2 - 4g_R^4}{16\pi^2}\left(\frac{2}{\epsilon} + \log\frac{4\pi\mu^2}{M^2} - \gamma_E\right). \tag{4.43}$$

Using Eq. (4.33), this means that the beta functions are:

$$\beta_\lambda = \frac{\mathrm{d}\lambda_R}{\mathrm{d}\log M} = \frac{1}{16\pi^2}(18\lambda_R^2 + 8\lambda_R g_R^2 - 8g_R^4),$$

(4.44)

$$\beta_g = \frac{\mathrm{d}g_R}{\mathrm{d}\log M} = \frac{5g_R^3}{16\pi^2},$$

(4.45)

$$\beta_{m_\phi^2} = \frac{\mathrm{d}m_{\phi R}^2}{\mathrm{d}\log M} = \frac{m_{\phi R}^2}{16\pi^2}(6\lambda_R + 4g_R^2(m_{\phi R}^2 - 2m_{\Psi R}^2)),$$

(4.46)

$$\beta_{m_\Psi} = \frac{\mathrm{d}m_{\Psi R}}{\mathrm{d}\log M} = -\frac{m_{\Psi R}g_R^2}{16\pi^2},$$

(4.47)

while the anomalous dimensions are:

$$\gamma_\phi = \frac{1}{Z_\phi^{1/2}}\frac{\mathrm{d}Z_\phi^{1/2}}{\mathrm{d}\log M} = \frac{2g_R^2}{16\pi^2},$$

(4.48)

$$\gamma_\Psi = \frac{1}{Z_\Psi^{1/2}}\frac{\mathrm{d}Z_\Psi^{1/2}}{\mathrm{d}\log M} = \frac{g_R^2}{32\pi^2}.$$

(4.49)

We can do essentially the same thing with the $-g\phi\bar{\Psi}\Psi$ theory if we wish. In that case, however, there will be diagrams like fig. (4.3) that do not vanish identically. To remove divergences like this, we require a $\lambda_3\phi^3/3$ term in the Lagrangian. In the Standard Model, this is forbidden by the requirement of $SU(2)$ symmetry for the Higgs doublet, but in this model it is in principle allowed. If we include it, we obtain additional diagrams (see figs. 4.8 and 4.9). We will also need to write the Lagrangian as:

$$\mathcal{L}_{\text{Yuk}} = \frac{1}{2}\partial_\mu\phi\partial^\mu\phi + \bar{\Psi}(i\gamma^\mu\Psi - m_\Psi)\Psi - \frac{1}{2}m_\phi^2\phi^2 - \lambda_1\phi - \frac{\lambda_3}{3}\phi^3 - \frac{\lambda}{4}\phi^4 - g\phi\bar{\Psi}\Psi.$$

(4.50)

Note that tadpole diagrams renormalising λ_1 do not contribute to higher n 1PI diagrams, as when included they can always be split into two diagrams. Including the diagrams of fig. 4.10, we find for Γ_ϕ:

$$\Gamma_\phi = -i\lambda_{1R} - i\delta\lambda_1 + \frac{\lambda_{3R}im_{\phi R}^2}{16\pi^2}\left(\frac{2}{\epsilon} + 1 - \gamma_E + \log\frac{4\pi\mu^2}{m_\phi^2}\right) - \frac{4g_R im_{\Psi R}^3}{16\pi^2}\left(\frac{2}{\epsilon} + 1 - \gamma_E + \log\frac{4\pi\mu^2}{m_{\Psi R}^2}\right).$$

(4.51)

Consequently the counter term $\delta\lambda_1$ defined by $\lambda_{1B}Z_\phi^{1/2} = \lambda_{1R} + \delta\lambda_1$ is:

$$\delta\lambda_1 = \frac{\lambda_{3R}m_{\phi R}^2 - 4g_R m_{\Psi R}^3}{16\pi^2}\left(\frac{2}{\epsilon} - \gamma_E + \log\frac{4\pi\mu^2}{M^2}\right).$$

(4.52)

Likewise we compute $\delta\lambda_3$ defined by $\lambda_{3B}Z_\phi^{3/2} = \lambda_{3R} + \delta\lambda_3$. In this case, the final triangle diagram with three 3-point scalar vertices gives only a finite contribution, so doesn't affect the counter term. We find:

$$\Gamma_{\phi^3} = -2i\lambda_{3R} - 2i\delta\lambda_3 + \frac{6\lambda_R\lambda_{3R}i}{16\pi^2}\left(\frac{2}{\epsilon} - \gamma_E + \log\frac{4\pi\mu^2}{m_{\phi}^2}\right) - \frac{3g_R^3 m_{\Psi R}i}{16\pi^2}\left(\frac{2}{\epsilon} - \gamma_E + \log\frac{4\pi\mu^2}{m_{\Psi R}^2}\right) + \text{(finite terms)}.$$

(4.53)

Thus:

$$\delta\lambda_3 = \frac{(3\lambda_R\lambda_{3R} - \frac{3}{2}g_R^3 m_{\Psi R})}{16\pi^2}\left(\frac{2}{\epsilon} - \gamma_E + \log\frac{4\pi\mu^2}{M^2}\right).$$

(4.54)

We now seek to compute Γ_{ϕ^4}. Note that the only additional diagram here is the scalar box diagram in figure 4.8, however this gives only a finite contribution. The fermion diagram changes, however, due to the absence of the $i\gamma^5$ terms. We have to recompute the trace of the divergent part:

$$\mathrm{Tr}([i(\not{p}+m_{\Psi R})]^4) = \mathrm{Tr}(\not{p}^4 + 4m_{\Psi R}\not{p}^3 + 6m_{\Psi R}^2\not{p}^2 + 4m_{\Psi R}^3\not{p} + m_{\Psi R}^4) = 4(p^2 - m_{\Psi R}^2)^2 + 32p^2 m_{\Psi R}^2, \tag{4.55}$$

$$\mathrm{Tr}([i(\not{p}+m_{\Psi R})i\gamma^5]^4) = \mathrm{Tr}([(\not{p}+m_{\Psi R})(-\not{p}+m_{\Psi R})]^2) = 4(p^2 - m_{\Psi R^2})^2. \tag{4.56}$$

These differ by a term $32p^2 m_{\Psi R}^2$, however, as the denominator is $(p^2 - m_{\Psi R}^2)^4$, this does not matter - it contributes only to the finite terms so doesn't affect the counter term. Thus, the difference between using $i\gamma^5$ in the Yukawa coupling or not yields only a finite piece in the fermion box diagram, and has no affect on the divergence. Consequently, we can use the same result as in the $-ig\phi\bar{\Psi}\gamma^5\Psi$ theory:

$$\delta\lambda = \frac{9\lambda_R^2 - 4g_R^4}{16\pi^2}\left(\frac{2}{\epsilon} + \log\frac{4\pi\mu^2}{M^2} - \gamma_E\right). \tag{4.57}$$

Similarly, fig. 4.9 shows that we have an additional diagram contributing to δg, but this is also finite, so doesn't change the counter term. Hence:

$$\delta g = \frac{g_R^3}{16\pi^2}\left(\frac{2}{\epsilon} - \gamma_E + \log\frac{4\pi\mu^2}{M^2}\right). \tag{4.58}$$

The most significant changes occur in Γ_{ϕ^2} and $\Gamma_{\bar{\Psi}\Psi}$. From figure 4.8 we see that Γ_{ϕ^2} has an extra scalar loop. The fermion loop is also different due to the lack of $i\gamma^5$ terms. Putting these together we find:

$$\Gamma_{\phi^2} = i(k^2\delta Z_\phi - \delta m_\phi^2) + \frac{3\lambda_R m_{\phi R}^2 i}{16\pi^2}\left(\frac{2}{\epsilon} + \log\frac{4\pi\mu^2}{m_{\phi R}^2} + 1 - \gamma_E\right) - \frac{12g_R^2}{16\pi^2}(m_{\Psi R} - \frac{k^2}{6})\left(\frac{2}{\epsilon} - \gamma_E + \log\frac{4\pi\mu^2}{m_{\Psi R}^2}\right). \tag{4.59}$$

The important change for the fermion contribution here is a change in sign for the k^2 dependent piece, due to the lack of $i\gamma^5$ pieces. From this we extract:

$$\delta m_\phi^2 = \frac{3\lambda_R m_{\phi R}^2 + 2\lambda_3^2 - 12g_R^2 m_{\Psi R}^2}{16\pi^2}\left(\frac{2}{\epsilon} - \gamma_E + \log\frac{4\pi\mu^2}{M^2}\right), \tag{4.60}$$

$$\delta Z_\phi = -\frac{2g_R^2}{16\pi^2}\left(\frac{2}{\epsilon} - \gamma_E + \log\frac{4\pi\mu^2}{M^2}\right). \tag{4.61}$$

Note that the anomalous dimension is unchanged for ϕ. Finally we compute $\Gamma_{\bar{\Psi}\Psi}$. No additional diagrams appear at one-loop level, but the different coupling produces a different result:

$$\Gamma_{\bar{\Psi}\Psi} = i(\not{k}\Delta Z_\Psi - \delta m_\Psi) + \frac{ig_R^2}{16\pi^2}\left(\frac{\not{k}}{2} + m_{\Psi R}\right)\left(\frac{2}{\epsilon} - \gamma_E + \log\frac{4\pi\mu^2}{m_{\Psi R}^2}\right) + (\text{finite terms}). \tag{4.62}$$

Hence, δZ_Ψ is unchanged, but, δm_Ψ is:

$$\delta Z_\Psi = -\frac{g_R^2}{32\pi^2}\left(\frac{2}{\epsilon} - \gamma_E + \log\frac{4\pi\mu^2}{M^2}\right), \tag{4.63}$$

$$\delta m_\Psi = \frac{g_R^2}{16\pi^2}\left(\frac{2}{\epsilon} - \gamma_E + \log\frac{4\pi\mu^2}{M^2}\right). \tag{4.64}$$

Putting these all together, the beta functions are:

$$\beta_\lambda = \frac{1}{16\pi^2} \left(18\lambda_R^2 + 8\lambda_R g_R^2 - 8g_R^4\right), \tag{4.65}$$

$$\beta_{\lambda_1} = \frac{1}{16\pi^2} \left(2\lambda_{1R} g_R^2 + 2\lambda_{3R} m_{\phi R}^2 - 8g_R m_{\Psi R}^3\right), \tag{4.66}$$

$$\beta_{\lambda_3} = \frac{1}{16\pi^2} \left(6\lambda_{3R} g_R^2 + 6\lambda_R \lambda_{3R} - 3g_R^2 m_{\Psi R}\right), \tag{4.67}$$

$$\beta_g = \frac{5g_R^3}{16\pi^2}, \tag{4.68}$$

$$\beta_{m_\phi^2} = \frac{1}{16\pi^2} \left(4g_R^2(m_{\phi R}^2 - 3m_{\Psi R}^2) + 6\lambda_R m_{\phi R}^2 + 4\lambda_3^2\right), \tag{4.69}$$

$$\beta_{m_\Psi} = \frac{5m_{\Psi R} g_R^2}{16\pi^2}. \tag{4.70}$$

Note that setting $m_{\Psi R} = \lambda_{3R} = \lambda_{1R} = 0$ is consistent, as this describes a fixed point of the beta functions. This gives the especially simple effective potential:

$$\begin{aligned}
V_{\text{eff}}(\phi_{\text{cl}}) = &\frac{1}{2}m_{\phi R}^2(\mu)Z_\phi(\mu)\phi_{\text{cl}}^2 + \frac{\lambda_R(\mu)}{4}Z_\phi^2(\mu)\phi_{\text{cl}}^4 \\
&+ \frac{(m_{\phi R}^2(\mu) + \lambda_R(\mu)Z_\phi(\mu)\phi_{\text{cl}}^2)^2}{64\pi^2}\left[\log\frac{(m_{\phi R}^2(\mu) + 3\lambda_R(\mu)Z_\phi(\mu)\phi_{\text{cl}}^2)}{\mu^2} - \frac{3}{2}\right] \\
&- \frac{4g_R^4(\mu)Z_\phi^2(\mu)\phi_{\text{cl}}^4}{64\pi^2}\left[\log\frac{g_R^2(\mu)Z_\phi(\mu)\phi_{\text{cl}}^2}{\mu^2} - \frac{3}{2}\right],
\end{aligned} \tag{4.71}$$

where we can solve the beta functions for $g_R(\mu)$, $\lambda_R(\mu)$ and $m_{\phi R}^2(\mu)$ analytically. For example:

$$g(\mu) = \frac{g_0}{\sqrt{1 - \frac{10g_0^2}{16\pi^2}\log\frac{\mu}{\mu_0}}}, \tag{4.72}$$

where $g(\mu_0) = g_0$. The result for $\lambda_R(\mu)$ and $m_{\phi R}(\mu)$ is complicated - and unenlightening. An example with $\lambda(\mu_0) = 0.05$, $g(\mu_0) = 0.45$ is plotted in fig. 4.11. The effective potential Eq. (4.71) is plotted in figure 4.12. The essential point is that we have a one-loop expression for the effective potential, evaluated at scale μ. What value of μ should we choose? The conventional choice is to pick $\mu = \phi$, which ensures that μ is at least the same order of magnitude as M_ϕ and M_Ψ. In general, however, there is no perfect way to do this when multiple mass scales are involved. Several methods have been proposed to deal with this, including using different renormalisation scales for different couplings [149, 150, 151], and decoupling methods [145, 152]. Other methods that have been proposed include [153], and a more recent method of selecting the renormalisation scale in a field dependent manner, $\mu(\phi)$, such that the loop corrections vanish [154, 3]. We considered this method in our recent paper, [3], which we will summarise later in this chapter. There is still much to be understood about how this should properly be done, however [155, 154, 3], and it is unclear whether it is possible to choose the scale in a systematic way that works for all cases.
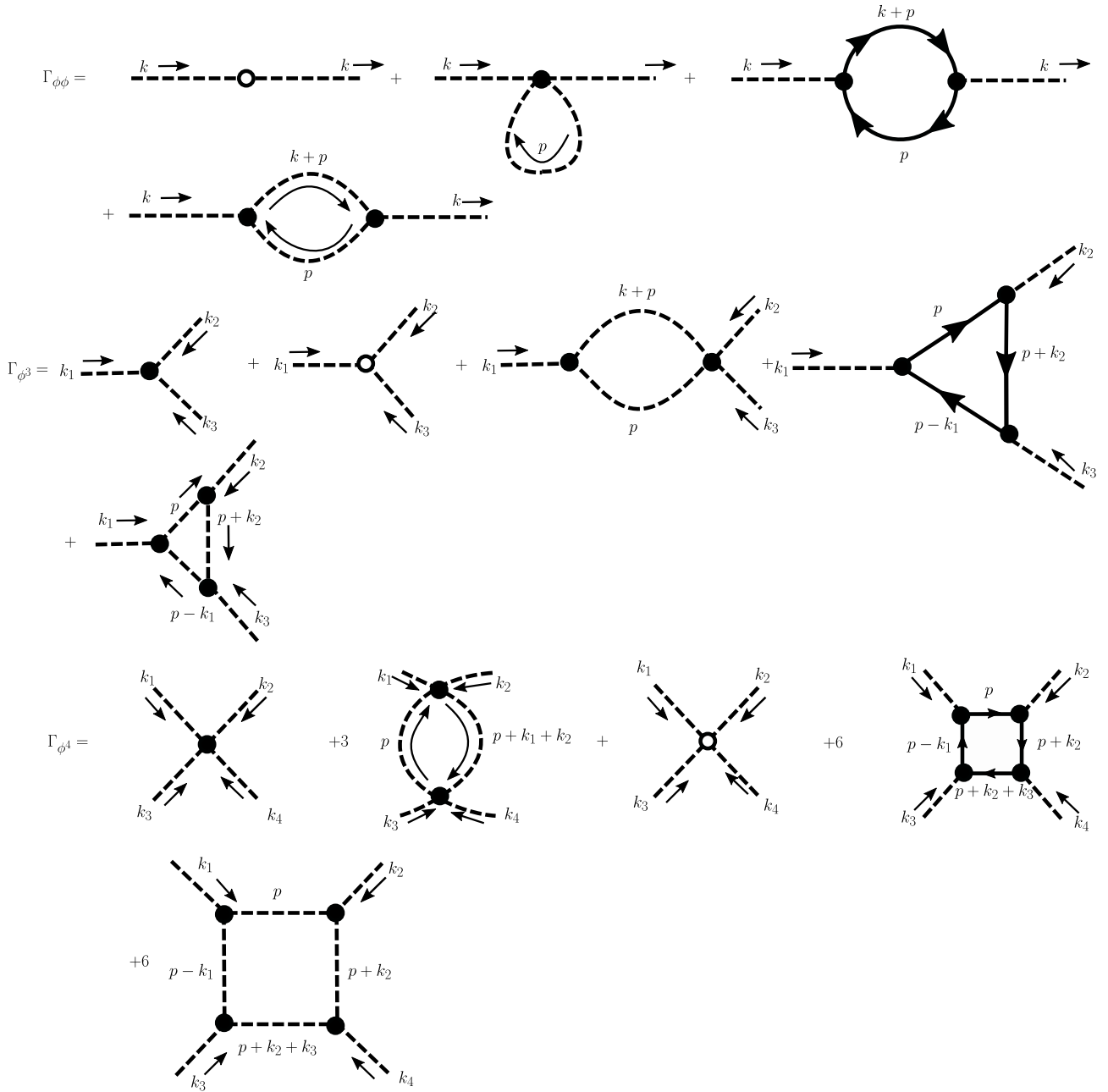
Figure 4.8: Diagrams contributing to the renormalisation of the scalar n-point functions in $ig\phi\bar{\Psi}\Psi$ theory.
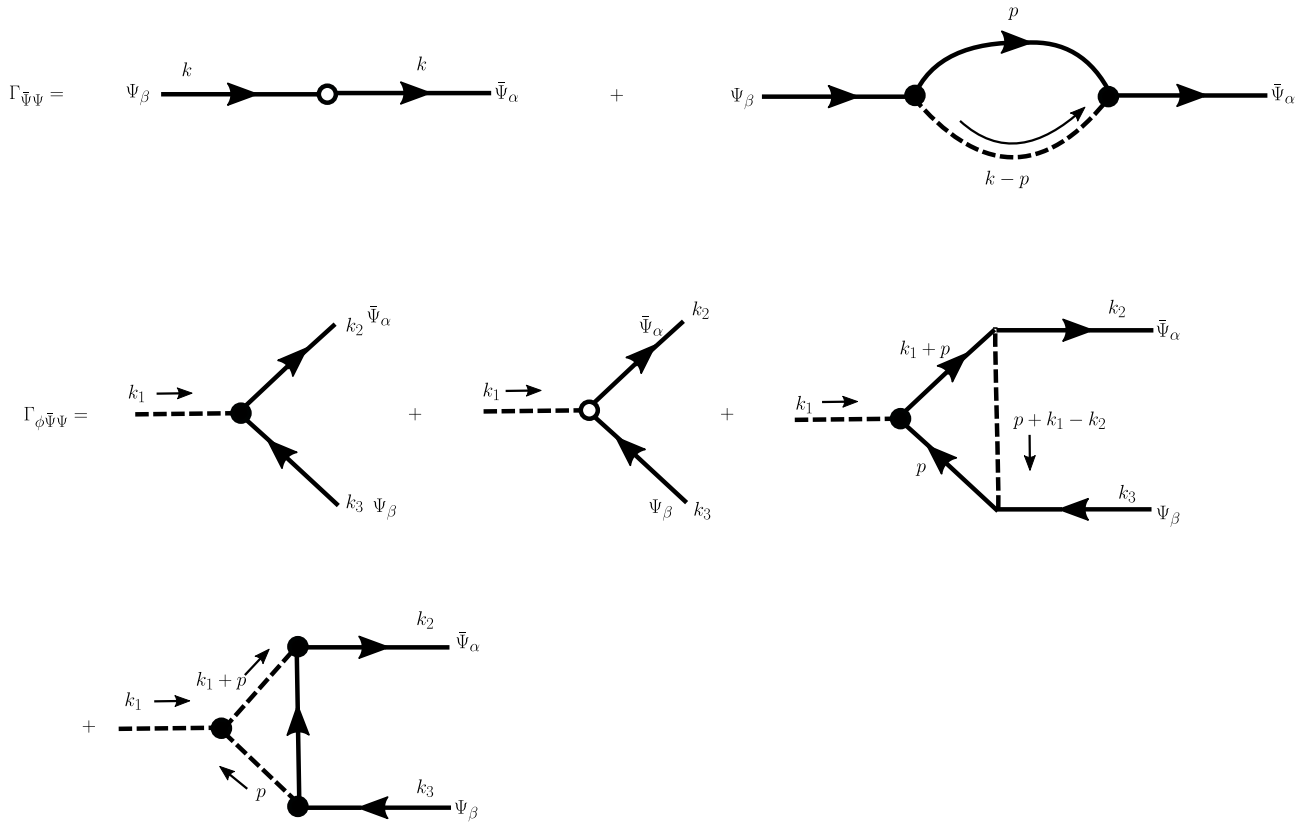
Figure 4.9: Diagrams contributing to the renormalisation of the fermion n-point functions in $ig\phi\bar{\Psi}\Psi$ theory. The only change is the last triangle diagram in $\Gamma_{\phi\bar{\Psi}\Psi}$, which gives only a finite contribution.

Figure 4.10: Tadpole diagrams contributing to the renormalisation of λ_1.
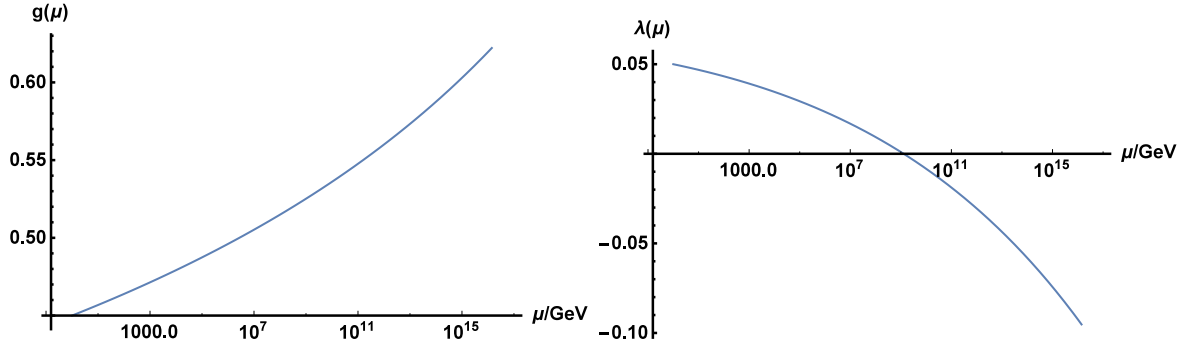
(a) Running of the Yukawa coupling, g, in the scalar model for $g_0 = 0.45, \lambda_0 = 0.05$.

(b) Running of the self-coupling, λ, in the scalar model for $g_0 = 0.45, \lambda_0 = 0.05$.
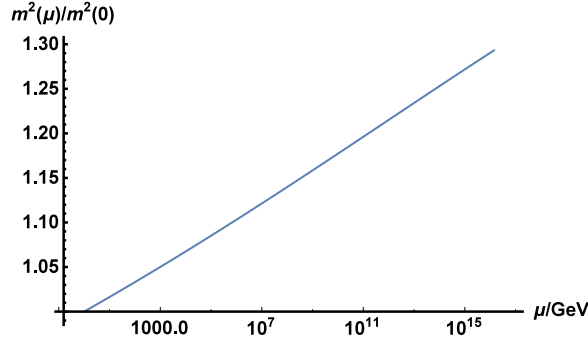
(c) Running of the scalar mass squared, m_ϕ^2, in the scalar model for $g_0 = 0.45, \lambda_0 = 0.05$.

Figure 4.11
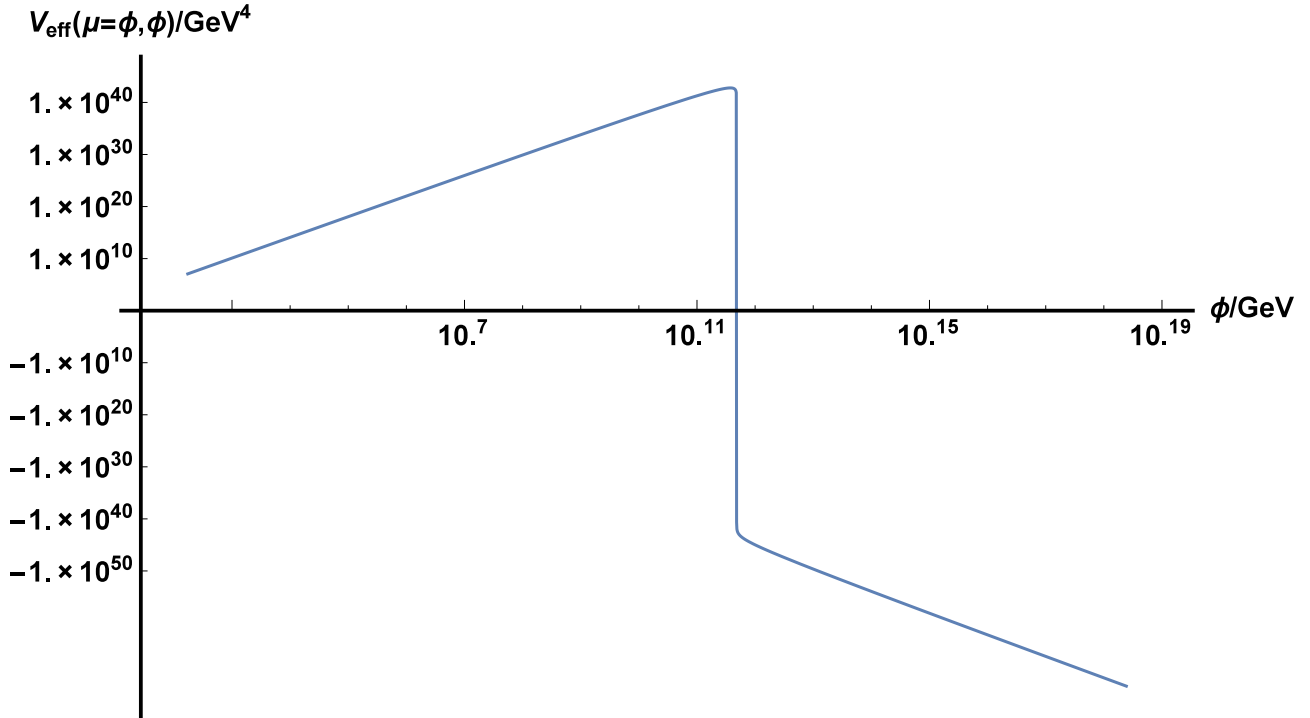
Figure 4.12: Renormalisation group improved effective potential for the scalar Yukawa theory with $g_0 = 0.45, \lambda_0 = 0.05$. The y axis is scaled with $\mathrm{sign}(y)\log(1 + |y|)$ to display all features logarithmically, including negative V regions.

4.3 Standard Model Effective Potential

For realistic calculations, we need to know the effective potential of the Standard Model. In particular, we need to perform its renormalisation group improvement. This requires the beta functions. To one loop, these are [156, 35, 10, 157, 158, 159]:

$$\beta_{y_t} = \frac{y_t}{16\pi^2} \left[\frac{3}{2}(y_t^2 - y_b^2) + Y_2 - \left(\frac{17}{12}(g')^2 + \frac{9}{4}g^2 + 8g_3^2 \right) \right], \tag{4.73}$$

$$\beta_{y_b} = \frac{y_b}{16\pi^2} \left[\frac{3}{2}(y_b^2 - y_t^2) + Y_2 - \left(\frac{5}{12}(g')^2 + \frac{9}{4}g^2 + 8g_3^2 \right) \right], \tag{4.74}$$

$$\beta_{y_l} = \frac{y_l}{16\pi^2} \left[\frac{3}{2}y_l^2 + Y_2 - \left(\frac{45}{12}(g')^2 + \frac{9}{4}g^2 \right) \right], \tag{4.75}$$

$$\beta_\lambda = \frac{1}{16\pi^2} \left(24\lambda^2 - 3\lambda \left((g')^2 + 3g^2 \right) + \frac{3}{4} \left(\frac{1}{2}(g')^4 + (g')^2g^2 + \frac{3}{2}g^4 \right) + 4Y_2\lambda - 2Y_4 \right), \tag{4.76}$$

$$\beta_{m^2} = \frac{m^2}{16\pi^2} \left[12\lambda - \frac{3}{2}(g')^2 - \frac{9}{2}g^2 + 2Y_2 \right], \tag{4.77}$$

$$\beta_{g'} = \frac{41}{6} \frac{(g')^3}{16\pi^2}, \tag{4.78}$$

$$\beta_g = -\frac{19}{6} \frac{g^3}{16\pi^2}, \tag{4.79}$$

$$\beta_{g_3} = -7 \frac{g_3^4}{16\pi^2}, \tag{4.80}$$

$$Y_2 \equiv 3(y_u^2 + y_c^2 + y_t^2) + 3(y_d^2 + y_s^2 + y_b^2) + (y_e^2 + y_\mu^2 + y_\tau^2),$$

$$Y_4 \equiv 3(y_u^4 + y_c^4 + y_t^4) + 3(y_d^4 + y_s^4 + y_b^4) + (y_e^4 + y_\mu^4 + y_\tau^4), \tag{4.81}$$

where β_{y_l} is the lepton beta function for $l = e, \mu, \tau$. For reference, g' is the $U(1)$ coupling, which can be related to the frequently used SU(5) normalisation by $g' = \sqrt{\frac{3}{5}}g_1$. g is the SU(2) coupling, and g_3 the $SU(3)$ coupling. Beta functions for the other generations of fermions can be obtained from eqs. (4.73) and (4.74) by substituting $y_t \to y_u, y_c$ and $y_b \to y_d, y_s$, leaving the gauge couplings and Y_2 the same.

For the calculation in [1, 2], and chapters 5 and 6 we in fact used the three loop running, available in the literature [35, 160, 161]. In that case, we approximated the Standard Model effective potential as:

$$V_{\text{eff}}(h) \approx \frac{\lambda(h)}{4}h^4, \tag{4.82}$$

which is equivalent to the scale choice $\mu = \phi 4$ and ignoring field renormalisation. This is a good approximation at large field values, since the quartic term is dominant and the scale choice $\mu = \phi$ is intended to suppress the size of the loop corrections to the Coleman Weinberg potential. This potential is plotted in figure 4.13.

For numerical calculations, it is computationally expensive to integrate the beta functions every time we wish to evaluate the effective potential. To avoid this, we solve the 3-loop beta functions (available, for example, at [161]), and take the discrete data of the couplings (t_n, g_{in}) where $t = \log(\mu)$ as the input for a piecewise polynomial potential, that is, we fit a polynomial to running $\lambda(\mu)$ between each set of adjacent points (t_n, t_{n+1}) (we do this in log space since the potential varies slowly with respect to μ so is not well represented by a polynomial). There are
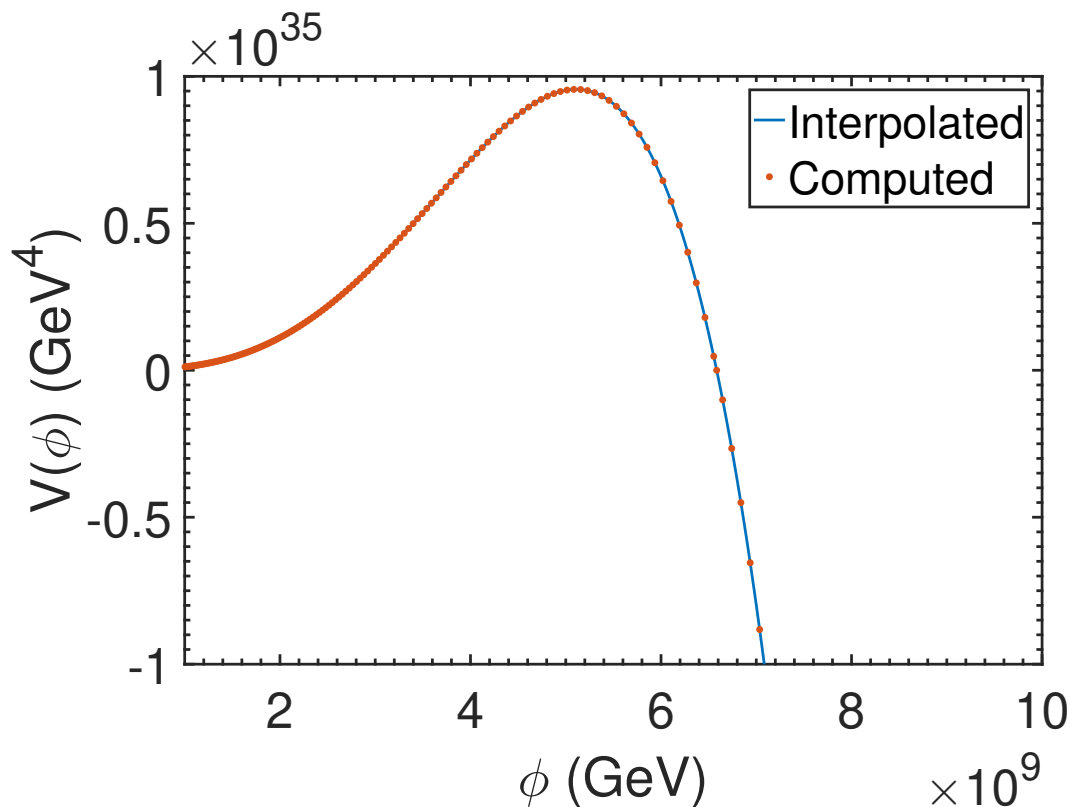
Figure 4.13: Plot of the effective potential as evaluated by integrating the beta functions (dotted line) against a piecewise polynomial interpolation.

several ways of performing this fit. The generic cubic fit with N data pairs (x_n, y_n) is given by a set of $N-1$ polynomials:

$$p_n(x) = (1 - u_n(x))y_n + u_n(x)y_{n+1} + u_n(x)(1 - u_n(x))[a_n(1 - u_n(x)) + b_n u_n(x)], \quad (4.83)$$

$$u_n(x) \equiv \frac{x - x_{n+1}}{x_{n+1} - x_n}, \quad (4.84)$$

$$a_n \equiv k_n(x_{n+1} - x_n) - (y_{n+1} - y_n), \quad (4.85)$$

$$b_n \equiv -k_{n+1}(x_{n+1} - x_n) + (y_{n+1} - y_n). \quad (4.86)$$

It is easy to verify that this choice is continuous and has continuous first derivatives at x_n and x_{n+1}. There are N free parameters, k_n, which are the derivatives of the interpolating piecewise polynomial at each x_n, and different choices of k_n define different interpolation schemes. A popular choice is the cubic spline, which is defined by requiring continuity of the second derivatives: $p''_{n-1}(x_n) = p''_n(x_n)$. This leads to the tridiagonal set of simultaneous equations:

$$\frac{k_{n-1}}{(x_n - x_{n-1})^2} + \left[\frac{2}{(x_n - x_{n-1})^2} + \frac{2}{(x_{n+1} - x_n)^2} \right] k_n + \frac{k_{n+1}}{(x_{n+1} - x_n)^2} = \frac{3(y_{n+1} - y_n)}{(x_{n+1} - x_n)^2} + \frac{3(y_n - y_{n-1})}{(x_n - x_{n-1})^2}. \quad (4.87)$$

The boundaries are usually specified with $p''_0(x_0) = p''_{N-1}(x_N) = 0$, but other choices are possible. The advantage of the spline is the high degree of continuity, however, it is not the only possible choice, and in fact tends to result in a mismatch between the derivatives of the running coupling, $\lambda(\mu)$, and the derivatives obtained by solving Eq. (4.87). This results in

spurious oscillations in the potential which are undesirable. A better choice is to use the beta functions to constrain the t-derivatives of λ:

$$k_n = \beta_\lambda(\lambda_n, g_{in}), \tag{4.88}$$

where g_{in} are the other couplings evaluated at t_n. This yields a piecewise polynomial $p_n(x)$ which matches the derivatives of $\lambda(t)$ obtained from the running, as well as matching $\lambda(t_n)$, but has *discontinuous* second derivatives. It is, however, generally a more faithful representation than the cubic spline. Figure 4.13 illustrates how this piecewise function interpolates the Standard Model effective potential. This is the potential used for numerics, and as figure 4.14 shows, the results of the calculation of decay exponents rapidly converge as N is increased.
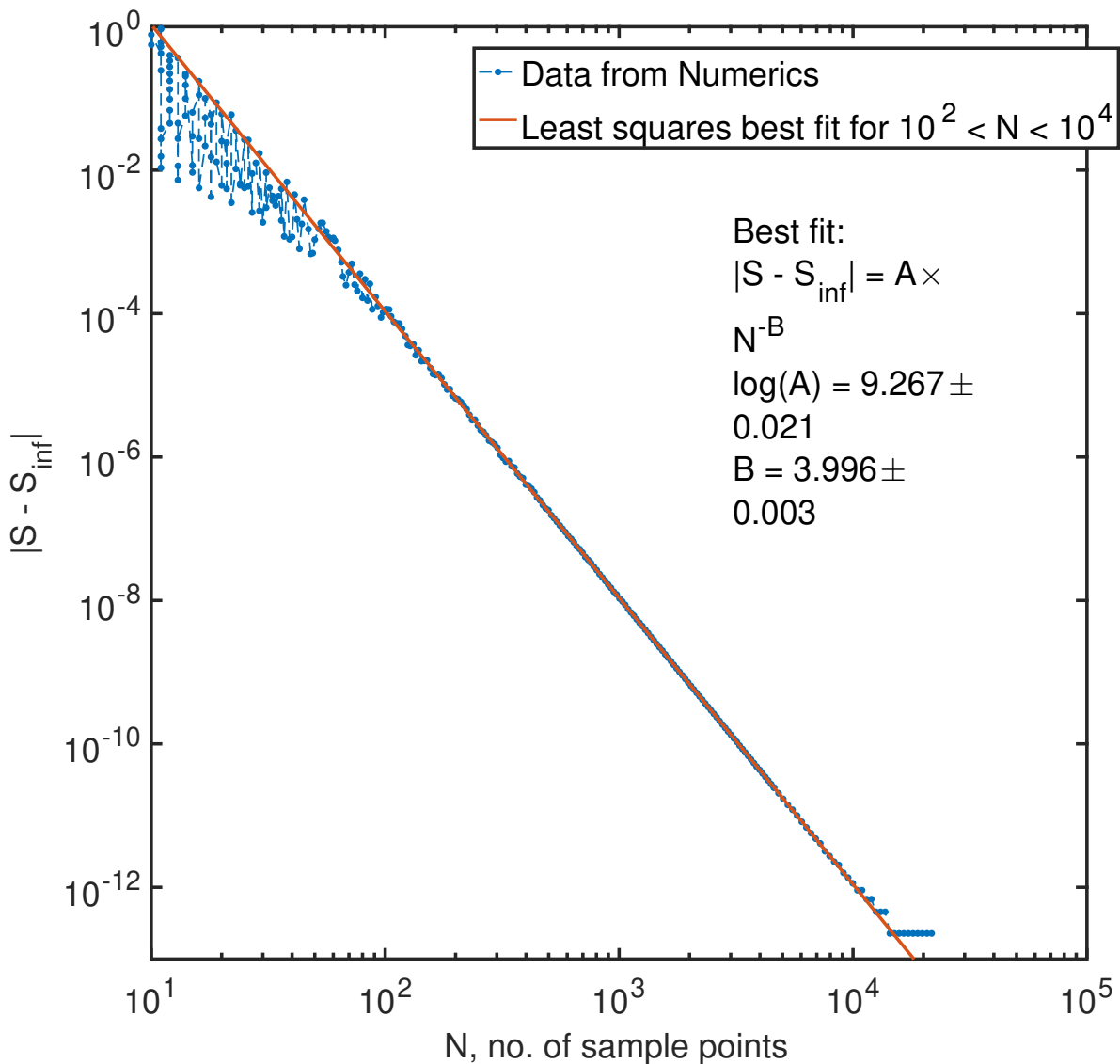
Figure 4.14: Plot of the action convergence as a function of the number of sample points used to approximate the potential (the apparent deviation at large N is due to floating round-off error in $|S - S_{\text{inf}}|$). Originally published in [1]

4.4   Renormalisation Group Running in De Sitter Space

Up to now, we have considered only the potential in flat space. In curved space, however, the result can be quite different. The loop integrals that contribute to the effective potential can be quite convoluted. One way to approach this, which we used in a recent paper [3], is through the method of heat kernels. A good review of this topic can be found at [162]. Another approach to the effect of non-minimal coupling in the effective potential is discussed in [163].

The fundamental idea of the heat kernel method it to make use of solutions to the heat-transfer equation:

$$\left(\frac{\partial}{\partial t} + D \right) K(t, x, y, D) = 0, \tag{4.89}$$

subject to the boundary conditions $K(0, x, y, D) = \delta(x - y)$. The advantage of this is that it allows us to express the Green's function for the operator D as:

$$D^{-1}(x, y) = \int_0^\infty dt K(t, x, y, D), \tag{4.90}$$

since:

$$D(x, y) \int_0^\infty dt K(t, x, y, D) = - \int_0^\infty dt \frac{\partial}{\partial t} K(t, x, y, D) = -[K(t, x, y, D)]_0^\infty$$
$$= K(0, x, y, D) - K(\infty, x, y, D) = \delta(x, y), \tag{4.91}$$

provided we satisfy $K(t \to \infty, x, y, D) \to 0$, which holds in most cases. For example, the operator:

$$D_0 = -\nabla_\mu \nabla^\mu + m^2, \tag{4.92}$$

with flat metric on $\mathbb{R}^n$ can be solved with [162]:

$$K(t, x, y, D_0) = \frac{1}{(4\pi t)^{n/2}} \exp \left(-\frac{(x - y)^2}{4t} - tm^2 \right). \tag{4.93}$$

The real power of this method, however, comes from the fact that we can express generic operators, D, in terms of expansions around simpler operators, D_0. In the curved space case, for example, it is possible to find an expression for the heat kernel of the operator $D_0 = \Box + X$ in the form [164, 165]:

$$K(\tau, x, x, D_0) = \frac{i}{(4\pi i\tau)^{n/2}} \exp \left(-i\tau \left(X - \frac{R}{6} \right) \right) \Omega(\tau). \tag{4.94}$$

In general, X can be a matrix, which makes this an exceptionally powerful technique. Generic operators can then be included as a heat kernel expansion with $\Omega(\tau)$ of the form:

$$\Omega(\tau) = \sum_{k=0}^\infty a_k (i\tau)^k. \tag{4.95}$$

The real usefulness of this approach, however, comes from the fact that it can be used to express the 1-loop corrections to the action of an arbitrary theory:

$$\Gamma^{(1)}[\phi] = \frac{i}{2} \mathrm{Tr}(\log(D)). \tag{4.96}$$

Note that up to a divergent constant (which we will regularise away):

$$\log \lambda = \int_0^\infty \mathrm{d}\tau \frac{1}{\tau} e^{-\lambda \tau}. \tag{4.97}$$

Hence we can express the one loop calculation as [162]:

$$\frac{i}{2} \mathrm{Tr}(\log(D)) = -\frac{i}{2} \mathrm{Tr} \left(\int_0^\infty \tau \frac{1}{\tau} e^{-i\tau D} \right). \tag{4.98}$$

Note that $\exp(-i\tau D)$ is the solution of:

$$\left(i \frac{\partial}{\partial \tau} - D \right) K(\tau, x, y, D) = 0, \tag{4.99}$$

which will yield the heat kernel. Hence:

$$\frac{i}{2} \mathrm{Tr}(\log(D)) = -\frac{i}{2} \int \mathrm{d}^4 x \sqrt{-\det(g)} \int_0^\infty \mathrm{d}\tau \frac{1}{\tau} K(\tau, x, x, D_0) \sum_{k=0}^\infty a_k (i\tau)^k. \tag{4.100}$$

The coefficients a_k can be determined for generic space-times [164, 165], and used to derive the curved-space effective potential for any theory, including the Standard Model. Some care has to be taken to apply this to fermionic and vector contributions, but in the end we obtain an approximate one loop expression for the renormalisation group improved effective potential in a fixed de Sitter background [3]:

$$V_{\mathrm{RGI}}^{\mathrm{1loop}}(\phi_{\mathrm{cl}}) = \frac{1}{2} \left[-m^2(\mu(\phi_{\mathrm{cl}})) + \xi(\mu(\phi_{\mathrm{cl}}))R \right] \phi(\mu(\phi_{\mathrm{cl}}))^2 + \frac{\lambda(\mu)}{4} \phi(\mu(\phi_{\mathrm{cl}}))^4 + V_\Lambda(\mu(\phi_{\mathrm{cl}})) - 12\kappa(\mu(\phi_{\mathrm{cl}}))$$

$$+ \alpha(\mu(\phi_{\mathrm{cl}}))H^4 + \frac{1}{64\pi^2} \sum_i \left[n_i M_i^4(\phi_{\mathrm{cl}}) \left(\log \frac{|M_i^2(\phi_{\mathrm{cl}})|}{\mu(\phi_{\mathrm{cl}})^2} - d_i \right) + n_i' H^4 \log \frac{|M_i^2(\phi_{\mathrm{cl}})|}{\mu(\phi_{\mathrm{cl}})^2} \right]. \tag{4.101}$$

The coefficients n_i, n_i', d_i are given in [3], and M_i^2 are Higgs field dependent masses defined in Eq. (4.108). Here we include some gravitational terms, which correspond to the running of various gravitation-related couplings, whose 1-loop beta functions are [3]:

$$\beta_\xi = \frac{(\xi - 1/6)}{16\pi^2} \left[12\lambda + 2Y_2 - \frac{3g'^2}{2} - \frac{9g^2}{2} \right], \tag{4.102}$$

$$\beta_{V_\Lambda} = \frac{2m^4}{16\pi^2}, \tag{4.103}$$

$$\beta_\kappa = \frac{4m^2}{16\pi^2} \left(\xi - \frac{1}{6} \right), \tag{4.104}$$

$$\beta_{\alpha_1} = \frac{1}{16\pi^2} \left(2\xi^2 - \frac{2}{3}\xi - \frac{277}{144} \right), \tag{4.105}$$

$$\beta_{\alpha_2} = \frac{1}{16\pi^2} \frac{571}{90}, \tag{4.106}$$

$$\beta_{\alpha_3} = -\frac{1}{16\pi^2} \frac{293}{720}, \tag{4.107}$$

where Y_2 is as defined in Eq. (4.81) and the three couplings $\alpha_1, \alpha_2, \alpha_3$ are for the next order Riemann-squared couplings of gravity: $\alpha_1 R^2 + \alpha_2 R_{\mu\nu} R^{\mu\nu} + \alpha_3 R_{\mu\nu\rho\sigma} R^{\mu\nu\rho\sigma}$. In de Sitter space, and in fact any maximally symmetric space-time, these combine into a single αH^4. Defining the effective potential then only requires a definition of $\mu(\phi_{\mathrm{cl}})$, the scale as a function of the classical field.

4.5 The Renormalisation Group Improved Higgs Potential in De Sitter Space

One complication in de Sitter space is the form of the mass-terms that appear in Eq. (4.101). Generally speaking, they are of the form:

$$M_i^2(\mu, \phi_{\rm cl}) = \kappa_i(\mu)Z(\mu)\phi_{\rm cl}^2 - \kappa_i'(\mu) + \theta_i(\mu)R, \tag{4.108}$$

where $\kappa_i, \kappa_i', \theta_i$ are coefficients that depend on the couplings of the theory [57, 86, 3]. Recall that in flat space, the scale choice $\mu(\phi_{\rm cl}) = \phi_{\rm cl}$ is chosen because, generally speaking, it matches the masses which are proportional to ϕ, at large ϕ. Due to the Higgs mechanism, for example, the mass of a fermion with Yukawa coupling y_f is $m_f = y_f\phi_{\rm cl}$, thus choosing $\mu = \phi_{\rm cl}$ will generically ensure that the log terms remain relatively small over the whole range of ϕ.

However, in curved space, there is an additional $\theta_i R = 12\theta_i H^2$ term present in the 'mass'. This complicates matters. Markkanen et al. [57, 86] argue that to ensure the accuracy of the renormalisation group improvement at all scales, it is necessary to choose μ to be of the form:

$$\mu^2(\phi_{\rm cl}) = \alpha\phi_{\rm cl}^2 + \beta R. \tag{4.109}$$

This has dramatic and important consequences for the behaviour of the vacuum during inflation. Most notably, at small ϕ, the form of the potential is *completely different* to the flat space case: instead of $\mu = \phi$ being the optimal choice, $\mu \sim H$. If H is large, this can mean that $\lambda < 0$ holds even at small ϕ, making the potential not only metastable, but *completely unstable.*

This phenomenon does make some sense - at large H, light scalar fields such as the Higgs receive large fluctuations, of order $\langle\phi^2\rangle \sim H^2$ [107]. If $H \gg \Delta V(\phi)^{1/4}$, then the Higgs will generally fluctuate over the barrier freely due to the large Gibbons-Hawking temperature. It makes some sense, therefore, that the potential would be completely unstable in this regime, and the decay rate consequently less well defined. In fact, we proved that potentials with no barrier do not have de Sitter solution in lemma 6.

Another way of choosing the renormalisation scale is to simply choose μ so that the sum of the quantum corrections is set to zero, as was recently suggested by [154] and considered in [3]. That is, we choose $\mu(\phi_{\rm cl})$ to satisfy:

$$\sum_i \left[n_i M_i^4(\phi_{\rm cl}) \left(\log \frac{|M_i^2(\phi_{\rm cl})|}{\mu(\phi_{\rm cl})^2} - d_i \right) + n_i' H^4 \log \frac{|M_i^2(\phi_{\rm cl})|}{\mu(\phi_{\rm cl})^2} \right] = 0. \tag{4.110}$$

Generically, Eq.(4.110) must be solved for numerically: although the $\log \mu$ terms can be isolated, the couplings depend implicitly on μ.

As it turns out, however, doing so is no straightforward matter. Consider figure 4.15, for example. This demonstrates there are multiple ways of solving Eq. (4.110). This is important, because both solutions will lead to *different* potentials - see fig. 4.16 These results are very strange, at first glance. Taken literally, it would imply there are two different effective potentials, which both give qualitatively different conclusions about the stability of the vacuum - one potential appears to be metastable (solution 2), while the other is completely unstable (solution 1). This is physically unacceptable - the effective potential is supposed to be independent of the renormalisation scale, so one or both of these solutions must be spurious. In fact, an analysis
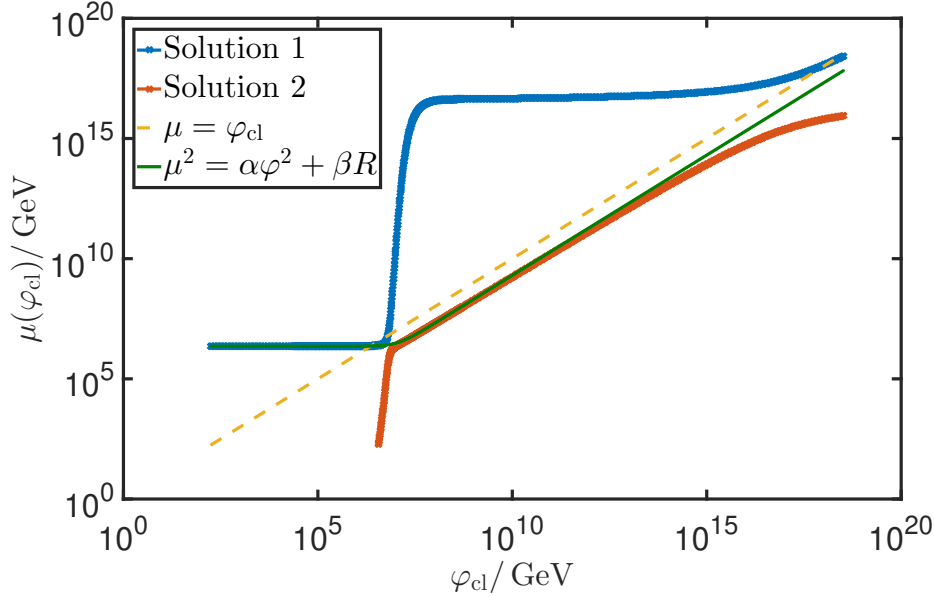
Figure 4.15: Plot of two different solutions of Eq. (4.110). Solution one appears to resemble the $\mu^2 = \alpha\phi^2 + \beta R$ rule at small ϕ, but solution 2, which does not exist at small ϕ, resembles the large ϕ behaviour. Here, $H = 10^6$ GeV and $\xi_{\text{EW}} = \xi(\mu = 0) = -1$.

of the size of the log terms in figure 4.17 reveals what is going on. There are indeed some cases where it is better to use the model of Eq. (4.109), as in the right hand plot of figure 4.17. In that case, we see that the logs remain small for solution 1 at small ϕ and for solution 2 at large ϕ. Some sort of model interpolating between the two is thus a good approximation that will keep the logs small throughout. Cases like the left hand panel of fig. 4.17 are more troubling, however: there is appears that there is no good approximation for small ϕ. This case is particularly exceptional, however. It corresponds to the conformal value of ξ_{EW}. This is important because the Higgs boson 'mass'-term appearing in Eq. (4.101) is [3]:

$$M^2 = m_h^2 + 12(\xi - 1/6)H^2. \tag{4.111}$$

Thus, for $\xi \neq 1/6$, one finds that the mass term is of the form Eq. (4.108). However, this ceases to be the case for $\xi = 1/6$, and a $\mu \propto \phi$ model proves a better approximation.

This begs the question: why are there multiple solutions to Eq. (4.110)? An closer examination of the equation reveals why: the n_i coefficients can be of varying sign, for the most part determined by whether i corresponds to a fermion or boson loop. However, this means that it is possible to solve Eq. (4.110), setting the sum of the loops to zero, even while the individual logs remain large, because log terms appear with opposing signs and can thus cancel each other. This tells us that choosing Eq. (4.110) to vanish is not a universally good way to choose $\mu(\phi)$. More careful procedures are necessary, and care should be taken to ensure that all the log terms are small. For example, one can use Eq. (4.109) with α and β chosen in such a way as to minimise:

$$S = \frac{\sum_i M_i^4 \log(M_i^2/\mu^2)^2}{\sum_i M_i^4}. \tag{4.112}$$

This is a weighted sum over the squares of the log terms. Note that we weight this by the mass because the heavier masses will give the greatest contribution to the potential, and we do not
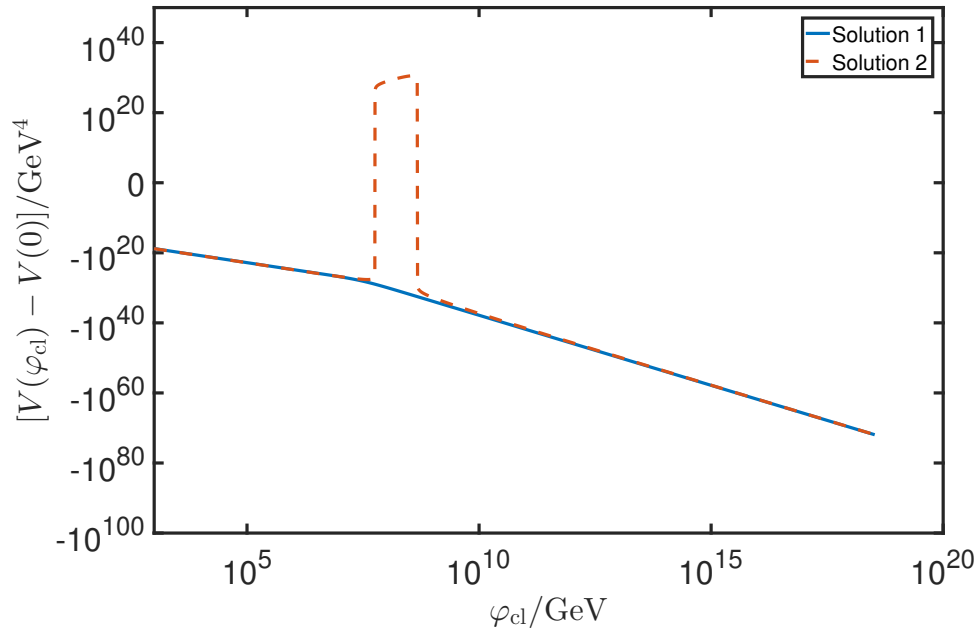
Figure 4.16:   Effective potentials resulting from choosing the two different solutions in Eq. (4.15). These lead to qualitatively different conclusions about the stability of the electroweak vacuum during inflation.

want to result to be adversely affected by masses which vanish for some $\phi_{\rm cl}$. In principle, such vanishing masses should be dealt with by some sort of decoupling scheme [145, 152].
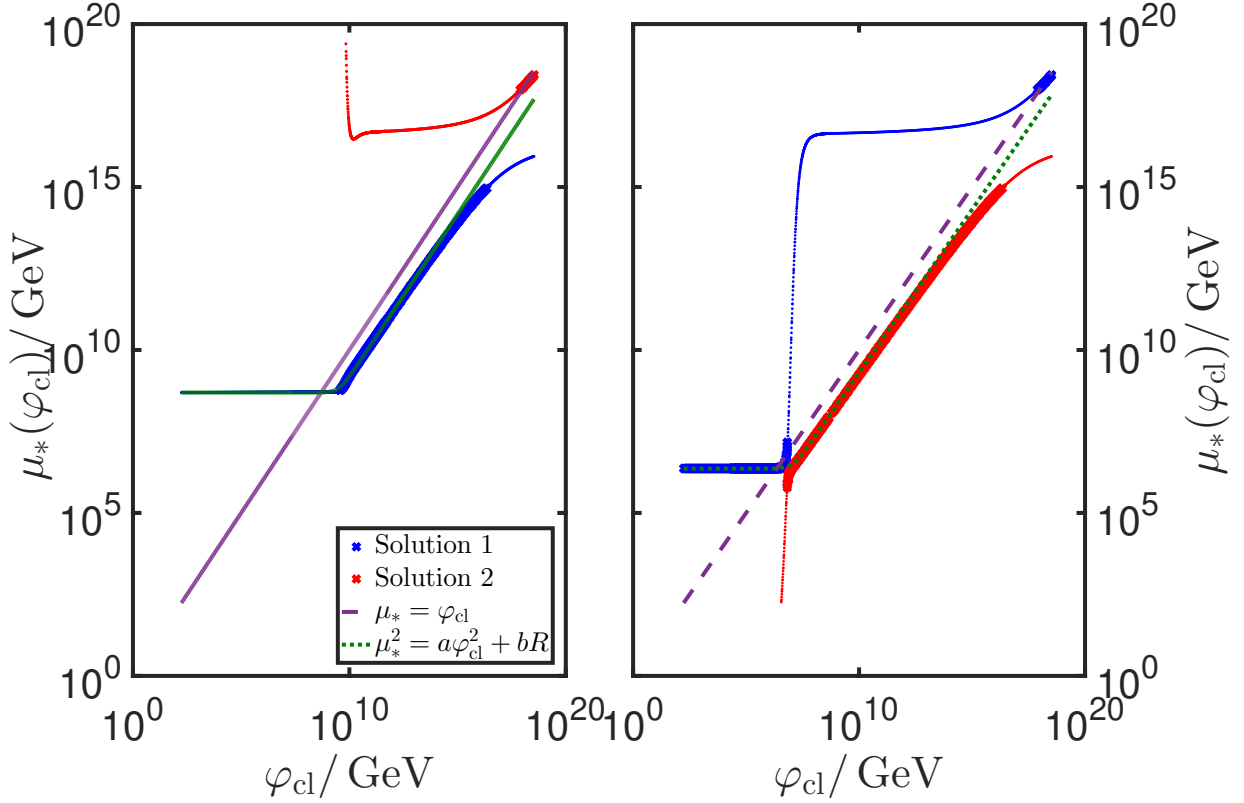
Figure 4.17: Figure 1. Two solutions of Eq. (4.110) for two different values of ξ_{EW} and H. A 'best fit' choice as in Eq. (4.109) is also plotted, along-side the $\mu = \phi_{\text{cl}}$ choice. Left: $\xi_{\text{EW}} = \xi(M_t) = 1/6, H = 10^9 \,\text{GeV}, \alpha = 0.0215$ and $\beta = 0.0203$. Right: $\xi_{\text{EW}} = \xi(M_t) = 1, H = 10^6 \,\text{GeV}, \alpha = 0.0414, \beta = 0.4332$. Large crosses denote points where the log contributions of the dominant fields, W, Z, ϕ, t, all satisfy $\log|M^2/\mu^2| < 5$, and small dots where this is not true.

Chapter 5

Back-reaction and Non-minimal Coupling: $V_0 = 0$ Case

As discussed previously, the $V_0 = 0$ case necessarily results in non-compact bounce solutions, that consequently resemble their flat space counterparts, at least on the exterior of the bounce. Here we consider the effect of including gravity on these flat false vacuum bounces, and their relationship to bounce in the $V_0 = 0$ limit. We also consider how a non-minimal coupling to gravity affects bounce solutions and their nucleation rate in the Standard Model, uncovering interesting affects, especially in the case of conformal coupling.

5.1 Bounces and Non-minimal Higgs-Curvature Coupling

When considering bounces in de Sitter backgrounds, the most complete scalar action is not Eq. (3.2), but:

$$S[\phi, g_{\mu\nu}] = \int \mathrm{d}^4x \sqrt{|\det(g)|} \left[\frac{1}{2} \nabla_\mu \phi \nabla^\mu \phi + V(\phi) - \frac{M_{\mathrm{P}}^2}{2} \left(1 - \xi \frac{\phi^2}{M_{\mathrm{P}}^2} \right) R \right]. \tag{5.1}$$

The term $\frac{1}{2}\xi\phi^2 R$ is required to be present in order for the scalar field to be re normalisable in a curved background. In principle, for consistency, we should also include terms which are expected (in the effective field theory approach) to be of the same order in M_{P}^2. For example, $g\phi^2/M_{\mathrm{P}}^2$ terms and $\beta\phi^2\partial_\mu\phi\partial^\mu\phi/M_{\mathrm{P}}^2$. The effect of the ϕ^6 term, for example, can stabilise the potential altogether if sufficiently large. It is possible to eliminate the $\phi^2\partial_\mu\phi\partial^\mu\phi$ term and $\xi\phi^2 R$ term by field redefinitions. We will do this for the $\phi^2\partial_\mu\phi\partial^\mu\phi$ term here for simplicity, and also neglect the ϕ^6 term so as to focus on the effect of non-minimal coupling, ξ. In general, there is no reason to assume that ξ is necessarily zero in a flat ($V_0 = 0$) background. Figure 1.5 shows the solution of beta function Eq. (3.1), for the initial values $M_t = 174.34\,\mathrm{GeV}, M_h = 125.15\,\mathrm{GeV}, \xi = 0$. This demonstrates that even if $\xi = 0$ holds in the Electroweak vacuum, it will not generally be true for all energy scales, as ξ runs with energy. Furthermore, there is no particular reason to suppose that $\xi = 0$ is the value in the electroweak vacuum: the best available bounds [105] suggest in fact that $|\xi| < 2.6 \times 10^{15}$, which leaves considerable parameter space unexplored.

There are two ways of approaching this sort of problem. One way is to perform a field transformation to the Einstein frame:

$$\tilde{g}_{\mu\nu} = \left(1 - \frac{\xi\phi^2}{M_{\mathrm{P}}^2} \right) g_{\mu\nu}, \tag{5.2}$$

$$\tilde{\phi} = \int_0^\phi \mathrm{d}\phi \frac{\sqrt{1 - \frac{\xi(1-6\xi)\phi^2}{M_{\mathrm{P}}^2}}}{\left(1 - \frac{\xi\phi^2}{M_{\mathrm{P}}^2} \right)}, \tag{5.3}$$

which decouples the scalar field from the metric:

$$S[\tilde{\phi}, \tilde{g}_{\mu\nu}] = \int \mathrm{d}^4x \sqrt{\det(\tilde{g})} \left[\frac{1}{2} \tilde{\nabla}_\mu \tilde{\phi} \tilde{\nabla}^\mu \tilde{\phi} + \frac{V(\phi(\tilde{\phi}))}{\left(1 - \frac{\xi\phi(\tilde{\phi})^2}{M_{\mathrm{P}}^2} \right)^2} - \frac{M_{\mathrm{P}}^2}{2} \tilde{R} \right]. \tag{5.4}$$

Instead of coupled scalar-field-gravity equations, this means that the effect of non-minimal coupling is transferred to the potential, which takes the Einstein-frame form:

$$\tilde{V}_{\mathrm{Einstein}}(\tilde{\phi}) = \frac{V_{\mathrm{Jordan}}(\phi(\tilde{\phi}))}{\left(1 - \frac{\xi\phi^2(\tilde{\phi})}{M_{\mathrm{P}}^2} \right)^2}. \tag{5.5}$$

Note that the potential is complicated by the fact that we need to know $\phi(\tilde{\phi})$. Integrating Eq. (5.3) gives the inverse of this:

$$\tilde{\phi}(\phi) = \sqrt{6} M_{\mathrm{P}} \tanh^{-1}\left(\frac{\sqrt{6} M_p \phi}{\sqrt{1 - \frac{\xi(1-6\xi)\phi^2}{M_{\mathrm{P}}^2}}} \right) + \sqrt{\frac{1-6\xi}{6\xi}} M_{\mathrm{P}} \sin^{-1}\left(\frac{\sqrt{\xi(1-6\xi)}\phi}{M_{\mathrm{P}}} \right). \tag{5.6}$$

In principle, we can invert this numerically. Another way is to leave Eq. (5.1) as it is, and derive the Jordan frame equations of motion:

$$\ddot{\phi} + \frac{3\dot{a}}{a}\dot{\phi} - V'(\phi) - \xi\phi R = 0, \tag{5.7}$$

$$\dot{a}^2 = 1 - \frac{a^2}{3M_{\mathrm{P}}^2\left(1 - \frac{\xi\phi^2}{M_{\mathrm{P}}^2}\right)}\left(-\frac{\dot{\phi}^2}{2} + V(\phi) - \frac{6\xi\dot{a}}{a}\phi\dot{\phi} \right), \tag{5.8}$$

$$\ddot{a} = -\frac{a}{3M_{\mathrm{P}}^2\left(1 - \frac{\xi\phi^2}{M_{\mathrm{P}}^2}\right)}\left(\dot{\phi}^2 + V(\phi) - 3\xi(\dot{\phi}^2 + \phi\ddot{\phi} + \frac{\dot{a}}{a}\phi\dot{\phi}) \right), \tag{5.9}$$

$$R = \frac{\dot{\phi}^2(1-6\xi) + 4V(\phi) - 6\xi\phi V'(\phi)}{M_{\mathrm{P}}^2\left(1 - \frac{\xi(1-6\xi)\phi^2}{M_{\mathrm{P}}^2}\right)}. \tag{5.10}$$

Note that for our numerical results, we use Eqs. (5.7) and (5.9) (which avoids problems when $\dot{a} = 0$, which occurs for de Sitter bounces), and use Eq. (5.8) to impose the second boundary condition, $\dot{a}(0) = 1$, at $\chi = 0$ needed to solve Eq. (5.9).

Using these Jordan frame equations, the potential is much simpler to evaluate since it does not need inversion of Eq. (5.6) at every step. In order to draw conclusions about the bounces, we can always move to the Einstein-frame, which can tell us, among other things, that the bounce solutions are well defined, and must be non-compact (since the equivalent Einstein frame bounce is non-compact). Note that the action in both the Jordan and Einstein frames is identical, since by definition one transforms from one frame to the other by keeping the action the same, but transforming the fields: consequently the action in the Einstein frame is just a re-writing of the Jordan frame action in different variables, and cannot actually differ for the same solution. Since the decay rate depends only on the action of the solution, it doesn't matter which frame we choose to evaluate it in, and so we are free to use whichever frame is most convenient - in this case the Jordan frame.

5.2   Results

We refer now to results that we published previously in [1], in which we performed detailed numerical calculations of bounces, including gravitational effects and non-minimal Higgs-curvature coupling. The method of solution is essentially the same as in flat space, since the bounces are non-compact: pick a value of $\phi(0)$ and compute the resulting solution: classify it either as an undershoot or an overshoot, then bisect until a solution sufficiently close to the bounce is found.

Example solutions are plotted in fig. 5.1.

The first thing we note is that simply including gravitational corrections, without non-minimal coupling ($\xi = 0$), produces a shift in the shape of the bounce at around its peak.
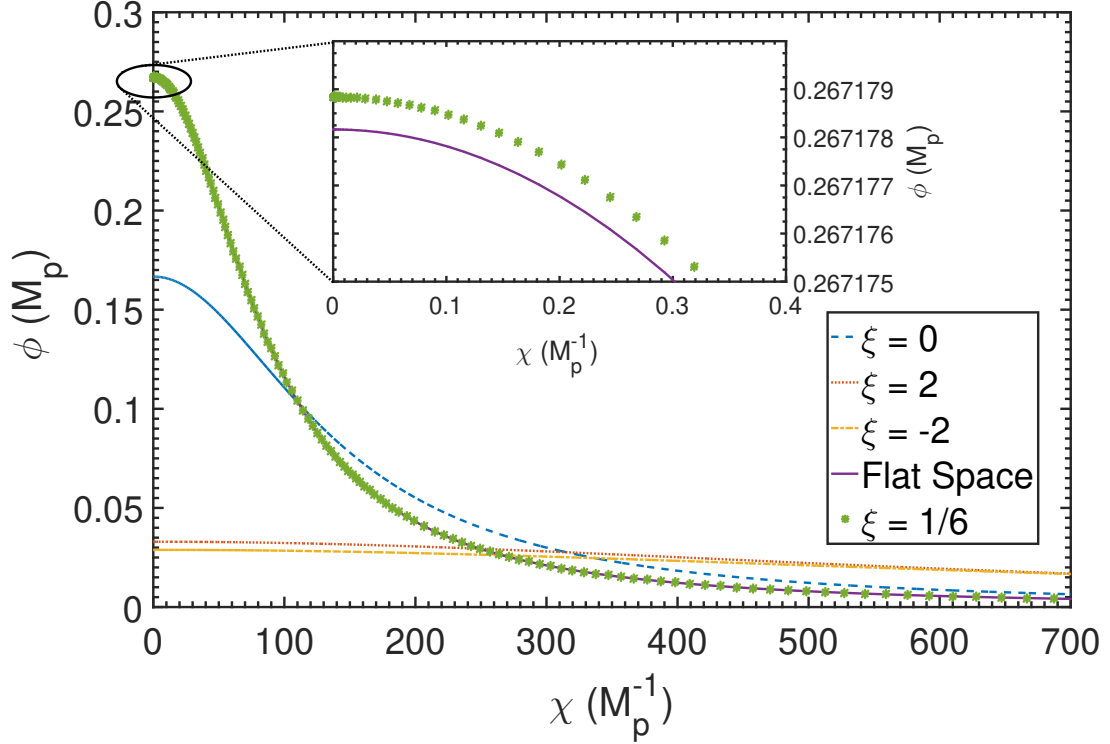
Figure 5.1: Various bounce solutions with $M_t = 173.34\,\text{GeV}$, $M_h = 125.16\,\text{GeV}$ when gravitational backreaction and non-minimal coupling are included. Note that the $\xi = 1/6$ bounce is similar to the flat space bounce, but the bounce with only gravitational corrections and $\xi = 0$ is different. Originally published in [1]

The reason for this can be understood by using a perturbative approach [28], consisting of perturbing around the flat space solution for the $\lambda\phi^4$ potential with constant negative λ. This predicts that the action is:

$$S = \frac{8\pi^2}{3|\lambda|} + \frac{32\pi^2}{45R^2 M_P^2 |\lambda|^2}. \tag{5.11}$$

In flat space, the value of λ that dominates in the Standard Model was found to be that which minimises the action [18]. Neglecting gravitational effects, this means the value at which $|\lambda|$ is maximised, or in other words, λ is minimised (since this must occur for negative λ). Including the gravity corrections in Eq. (5.11), this instead means (remembering that $R = 1/\mu$):

$$\frac{\mathrm{d}S}{\mathrm{d}\mu} - \left(\frac{8\pi^2}{3|\lambda|^2} + \frac{64\pi^2\mu^2}{45M_P^2|\lambda|^3} \right) \frac{\mathrm{d}|\lambda|}{\mathrm{d}\mu} + \frac{64\pi^2\mu}{45M_P^2|\lambda|^2} = 0. \tag{5.12}$$

This produces a shift from the minimum of λ, and the resulting change in the scale μ is what accounts for the shift in the peak of bounce evident for $\xi = 0$ in fig. 5.1.

Another feature of fig. 5.1 is the fact that the bounce for $\xi = 1/6$ closely resembles that for *flat* space (for which, note, ξ is irrelevant since $R = 0$ everywhere). There is a slight difference in the two solutions, however. The fact that this occurs near $\xi = 1/6$ suggests that it is something to do with conformal symmetry. In fact, this is relatively easy to show using the expression for R, Eq. (5.10), since in the conformal case for a potential of the form $\frac{\lambda(h)h^4}{4}$ we obtain:

$$R = \frac{-\lambda'(h)h^5}{4M_P^2}. \tag{5.13}$$

97

For constant λ then, this implies that R would be exactly zero, and Eqs. (5.7) and (5.9) would reduce to the flat space equations. In the cases where λ varies only slowly - which is the case in the Standard Model since λ runs logarithmically with energy - then R is small everywhere near $\xi = 1/6$, and thus the bounce can be expected to resemble its flat space equivalent.

This can be understood as a sort of residual effect of conformal symmetry - the flat space Higgs potential is conformally symmetric at large ϕ, but this effect is mildly broken by quantum corrections that cause the Higgs self coupling to run with energy. Consequently, the $\xi = 1/6$ bounces are close to, but not exactly the same as, the flat space bounces.

Related to this, one finds that the action of bounce solutions in the vicinity of $\xi = 1/6$ is close to the flat space action. This can be seen in figs. 5.2 and 5.3, which also shows that the minimum of the curve is deflected slightly from $\xi = 1/6$. This again is due to the slight breaking of conformal symmetry.
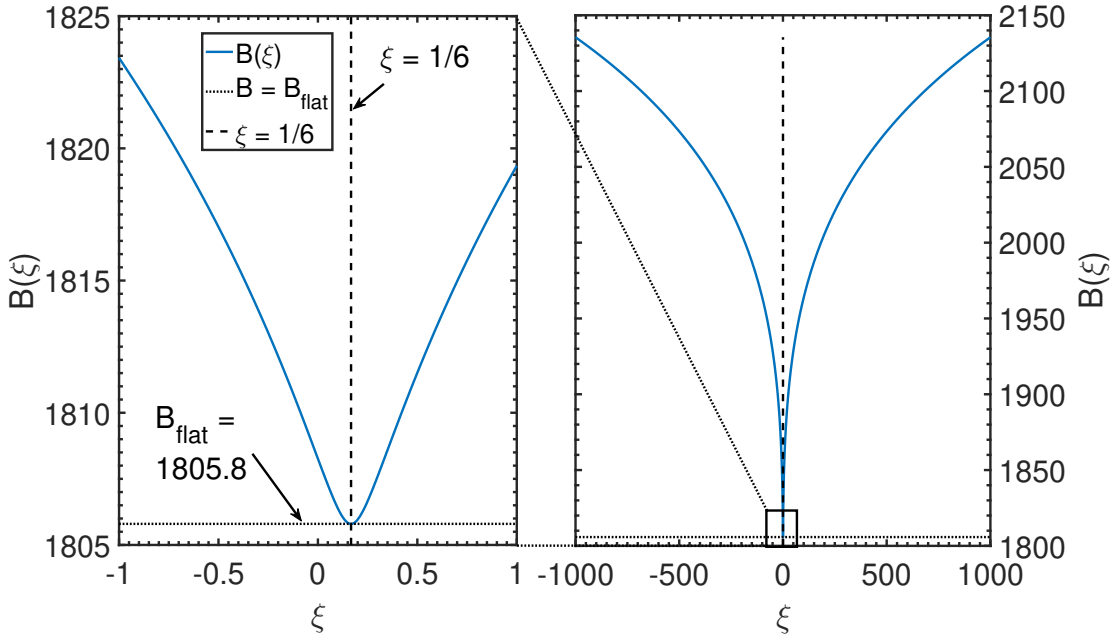
Figure 5.2: Plot of the decay exponent as a function of ξ for $M_h = 125.15\,\text{GeV}, M_t = 173.34\,\text{GeV}$. Note the displacement from $\xi = 0$ - the conformal coupling at $\xi = 1/6$ is in fact the approximate centre here. Originally published in [1].

It is possible to understand this deflection by deriving an expression for the location of the minimum of the curve $B(\xi)$ that describes the decay exponent as a function of ξ. Starting from:

$$\frac{\mathrm{d}B}{\mathrm{d}\xi} = \frac{\partial S_\xi[\phi_\xi, g_{\xi,\mu\nu}]}{\partial \xi}\bigg|_{\phi,g_{\mu\nu}} + \frac{\delta S_\xi[\phi_\xi, g_{\xi,\mu\nu}]}{\delta\phi}\bigg|_{\xi,g_{\mu\nu}} \frac{\partial\phi_\xi}{\partial\xi} + \frac{\delta S_\xi[\phi_\xi, g_{\xi,\mu\nu}]}{\delta g_\xi^{\mu\nu}}\bigg|_{\xi,\phi} \frac{\partial g_\xi^{\mu\nu}}{\partial\xi}. \tag{5.14}$$

98
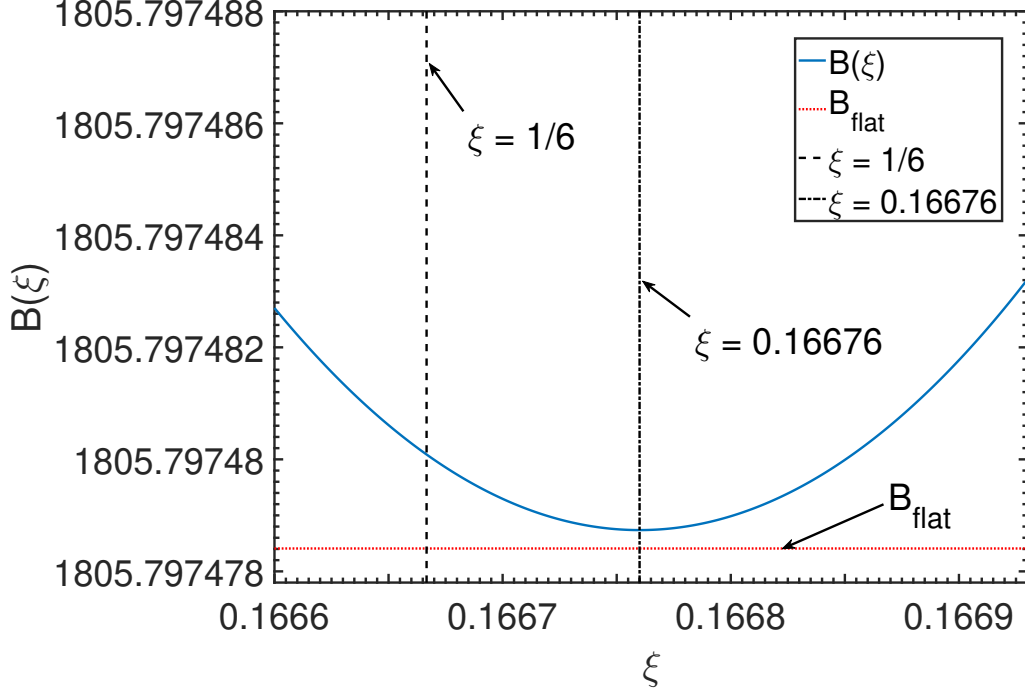
Figure 5.3: Zoom on the bottom of Fig. 5.2, showing that the centre is actually displaced from $\xi = 1/6$, and takes on a 'near conformal' value. The decay exponent is slightly above the flat space value. Originally published in [1].

For reference we define:

$$S_\xi[\phi, g_{\mu\nu}] = \int d^4x \sqrt{|\det g|} \left[\frac{1}{2} \nabla_\mu \phi \nabla^\mu \phi + V(\phi) + \frac{1}{2} \xi \phi^2 R - \frac{M_P^2}{2} R \right], \tag{5.15}$$

$$\Delta S[\phi, g_{\mu\nu}] = \int d^4x \frac{1}{2} \phi^2 R. \tag{5.16}$$

Note that evaluated at the bounce solution, the functional derivatives vanish, and thus we are only interested in the partial derivative with respect to ξ at constant $\phi, g_{\mu\nu}$. Hence:

$$\frac{dB}{d\xi} = \Delta S[\phi_\xi, g_{\xi,\mu\nu}] = \pi^2 \int_0^\infty d\xi a_\xi^3(\chi) \phi_\xi^2(\chi) R_\xi(\chi). \tag{5.17}$$

Hence, if we had an exact conformal symmetry, then $R_\xi = 0$ everywhere, and thus $B'(1/6) = 0$. So for exact conformal symmetry, $\xi = 1/6$ is the minimum of the $B(\xi)$ curve. Because $R_{\frac{1}{6}} \approx 0$, then we find that even in the Standard Model, $\xi = 1/6$ (and not $\xi = 0$) is close to (but not exactly at) the minimum of the curve. For example, with $M_t = 173.34 \,\text{GeV}$ and $M_h = 125.15 \,\text{GeV}$, the minimum is found numerically to lie at $\xi_{\min} - \frac{1}{6} = 9.3354 \times 10^{-5}$.

5.3 Ricci Curvature in the Interior of the Bounce

On striking conclusion of this analysis is that fig. 5.4 appears to show that for some $\xi > \frac{1}{6}$, e.g. $\xi = 1/3$, the Ricci curvature in the centre of the bounce is *positive*. This would be a surprising conclusion if true, because at first glance it would appear to imply that when a vacuum bubble

nucleates, it creates an expanding region of positive Ricci curvature, that then presumably inflates, potentially creating a new universe.

However, this scenario is in fact unlikely. To see why, we need to transform back to the Einstein frame. For an arbitrary conformal transformation, $\tilde{g}_{\mu\nu} = \Omega^2(x)g_{\mu\nu}$, the Ricci scalars are related by:

$$\tilde{R} = \frac{1}{\Omega^2}\left[R - 2(d-1)\nabla_\rho\nabla^\rho\log\Omega - (d-1)(d-2)\nabla_\lambda\log\Omega\nabla^\lambda\log\Omega\right]. \tag{5.18}$$

Substituting in $\Omega^2 = 1 - \frac{\xi\phi^2}{M_{\mathrm{P}}^2}$, as we need here, one obtains:

$$\tilde{R} = \frac{1}{M_{\mathrm{P}}^2}\left[4\frac{V(\phi)}{\left(1 - \frac{\xi\phi^2}{M_{\mathrm{P}}^2}\right)^2} + \frac{1 - \frac{\xi(1-6\xi)\phi^2}{M_{\mathrm{P}}^2}}{\left(1 - \frac{\xi\phi^2}{M_{\mathrm{P}}^2}\right)^3}\dot{\phi}^2\right]. \tag{5.19}$$

Taking account of the field transformation Eq. (5.6), and that the radial co-ordinate in the Einstein frame, $\tilde{\chi}$ is related to that in the Jordan frame, χ, by:

$$\mathrm{d}\tilde{\chi}^2 = \left(1 - \frac{\xi\phi^2}{M_{\mathrm{P}}^2}\right)\mathrm{d}\chi^2, \tag{5.20}$$

then we see that this is just the Einstein-frame form of Eq. (3.15), using the Einstein-frame potential Eq. (5.5). Consequently, it is fairly straightforward to see from Eq. (5.19) that the bounce will never describe a situation in which interior of the bounce is positive energy, (and thus expanding), since this would violate energy conservation in the Einstein frame. The fact that R appears to be negative in fig. (5.4) is just an artefact of the unusual form of the equations of motion in the Jordan frame.

It makes sense, at this point, to try and interpret this result physically. We have established that the Ricci curvature at the centre of a bounce solution is always negative. Ricci curvature can be interpreted as being related to the ratio of the volume and/or area of a ball radius ε at some point in a curved space to a ball of the same radius in flat space, in the $\varepsilon \to 0$ limit [166, 167]:

$$R = \lim_{\varepsilon\to 0}\frac{6(d+2)}{\varepsilon}\left[1 - \frac{V_{\mathrm{curved}}(\varepsilon)}{V_{\mathrm{flat}}(\varepsilon^2)}\right], \tag{5.21}$$

$$= \lim_{\varepsilon\to 0}\frac{6d}{\varepsilon}\left[1 - \frac{A_{\mathrm{curved}}(\varepsilon)}{A_{\mathrm{flat}}(\varepsilon^2)}\right], \tag{5.22}$$

where $V(\varepsilon)$ denotes the volume, and $A(\varepsilon)$ the surface area of the balls, respectively. This means, for example, if $R < 0$, then the volume of a ball in this space is *larger* than the equivalent ball in flat space, and the same holds for the surface areas. However, note that the volume ratio is closer to 1 than the area ratio - this is important, as it means that the surface area to volume ratio is different with a different Ricci curvature:

$$\frac{\left(\frac{A_{\mathrm{curved}}}{V_{\mathrm{curved}}}\right)}{\left(\frac{A_{\mathrm{flat}}}{V_{\mathrm{flat}}}\right)} = \frac{\left(\frac{V_{\mathrm{flat}}}{V_{\mathrm{curved}}}\right)}{\left(\frac{A_{\mathrm{flat}}}{A_{\mathrm{curved}}}\right)} = \frac{1 + \frac{\varepsilon^2 R}{6(d+2)}}{1 + \frac{\varepsilon^2 R}{6d}} \approx 1 - \frac{\varepsilon^2 R}{6}\left(\frac{1}{d} - \frac{1}{d+2}\right). \tag{5.23}$$

That is, the surface-area to volume ratio of such a ball *decreases*. This gives a physical interpretation of why the action of bounces seems to decrease: the surface-area to volume ratio decreases, and so so surface terms (which tend to suppress decay due to the positive energy of the gradient) have less impact than volume terms (which tend to enhance decay due to the negative energy present in the interior). Thus, the general tendency of the Ricci terms is to increase the decay rate, essentially by increasing the 'amount' of negative energy that can fit inside a nucleated bubble.
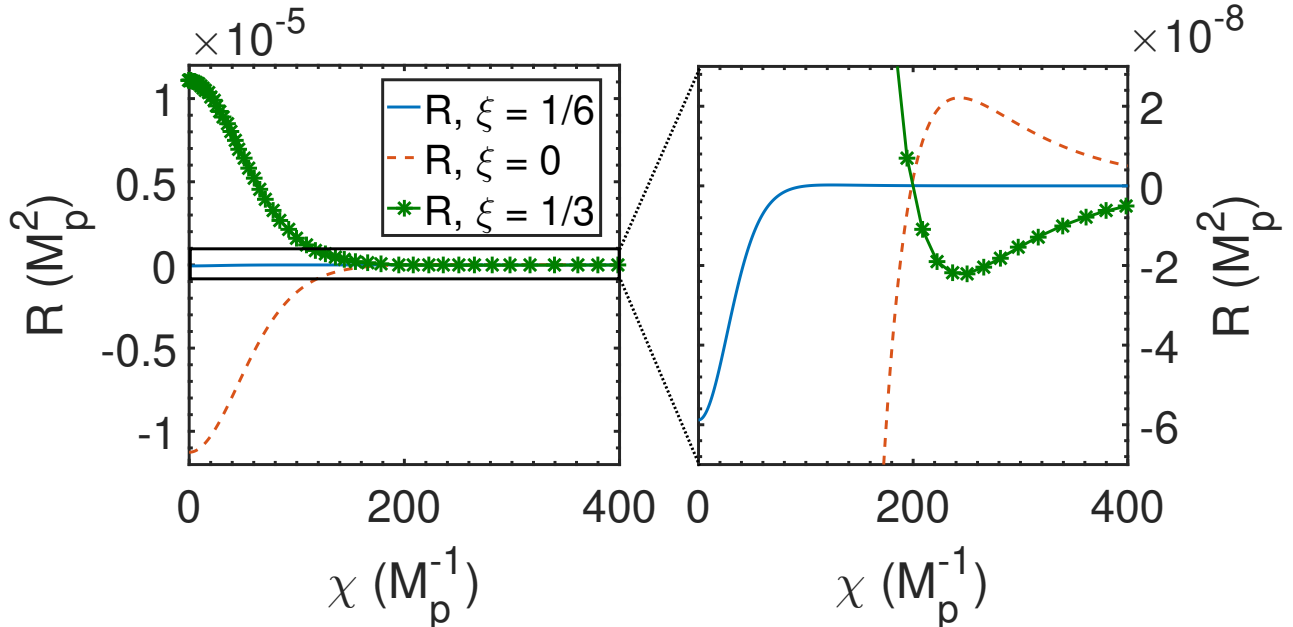
Figure 5.4: Plot of the Ricci scalar as a function of radial parameter, χ, for the bounces resulting from different values of ξ with $M_t = 173.34\,\text{GeV}$, $M_h = 125.16\,\text{GeV}$. The $\xi = 1/6$ case has (nearly) cancelling back-reaction corrections. Originally published in [1].

5.4   Effect on Stability for $V_0 = 0$

For $V_0 = 0$, the background space-time has no intrinsic Ricci curvature that the Higgs field can couple to, which is one reason ξ is difficult to constrain in collider experiments. As we have discussed, the back-reaction of bounces and the resulting nucleated bubbles creates a region of negative Ricci curvature, which can interact strongly with the bounce. This effect is especially significant when the Standard Model potential is deep and bounce solutions penetrate far into the negative curvature region. Fig. 5.2 showed that the effect of ξ is, quite generically, to suppress tunnelling by increasing the action. This can have a significant effect on the life-time of the vacuum, which we plot in figure 5.5. The net effect of this is to push back the boundary between the meta-stability and instability (defined as having a life-time shorter than the age of the visible universe) regions of (M_h, M_t) parameter space. This is plotted in fig. 5.6, where the beige region shows the shift in the instability-metastability boundary for a few different values of ξ. Note that because the true minimum is necessarily very shallow around the stability-meta-stability boundary, there isn't expected to be a significant effect on this. This means that physically speaking, non-minimal coupling when $V(\phi_{\text{fv}}) = 0$ doesn't change much, other than to significantly extend the life-time of the metastable vacuum: one might argue, however, that
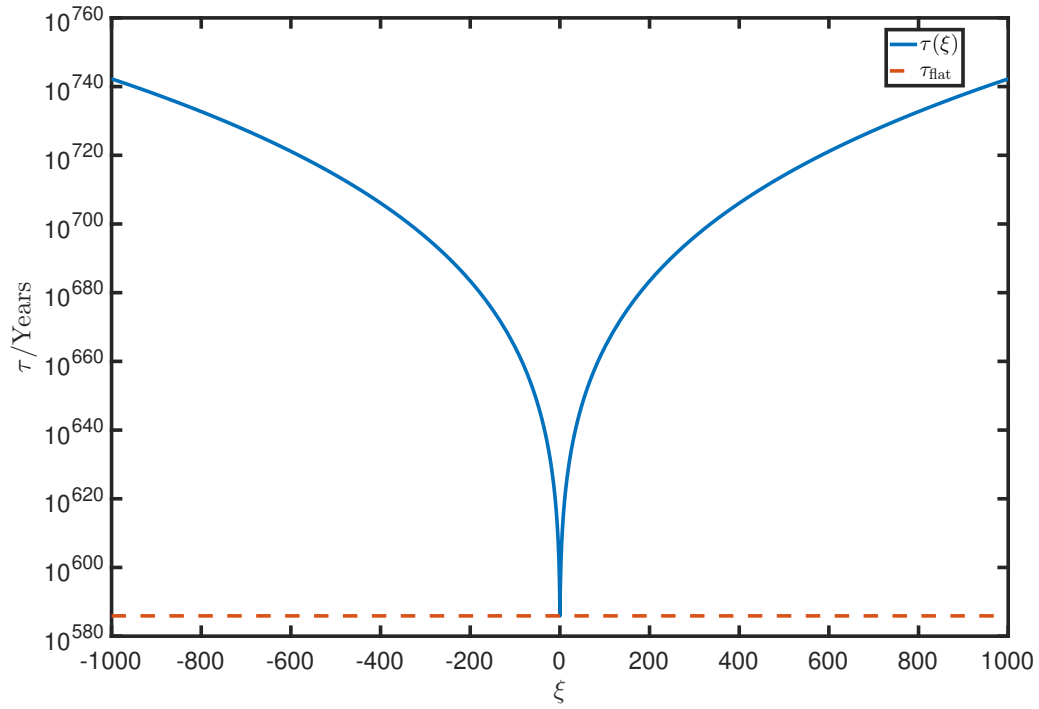
Figure 5.5: Life-time of the vacuum for $M_t = 173.34\,\text{GeV}, M_h = 125.15\,\text{GeV}, \alpha_S = 0.1184$, for different values of ξ compared to the flat space (no back-reaction) lifetime.

there isn't much of a practical difference between a life-time of 10^{580} years and 10^{780} years: both describe exceedingly rare events.
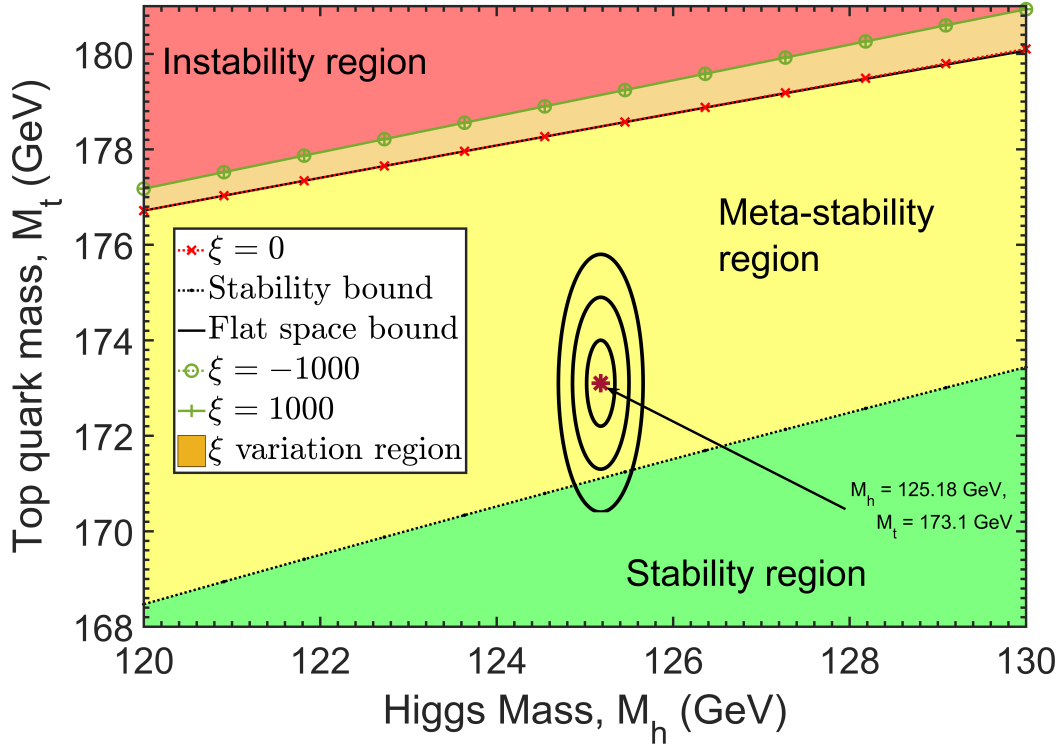
Figure 5.6: Effect on stability of gravitational corrections to the bounce for different top and Higgs masses. Increasing $|\xi|$ tends to stabilise the vacuum. Bounds on the top and Higgs masses are displayed as ellipses, representing 1,2, and 3σ bounds; $M_h = 125.18 \pm 0.16\,\text{GeV}, M_t = 173.1 \pm 0.9\,\text{GeV}$ from [4]. Figure based on [1].

5.5 Effect of Non-minimal Coupling in De Sitter Space

With the de-Sitter space effective potential of the Standard Model in place, it is also possible to ask questions not only about how gravity affects tunnelling rates, but about how the non-minimal coupling affects them. This results in an improvement over the previous analysis of this chapter which assumed a constant ξ and uses the flat space potential.

Although we do not consider bounces here, which will be left for a later work, it is possible to get an idea of how non-minimal Higgs-curvature coupling affects the Standard Model potential through the use of the Hawking-Moss instanton. This is most easily done by switching to the Einstein-frame, where the Higgs field and gravity are decoupled, and the potential takes the form:

$$\tilde{V}(\tilde{\phi}) = \frac{V(\phi(\tilde{\phi}))}{\left(1 - \frac{\xi\phi^2(\tilde{\phi})}{M_{\text{P}}^2}\right)^2}, \tag{5.24}$$

where $\tilde{\phi}$ is related to the Jordan-frame field by:

$$\frac{\mathrm{d}\tilde{\phi}}{\mathrm{d}\phi} = \frac{\sqrt{1 - \frac{\xi(1-6\xi)\phi^2}{M_{\text{P}}^2}}}{\left(1 - \frac{\xi\phi^2}{M_{\text{P}}^2}\right)}. \tag{5.25}$$

The decay exponent of the Hawking-Moss solution is thus:

$$B = 24\pi^2 M_P^4 \left(\frac{1}{V(\phi(\tilde{\phi}_{fv}))} \left(1 - \frac{\xi\phi(\tilde{\phi}_{fv})^2}{M_P^2}\right)^2 - \frac{1}{V(\phi(\tilde{\phi}_{max}))} \left(1 - \frac{\xi\phi(\tilde{\phi}_{max})^2}{M_P^2}\right)^2 \right). \quad (5.26)$$

Note that $\phi(\tilde{\phi}_{max})$ does not necessarily coincide with ϕ_{max}, as the different potential in the Einstein and Jordan frames will change the location of the stationary points. However, the solution exists and is will defined. In the fixed-background limit, the action of a generic solution in the Jordan frame can be written as:

$$S = \frac{2\pi^2}{H^3} \int_0^{\pi/H} d\chi \sin^3(H\chi) \left[\frac{\dot{\phi}^2}{2} + V(\phi) - \frac{M_P^2}{2}\left(1 - \frac{\xi\phi^2}{M_P^2}\right) R \right]. \quad (5.27)$$

Thus, if R is fixed, we can write B as:

$$B = \frac{8\pi^2}{3H^4} \left[V(\phi_{max}) + \frac{1}{2}\xi\phi_{max}^2 R - V(\phi_{fv}) - \frac{1}{2}\xi\phi_{fv}^2 R \right] = \frac{8\pi^2 \Delta V_\xi(\phi_{max})}{3H^4}, \quad (5.28)$$

where $\Delta V_\xi(\phi) = V(\phi) + \frac{1}{2}\xi\phi^2 R - V(\phi_{fv}) - \frac{1}{2}\xi\phi_{fv}^2 R$. That is, we can obtain the action simply by computing the difference between the top of the barrier and the false vacuum, as if the $\frac{1}{2}\xi\phi^2 R$ term *were part of the effective potential*. This is consistent with what we have written for the effective potential in Eq. (4.101), and thus computing the decay exponent is as simple as computing the potential with the extra $\xi\phi^2 R/2$ piece and computing the height difference between the false vacuum and barrier. This trick avoids a complicated conversion of the Einstein-frame solution back to the Jordan frame.

Rather than the more complicated discussion of section 3.8, we used a slightly simpler analysis to obtain the probability of nucleating a bubble in our past light cone. Let us assume that we have some number N e-folds of inflation visible, which splits the visible universe into approximately e^{3N} Hubble volumes that could have decayed during inflation. Furthermore, assume some scale $A = \mu^4$, then the probability per unit time of a decay occurring within one Hubble volume is:

$$\gamma = \frac{4\pi\mu^4}{3H^3}e^{-B}. \quad (5.29)$$

Hence the probability of a decay occurring between t_1 and t_2 is:

$$p(N, 1) = \frac{4\pi\mu^4}{3} \int_{t_1}^{t_2} dt \frac{\mu^4}{H^3} e^{-B(H)}. \quad (5.30)$$

In principle, H can be time dependent, but it is convenient to express this in terms of the number of e-folds, $dN/N = Hdt$

$$p(N, 1) = \frac{4\pi\mu^4}{3} \int_1^N \frac{dN}{\dot{N}^4} N^3 e^{-B(N)}. \quad (5.31)$$

For constant H, this can be evaluated as:

$$p(N, 1) = \frac{4\pi}{3} \left(\frac{\mu}{H}\right)^4 e^{-B} \log(N). \quad (5.32)$$

This gives the total probability that a bubble was nucleated within a given Hubble volume, during inflation. Within the observable universe, if we can see N e-folds of inflation, then we
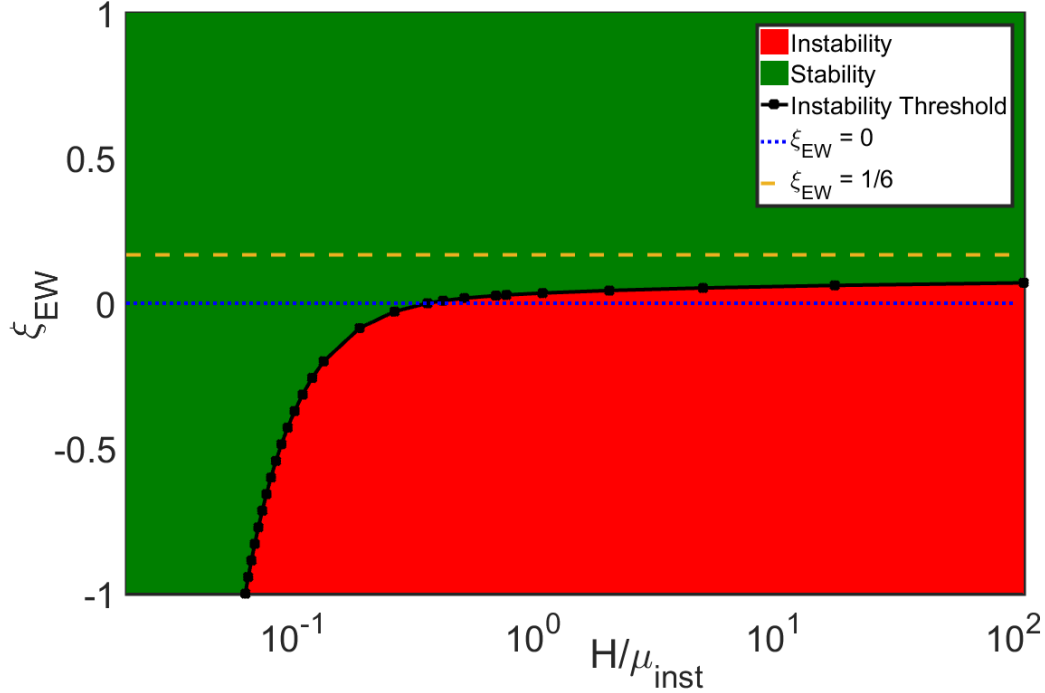
Figure 5.7: Stability of the electroweak vacuum for different values of ξ_{EW} and H. Negative ξ tends to destabilise the potential, while positive ξ can rescue it, even for large H. Originally published in [5]. Compare with results in [6, 7].

expect of order e^{3N} such Hubble volumes [65], and thus the expected number of Hubble volumes which decay during inflation is $e^{3N}p(N,1)$. If even one such Hubble volume were to survive inflation, then it would expand to fill the whole universe. Consequently, for stability, we require $e^{3N}p(N,1) < 1$, or:

$$B > 3N + \log\left(\frac{4\pi}{3}\left(\frac{\mu}{H}\right)^4\right) + \log(\log(N)). \qquad (5.33)$$

In the case of the Hawking-Moss solution, for example, this would impose the condition:

$$H < A\Delta V(\phi_{\text{bar}})^{\frac{1}{4}}_{\xi}, \qquad (5.34)$$

where:

$$A = \left[\frac{8\pi^2}{3\left(3N + \log\left(\frac{4\pi}{3}\left(\frac{\mu}{H}\right)^4\right) + \log(\log(N))\right)}\right]^{\frac{1}{4}}. \qquad (5.35)$$

The scale μ is somewhat arbitrary and is meant to absorb various factors (such as cosmological history since the end of inflation, and the precise pre-factor for Hawking-Moss bubbles computed including graviton fluctuations). However, A is only weakly dependent on this, so we assume for simplicity that $10^{-2} < \frac{4\pi\mu^4}{3H^4} < 10^2$ to give the ad hoc $A = 0.617 \pm 0.004$. This corresponds to out intuition that H must be comparable in height to the barrier for significant decays to occur, but here we take into account how non-minimal coupling affects the calculation, since we compare H to $\Delta V_\xi(\phi_{\text{bar}})^{1/4}$ rather than $\Delta V(\phi_{\text{bar}})^{1/4}$. This produces as threshold value of ξ for a given H that will lead to stability or instability. We plot this in figure 5.7. Similar results were also given by [6].

Chapter 6

Vacuum Decay in a De Sitter Background

Thus far, our results for the Standard Model have considered gravitational effects of vacuum decay in the flat false vacuum ($V_0 = 0$) limit. Now we consider non-zero, positive V_0.

6.1 Shooting Method for De Sitter Bounces

As discussed in section 3.4, for $V_0 > 0$, the bounce solutions are always compact. This is a substantial change from the $V_0 = 0$ case, which makes for a qualitative difference in how it is treated. Instead of one unknown initial value, $\phi_0 = \phi(0)$, it is also necessary to know the value on the other side of the barrier, $\phi_1 = \phi(\chi_{\max})$. Consequently, finding a solution in de Sitter space is, at minimum, twice as difficult, since one needs to apply the shooting method to *both* values.

There is an additional complication, however, in that instead of one singularity at $\chi = 0$ which must be avoided, there are two singularities, with a second appearing at $\chi = \chi_{\max}$. Worse, this singularity is *movable*, since it's position depends on the solution itself, being defined by the first $\chi_{\max} > 0$ at which $a(\chi_{\max}) = 0$. It is not, therefore, an option to simply integrate from $\chi = 0$ up to $\chi = \chi_{\max}$, since integrating into a co-ordinate singularity is generally unstable. This is easy to see from the field equation:

$$\ddot{\phi} + \frac{3\dot{a}}{a}\dot{\phi} - V'(\phi) = 0. \tag{6.1}$$

If $\dot{a} < 0$, then the second term of Eq. (6.1) becomes an anti-friction term, which in the mechanical analogy causes the ϕ to accelerate. As we approach $a = 0$, this anti-friction diverges and thus so does the solution, unless we approach $\dot{\phi} = 0$.

To deal with this, it is necessary to shoot from both sides. The procedure is as follows:

1. Pick values of ϕ_0, ϕ_1, on opposite sides of the barrier, i.e. $\phi_0 \in (\phi_{\mathrm{fv}}, \phi_{\mathrm{bar}})$ and $\phi_1 \in (\phi_{\mathrm{bar}}, \phi_{\mathrm{tv}})$.

2. Compute two solutions $\phi_{\mathrm{false}}(\chi)$ and $\phi_{\mathrm{true}}(\chi)$ with the initial conditions: $\phi_{\mathrm{false}}(0) = \phi_0, \dot{\phi}_{\mathrm{false}}(0) = 0, \phi_{\mathrm{true}}(0) = \phi_1, \dot{\phi}_{\mathrm{true}}(0) = 0$.

3. Classify these solutions as either undershoots or overshoots, according to the following definition:

   (a) Undershoots have some point $\chi > 0, \chi < \chi_{\max}$ satisfying $\dot{\phi}(\chi) = 0$.

   (b) Overshoots diverge without ever encountering $\dot{\phi} = 0$. This can be identified by ϕ_{false} passing through the true vacuum, and ϕ_{true} passing through the false vacuum with $\dot{\phi} \neq 0$.

4. By the arguments of [109], there must lie a bounce solution between any undershoot and overshoot. Find an undershoot and overshoot on each side of the barrier, and then bisect on this range until the relevant bounce is found.

5. Once a bounce starting on each side is found, match the two solutions. Truncate each solution at χ_{mid} defined by $\dot{a}(\chi_{\mathrm{mid}}) = 0$ (if no such point exists, then the solution is not sufficiently close to a bounce, so return to the bisection step - a bounce solution will *always* have such a point - see section 3.4).

6. Compute $\chi_{\text{max}} = \chi_{\text{mid,false}} + \chi_{\text{mid,true}}$. Now flip ϕ_{false} to define:

$$\phi_{\text{bounce}}(\chi) = \left\{ \begin{pmatrix} \phi_{\text{true}}(\chi) & \chi < \chi_{\text{mid,true}} \\ \phi_{\text{false}}(\chi_{\text{max}} - \chi) & \chi > \chi_{\text{min,true}} \end{pmatrix} \right. , \tag{6.2}$$

and similarly patch together $a(\chi)$ from the two halves of the solution. This gives the complete solution, from which we can compute the action.

The reason for the patching together of the two solutions at their midpoints, where $\dot{a} = 0$, is that it avoids the anti-friction region, where we might expect the solution to be less reliable. Note also that it is necessary to find both an undershoot *and* an overshoot to get the bisection started. Under certain conditions, we can exploit the fact that solutions sufficiently close to the critical points of the potential satisfy this. Recall that with Lemma 3 we proved that solutions starting sufficiently close to the false vacuum are always overshoots. This allows us to guarantee that an overshoot can always be found (note that this lemma applies equally well to the true vacuum, so we can always find an overshoot on the true vacuum side if there is a true vacuum in the potential). Lemma 4 on the other hand says that we can always find an undershoot by going sufficiently close to the top of the barrier (if it exists), provided:

$$\frac{V''(\phi_{\text{bar}})}{4} + \frac{V(\phi_{\text{bar}})}{3M_{\text{P}}^2} < 0. \tag{6.3}$$

This is related to the existence proof for CdL solutions given by [109] - that argument essentially amounts to saying that since an overshoot and an undershoot are proven to exist, then a CdL bounce necessarily exists if Eq. (6.3) is satisfied.

The more interesting case is if Eq. (6.3) is *not* satisfied. In that case, solutions starting close to any critical point of the potential are overshoots, and thus a CdL solution may not exist. However,this does not amount to a proof of it's non existence - in fact, as we will see, CdL solutions *can* exist in this situation, and this is crucial to the main results of this thesis.

Another point is that the method described here may fail if the solutions simply do not match at their respective $\dot{a} = 0$ points. There is no guarantee that a, ϕ will match, and if they do not, then this implies that the two halves found are actually *different* solutions. This will show up as a discontinuity in the computed solution, and reveals the presence of *multiple* CdL solutions.

6.2 The Critical Threshold and the CdL-HM Transition

As mentioned in section 3.3.3, there is always a second type of bounce, the Hawking-Moss solution, which sits at $\phi = \phi_{\text{bar}}$ and is a constant solution. In section 3.6 we computed the eigenvalue spectrum of the Hawking-Moss solution and found that it will have more than one negative eigenvalue if:

$$\frac{V''(\phi_{\text{bar}})}{4} + \frac{V(\phi_{\text{bar}})}{3M_{\text{P}}^2} < 0. \tag{6.4}$$

It is immediately striking that Eq. (6.4) is precisely the same condition as Eq. (6.3). This the first hint that there is link between the two. Re-arranging Eq. (6.4) and defining the background Hubble rate as:

$$H^2 = \frac{V(\phi_{\text{fv}})}{3M_{\text{P}}^2}, \tag{6.5}$$

then there exists a critical background Hubble rate:

$$H_{\text{crit}}^2 = -\frac{V''(\phi_{\text{bar}})}{4} - \frac{[V(\phi_{\text{bar}}) - V(\phi_{\text{fv}})]}{3M_{\text{P}}^2}, \tag{6.6}$$

below which, CdL solution necessarily exist, and Hawking-Moss solutions do not contribute to vacuum decay, owing to their additional negative eigenvalues. Above this, the Hawking-Moss solution does contribute to vacuum decay. The question is, does the CdL solution also contribute?

At this point, the naive answer seems to be that it shouldn't - the existence proof ceases to apply, and this *might* be a signal that the CdL solution no longer exists above this threshold. Is this the case?

One thing that appears to support this, at first glance, is that we can prove the number of solutions *definitely* changes in number:

Statement 7. *As H changes from $H < H_{\text{crit}}$ to $H > H_{\text{crit}}$, the number of CdL solutions changes by an odd number.*

Proof. By the results of [109],there must exist a bounce solution between every overshoot and undershoot. This means that we can split the space of initial conditions, $(\phi_{\text{fv}}, \phi_{\text{bar}})$ (considering only the false vacuum side is sufficient) into 'overshoot' and 'undershoot' regions. Wherever there is a transition between two regions of opposite character, a bounce solution exists. Now, by lemmas 3 and 4, when $H < H_{\text{crit}}$, solutions close to ϕ_{fv} are overshoots, and those close to ϕ_{bar} are undershoots. This means that there is an odd number of transitions, and thus an odd number of CdL solutions (not necessarily 1 solution). Vice versa, when $H > H_{\text{crit}}$, solutions near ϕ_{bar} are now overshoots, and so there must be an even number of (or zero) solutions. Either way, the number of CdL solutions changes by an odd number. $\square$

Lemma 7 thus appears to suggest that the CdL solution disappearing at H_{crit} is plausible. Solutions are *definitely* either created or destroyed across this threshold, and if there were only a single CdL solution for $H < H_{\text{crit}}$, it would be consistent for this to disappear at H_{crit}. Indeed, this seems to be what happens in many potentials. Consider for example the polynomial potential:

$$V(\phi) = \frac{1}{2}m^2\phi^2 + \frac{\lambda_4}{4}\phi^4 + \frac{\lambda_6}{6M_{\text{P}}^2}\phi^6. \tag{6.7}$$

For the parameters $\lambda_4 = -1, \lambda_6 = +1, m^2 = 0.1M_{\text{P}}^2$, we plot this potential in fig. 6.1.

For this potential, we plot solutions (fig. 6.2) and the decay rate (fig. 6.3). The critical Hubble rate in this case occurs at $V_{0\text{crit}} = 0.014822M_{\text{P}}^4$. As can be seen from the solutions in fig. 6.2, as $H \to H_{\text{crit}}$ from below, the CdL solutions increasingly decrease in amplitude until they resemble the Hawking-Moss solution, merging smoothly with it at $H = H_{\text{crit}}$. The decay exponent merges similarly smoothly in fig. 6.3, which also illustrates how this decay exponent approaches the flat false vacuum result as $H \to 0$, while the action of the Hawking-Moss diverges (and in any case, doesn't contribute to the decay rate).

This is in some sense the 'typical' behaviour that we would expect - CdL solutions dominate the decay rate below the critical threshold, and as we raise the Hubble rate, the solutions increasingly resemble the Hawking-Moss solution until they cease to exist at H_{crit}, and the
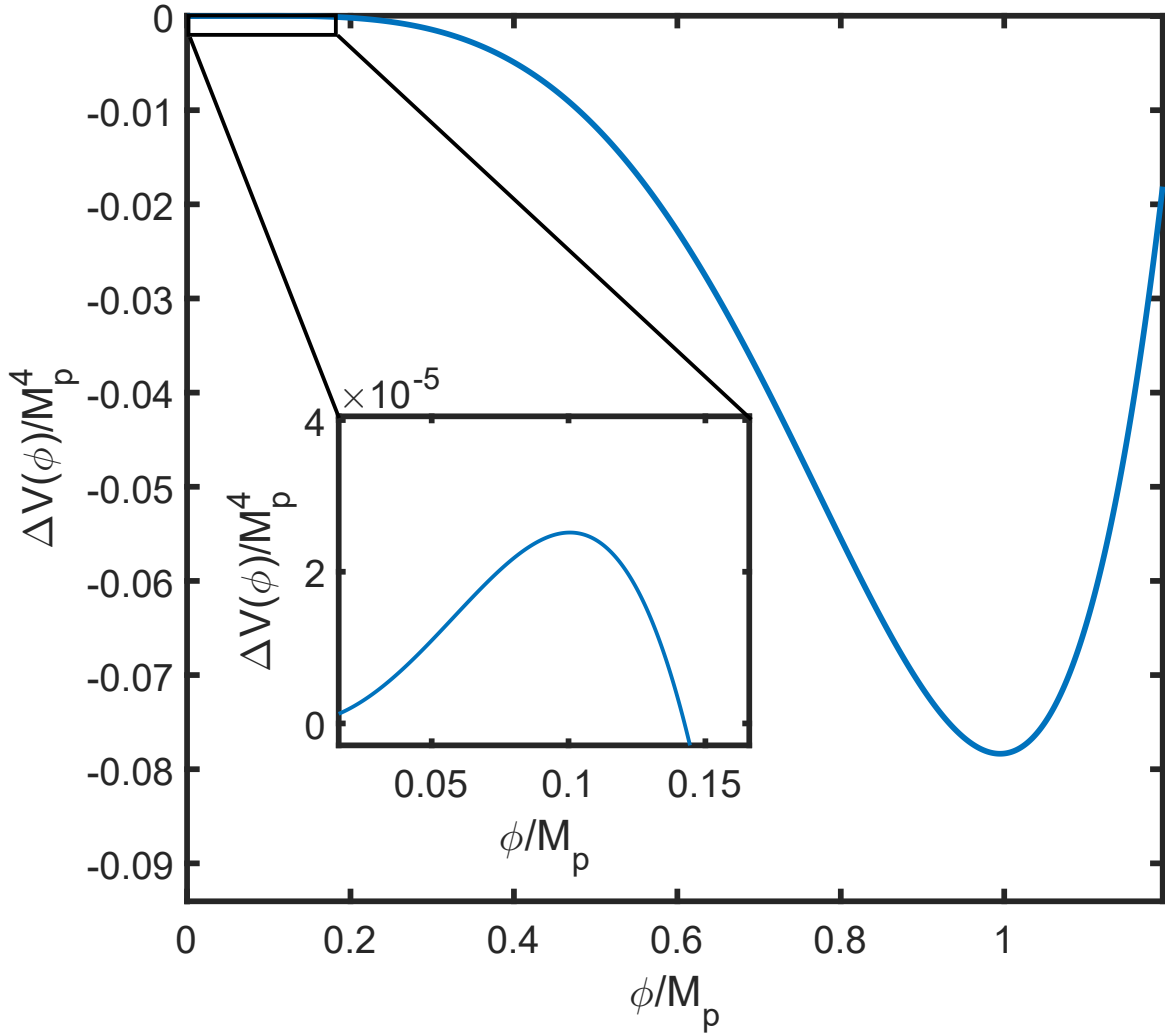
Figure 6.1: Plot of the polynomial potential on Eq. (6.7), with $\lambda_4 = -1, \lambda_6 = +1, m^2 = 0.1 M_{\mathrm{P}}^2$. The barrier is chosen to be much shallower than the true vacuum similar to the Standard Model case. Originally published in [2].
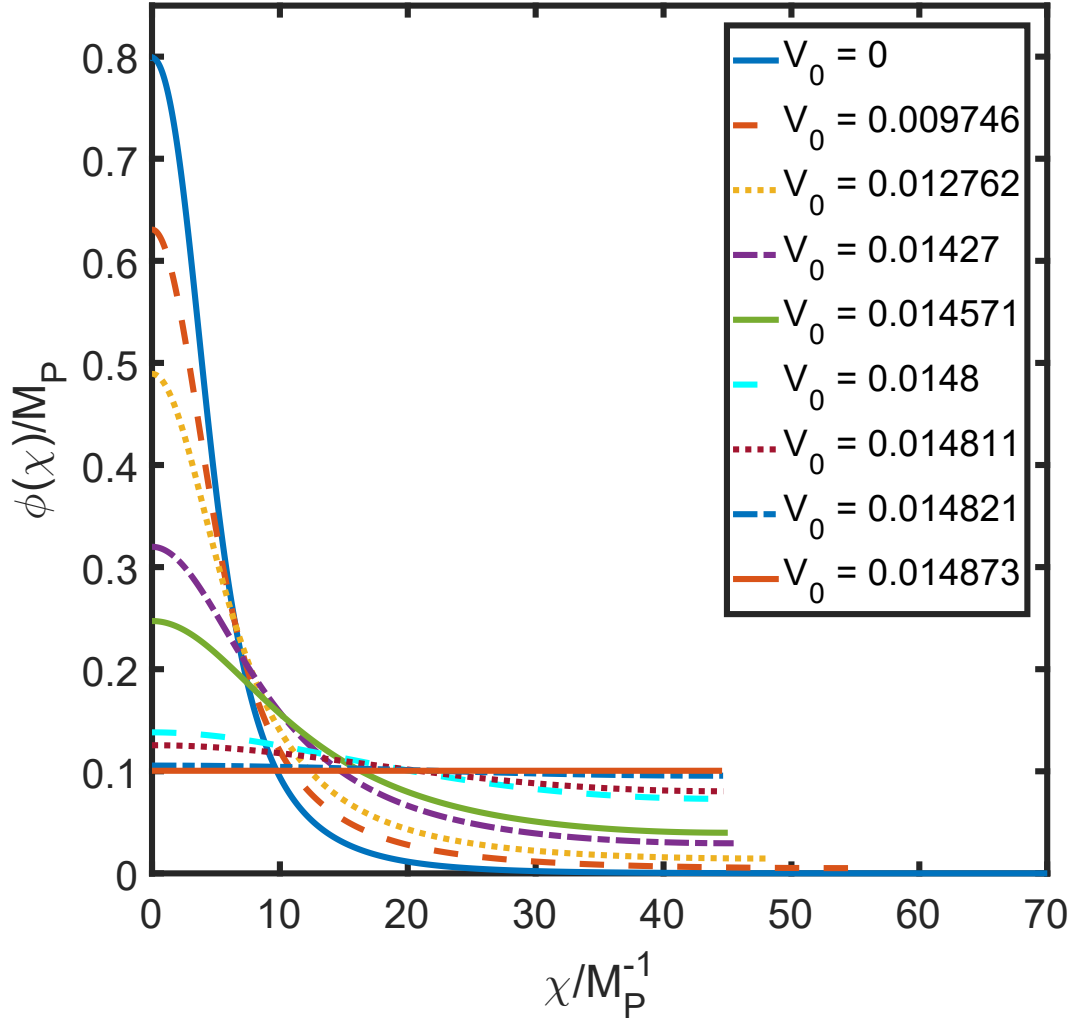
Figure 6.2: Plot of bounce solutions in the polynomial potential of fig. 6.1. Originally published in [2].

decay is entirely Hawking-Moss dominated. We can call this phenomenon the 'CdL-Hawking-Moss transition. As we will see, however, it is not a universal phenomenon.
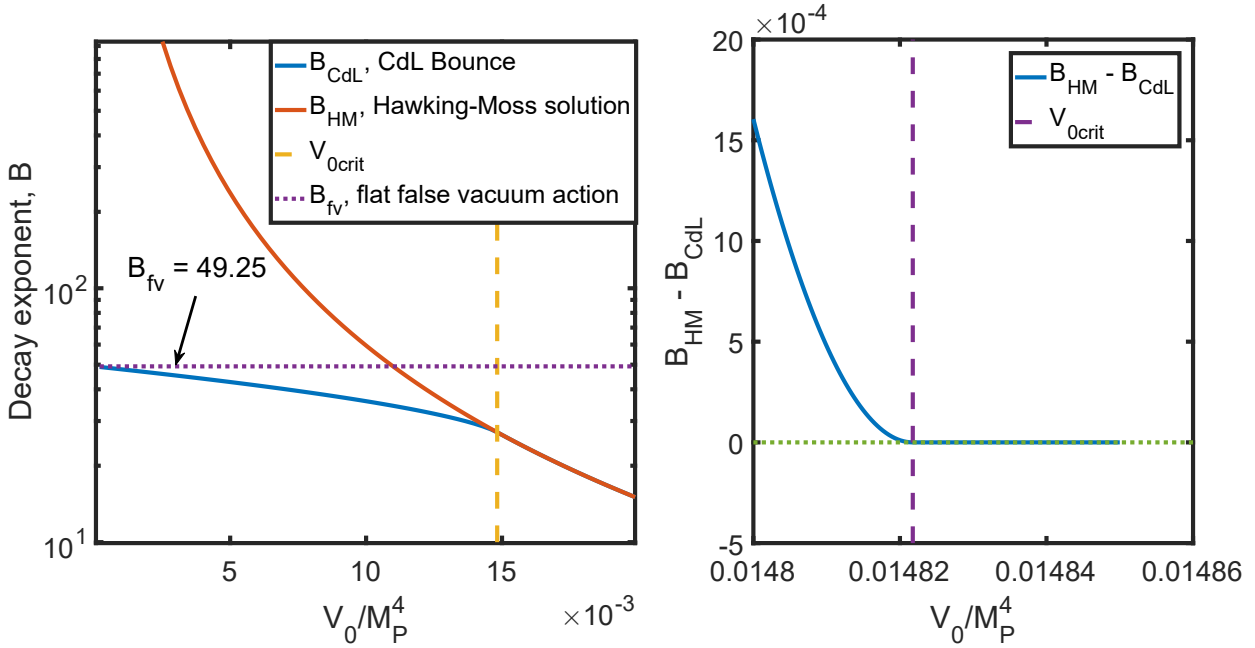
Figure 6.3: Plot of the decay exponent, B, in the polynomial potential of fig. 6.1. Originally published in [2].

6.3 CdL Solutions Around the Barrier

We can get a better understanding of the CdL-Hawking-Moss transition by considering the behaviour of bounce solutions around the critical threshold. For these bounces, it is possible to derive perturbative expressions for the solution - this was considered, for example, by [113, 112], and studied in the context of the Standard Model by [7].

Following [113], we expand the potential around the top of the barrier as:

$$V(\phi) = V(\phi_{\text{bar}}) + \frac{V''(\phi_{\text{bar}})}{2}(\phi - \phi_{\text{bar}})^2 + \frac{V^{(3)}(\phi_{\text{bar}})}{6}(\phi - \phi_{\text{bar}})^3 + \frac{V^{(4)}(\phi_{\text{bar}})}{24}(\phi - \phi_{\text{bar}})^4 + \ldots \quad (6.8)$$

We wish to find solutions when H is close to the critical threshold, H_{crit}. We will use a slight modification of the approach used by [113], and use the dimensionless perturbation parameter:

$$\epsilon^2 = -\Lambda \frac{3M_{\text{P}}^2}{V(\phi_{\text{bar}})}\left(H^2 - H_{\text{crit}}^2\right) = -\Lambda\left(\frac{3M_{\text{P}}^2 V''(\phi_{\text{bar}})}{V(\phi_{\text{bar}})} + 1\right). \quad (6.9)$$

This is equivalent to the parameter χ^2 used by [113] when $\Lambda = 1$, but introducing the arbitrary factor Λ will allow us to consider cases where $H > H_{\text{crit}}$, as well as $H < H_{\text{crit}}$ (as considered by [113]). As we will see, this will not make a different to the result. Additionally, instead of ϕ we will consider:

$$u = \frac{\Delta\phi}{\Delta\phi_0}, \quad (6.10)$$

where $\Delta\phi = \phi - \phi_{\text{bar}}$ and $\Delta\phi_0 = \Delta\phi(0)$ is the initial condition. Note that $\Delta\phi_0$ is ϵ dependent, since the solution will change with H. Note also when comparing with [113, 112, 7] that we define the Hubble rate as $H^2 = \frac{V(\phi_{\text{fv}})}{3M_{\text{P}}^2}$, rather than at the top of the barrier, although the difference is Planck-suppressed. We now transform variables from χ to $x = \frac{\pi\chi}{\chi_{\text{max}}}$ where

112

$a(\chi_{\max}) = 0$ for the bounce solution. In fact, $\chi_{\max}$ depends on ϵ, but this variable transformation ensures that the boundaries are always at $x = 0, \pi$. In these new variables, the bounce equations become:

$$u'' + \frac{3a'}{a}u' - \frac{\chi_{\max}^2}{\pi^2}V''(\phi_{\mathrm{bar}})u - \frac{\chi_{\max}^2}{\pi^2}\Delta\phi_0\frac{V^{(3)}(\phi_{\mathrm{bar}})}{2}u^2 - \frac{\chi_{\max}^2}{\pi^2}\frac{V^{(4)}(\phi_{\mathrm{bar}})}{6}\Delta\phi_0^2 u^3 = 0, \quad (6.11)$$

$$a'' + \frac{a\Delta\phi_0^2}{3M_{\mathrm{P}}^2}\left(u'^2 + \frac{\chi_{\max}^2}{\pi^2}\frac{V''(\phi_{\mathrm{bar}})}{2}u^2 + \frac{\chi_{\max}^2}{\pi^2}\Delta\phi_0\frac{V^{(3)}(\phi_{\mathrm{bar}})}{6}u^3 + \frac{\chi_{\max}^2}{\pi^2}\Delta\phi_0^2\frac{V^{(4)}(\phi_{\mathrm{bar}})}{24}u^4\right)$$
$$- a\frac{\chi_{\max}^2}{\pi^2}\frac{V''(\phi_{\mathrm{bar}})}{4\left(1 + \frac{\epsilon^2}{\Lambda}\right)}. \tag{6.12}$$

We now write perturbative expressions for the solutions and their parameters $\Delta\phi_0$ and $\chi_{\max}$:

$$u(x) = u_0(x) + \epsilon u_1(x) + \epsilon^2 u_2(x) + \dots, \tag{6.13}$$

$$a(x) = a_0(x) + \epsilon a_1(x) + \epsilon^2 a_2(x) + \dots, \tag{6.14}$$

$$\Delta\phi_0 = \Delta\phi_0^{(0)} + \epsilon\Delta\phi_0^{(1)} + \epsilon^2\Delta\phi_0^{(2)} + \dots, \tag{6.15}$$

$$\chi_{\max} = \chi_{\max}^{(0)} + \epsilon\chi_{\max}^{(1)} + \epsilon^2\chi_{\max}^{(2)} + \dots. \tag{6.16}$$

For this to work, we need something to perturb around. In the $\epsilon = 0$ case, we have exactly $H = H_{\mathrm{crit}} = 0$. This means that the linearised bounce equations:

$$\Delta\ddot{\phi} + \frac{3\dot{a}}{a}\Delta\dot{\phi} - V''(\phi_{\mathrm{bar}})\Delta\phi = 0, \tag{6.17}$$

$$\ddot{a} + \frac{aV(\phi_{\mathrm{bar}})}{3M_{\mathrm{P}}^2}, \tag{6.18}$$

have a solution that can be made to satisfy the bounce boundary conditions, namely:

$$\Delta\phi(\chi) = \frac{\Delta\phi_0}{3}C_1^{(3/2)}(\cos(H_{\mathrm{HM}}\chi)), \tag{6.19}$$

$$a(\chi) = \frac{1}{H_{\mathrm{HM}}}\sin(H_{\mathrm{HM}}\chi), \tag{6.20}$$

where $H_{\mathrm{HM}}^2 = \frac{V(\phi_{\mathrm{bar}})}{3M_{\mathrm{P}}^2}$ and $C_n^{(3/2)}(u)$ is the nth Gegenbauer polynomial [128]. Note that Eq. (6.18) only has polynomial solutions when $\frac{-V''(\phi_{\mathrm{bar}})}{H_{\mathrm{HM}}^2} = n(n+3)$ where $n = 0, 1, 2, \dots$. These in fact correspond to the eigen-modes of the Hawking-Moss solution. In particular, $n = 1$ is the mode which changes the sign of it's eigenvalues at H_{crit}, and in that case $C_1^{(3/2)}(u) = 3u$ and the solution is just:

$$\Delta\phi(x) = \Delta\phi_0\cos(H_{\mathrm{HM}}\chi). \tag{6.21}$$

Note, however, that the linearised solution is only a solution of the bounce equations in the $\Delta\phi_0 \to 0$ limit - it is for this reason that it is known as a 'limit solution' [109]. Consequently, if we wish to consider solutions that continuously deform into the $n = 1$ eigen-mode of the Hawking-Moss as $H \to H_{\mathrm{crit}}$, then we should take the zeroth-order solution to be:

$$u_0(x) = \cos(x), \tag{6.22}$$

$$a_0(x) = \frac{\chi_{\max}}{\pi}\sin(x). \tag{6.23}$$

The astute reader will notice that u_0, a_0 thus defined are *not* the $\epsilon = 0$ solutions except when $\epsilon = 0$, because $\chi_{\max} \neq \chi_{\max}^{(0)}$. If we were to use the $\epsilon = 0$ solutions instead, we would encounter

secular terms in the perturbative expansion that complicate the calculations [168]. These secular terms are eliminated precisely by choosing $\chi_{\max}$ to vary as in Eq. (6.16), which is analogous to the way the frequency of a Duffing oscillator changes with the perturbation parameter [168].

This also has the effect of simplifying the boundary conditions for the perturbative expansion: we require $a(0) = a(\phi) = 0$ and $a'(0) = \frac{\chi_{\max}}{\pi}$ (i.e. $\dot{a}(0) = 1$). The apparent third boundary condition here is really what defines $\chi_{\max}$, so this system is not over-constrained. Similarly, $u'(0) = u'(\pi) = 0$ (the normal CdL bounce boundary conditions) and $u(0) = 1$ (which ensures $\Delta\phi_0 = \Delta\phi(0)$ to all orders of perturbation theory). Since Eqs. (6.22) and (6.23) already satisfy these conditions to all orders in ϵ, then the boundary conditions on the perturbative solutions are just:

$$u'_n(0) = u'_n(\pi) = u_n(0) = 0, \qquad (6.24)$$
$$a_n(0) = a_n(\pi) = a'_n(0) = 0, \qquad (6.25)$$

for all n. Again, the extra boundary condition here is simply to impose the definitions of $\Delta\phi_0$ and $\chi_{\max}$ at each order in perturbation theory: when we perform the expansion we will see that unknown terms like $\chi_{\max}^{(n)}, \phi_0^{(n)}$ will appear in each equation, and are fixed by the extra boundary conditions, so the system is not over-constrained.

The perturbative equations of motion are given in appendix A.2. At first glance, these equations appear hopelessly complicated, but in fact, they are solvable analytically. Start by solving Eq. (A.42), which is the inhomogeneous simple harmonic oscillator. Substituting the solution into Eq. (A.43) then gives the inhomogeneous Gegenbauer equation for $n = 1$, which has a solution in terms of $\cos(x)$. We can then substitute these solutions into the higher order equations, each time creating an inhomogeneous harmonic oscillator (for a_n) or Gegenbauer equation (for u_n), where the right hand side is always a polynomial in some number of trigonometric functions. This is because the general solution of the homogeneous Gegenbauer equation with $n = 1$ is:

$$y(x) = C_1 \cos(x) + C_2 \frac{1}{4(\cos^2(x) - 1)} \left[4 - 6\cos^2(x) + 3\cos(x)\log(1 - \cos(x)) \right.$$
$$\left. - 3\cos^3(x)\log(1 - \cos(x)) - 3\cos(x)\log(1 + \cos(x)) + 3\cos^3(x)\log(1 + \cos(x)) \right], \quad (6.26)$$

where the second solution here is the Gegenbauer equation of the second kind. This is divergent at the boundaries 0 and π, so the inhomogeneous terms in the solution must combine with C_2 and C_1 to cancel this divergence. This always results in a solution that is polynomial in $\cos(x)$ and $\sin(x)$, and the $\cos^2(x) - 1$ in the denominator cancels. Consequently, each order of perturbation theory, once the lower order solutions are substituted in, gives an inhomogeneous equation with a complicated polynomial of trigonometric functions, and thus is always solvable by the method of variation of parameters, with either sufficient patience, or computer assisted algebra.

Applying this technique, the solutions that match the boundary conditions, up to second

order in ϵ are:

$$a_1(x) = 0, \tag{6.27}$$

$$u_1(x) = -\frac{V^{(3)}(\phi_{\text{bar}})\Delta\phi_0^{(1)}}{6V^{(2)}(\phi_{\text{bar}})}(1 + \cos(x) - 2\cos^2(x)), \tag{6.28}$$

$$a_2(x) = \frac{\chi_{\max}^{(0)}(\Delta\phi_0^{(1)})^2}{8\pi M_{\text{P}}^2}\sin^3(x), \tag{6.29}$$

$$u_2(x) = \frac{(1 - \cos(x))}{12V^{(2)}(\phi_{\text{bar}})\Lambda(4(V^{(2)}(\phi_{\text{bar}}))^2 + \left(\frac{(V^{(3)}(\phi_{\text{bar}}))^2}{2} - 9V^{(2)}(\phi_{\text{bar}})V^{(4)}(\phi_{\text{bar}})\right)M_{\text{P}}^2)} \times$$

$$\left((V^{(2)}(\phi_{\text{bar}}))^2\left[-\frac{27}{2}V^{(2)}(\phi_{\text{bar}})\cos(x)(1 + \cos(x))\right.\right.$$

$$\left. -8V^{(3)}(\phi_{\text{bar}})\Lambda(1 + 2\cos(x))\Delta\phi_0^{(2)}\right]$$

$$-4M_{\text{P}}^2\left[-V^{(2)}(\phi_{\text{bar}})\left\{\frac{(V^{(3)}(\phi_{\text{bar}}))^2}{2} - 9V^{(2)}(\phi_{\text{bar}})V^{(4)}(\phi_{\text{bar}})\right.\right.$$

$$\left. +2\left(\frac{(V^{(3)}(\phi_{\text{bar}}))^2}{2} - 9V^{(2)}(\phi_{\text{bar}})V^{(4)}(\phi_{\text{bar}})\right)\cos(x)\right.$$

$$\left. +(-3(V^{(3)}(\phi_{\text{bar}}))^2 - 9V^{(2)}(\phi_{\text{bar}})V^{(4)}(\phi_{\text{bar}}))\cos(2x)\right\}$$

$$\left.\left. +V^{(3)}(\phi_{\text{bar}})\Lambda\left(\frac{(V^{(3)}(\phi_{\text{bar}}))^2}{2} - 9V^{(2)}(\phi_{\text{bar}})V^{(4)}(\phi_{\text{bar}})\right)(1 + 2\cos(x))\Delta\phi_0^{(2)}\right]\right). \tag{6.30}$$

While $\Delta\phi_0$ and $\chi_{\max}$ are found to be:

$$\chi_{\max} = \frac{2\pi}{\sqrt{-V''(\phi_{\text{bar}})}} + \epsilon^2\frac{\pi(12M_{\text{P}}^2 - \Lambda(\Delta\phi_0^{(1)})^2)}{12\sqrt{-V''(\phi_{\text{bar}})}\Lambda M_{\text{P}}^2} + O(\epsilon^4), \tag{6.31}$$

$$\Delta\phi_0 = \epsilon\Delta\phi_0^{(1)} + \epsilon^2\frac{V^{(3)}(\phi_{\text{bar}})(\Delta\phi_0^{(1)})^2}{6V^{(2)}(\phi_{\text{bar}})}, \tag{6.32}$$

$$(\Delta\phi_0^{(1)})^2 = \frac{21}{\Lambda\left(\frac{4}{M_{\text{P}}^2} + \frac{(V^{(3)}(\phi_{\text{bar}}))^2}{2(V^{(2)}(\phi_{\text{bar}}))^2} - \frac{3V^{(4)}(\phi_{\text{bar}})}{2V^{(2)}(\phi_{\text{bar}})}\right)}. \tag{6.33}$$

Eq. (6.33) is especially significant, as it gives the condition under which solutions exist. The LHS is manifestly positive, but the RHS can potentially be negative. Note that we can technically choose the sign of Λ to counteract this sign, but this has consequences for whether the expansion is well defined for $H > H_{\text{crit}}$ or $H < H_{\text{crit}}$. Since $\Lambda = \text{sign}(\text{H}_{\text{crit}}^2 - \text{H}^2)$, then we require:

$$\text{sign}(\text{H}_{\text{crit}}^2 - \text{H}^2)\left(\frac{4}{\text{M}_{\text{P}}^2} + \frac{(\text{V}^{(3)}(\phi_{\text{bar}}))^2}{2(\text{V}^{(2)}(\phi_{\text{bar}}))^2} - \frac{3\text{V}^{(4)}(\phi_{\text{bar}})}{2\text{V}^{(2)}(\phi_{\text{bar}})}\right) > 0. \tag{6.34}$$

This condition was previously derived in [113, 112]. More recently is was discussed by [7]. To relate the condition of [7] to Eq. (6.34), we use the fact that:

$$\epsilon^2 = -\frac{\Lambda}{4}\left(\frac{V^{(2)}(\phi_{\text{bar}})}{H_{\text{HM}}^2} + 4\right) \implies -V^{(2)}(\phi_{\text{bar}}) = 4H_{\text{HM}}^2\left(1 + \frac{\epsilon^2}{\Lambda}\right), \tag{6.35}$$

in order to write:

$$\Delta\phi_0^2 = -\frac{1}{4}\left(\frac{V^{(2)}(\phi_{\text{bar}})}{H_{\text{HM}}^2} + 4\right)\frac{21}{\left(\frac{4}{M_{\text{P}}^2} + \frac{(V^{(3)}(\phi_{\text{bar}}))^2}{32H_{\text{HM}}^4} + \frac{3V^{(4)}(\phi_{\text{bar}})}{8H_{\text{HM}}^2}\right)} + O(\epsilon^4). \tag{6.36}$$

Thus:

$$\left(\frac{V^{(2)}(\phi_{\text{bar}})}{H_{\text{HM}}^2} + 4\right) = -\frac{(\phi(0) - \phi_{\text{bar}})^2}{14 H_{\text{HM}}^2}\left(V^{(4)}(\phi_{\text{bar}}) + \frac{(V^{(3)}(\phi_{\text{bar}}))^2}{12 H_{\text{HM}}^2} + \frac{32 H_{\text{HM}}^2}{3 M_{\text{P}}^2}\right). \qquad (6.37)$$

Up to the Planck-suppressed $\frac{32 H_{\text{HM}}^2}{3 M_{\text{P}}^2}$ term, this is the same condition found by [7]. Note that $H_{\text{HM}}^2 = \frac{V(\phi_{\text{bar}})}{3 M_{\text{P}}^2}$. We can also compute the action of this perturbative solution - full calculation is given in appendix A.2:

$$S = S_{\text{HM}} + \frac{2\pi^2 (\phi(0) - \phi_{\text{bar}})^4}{15 H_{\text{HM}}^4}\left(-\frac{1}{14}\left[V^{(4)}(\phi_{\text{bar}}) - \frac{(V^{(3)}(\phi_{\text{bar}}))^2}{3 V^{(2)}(\phi_{\text{bar}})} - \frac{8 V^{(2)}(\phi_{\text{bar}})}{3 M_{\text{P}}^2}\right]\right), \qquad (6.38)$$

where we used Eq. (6.33) to eliminate Λ. With the substitution $V^{(2)}(\phi_{\text{bar}}) = -4 H_{\text{HMcrit}}^2 = -4 H_{\text{HM}}^2 + O(\epsilon^2)$, this agrees with the form of the action derived elsewhere [113, 112, 7]. Note that $\phi(0) - \phi_{\text{bar}} = O(\epsilon)$. There is an important conclusion we can draw from Eq. (6.38): the sign of Λ, and thus the sign of $H^2 - H_{\text{crit}}^2$ is what determines whether these solutions have lower or higher action than the appropriate Hawking-Moss solution. In particular, if $H < H_{\text{crit}}$, and solutions exist, this tells us that $\Lambda > 0$, so these solutions always have *lower* action than the Hawking-Moss. This agrees with what we have seen - for such potentials, the CdL bounce approaches the Hawking-Moss as $H \to H_{\text{crit}}$, with the action approaching from below.

Somewhat more interesting, however, is the opposite case, when $H > H_{\text{crit}}$. If solutions exist here (that is, Eq. (6.34) is satisfied), then $\Lambda < 0$ and they will have *higher* action than the Hawking-Moss. It should be noted. In this case, a new solution appears at $H = H_{\text{crit}}$, but it is always suppressed relative to the Hawking-Moss solution.

However, there is a far more interesting conclusion that can be drawn from this. Recall in section 6.2 where we proved (lemma 7) that at H_{crit} the number of CdL solutions must change by an odd number. We also know that there is always a solution for $H < H_{\text{crit}}$. But if a solution exists for $H > H_{\text{crit}}$, and the number of solutions always changes by an odd number, we are left with an inescapable conclusion: *there must be more than one solution.*

6.4 Potentials with Multiple CdL Solutions

The discussion of section 6.3 revealed a surprising conclusion - it is possible to have *multiple* CdL solutions in certain potentials. Whether the solution that merges with the Hawking-Moss exists or not is determined by the quantity:

$$\Delta \equiv -\frac{1}{14}\left(V^{(4)}(\phi_{\text{bar}}) - \frac{\left(V^{(3)}(\phi_{\text{bar}})\right)^2}{3 V^{(2)}(\phi_{\text{bar}})} - \frac{8 V^{(2)}(\phi_{\text{bar}})}{3 M_{\text{P}}^2}\right). \qquad (6.39)$$

Specifically, existence requires $\text{sign}(\Delta) = \text{sign}(H_{\text{crit}}^2 - H^2)$ (see Eq. (6.34)). The sign and factor $1/14$ are retained here so that we can write Eq. (6.38) in the form:

$$S = S_{\text{HM}} + \frac{2\pi^2 (\phi_0 - \phi_{\text{bar}})^4 \Delta}{15 H_{\text{HM}}^4}. \qquad (6.40)$$

It is worth emphasising here that this leads to two different classes of potentials:

1. $\Delta < 0$, for which solutions only exist if $H < H_{\text{crit}}$. These solutions have lower action than the Hawking-Moss, and probably correspond to the CdL solution found numerically in figure 6.1.

2. $\Delta > 0$, for which solutions only exist if $H > H_{\text{crit}}$. Furthermore, there are at *least* two CdL solutions, one of which is not found perturbatively.

The $\Delta < 0$ case is the more 'typical' case - any potential with $V^{(4)}(\phi_{\text{bar}}) > 0$ will immediately fall into this category. But it is not necessarily more physical. Let us consider examples.

6.4.1 Polynomial Model
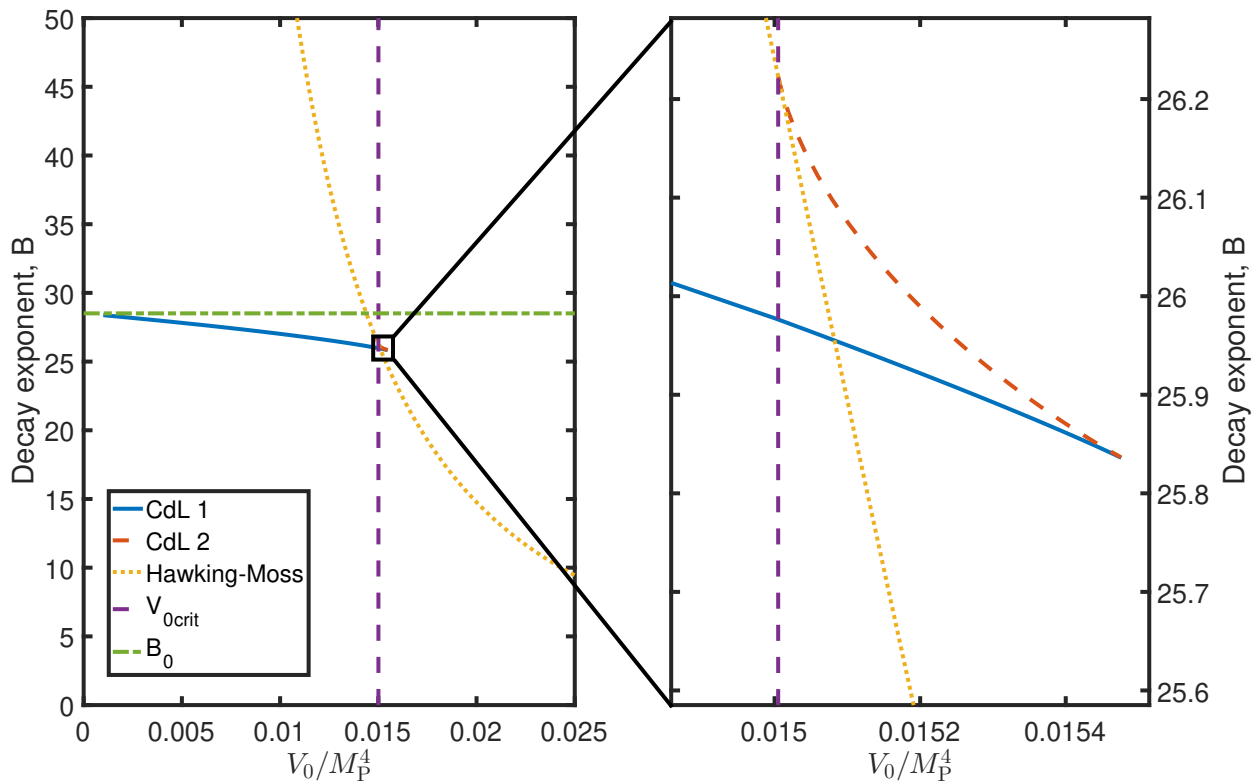
Figure 6.4: Plot of the decay exponent, B, as a function of $V_0 = V(0)$ for the potential in Eq. (6.41) using $g = -\frac{1}{5M_{\text{P}}^2}, m = 0.1M_{\text{P}}, \lambda = -1$. A second solution appears at $V_{0\text{crit}}$, which eventually merges with the usual CdL solution at higher V_0. The flat space decay exponent, B_0, is shown for reference.

Consider the potential:

$$V(\phi) = V_0 + \frac{1}{2}m^2\phi^2 + \frac{\lambda}{4}\phi^4 + \frac{g}{6}\phi^6, \tag{6.41}$$

with $m^2, g > 0$ and $\lambda < 0$. This is one of the simplest examples of a potential that exhibits tunnelling, and has the advantage that the barrier and true vacuum can be found in closed

form:

$$\phi_{\text{fv}} = 0, \tag{6.42}$$

$$\phi_{\text{bar}} = \sqrt{\frac{|\lambda| - Q}{2g}}, \tag{6.43}$$

$$\phi_{\text{tv}} = \sqrt{\frac{|\lambda| + Q}{2g}}, \tag{6.44}$$

$$Q \equiv \sqrt{|\lambda|^2 - 4m^2 g} < |\lambda|. \tag{6.45}$$

The derivatives at the barrier are given by:

$$V^{(2)}(\phi_{\text{bar}}) = \frac{Q(Q - |\lambda|)}{g}, \tag{6.46}$$

$$V^{(3)}(\phi_{\text{bar}}) = \sqrt{2}(2|\lambda| - 5Q)\sqrt{\frac{|\lambda| - Q}{g}}, \tag{6.47}$$

$$V^{(4)}(\phi_{\text{bar}}) = 6(4|\lambda| - 5Q). \tag{6.48}$$

H should be evaluated at the critical threshold and including the full height of the barrier, so $H = H_{HM} = \sqrt{-V^{(2)}(\phi_{\text{bar}})/4}$. This gives:

$$\Delta \propto -6(4|\lambda| - 5Q) + \frac{2(2|\lambda| - 5Q)^2(|\lambda| - Q)}{3Q(Q - |\lambda|)} + \frac{8Q(Q - |\lambda|)}{3gM_{\text{P}}^2}. \tag{6.49}$$

The last two terms are always negative. It can be shown that there is an upper limit to g for which tunnelling occurs, namely when the true and false vacua are of equal height and the potential never dips below V_0. This occurs at $g = 3|\lambda|^2/16m^2$, or $Q = |\lambda|/2$. In this limit, $\Delta < 0$, so for $\Delta > 0$ to occur, a necessary condition is that there exist a solution to $\Delta = 0$, or:

$$40Q^3 + \left(8|\lambda| - \frac{32m^2}{M_{\text{P}}^2}\right)Q^2 - 40|\lambda|^2 Q - 8|\lambda|^3 = 0. \tag{6.50}$$

for some $0 < Q < |\lambda|$. This can be factorised in the $m^2 \ll M_{\text{P}}^2$ limit:

$$(Q + |\lambda|)(40Q^2 - 32|\lambda|Q - 8|\lambda|^2) = 0, \tag{6.51}$$

which has zeros at $Q = -|\lambda|$, $Q = +|\lambda|$ and $Q = -\frac{|\lambda|}{5}$. The net effect of the $-32m^2 Q^2/M_{\text{P}}^2$ term is to reduce the (negative) value of the polynomial on the $Q > 0$ region, which means that the $Q = +|\lambda|$ root is pushed to higher Q, and no more positive Q roots are introduced. Hence, the positive root always satisfies $Q \geq |\lambda|$, while the other roots are always negative. This means that $\Delta < 0$ on the range $0 < Q < |\lambda|$, which is that covered by solutions possessing a barrier, and thus this simple polynomial model with a well defined true vacuum (i.e. $g > 0$) can *never* produce the unusual $\Delta > 0$ behaviour. A perturbative estimate for the positive root with $\epsilon = m^2/M_{\text{P}}^2$ is:

$$Q_{\text{pos}} = |\lambda| + \frac{\epsilon}{3} + \frac{2\epsilon^2}{27|\lambda|} + O(\epsilon^3). \tag{6.52}$$

There is a possible exception to this with $g < 0$, which can have a barrier, but no true vacuum

(this is similar to the situation in the Standard Model, for sub-Planckian field values). In that case, $Q > |\lambda|$, and $V^{(4)}(\phi_{\text{bar}}) < 0$ is always true. Perturbatively, we find that if:

$$g < -\frac{|\lambda|}{6M_\text{P}^2} - \frac{7\epsilon}{108M_\text{P}^2} + O(\epsilon^2), \qquad (6.53)$$

then $\Delta > 0$ is achieved. The exact expression can in principle be obtained by using the cubic formula on Eq. (6.50), but for most cases this is not necessary.

An example of the decay rates with $g = -\frac{1}{5M_\text{P}^2}, m = 0.1M_\text{P}, \lambda = -1$ is computed numerically and plotted in figure 6.4. The results when zoomed out are qualitatively similar to figure 6.3, but closer inspection of the area around the critical threshold reveals the presence of a second CdL solution. In this case, the solution soon merges into the usual CdL solution at sufficiently large V_0, which happens after the Hawking-Moss solution comes to dominate the decay. Unlike the $g > 0$ case of fig. 6.3, however, there is no smooth merging of the CdL into the Hawking-Moss.
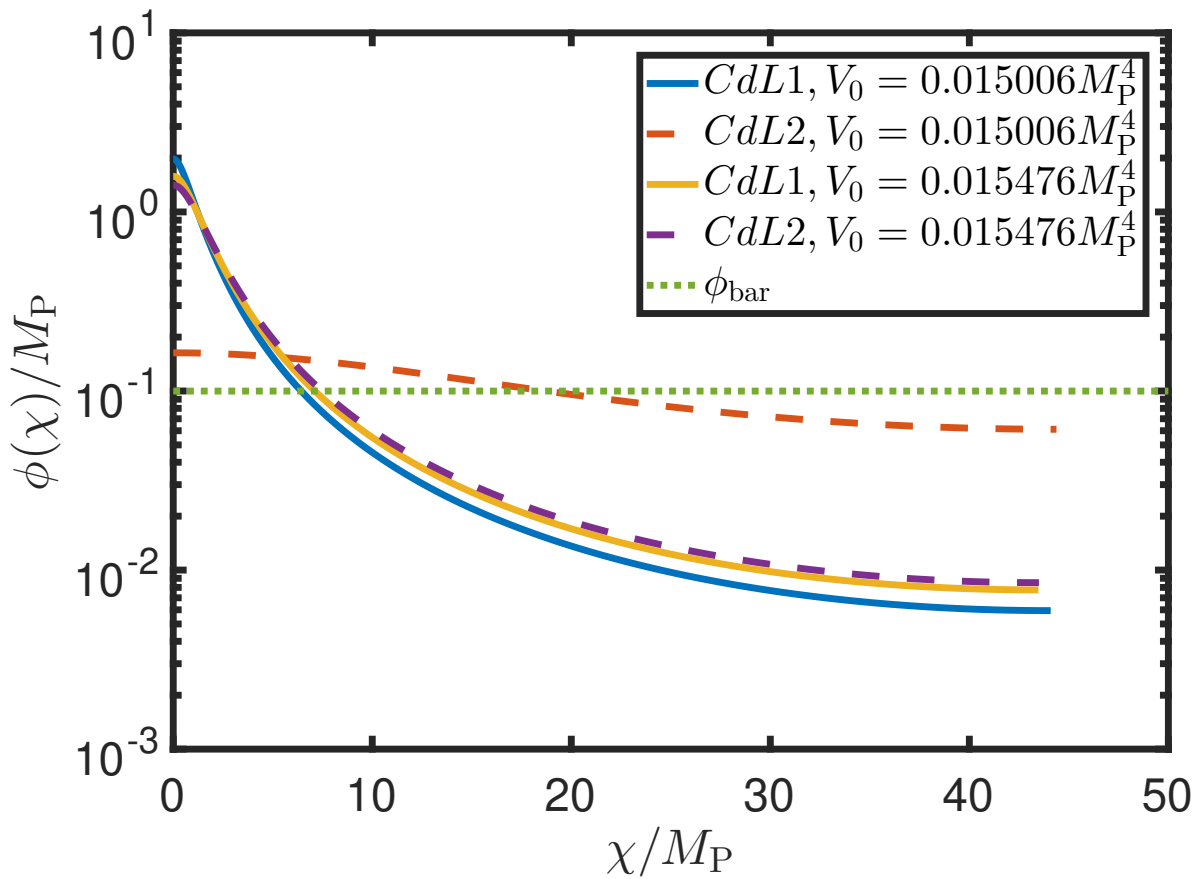
Figure 6.5: CdL solutions with the same parameters as fig. 6.4 for $V_0 = 1.015006M_\text{P}^4$ (blue and red) and $V_0 = 0.015476M_\text{P}^4$ (yellow and purple). The critical value is at $V_0 = 0.015005M_\text{P}^4$. As V_0 increases, the solutions become closer together.

Fig. 6.5 shows a plot of the solutions for a couple of different values of V_0. Notice that CdL 1 (the solution which exists in the $V_0 \to 0$ limit), continues to have a mostly large amplitude, while CdL 2 starts out with a small amplitude around the top of the barrier, and grows to meet CdL 1 until they merge. Unlike the $g > 0$ case, neither solution shrinks until it sits at the top of

the barrier - instead they disappear at some $V_0 > V_{crit}$. Note that it is not impossible that these solutions actually exist for all V_0 and simply move arbitrarily close together as V_0 increases - beyond the point where they appear to merge, the solutions become indistinguishable and the undershoot region between them becomes difficult to find numerically. Thus, it may *appear* that there are no CdL solutions, even though they in fact exist.

The example given here, with $g < 0$, is analogous to the Standard Model Higgs potential in that no true vacuum necessarily exists at large ϕ: the potential decreases without bound[1].

6.4.2 Linear Model

An example of a potential that has multiple solutions was considered by [110]. They considered the potential:

$$V(\phi) = \begin{cases} C(\phi + a) + V_0 & \phi < -a \\ V_0 & -a < \phi < a \\ -C(\phi - a) + V_0 & \phi > a \end{cases}.$$ (6.54)

In the fixed background approximation, with $H^2 = V_0/3M_P^2$ and $x = H\chi$, one finds the equation of motion to be:

$$\frac{1}{\sin^3(x)} \frac{d}{dx} \left(\sin^3(x) \frac{d\phi}{dx} \right) - \frac{\alpha}{H^2} = 0,$$ (6.55)

where $\alpha = C, 0, -C$ in the $\phi < -a, -a < \phi < a, \phi > a$ regions respectively. The general solution to this can be found analytically:

$$\phi(x) = \frac{\alpha}{H^2} \left[\frac{1}{3\sin^2(x)} - \frac{1}{3}\log|\sin(x)| \right] - D\left[\frac{1}{2}\log\left|\frac{\cos(x)+1}{\sin(x)}\right| + \frac{\cos(x)}{2\sin^2(x)} \right] + D.$$ (6.56)

Using this form, we fix D, E in each of the three regions, by matching the $\dot\phi(0) = \dot\phi(\pi/H) = 0$ boundary conditions and requiring that the solution be continuous in the first and second derivatives at the two potential gradient discontinuities at $\phi = \pm a$. Note that we do not know at what χ these occur, but we can remedy this by defining these matching points to occur at arbitrary points $\phi(x_\pm) = \pm a$, and then requiring that this be true for both parts of the solution at the matching point. This gives eight unknowns $(D_L, E_L, D_C, E_C, D_R, E_R, x_-, x_+)$ and eight equations to be satisfied:

$$\dot\phi_L(0) = 0, \qquad\qquad\qquad \dot\phi_R(\pi/H) = 0, \qquad\qquad (6.57)$$
$$\phi_L(x_-) = -a, \qquad\qquad\qquad \phi_C(x_-) = -a, \qquad\qquad (6.58)$$
$$\phi_R(x_+) = +a, \qquad\qquad\qquad \phi_C(x_+) = +a, \qquad\qquad (6.59)$$
$$\dot\phi_L(x_-) = \dot\phi_C(x_{-1}), \qquad\qquad \dot\phi_R(x_+) = \dot\phi_C(x_+), \qquad\qquad (6.60)$$

where ϕ_L, ϕ_C, ϕ_R are the solutions in the $\phi < -a, -a < \phi < a, \phi > a$ regions respectively, and D_L, E_L the respective arbitrary constants to be fixed. Starting with the $\dot\phi_L(0) = 0$ condition, we find:

$$\dot\phi_L(x) = \frac{C}{H^2} \left(-\frac{2}{3}\frac{\cos(x)}{\sin^3(x)} - \frac{\cos(x)}{3\sin(x)} \right) + \frac{D_L}{\sin^3(x)}.$$ (6.61)

---

[1]In fact, under a literal reading, the Standard Model potential does have a true vacuum since λ is eventually driven to positive values by the Landau pole of the U(1) coupling, but this happens far beyond the Planck scale, and has no effect on tunnelling rates since bounce solutions do not penetrate that far into the true vacuum.

Taylor expanding for small x we find:

$$\dot{\phi}_L(x) = \frac{C}{H^2}\left(-\frac{2}{3x^3} + \frac{1}{3x}\right) + D_L\left(\frac{1}{x^3} - \frac{1}{2x}\right) + O(x). \tag{6.62}$$

Hence to match $\dot{\phi}_L(0) = 0$ we require:

$$D_L = \frac{2C}{3H^2}. \tag{6.63}$$

The $\dot{\phi}_R(\pi) = 0$ solution is similar to this, and instead we find:

$$D_R = -\frac{2C}{3H^2}. \tag{6.64}$$

The remaining six equations then become:

$$-a = E_L + \frac{C}{H^2}\left[\frac{1}{3\sin^2(x_-)} - \frac{1}{3}\log|\sin(x_-)| - \frac{1}{3}\log\left|\frac{\cos(x_-)+1}{\sin(x_-)}\right| - \frac{\cos(x_-)}{3\sin^2(x_-)}\right], \tag{6.65}$$

$$-a = E_C + D_C\left[-\frac{1}{2}\log\left|\frac{1+\cos(x_-)}{\sin(x_-)}\right| - \frac{\cos(x_-)}{2\sin^2(x_-)}\right], \tag{6.66}$$

$$\frac{C}{H^2}\left[-\frac{2}{3}\frac{\cos(x_-)}{\sin^3(x_-)} - \frac{1}{3}\frac{\cos(x_-)}{\sin(x_-)} + \frac{2}{3\sin^3(x_-)}\right] = \frac{D_C}{\sin^3(x_-)}, \tag{6.67}$$

$$+a = E_R - \frac{C}{H^2}\left[\frac{1}{3\sin^2(x_+)} - \frac{1}{3}\log|\sin(x_+)| + \frac{1}{3}\log\left|\frac{\cos(x_+)+1}{\sin(x_+)}\right| + \frac{\cos(x_+)}{3\sin^2(x_+)}\right], \tag{6.68}$$

$$+a = E_C + D_C\left[-\frac{1}{2}\log\left|\frac{1+\cos(x_+)}{\sin(x_+)}\right| - \frac{\cos(x_+)}{2\sin^2(x_+)}\right], \tag{6.69}$$

$$-\frac{C}{H^2}\left[-\frac{2}{3}\frac{\cos(x_+)}{\sin^3(x_+)} - \frac{1}{3}\frac{\cos(x_+)}{\sin(x_+)} - \frac{2}{3\sin^3(x_+)}\right] = \frac{D_C}{\sin^3(x_+)}. \tag{6.70}$$

The first step is to solve Eqs. (6.66) and (6.69) for E_C, D_C respectively:

$$E_C = \frac{a(f(x_-) + f(x_+))}{f(x_-) - f(x_+)}, \tag{6.71}$$

$$D_C = \frac{2a}{f(x_+) - f(x_-)}, \tag{6.72}$$

where:

$$f(x) = -\frac{1}{2}\log\left|\frac{\cos(x)+1}{\sin(x)}\right| - \frac{\cos(x)}{2\sin^2(x)}. \tag{6.73}$$

Next, equating D_C from Eqs. (6.67) and (6.70), we obtain:

$$g(x_+) = -g(x_-), \tag{6.74}$$

where:

$$g(x) = -\frac{2}{3}\cos(x) - \frac{1}{3}\cos(x)\sin^2(x). \tag{6.75}$$

It is trivial to show that $g(x)$ is an odd function about $x = \frac{\pi}{2}$, and that $g'(x) = \sin^3(x)$, which makes it monotonic. Consequently, the only solution to Eq. (6.74) is when:

$$x_+ + x_- = \pi, \tag{6.76}$$

121
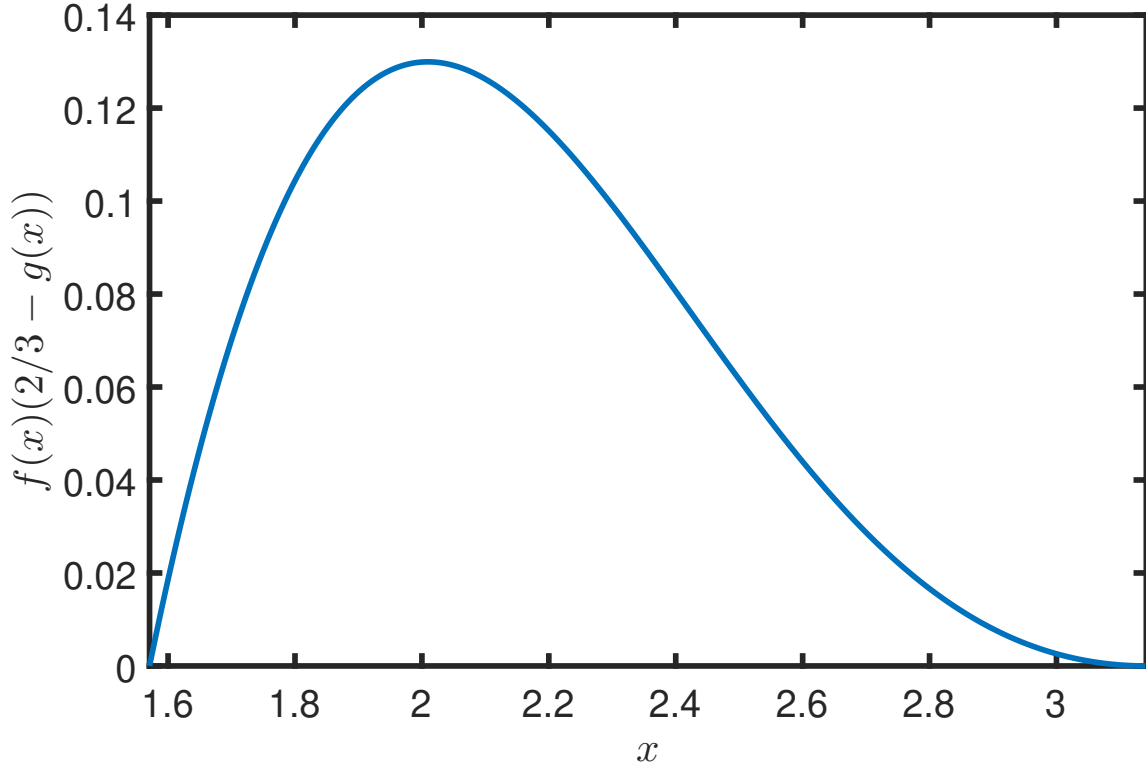
Figure 6.6: Plot of $f(x_+)(2/3 - g(x_+))$ against x_+. Maximum height is at $x_+ \approx 2.01$ with height 0.130.

that is, they are equidistant from $\frac{\pi}{2}$. This corresponds to what we would expect on symmetry grounds, since the potential is symmetric about the top of the barrier. Furthermore, one can show that the same is true of $f(x)$:

$$f(x_+) = -f(x_-), \tag{6.77}$$

since $\cos(\pi - x) = -\cos(x), \sin(\pi - x) = \sin(x)$ and:

$$\log\left|\frac{1 + \cos(x)}{\sin(x)}\right| + \log\left|\frac{1 - \cos(x)}{\sin(x)}\right| \equiv 0. \tag{6.78}$$

This immediately yields $E_C = 0$ and $D_C = a/f(x_+)$, allowing us to define an equation for x_+:

$$f(x_+)(-g(x_+) + 2/3) = \frac{aH^2}{C}. \tag{6.79}$$

Figure 6.6 shows the LHS of Eq. (6.79), revealing the two solutions for x_+ exist for $H^2 < 0.130C/a$, and none otherwise. These two values of x_+ thus correspond to two different solutions of the bounce equations of motion, as Eqs. (6.65) and (6.66) then yield E_L, E_R. It is worth noting that this piecewise potential does not actually satisfy $\Delta > 0$, despite having multiple solutions - in fact $\Delta < 0$, which would appear to imply it should not have multiple solutions by our previous argument. However, this is a consequence of the fact that the potential is completely flat around the top of the barrier (a constant): the perturbative solutions don't really apply here any more. One might argue that this potential is somewhat artificial - and it is - but multiple solutions, as we have shown, can also exist in non-physical potentials, such as the Standard Model, as we will now see.

6.5 Multiple CdL Solutions in the Standard Model

Now that we have deduced that multiple CdL solutions are possible, we move to consider the Standard Model. First, we consider the dimensionless quantity Δ defined by Eq. (6.39), which for $m_t = 173.34\,\text{GeV}, m_h = 125.15\,\text{GeV}$ gives $\Delta = +3.6992 \times 10^{-4}$. This is small, but positive nonetheless, indicating that extra solutions may well be possible. We considered this scenario in depth in [2], and here we will present the main results of that paper. We also note the critical Hubble rate in this case, which is:

$$H_{\text{crit}} = \sqrt{-\frac{V''(h_{\text{bar}})}{4} - \frac{\Delta V(h_{\text{bar}})}{3M_{\text{P}}^2}} = 1.1931 \times 10^8 \,\text{GeV}. \tag{6.80}$$

where $h_{\text{bar}} = 5.11 \times 10^9 \,\text{GeV}$ is the location of the barrier in the Standard Model for these top-quark and Higgs-boson mass parameters.

6.5.1 Scan-plots

As previously, we apply the undershoot/overshoot method, and try to find bounces that lie between an overshoot and an undershoot. To visualise the structure of overshoots/undershoots, and aid in searching for solutions, we plot the following function:

$$\phi_{\text{end}}(\phi_0) = \begin{cases} \phi(\chi_{\text{turn}}) & \phi_0 \text{ undershoot} \\ \phi_{\text{fv}} & \phi_0 \text{ overshoot}, \phi_0 \in (\phi_{\text{bar}}, \phi_{\text{tv}}) \,, \\ \phi_{\text{tv}} & \phi_0 \text{ overshoot}, \phi_0 \in (\phi_{\text{fv}}, \phi_{\text{bar}}) \end{cases} \tag{6.81}$$

where χ_{turn} is the first non-zero χ where the solution $\phi(\chi, \phi_0)$ with initial conditions $\phi(0, \phi_0) = \phi_0, \dot{\phi}(0, \phi_0) = 0$ satisfies $\phi(\chi_{\text{turn}}, \phi_0) = 0$. Note that for bounce solutions, $\chi_{\text{turn}} = \chi_{\text{max}}$ (the point at which $a(\chi_{\text{max}}) = 0$) by definition, so when ϕ_0 is close to a bounce, the function ϕ_{end} approaches the other end of the bounce solution from the undershoot side. In the Standard Model, with $\phi = h$, we note also that h_{tv} is generically far beyond the Planck scale, thus to avoid numerical problems, we replace this threshold with appropriate cut-off, $h_{\text{tv}} = M_{\text{P}}$ in most cases, beyond which we assume there are no bounce solutions and thus all values of $\phi_0 > \phi_{\text{tv}}$ are expected to be overshoots[2].

Equation (6.81) defines what we call an 'Overshoot-Undershoot scan-plot', which shows at a glance the structure of overshoots and undershoots, coloured for ease of visualisation. The first thing we notice about fig. 6.7 is that unlike the $\Delta < 0$ polynomial models, something completely different happens: the undershoot solutions do not disappear. However, the expected behaviour near the top of the barrier - always overshoots - does occur. This is verified by a closer zoom (see fig. 6.9). However, this is not the only feature present: zooming in further in figs. 6.8a and 6.8b, we see that there are *additional* overshoot regions, narrow in width, that are not immediately apparent from fig. 6.7.

---

[2]Given the nature of our results, it is always possible that this assumption is false, but if so, it doesn't affect the solutions found which do not involve trans-planckian field values. At the very least, we can say that no such solutions exist in flat space for the range of parameters considered.
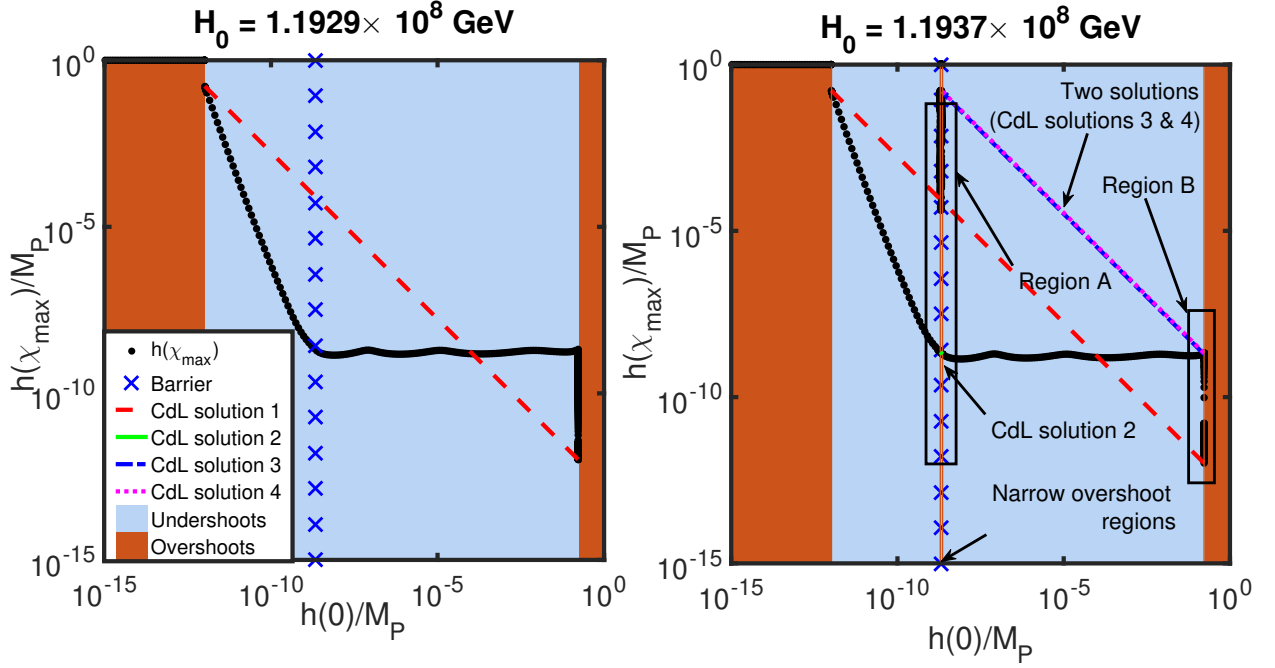
Figure 6.7: Scan plot from [2] for two different Hubble rates. Left: $H < H_{\text{crit}}$. Note that all intermediate solutions, including those around the barrier, are undershoots. Right: $H > H_{\text{crit}}$. Note that a thin line overshoots appears near the barrier. Zoomed plots for regions A and B are shown in figures 6.8a and 6.8b respectively. Dots indicate the $h_{\text{end}}(h_0)$ function.
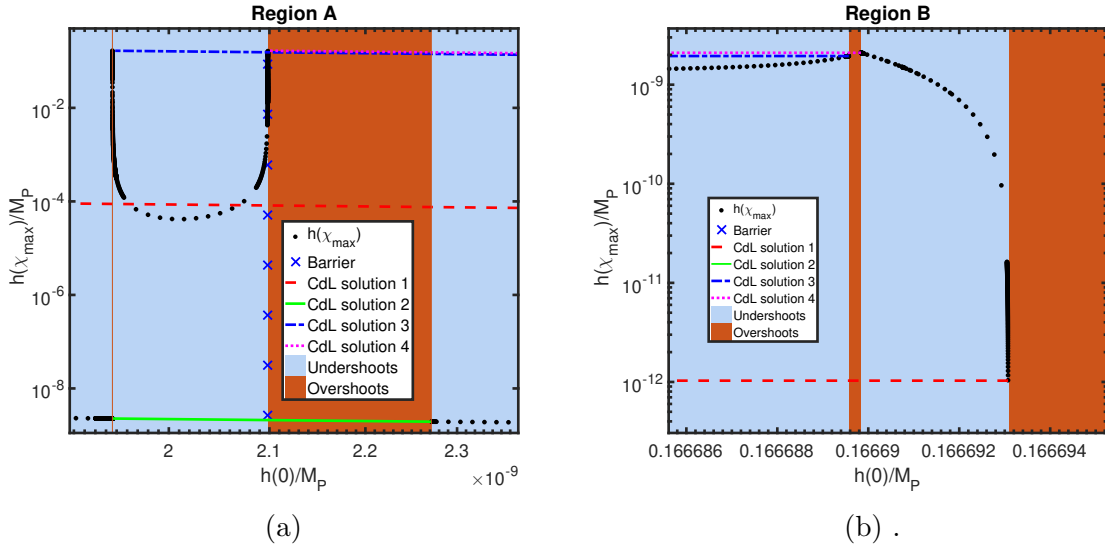
Figure 6.8: Zoomed in plots of fig. 6.7, from [2], which show the expected region of overshoots near the top of the barrier, together with two even narrower overshoot regions that appear on either side.
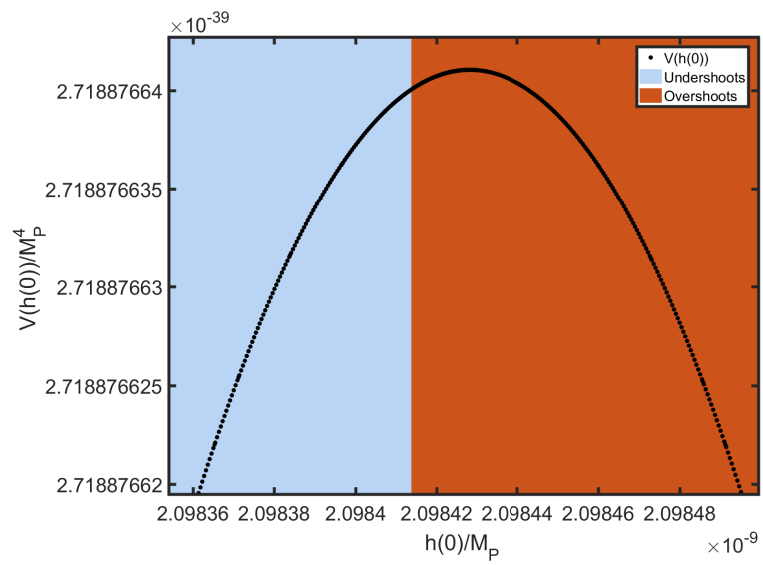
Figure 6.9: Overshoot/Undershoot structure around the top of the barrier for $H > H_{\text{crit}}$. This verifies the linear analysis that argued these solutions should be overshoots sufficiently close to the barrier. The potential is overlayed on top of this. Originally published in [2].

6.5.2 Solution Structure

The existence of these additional overshoot/undershoot regions makes the Standard Model potential even more mysterious, since by counting overshoot/undershoot transitions, we can argue that there are not one, but *four* CdL-type solutions. The structure of these solutions is difficult to see from fig. 6.7, so we sketch them (not to scale) superimposed on the potential in fig. 6.10. Specific data on these solutions is given in table 6.1, and we plot the four solutions in fig. 6.11. Some points about these solutions:

1. CdL 1 is much the same as the flat space solution, having similar decay exponent. It is also the largest amplitude solution.

2. CdL 2 is smallest in amplitude, and closely resembles the perturbative solution we have considered before.

3. CdL 3 and 4 are the unusual solutions, which appear to be related to the additional narrow overshoot regions. Notice (see fig. 6.10) that CdL 2 has larger amplitude on the false vacuum side than either CdL 3 or 4.

The immediate suspicion here is that CdL 2, with its small amplitude, is related to the perturbative solution found earlier. Indeed, comparison of the action obtained at different H in both cases demonstrates that this is likely true (see figs. 6.12a and 6.12b). Since we know that this solution disappears at $H = H_{\mathrm{crit}}$, then the structure present in fig. 6.10 suggests that solutions CdL3 and CdL4 will also disappear at $H = H_{\mathrm{crit}}$, since their false vacuum side starting points lie between that of CdL 2 and the barrier, an interval that shrinks to zero as $H \to H_{\mathrm{crit}}$. It is conceivable that they instead emerge at some $H > H_{\mathrm{crit}}$, but there is no numerical evidence to support this as all the cases considered have presented the same structure. As it is, both these solutions have fairly high action compared to the Hawking-Moss solution, so are likely irrelevant to tunnelling.

6.5.3 Robustness of results

Since we use a piecewise polynomial to describe the standard model effective potential, a reasonable question is whether the apparent new solutions are some sort of numerical artefact. There are several reasons to think this is not the case. First, it is possible to construct potentials of the form:

$$V(\phi) = \frac{1}{4} \left(a + b \log \left(\frac{\phi^2}{M^2} \right) + c \log \left(\frac{\phi^2}{M^2} \right)^2 \right) \phi^4, \tag{6.82}$$

which were used, for example, by [83, 82, 84] to approximate the Standard Model potential by fitting the coefficients a, b, c to approximate the running of $\lambda(\phi)$ in the Standard Model. This potential, although a simplified model compared to the full Standard Model effective potential, does not suffer from the same defects as a piecewise polynomial (namely discontinuities in the second and higher derivatives). Yet for appropriate parameters, this potential can also be chosen to satisfy the $\Delta > 0$ condition and exhibit multiple solutions. Furthermore, we have shown that the polynomial potential of Eq. (6.7) exhibits this behaviour for sufficiently negative ϕ^6 coupling. On this basis, it seems reasonable to accept that the numerics are giving the correct result. Indeed, the code has been tested using arbitrary precision arithmetic with 100 decimal place precision and extremely restrictive relative and absolute tolerances:
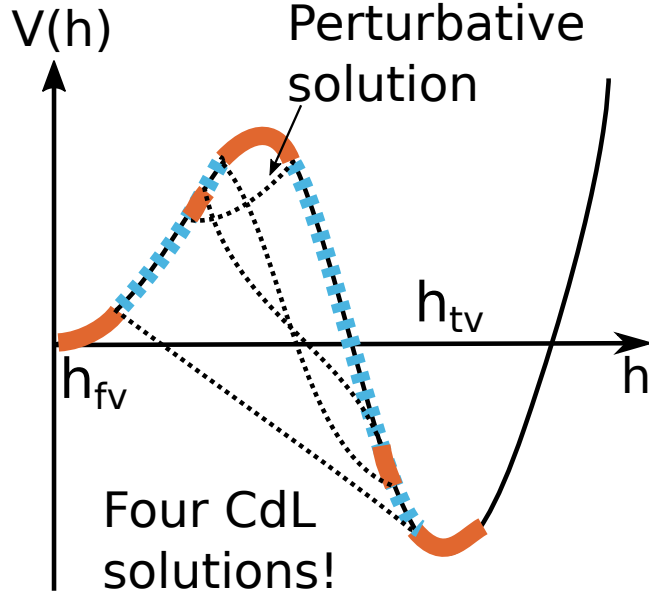
Figure 6.10: Sketch of four solutions in the Standard Model effective potential (neither potential nor solutions are to scale), illustrating their convoluted relationship to the overshoot/undershoot structure. Each transition on one side of the barrier corresponds to a transition on the other side.

Bounces with back-reaction	$h(0)/\mathrm{GeV}$	$h(\chi_{\mathrm{max}})/\mathrm{GeV}$	Decay exponent, B	$H_0\chi_{\mathrm{max}}/\pi - 1$
CdL solution 1	4.0589763×10^{17}	2.5097992×10^{6}	1808.261	-3.99325×10^{-12}
CdL solution 2	5.5306295×10^{9}	4.7385411×10^{9}	12388.87	-1.89647×10^{-19}
CdL solution 3	4.0588911×10^{17}	4.7385591×10^{9}	14197.13	-3.99303×10^{-12}
CdL solution 4	4.0588976×10^{17}	5.1096372×10^{9}	14197.08	-3.99303×10^{-12}
Hawking-Moss solution	5.1096727×10^{9}	5.1096727×10^{9}	12388.82	-3.77098×10^{-19}

Table 6.1: Table of initial and final values of the bounce solutions for $V_0 = 7.210 \times 10^{-21}M_{\mathrm{P}}^4$, $(H_0 = 1.1937 \times 10^8 \mathrm{GeV})$, together with the associated decay exponents. The ending values of χ_{max} are all nearly the same as in the fixed background approximation, but this does not mean the effects of gravitational back-reaction are negligible. Note that CdL solution 2 and the Hawking-Moss solution have χ_{max} significantly closer to the flat false vacuum result, as they probe only the barrier, which is closer to the false vacuum, while the other solutions probe the depth of the Standard Model potential and thus receive larger back-reaction corrections. From [2]
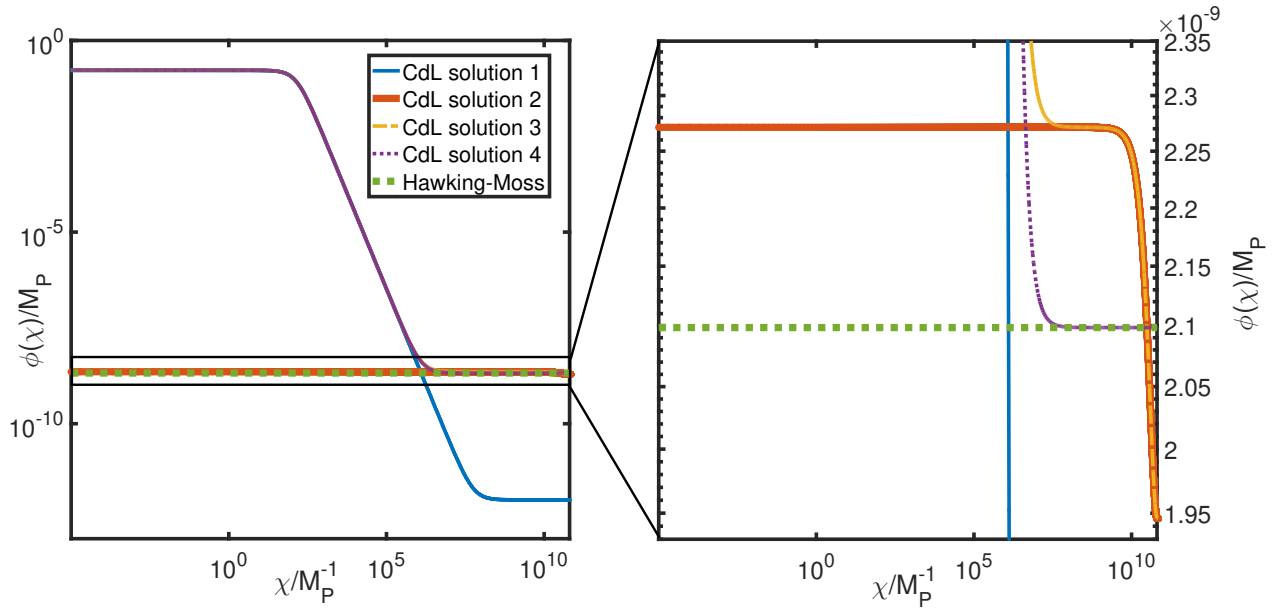
Figure 6.11: Plot of the four CdL bounce solutions in the Standard Model. One solution (CdL 1) has large amplitude on both sides of the barrier, and resembles the $V_0 = 0$ bounce. CdL 2 is small amplitude on both sides, while CdL 3 and 4 resemble CdL 1 at large h, while having small amplitude around the barrier on the false vacuum side. Originally published in [2].

$\epsilon_{\text{rel}} = 10^{-30}, \epsilon_{\text{abs}} = 10^{-80}$, where the error in component y of a Runge-Kutta solution is estimated to satisfy $|\Delta y| < |\epsilon_{\text{rel}} y + \epsilon_{\text{abs}}|$. The effect persists, giving confidence that these solutions are real, and not numerical artefacts. Finally, the observation of fig. 6.12 that the action of CdL 2 lies very close to that predicted by the perturbative analysis, even when the difference between S_{HM} and the solution's action is in the seventh significant figure, demonstrates that CdL 2 is certainly no artefact, giving even more confidence that the solutions like CdL 3 and 4, which are known only numerically, are similarly robust.

As a further check, it is possible to consider what happens in the fixed back-ground approximation, when we ignore back-reaction. In this case, we also obtain the same four solutions (with slightly different actions). This demonstrates that the result is not due to the problems incorporating backreaction effects into the calculation (see table 6.2).
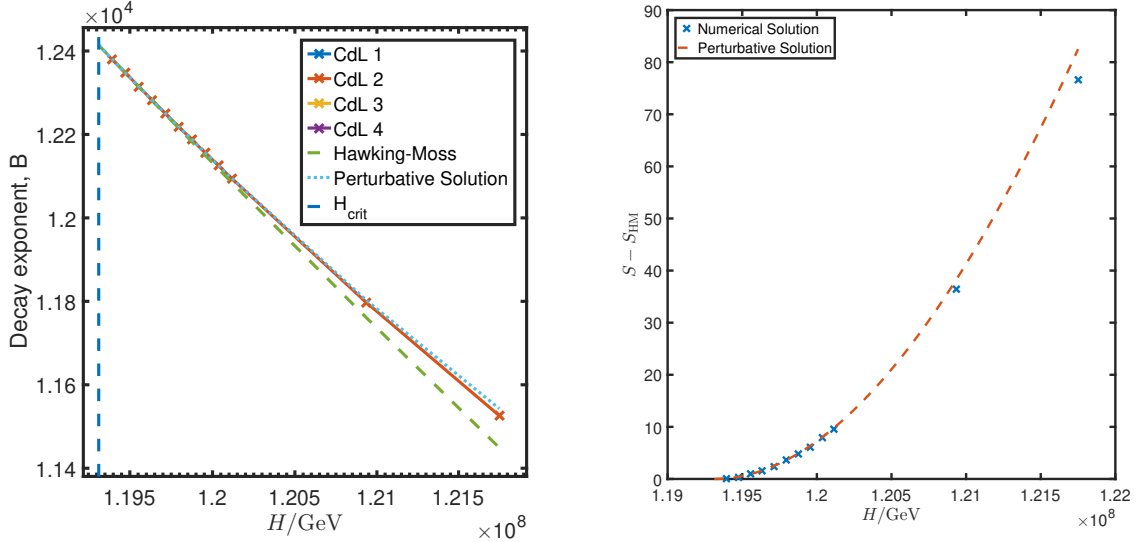
(a) Plot of the CdL 2 decay exponent (numerical) against the perturbative value and the Hawking-Moss.

(b) Difference between CdL 2 and the Hawking-Moss action, compared to the perturbative prediction.

Figure 6.12

Bounces with fixed dS background	$h(0)/\text{GeV}$	$h(\chi_{\max})/\text{GeV}$	Decay exponent, B
CdL solution 1	6.5057883×10^{17}	2.1207789×10^{6}	1805.797
CdL solution 2	5.5306295×10^{9}	4.7385412×10^{9}	12388.88
CdL solution 3	6.5056176×10^{17}	4.7385523×10^{9}	14194.68
CdL solution 4	6.5056306×10^{17}	5.1096372×10^{9}	14194.62
Hawking-Moss solution	5.1096727×10^{9}	5.1096506×10^{9}	12388.82

Table 6.2: Table of initial and final values of the bounce solutions using a fixed de Sitter background, for $V_0 = 7.210 \times 10^{-21} M_{\text{P}}^4$, ($H_0 = 1.1936 \times 10^8 \text{GeV}$), together with the associated decay exponents. As the metric is fixed at the de Sitter space of the false vacuum, $\chi_{\max} = \frac{\pi}{H_0}$ for all solutions. From [2].

6.6 Computing the action

The decay exponent of an $O(4)$ symmetric bounce, including gravitational backreaction, is given by (inserting the equations of motion to simplify):

$$B = \frac{24\pi^2 M_{\text{P}}^4}{V_0} - 2\pi^2 \int_0^{\chi_{\max}} \mathrm{d}\chi a^3(\chi) V(\phi(\chi)). \tag{6.83}$$

Note that the gradient terms here actually cancel out due to the equivalent contribution of the gradients to $M_{\text{P}}^2 R/2$, leaving only (direct) dependence on the potential. Again, note that this only applies to solutions that satisfy the equations of motion. The first observation here is that we will encounter problems in the $V_0 \to 0$ limit, since the decay exponent must then be computed from a cancellation of two large numbers. This problem is best illustrated by the

analytic Hawking-Moss solution, whose decay exponent is:

$$B_{\mathrm{HM}} = 24\pi^2 M_{\mathrm{P}}^4 \left[\frac{1}{V_0} - \frac{1}{V_0 + \Delta V(\phi_{\mathrm{bar}})} \right]. \tag{6.84}$$

In the regime $\Delta V(\phi) \ll V_0 \ll M_{\mathrm{P}}^4$ (which is a considerable portion of the interesting parameter space), Eq. (6.84) is difficult to evaluate numerically, as round-off error will result in an answer of zero. Taylor-expansion in $\Delta V(\phi_{\mathrm{bar}})/V_0$ predicts:

$$B_{\mathrm{HM}} \approx \frac{24\pi^2 M_{\mathrm{P}}^4 \Delta V(\phi_{\mathrm{bar}})}{V_0^2} = \frac{8\pi^2 \Delta V(\phi_{\mathrm{bar}})}{3H^4}. \tag{6.85}$$

However, especially for solutions like CdL 2 that are close to the Hawking-Moss, the same issue occurs for CdL solutions. However for these, it is problematic to perform such a cancellation analytically because the solution is only known numerically, and any errors in evaluating the action integral will be magnified, ruining the precision of the result. This is one reason that such calculations are often performed in the fixed background approximation, which assumes that the height of the barrier and gradient terms give no significant contribution to metric, and that only the background V_0 matters. That is, one assumes the scale factor takes on the approximate solution:

$$a(\chi) = \frac{1}{H} \sin(H\chi). \tag{6.86}$$

This approximation is certainly reasonable, as the small differences in tables 6.1 and 6.2 provide a (post-hoc) justification for. However, it is not immediately obvious that this should apply in the Standard Model, because of the depth of the potential true minimum. Is it necessarily the case that we can ignore the contribution from this region? To answer this, we constructed a new way of splitting up the exponent Eq. (6.83). The basic idea is to attempt to extract the part of the metric solution, a, that comes from the fixed background V_0, splitting it into two parts:

$$a(\chi) = \frac{1}{H} \sin(H[\chi_{\mathrm{max}} - \chi]) + \delta a(\chi), \tag{6.87}$$

where $H^2 = V_0/3M_{\mathrm{P}}^2$, and δa carries the deviation from the fixed background metric. The reason we have shifted the fixed-back background solution from $\sin(H\chi)$ to $\sin(H(\chi_{\mathrm{max}} - \chi))$ is for convenience that will become clear later - it amounts to a choice of which pole of the (distorted) 4-sphere geometry to expand around. We now proceed to split the decay exponent into three pieces:

$$B = B_1 + B_2 + B_3, \tag{6.88}$$

where:

$$B_1 = -2\pi^2 \int_0^{\chi_{\mathrm{max}}} \mathrm{d}\chi\, a^3(\chi) \Delta V(\phi), \tag{6.89}$$

$$B_2 = -6\pi^2 M_{\mathrm{P}}^2 \int_0^{\chi_{\mathrm{max}}} \mathrm{d}\chi \left[3\sin^2(H(\chi_{\mathrm{max}} - \chi))\delta a(\chi) + 3H\sin(H(\chi_{\mathrm{max}} - \chi))\delta a^2(\chi) + H^2\delta a^3(\chi) \right], \tag{6.90}$$

$$B_3 = \frac{24\pi^2 M_{\mathrm{P}}^4}{V_0} - \int_0^{\chi_{\mathrm{max}}} \mathrm{d}\chi \frac{1}{H^3} \sin^3(H(\chi_{\mathrm{max}} - \chi)) V_0 \tag{6.91}$$

$$= -\frac{2\pi^2 M_{\mathrm{P}}^2}{H^2} (1 + \cos(H\chi_{\mathrm{max}}))^2 (\cos(H\chi_{\mathrm{max}}) - 2). \tag{6.92}$$

Here, B_1 essentially carries the action with most of the large V_0 dependent terms cancelled off. B_2 and B_3 are residue terms of the cancellation, B_2 corresponding to the fact that a differs from the fixed background scale factor, and B_3 to the fact that χ_{max} differs from the fixed background value of π/H. The majority of the cancellation takes place in the analytic B_3 term.

6.7 Flat False Vacuum Limit

6.7.1 Smoothness of the $H \to 0$ Limit

An interesting application of the splitting in Eq. (6.88) is that we can deduce an expression for how $\chi_{\mathrm{max}}(H_0)$ behaves for small H. It is clear that the $H \to 0$ limit of Eq. (6.92) will be divergent, unless $H\chi_{\mathrm{max}} \to - > \pi$, which allows us to write the following power series expansion:

$$\chi_{\mathrm{max}}(H) = \frac{\pi}{H} + \alpha_0 + \alpha_1 H + O(H^2), \tag{6.93}$$

where $\alpha_0, \alpha_1, \ldots$ are appropriate constants. Substituting this into Eq. (6.87) and taking the $H \to 0$ limit, we find:

$$a_0(\chi) = \chi - \alpha_0 + \delta a_0(\chi). \tag{6.94}$$

Here, a_0 is the scale factor at $H = 0$ (note that this is emphatically *not* the same thing as the fixed-background scale factor - it is the scale factor in the flat false vacuum limit, $V_0 = 0$, but includes back-reaction of the bounce). Also, $\delta a_0(\chi \to \infty) \to 0$, by definition, since for any bounce, $a(\chi_{\mathrm{max}}) = 0$ and thus $\delta a(\chi_{\mathrm{max}}) = 0$ if defined as in Eq. (6.87) (which is why we chose to define it that way rather than expanding around $\sin(H\chi)$). Since $\chi_{\mathrm{max}} \to \infty$ in the $H \to 0$ limit, $\delta a_0(\chi \to \infty) \to 0$ and we can thus compute α_0 simply by solving for $a_0(\chi)$ at $V_0 = 0$. In fact, solving for $V_0 = 0$ is considerably easier than solving for $V_0 > 0$ close to but not exactly zero. This is because the decay exponent Eq. (6.83) takes a different form:

$$B_{H=0} = -2\pi^2 \int_0^\infty \mathrm{d}\chi a^3(\chi)\Delta V(\phi). \tag{6.95}$$

The essential reason for this is that there is a discontinuity in the false vacuum action (obtainable from Eq. (6.95) by substituting $a = \sin(H\chi)/H, V(\phi) \to V_0, \infty \to \pi/H$):

$$S_{\mathrm{fv}} = \begin{cases} -\frac{24\pi^2 M_{\mathrm{P}}^4}{V_0} & V_0 > 0 \\ 0 & V_0 = 0 \end{cases}. \tag{6.96}$$

Consequently, it is numerically fairly easy to compute the limit:

$$\alpha_0 = \lim_{\chi \to \infty}(\chi - a_0(\chi)), \tag{6.97}$$

since we know that the $V_0 = 0$ solution approaches the false vacuum as $\chi \to \infty$, and thus $a_0(\chi)$ approaches the flat space form $\chi + C$, where C is some constant (namely, $C = -\alpha_0$). This allows us to numerically compute α_0, which for the values $m_t = 173.34\,\mathrm{GeV}, m_h = 125.15\,\mathrm{GeV}$ we consider here, gives $\alpha_0 = -0.2559 M_{\mathrm{P}}^{-1}$. Even at first order, this proves an excellent approximation to the actual value of χ_{max} for different H (see figure 6.13). Additionally, we would like to be sure that the action approaches the $V_0 = 0$ action smoothly. For this to be true, we require that B_2 does not diverge. This can be shown by considering the $H \to 0$ limit:

$$B_2(H = 0) = -6\pi^2 M_{\mathrm{P}}^2 \lim_{H \to 0} H^2 \int_0^{\frac{\pi}{H} + \alpha_0 + \cdots} \mathrm{d}\tilde{\chi} \left[3(\chi - \alpha_0)^2 \delta a_0(\chi) + 3(\chi - \alpha_0)\delta a_0^2(\chi) + \delta a_0^3(\chi) + O(H^2)\right].$$
$$\tag{6.98}$$
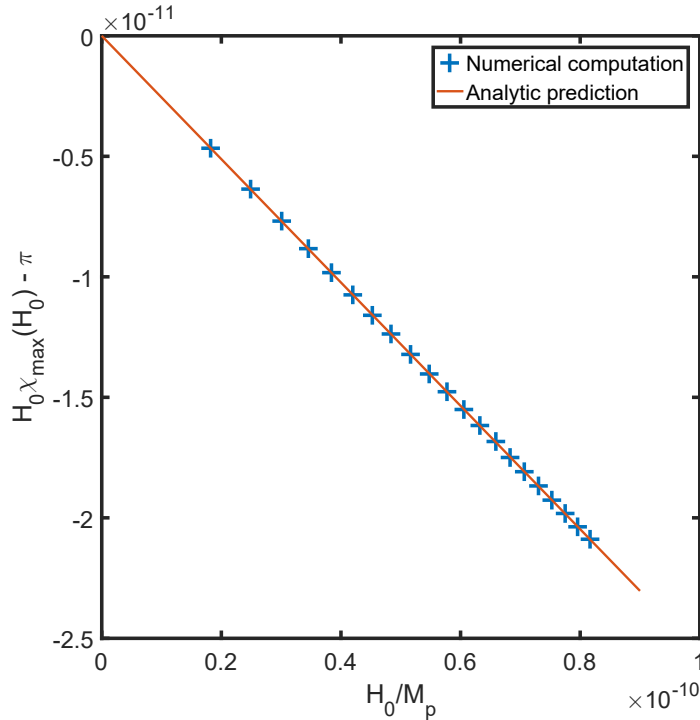
Figure 6.13: Plot of $H_0 \chi_{\mathrm{max}}(H_0) - \pi$ against H_0 for a range of CdL bounces in the Standard Model, computed numerically (crosses) and compared to the analytic prediction $\chi_{\mathrm{max}} \approx \frac{\pi}{H_0} - 0.2559 M_P^{-1} + \ldots$ of Eq. (6.93). Figure from [2].

Although proportional to H, we must actually be slightly careful here because the integral may diverge in the $H \to 0$ limit. Thus, it is not immediately obvious that B_2 does not diverge. To assess whether it does or not, we consider the $\chi \to \infty$ limit of the $V_0 = 0$ solution, for which the scalar field $\Delta\phi = \phi - \phi_{\mathrm{fv}}$ asymptotically satisfies:

$$\Delta\ddot{\phi} + \frac{3}{\chi}\Delta\dot{\phi} - m^2\Delta\phi = 0, \qquad (6.99)$$

where $m^2 = V''(\phi_{\mathrm{fv}})$ (the situation is somewhat more complicated in the massless limit). The solution to this equation is known in terms of Bessel functions, specifically, $\Delta\phi(\chi) \propto K_1(m\chi)/\chi$, which takes the asymptotic form:

$$\Delta\phi = \frac{C}{\chi^{3/2}}e^{-m\chi}. \qquad (6.100)$$

The asymptotic form is sufficient for our purposes, since the only thing that can cause a divergence (and thus avoid $B_2 = 0$), is the tail end $\chi \to \infty$ limit of the integral. The scale factor deviation satisfies:

$$\delta\ddot{a}_0 = -\frac{(\chi - \alpha_0 + \delta a_0)}{3M_{\mathrm{P}}^2}\left(\dot{\phi}^2 + V(\phi)\right). \qquad (6.101)$$

We are concerned here with the large χ limit, and since we know $\delta a_0 \to 0$, in this limit we find $\chi \gg \delta a_0 - \alpha_0$ for which this equation becomes approximately:

$$\delta\ddot{a}_0 \sim -\frac{\chi}{3M_{\mathrm{P}}^2}\left[\frac{3m^2 C^2}{2\chi^3}e^{-2m\chi} + O\left(\frac{1}{\chi^4}e^{-2m\chi}\right)\right]. \qquad (6.102)$$

132

Integrating this, we obtain:

$$\delta a_0(\chi) = -\frac{m^2 C^2}{2M_{\rm P}^2}\left[-e^{-2m\chi} - (1 + 2m\chi){\rm Ei}(-2{\rm m}\chi)\right] + D + E\chi, \qquad (6.103)$$

where Ei is the exponential integral function:

$$ {\rm Ei}(x) = -\int_{-x}^{\infty}\frac{e^{-t}}{t}{\rm d}t. \qquad (6.104) $$

This can be related to the En function for $x > 0$ by ${\rm Ei}(-{\rm x}) = -{\rm E}_1({\rm x})$ where [169]:

$$ {\rm En}(x) = \int_1^{\infty}{\rm d}t\frac{e^{-xt}}{t^n}{\rm d}t. \qquad (6.105) $$

The En function has a known asymptotic expansion for large x, namely [169]:

$$ E_n(z) \sim \frac{e^{-z}}{z}\left[1 - \frac{n}{z} + \frac{n(n+1)}{z^2} - \frac{n(n+1)(n+2)}{z^3} + O\left(\frac{1}{z^4}\right)\right]. \qquad (6.106) $$

Hence, to match $\delta a_0(\chi \to \infty) \to 0$ we need $D = E = 0$, and $\delta a_0(\chi)$ is asymptotically:

$$ \delta a_0(\chi) \sim \frac{m^2 C^2}{2M_{\rm P}^2}\left[\frac{1}{4m^2\chi^2}e^{-2m\chi} + O\left(\frac{1}{8m^3\chi^3}e^{-2m\chi}\right)\right]. \qquad (6.107) $$

With these asymptotics, it is clear that the integral in Eq. (6.98) remains finite, and thus B_2 vanishes in the $H \to 0$ limit. Since B_1 (Eq. (6.89)) trivially approaches the $V_0 = 0$ decay exponent as $H \to 0$, this proves that the action limit is smooth, *provided* there exists a sequence of bounce solutions for all H that satisfies Eq. (6.93) (solutions can potentially exist that fail to satisfy this - they will have divergent action in the $H \to 0$ limit however). We have already shown that a solution always exists for $H < H_{\rm crit}$, so the only question is whether it approaches the false vacuum in the $H \to 0$ limit (if it doesn't, then this argument doesn't apply).

The massless case is similar, but in this case the asymptotic form of $\Delta\phi \sim 1/\chi^2$. Hence, at large χ, $\delta\ddot{a}_0 \sim 1/\chi^5$ and so $\delta a_0 \sim 1/\chi^3$. This means that the integral appearing in Eq. (6.98) is logarithmically divergent, but due to the prefactor of H^2, and the upper limit $\sim \pi/H$, it is clear that B_2 in fact vanishes as $H^2 \log H$ in the $H \to 0$ limit. Hence, the action smoothly approaches the $V_0 = 0$ case here too.

6.7.2 Existence of Solutions Approaching the $V_0 = 0$ Solution

The only remaining loose end is whether or not a family of solutions actually exists that approach the $H = 0$ solution satisfying $\phi(\chi \to \infty) \to \phi_{\rm fv}$ in the $H \to 0$ limit, together with the related question of whether that solution itself exists at $H = 0$. This is crucial: notice that the arguments given above for the vanishing of B_2 and B_3 depend on the assumption that $\delta a_H(\chi)$ smoothly approaches the $H = 0$ case, $\delta a_0(\chi)$. If this isn't the case, then B_2 will not smoothly approach zero. Likewise, if $H\chi_{\rm max}(\chi) - \pi$ doesn't smoothly approach 0, then B_3 diverges. Thus, to ensure continuity we need to ensure that there exists some sequence of solutions, $(\phi_H(\chi), \delta a_H(\chi))$ whose limit is $(\phi_0(\chi), \delta a_0(\chi))$, the $H = 0$ solution. There is already numerical evidence that this is the case in the Standard Model (see fig. 6.13). Is it true in

general?

In section 3.4.4 we argued that for $H > 0$, solutions starting sufficiently close to the false vacuum are always overshoots. This was done using approximately linear solutions, which is valid when ϕ is close to ϕ_{fv}. Outside this region, the linear solutions do not apply, and this is precisely regime where the overshoot divergence will take the solution. This isn't a problem in the $H > 0$ case, because we can argue on energy grounds that the solution will diverge even in the non-linear regime. Consider re-writing the equation of motion for the scalar field as:

$$\frac{\mathrm{d}}{\mathrm{d}\chi}\left(\frac{\dot{\phi}^2}{2} - V(\phi)\right) = -\frac{3\dot{a}}{a}\dot{\phi}^2, \tag{6.108}$$

where $E = \dot{\phi}^2/2 - V(\phi)$ is the "energy". We note that Coleman originally phrased the overshoot/undershoot argument in terms of this mechanical analogue [98, 99]. In flat space, we always have $\dot{a} > 0$, so energy can only decrease. This means that solutions that start close to the true vacuum always overshoot because they stay there sufficiently long that the friction term drops to zero, and then have too much energy to undershoot. Likewise, solutions close to the false vacuum always *undershoot* because they also stay close to the false vacuum sufficiently long that the friction drops to zero, and then lack the energy to climb back up to the true vacuum. This is a different result to $H > 0$, where solutions starting close to ϕ_{fv} always *overshoot*. The reason for the difference is that for $H > 0$, friction eventually goes negative in the $\dot{a} < 0$ region, adding energy to the system. This is why solutions starting close to ϕ_{fv} overshoot: if we attempt to delay their departure from the vicinity of ϕ_{fv} by making $\Delta\phi_0 = \phi_0 - \phi_{\text{fv}}$ sufficiently small, then they will eventually hit a singularity at some finite $\chi \approx \pi/H$, and diverge with infinite energy as overshoots.

The question then, is whether the $H = 0$ case (which, it should be remembered, is *not* the same as flat space as we are including back-reaction) behaves in the same way as the flat space case, or whether gravitational effects will render it like the $H > 0$ case. The linear equation for fluctuations near the false vacuum is:

$$\Delta\ddot{\phi} + \frac{3}{\chi}\Delta\dot{\phi} - V''(\phi_{\text{fv}})\Delta\phi = 0, \tag{6.109}$$

which has solution:

$$\Delta\phi(\chi) = \frac{2\Delta\phi_0}{\sqrt{V''(\phi_{\text{fv}})}}\frac{I_1(\sqrt{V''(\phi_{\text{fv}})}\chi)}{\chi}, \tag{6.110}$$

where I_1 is the Modified Bessel function of the first kind. This solution is divergent, but not at finite χ which means we have to take into account the behaviour of the solution in the non-linear regime. The first thing we should note about the non-linear solution is that it will necessarily undershoot if it reaches the point ϕ_{inst} on the other side of the barrier, where $V(\phi_{\text{inst}}) = V(\phi_{\text{fv}}) = 0$, without sufficient energy to reach the true vacuum. This is analogous to the reason that a solution in flat space starting on the range $(\phi_{\text{fv}}, \phi_{\text{bar}})$ always undershoots: in that case, the friction is always positive, and so since it lacks the energy to reach ϕ_{tv} without friction, it will certainly lack the energy including it. The only thing that can potentially change this when including gravity is if the friction term, $\dot{a}/a$ becomes *negative*. If we can show that this never happens for solutions starting sufficiently close to ϕ_{fv}, then we will have established that solutions starting sufficiently close to ϕ_{fv} are undershoots for $V(\phi_{\text{fv}}) = 0$, even taking gravity into account.

At large χ, the solution is asymptotically:

$$\Delta\phi(\chi) \sim \frac{2\Delta\phi_0 e^{\sqrt{V''(\phi_{\mathrm{fv}})}\chi}}{\sqrt{2\pi}\,(V''(\phi_{\mathrm{fv}})\chi)^{3/2}}. \tag{6.111}$$

By choosing $\Delta\phi_0$ sufficiently (exponentially in this case) small, we can always ensure that this asymptotic form is accurate up to some χ_{nl} where non-linearity approximately starts by ensuring $\Delta\phi$ remains small (how small depends on the shape of the potential). Staying in the linear regime thus requires $\Delta\phi_0$ to be exponentially small compared to χ_{nl}. At large χ, however, since we stay close to ϕ_{fv} and $V(\phi_{\mathrm{fv}}) = 0$, $a(\chi) \sim \chi + C$ where C is some constant, so $\dot{a}/a$ falls to zero for this solution, and the friction is essentially negligible. Thus the non-linear solution will (approximately) conserve energy provided $\dot{a}/a$ remains small. This will remain true up until $\dot{a}$ crosses zero, when the form of the friction term will begin to change drastically. $\dot{a}$ is controlled by:

$$\dot{a}^2 = 1 + \frac{a^2 E}{3M_{\mathrm{P}}^2}, \tag{6.112}$$

and so we require $a^2 E/(3M_{\mathrm{P}}^2) \ll 1$ to ensure that the friction remains small. The energy in the linear regime (before the field starts to roll down the barrier significantly) is asymptotically:

$$E \sim \frac{\Delta\phi_0^2 e^{2\sqrt{V''(\phi_{\mathrm{fv}})}\chi}}{4\pi\sqrt{V''(\phi_{\mathrm{fv}})}\chi^4}\left[-\frac{12}{\sqrt{V''(\phi_{\mathrm{fv}})}} + O\left(\frac{1}{\sqrt{V''(\phi_{\mathrm{fv}})}\chi}\right)\right]. \tag{6.113}$$

Thus for example choosing $\Delta\phi_0$ suppressed by a factor $e^{-k\sqrt{V''(\phi_{\mathrm{fv}})}\chi_{\mathrm{nl}}}$ where $k \geq 1$ ensures that the energy is exponentially suppressed, and we would need a to grow to $a > a(\chi_{\mathrm{nl}})e^{(k-1)\sqrt{V''(\phi_{\mathrm{fv}})}\chi_{\mathrm{nl}}/2}$ to overcome this and produce a significant deviation from $\dot{a} \approx 1$. Since $a \sim \chi$, this means we can push the point where $\dot{a} \to 0$ to arbitrarily large χ simply by choosing $\Delta\phi_0$ sufficiently small, and consequently, we can keep $\dot{a} \approx 1$ and $\dot{a}/a \ll 1$ for arbitrarily large χ this way. This is crucial, because it means that such solutions will behave like their flat space analogues, and undershoot, bouncing backwards when they reach $\phi \approx \phi_{\mathrm{inst}}$.

Notice that this argument depends crucially on $V(\phi_{\mathrm{fv}}) = 0$ being *exactly* true. If $V(\phi_{\mathrm{fv}}) > 0$, even with a very small value, then it is *not* possible to delay the potential rolling down the barrier for arbitrarily long just by choosing $\Delta\phi_0$ small enough. This is because however small $\Delta\phi_0$, when $V(\phi_{\mathrm{fv}}) > 0$, there is an upper limit at which the linearised solution encounters a singularity in a and diverges with infinite energy as an overshoot (see Eq. (3.38)).

Why does this matter? The conclusion is that for $V(\phi_{\mathrm{fv}}) > 0$, solutions sufficiently close to ϕ_{fv} are always overshoots. Yet we have just argued that for $V(\phi_{\mathrm{fv}}) = 0$, such solutions are *undershoots*. Since we know that a bounce exists between every overshoot and undershoot, we can conclude only one thing: there exists *some* family of bounce solutions with different H that approach a solution satisfying $\phi(\chi \to \infty) \to \phi_{\mathrm{fv}}$ in the $H \to 0$ limit. This is the final link in the chain: having proven that such a solution exists, we have established previously that it must smoothly approach the $V_0 = 0$ action, proving that the decay rate is continuous across the $H = 0$ transition.

6.8 Decay Rate as a Function of H

The existence of multiple CdL solutions in the Standard Model complicates the question of what the actual decay rate is. We can track the decay rate of the four CdL solutions and the

Hawking-Moss - this is plotted in fig. 6.14. It appears then, that the extra solutions always
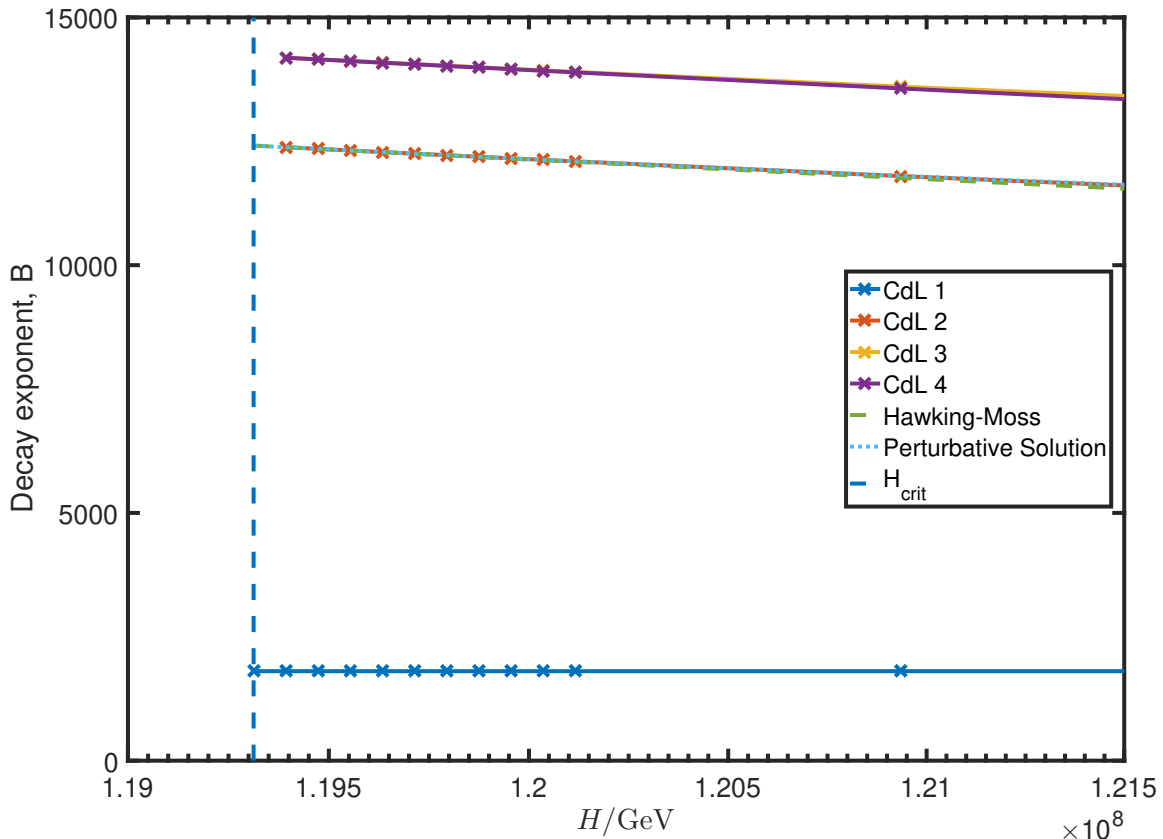
Figure 6.14: Decay exponents of the four CdL solutions found in the Standard Model. Below the critical threshold, only the large amplitude CdL 1 and the Hawking-Moss exist. Above H_{crit}, extra solutions appear. CdL 2 splits off from the Hawking-Moss, closely following the perturbative prediction of Eq. (6.38) (see fig. 6.12b). CdL 3 and 4 have a higher action.

have higher action than the Hawking-moss solution, although whether this is always the case is unclear. The perturbative result of Eq. (6.38) proves that this is true for CdL 2, but it remains conjecture for CdL 3 and 4, or any other solutions that may exist.

Assuming that CdL 1 is always the dominant CdL solution, it is possible to deduce the decay rate as a function of H, which we plot in fig. 6.15. A notable feature of this plot is that the transition between Hawking-Moss and CdL is sharp, unlike the smooth transition observed in fig. 6.3. This means that a reasonable approximation of the decay rate in the Standard Model from instantons is given by:

$$B_{\text{SM}}(H) = \begin{cases} B_0 & H < H_{\text{cross}} \\ \frac{8\pi^2 \Delta V(h_{\text{bar}})}{3H^4} & H > H_{\text{cross}} \end{cases}, \tag{6.114}$$

where B_0 is the flat false vacuum $(H = 0)$ decay exponent, and;

$$H_{\text{cross}} \approx \sqrt{\frac{\Delta V(h_{\text{bar}})}{6M_{\text{P}}^2} \left(-1 + \sqrt{1 + \frac{96\pi^2 M_{\text{P}}^4}{\Delta V(h_{\text{bar}}) B_0}} \right)}. \tag{6.115}$$

This expression for H_{cross} is obtained by equating S_{HM} with B_0 and solving for H. Note that it applies without using the fixed background approximation: if $\Delta V(h_{\text{bar}}) \ll V_0$, then we can further approximate H_{cross} as:

$$H_{\text{cross}} \approx \left(\frac{24\pi^2 \Delta V(h_{\text{bar}})}{9 B_0} \right)^{1/4}. \tag{6.116}$$

The reason that this works well is that the Standard Model potential has a wide range of scales present: For $M_t = 173.34\,\text{GeV}, M_h = 125.15\,\text{GeV}, \alpha_S = 0.1184$, the scale $\mu_{\text{min}} = 2.79 \times 10^{17}\,\text{GeV}$ at which $\lambda(\mu)$ takes its minimum value controls the nucleation of vacuum bubbles, which is orders of magnitude different to barrier scale of $7.70 \times 10^9\,\text{GeV}$. This means that for small $(H \ll \mu_{\text{min}})$ Hubble rates, $B(H)$ varies only slowly with H and is nearly constant. The Hawking-Moss solution then comes to dominate at a scale determined by the height of the barrier, H_{cross}. It should be noted, however, that this discussion is modified if the effective potential in de Sitter space is properly properly computed as in chapter 4, to account for the running of the couplings at non-zero H.
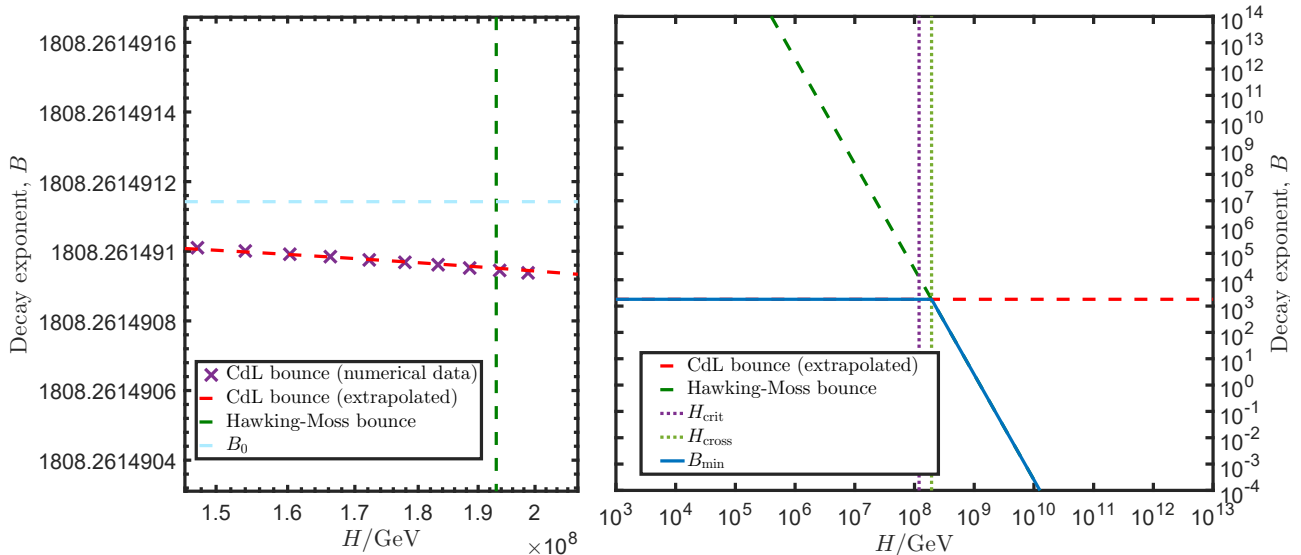
Figure 6.15: Right: Smallest decay exponent, B_{min}, in the Standard Model, with $M_t = 173.34\,\text{GeV}, M_h = 125.15\,\text{GeV}, \alpha_S = 0.1184$, assuming that CdL 1 (the largest amplitude bounce) is always the smallest action CdL solution. At $H < H_{\text{cross}}$ (rather than H_{crit}), the CdL solution dominates with nearly the same action as the $H = 0$ case. Above this, the Hawking-Moss solution dominates, and rapidly becomes so small in action that the semi-classical approximation no longer applies. Left: zoom in on cross-over region, showing slow variation of $B_{\text{CdL1}}(H)$ compared to B_0, the $H = 0$ value. Dashed red line is extrapolated from numerical data indicated by crosses.

Chapter 7

Conclusions

7.1 Backreaction and Non-minimal Coupling in Standard Model Bubble Nucleation

As we have seen, the depth of the Standard Model effective potential is such that back-reaction of the bounce is not negligible. The shape of the bounce solution changes significantly, and the curvature in the centre of the bounce is non negligible. From the point of view of the future state of the universe this is especially important - the large negative Ricci curvature leads to a collapsing AdS region with a big-crunch like singularity, an effect not seen with a fixed, flat background.

With regards the actual effect of the decay rates, however, backreaction has a small effect on the life-time of the vacuum. In part this is due to the fact that the interior of the bounce, where the Higgs field, ϕ, is deep in the potential, is where the strongest effects are concentrated. However, this is not where the action of the solution is determined, by and large. Even with back-reaction, the bounce solution is well approximated by it's constant λ form:

$$h(\chi) = \sqrt{\frac{2}{|\lambda(\mu)|}} \frac{2R(\mu)}{R(\mu)^2 + \chi^2}, \tag{7.1}$$

$$S \approx \frac{8\pi^2}{3|\lambda(\mu)|}, \tag{7.2}$$

where μ is the characteristic scale of the bounce. The main effect of back-reaction is to shift this scale, while producing a Planck-suppressed correction to the action. This means that despite a significant change in the *shape* of the solution, corresponding to a change in μ, the actual action varies only weakly with μ, since λ varies only logarithmically with μ. Thus, while there is a small suppression of the decay rate relative to the fixed background approximation, this is not sufficient to change the stability of the vacuum considerably.

However, direct gravitational suppression of vacuum decay is not the only result of back-reaction. As we have seen from the discussion in chapter 5, the large negative Ricci curvature in the centre of the bounce solution is can couple to the Higgs field in a significant way, and this *does* substantially shift the boundary between stability and metastability. Including this in our numerical calculations, we produced a complete analysis of the top quark/Higgs boson phase plane, including the effect of different values of ξ, summarised in fig. 5.6. This shows that both positive and negative ξ can have significant effects on the boundary between metastability and instability.

However, this is not all. We also showed that the effect of ξ is sensitive to the near conformal symmetry in the Standard Model effective potential at large h. This is largely due to the way the Ricci scalar depends on the Higgs field in the Jordan frame:

$$R = \frac{(1 - 6\xi)\dot{h}^2 + 4V(h) - 6\xi\phi V'(h)}{M_P^2 \left(1 - \frac{\xi(1 - 6\xi)h^2}{M_P^2}\right)}. \tag{7.3}$$

The case $\xi = 1/6$ is a special value in 4D, since it corresponds to exact conformal symmetry with a conformally symmetry potential like $\lambda\phi^4$ with constant λ. For such a potential, it is clear that the conformal symmetry ensures the vanishing of R everywhere. Since conformally symmetry is only lightly broken by quantum corrections at large ϕ, this means that $\xi = 1/6$ should be

roughly equivalent to having an exactly fixed flat background, with no back-reaction at all. This also means that $\xi = 1/6$ is the point at which the decay exponent, $B(\xi)$, is minimised if the back-reaction exactly cancels:

$$\frac{\mathrm{d}B}{\mathrm{d}\xi} = \pi^2 \int_0^\infty \mathrm{d}\chi a_\xi^3(\chi)\phi_\xi^2(\chi)R_\xi(\chi) = 0. \tag{7.4}$$

However, the running of $\lambda(\mu)$ breaks this conformal symmetry, and spontaneously generates a new scale, $\mu_{\min}$, at which λ is minimised. This breaking also means that $\xi = 1/6$ is *not* the minimum of $B(\xi)$, which shifts slightly, as is clearly seen in fig. 5.3. However, it maintains the approximate conformal symmetry. These numerical results also show that the large ξ behaviour is far from quadratic at large ξ.

7.2 New CdL Solutions in the Standard Model

Perhaps the most important of the results we now summarise is the surprising observation that the Standard Model potential does not have typical behaviour in de Sitter space. As he have discussed, there is a critical threshold for the Hubble rate:

$$H_{\mathrm{crit}} = \sqrt{-\frac{V''(\phi_{\mathrm{bar}})}{4} - \frac{[V(\phi_{\mathrm{bar}}) - V(\phi_{\mathrm{fv}})]}{3M_{\mathrm{P}}^2}}, \tag{7.5}$$

below which CdL solutions exist in all potentials. In many potentials, CdL solutions do not exist for $H > H_{\mathrm{crit}}$ and there is a smooth transition at $H = H_{\mathrm{crit}}$ to dominance by Hawking-Moss type solutions. However in others, such as the Standard Model and $g\phi^6$ potentials with sufficiently negative g, this doesn't happen: instead a new solution emerges at H_{crit}. The reason for this peculiar behaviour can be understood by using a perturbative analysis of solutions in the vicinity of $H \sim H_{\mathrm{crit}}$. This analysis shows that there is a critical quantity, Δ:

$$\Delta = -\frac{1}{14}\left(V^{(4)}(\phi_{\mathrm{bar}}) - \frac{(V^{(3)}(\phi_{\mathrm{bar}}))^2}{3V^{(2)}(\phi_{\mathrm{bar}})} - \frac{8V^{(2)}(\phi_{\mathrm{bar}})}{3M_{\mathrm{P}}^2}\right), \tag{7.6}$$

which allows us to classify potentials:

1. $\Delta < 0$: the 'typical' potentials. The perturbative solution only exists for $H < H_{\mathrm{crit}}$, and describes the smooth merging of the CdL solution with the Hawking-Moss at H_{crit}. It has *lower* action than the Hawking-Moss, showing that we can easily split the Hubble rates into a CdL-dominated region for $H < H_{\mathrm{crit}}$ and a Hawking-Moss dominated region for $H > H_{\mathrm{crit}}$.

2. $\Delta > 0$: In this case, perturbative solutions only exist for $H > H_{\mathrm{crit}}$, thus they cannot describe the smooth merging of the CdL solution that exists for $H < H_{\mathrm{crit}}$ with the Hawking-Moss. This also implies the presence of *multiple* CdL solutions.

As we have seen, the Standard Model is in the latter category, and this has potential consequences. The most serious consequence is the disturbing questions it raises about the uniqueness of CdL bounces. As we have proven, CdL bounces are not unique, and multiple, non-oscillating solutions exist. At least one of these can be understood perturbatively, and appears to have higher action than the Hawking-Moss solution. If this were the only solution, then this would be a theoretically interesting, yet physically irrelevant fact: only the lowest action solution

contributes significantly due to the exponential dependence on the action.

However, as our analysis of the Standard Model in chapter 6 has shown, this is not the case. *At least* four solutions exist in the Standard Model potential for $H > H_{\text{crit}}$, and there is no way of ruling out additional solutions. Although all the solutions found to date are of higher action, there is no particular reason to think that this should be the case in general. Thus, it is possible to imagine, given the extremely difficult-to-spot signatures that these solutions have (see figures 6.8a and 6.8b for example), that additional solutions could lie undetected for other Hubble rates, and that these solutions could dominate vacuum decay.

If these solutions were low action, then they could lead to extremely rapid decay, which erodes confidence that we might have in calculations of the vacuum decay rate during inflation. Even the predictions of the stochastic approach and the Fokker-Planck equations might be suspect, since this depends on the coarse-graining of sub-horizon effects, which is precisely the regime CdL solutions describe. Although we deem this situation unlikely, it cannot be altogether ruled out.

7.3   Possible Future Directions

There remain a great many questions to be answered about the issues raised in this work. Most of these concern the extra CdL solutions found in the Standard Model. For example:

1. How many CdL solutions exist for a given Hubble rate?

2. Is the action of the extra solutions always higher than the Hawking-Moss solution?

3. What happens to the extra solutions as H is further increased?

Numerically, all the solutions found to date appear to support the assumption that the higher action solutions are generally of higher action, however, we wish to stress that there is no proof of this, and indeed no particular reason why it should be the case. Arguing from intuition, we might argue that raising H is much akin to raising the temperature, and thus we would expect that thermal fluctuation over the barrier (as described by the Hawking-Moss solution) should eventually come to dominate at sufficiently large H, where excitation up the barrier becomes more and more important. Certainly at $H \gg \Delta V(\phi_{\text{bar}})^{1/4}$ we would expect thermal fluctuations to be extremely rapid. Since S_{HM} eventually becomes $O(1)$, signalling the break-down of the dilute gas approximation used in deriving the decay rate [99], unless the same happens to the CdL solutions, they will eventually become irrelevant. This seems an unlikely behaviour, so it is not unreasonable to believe that Hawking-Moss solutions dominate for sufficiently high H.

Furthermore, some hints of what may happen in the Standard Model are found by looking to toy models. In chapter 6 we considered a $g\phi^6$ model with g sufficiently negative that it satisfied $\Delta > 0$. In this model, we found that the perturbative solution appeared as expected, but numerics then suggested that it rapidly merged with the CdL solution that existed for $H < H_{\text{crit}}$ (see fig. 6.4). If the same is repeated in the Standard Model, then it may well be the case that the extra solutions all merge as H is increased in the Standard Model too. More evidence would be required to conclude this, however.

Another direction of future investigation that may bear fruit is the effect of non-minimal coupling during de Sitter space. The methods we used to extract the back-reaction in chapter 6 would not work for the Jordan frame with non-zero ξ, however, the calculation may well be possible in the Einstein frame, if a way can be found to consistently compute the Einstein frame effective potential that takes into account the running of ξ. This would be necessary to go beyond the simplified analysis of chapter 4 of the effect of ξ on vacuum stability during inflation, which assumed only Hawking-Moss solutions were relevant. Furthermore, the effect of varying ξ upon the extra solutions found in chapter 6 has yet to be investigated, and we expect that the effects could well be significant. Since we have already established that the the effect of back-reaction alone does not produce particularly large shifts in the action compared to the fixed background approximation, even in de Sitter, significant information could even be gleaned from the fixed background approximation alone, even with non-zero ξ.

7.4 Final Words

Gravity is not an entirely irrelevant factor in vacuum decay. As we have seen, the Standard Model true minimum can be very deep, and this depth affects the shape of bounce solutions. Taken together with the inevitable non-minimal coupling that is produced in the Standard Model, this can result in a significant effect on the vacuum decay rate, which is sensitive to Planck scale effects because of the scale $\mu_{\min} \sim 10^{17}\,\mathrm{GeV}$ which controls the size of nucleated bubbles.

Perhaps the most interesting effect of gravity, however, is how curvature affects the decay rate itself, acting to excite the field partially up the barrier and providing thermal assistance to tunnelling. In part this is due to the vacuum state during de Sitter being different - a thermal Bunch-Davies state. However, curvature has other effects, such as altering the effective potential itself and changing how the running of the couplings affects it.

Most surprising, however, is that de Sitter backgrounds lead to the possibility of extra Coleman de Luccia solutions which can contribute to vacuum decay. This effect was unexpected, but seems to be related to the critical threshold, H_{crit} which is controlled by the shape (not the height) of the barrier. Although we ultimately believe that the effect will not change any results significantly, it does raise the prospect that any calculation of vacuum decay rates could be incorrect if a lower action solution exists, and more work is needed to understand vacuum decay in the vicinity of the critical threshold.

Bibliography

[1] A. Rajantie and S. Stopyra, *Standard Model vacuum decay with gravity*, Phys. Rev. **D95** (2017) 025008 [`1606.00849`].

[2] A. Rajantie and S. Stopyra, *Standard model vacuum decay in a de sitter background*, Phys. Rev. D **97** (2018) 025012.

[3] T. Markkanen, S. Nurmi, A. Rajantie and S. Stopyra, *The 1-loop effective potential for the standard model in curved spacetime*, Journal of High Energy Physics **2018** (2018) 40.

[4] M. Tanabashi, *Review of particle physics*, Phys. Rev. D **98** (2018) 030001.

[5] T. Markkanen, S. Nurmi, A. Rajantie and S. Stopyra, *The 1-loop effective potential for the Standard Model in curved spacetime*, `1804.02020`.

[6] X. Calmet, I. Kuntz and I. G. Moss, *Non-Minimal Coupling of the Higgs Boson to Curvature in an Inflationary Universe*, Found. Phys. **48** (2018) 110 [`1701.02140`].

[7] A. Joti, A. Katsis, D. Loupas, A. Salvio, A. Strumia, N. Tetradis et al., *(Higgs) vacuum decay during inflation*, JHEP **07** (2017) 058 [`1706.00792`].

[8] T. Aoyama, M. Hayakawa, T. Kinoshita and M. Nio, *Tenth-order qed contribution to the electron $g-2$ and an improved value of the fine structure constant*, Phys. Rev. Lett. **109** (2012) 111807.

[9] B. Odom, D. Hanneke, B. D'Urso and G. Gabrielse, *New measurement of the electron magnetic moment using a one-electron quantum cyclotron*, Phys. Rev. Lett. **97** (2006) 030801.

[10] M.-x. Luo and Y. Xiao, *Two loop renormalization group equations in the standard model*, Phys. Rev. Lett. **90** (2003) 011601 [`hep-ph/0207271`].

[11] M. Sher, *Electroweak Higgs Potentials and Vacuum Stability*, Phys. Rept. **179** (1989) 273.

[12] M. Lindner, M. Sher and H. W. Zaglauer, *Probing Vacuum Stability Bounds at the Fermilab Collider*, Phys. Lett. **B228** (1989) 139.

[13] P. B. Arnold, *Can the Electroweak Vacuum Be Unstable?*, Phys. Rev. **D40** (1989) 613.

[14] M. Sher, *Precise vacuum stability bound in the standard model*, Phys. Lett. **B317** (1993) 159 [`hep-ph/9307342`].

[15] J. A. Casas, J. R. Espinosa and M. Quiros, *Improved Higgs mass stability bound in the standard model and implications for supersymmetry*, *Phys. Lett.* **B342** (1995) 171 [`hep-ph/9409458`].

[16] J. R. Espinosa and M. Quiros, *Improved metastability bounds on the standard model Higgs mass*, *Phys. Lett.* **B353** (1995) 257 [`hep-ph/9504241`].

[17] B. Schrempp and M. Wimmer, *Top quark and Higgs boson masses: Interplay between infrared and ultraviolet physics*, *Prog. Part. Nucl. Phys.* **37** (1996) 1 [`hep-ph/9606386`].

[18] G. Isidori, G. Ridolfi and A. Strumia, *On the metastability of the standard model vacuum*, *Nucl. Phys.* **B609** (2001) 387 [`hep-ph/0104016`].

[19] J. Ellis, J. R. Espinosa, G. F. Giudice, A. Hoecker and A. Riotto, *The Probable Fate of the Standard Model*, *Phys. Lett.* **B679** (2009) 369 [`0906.0954`].

[20] J. Elias-Miro, J. R. Espinosa, G. F. Giudice, G. Isidori, A. Riotto and A. Strumia, *Higgs mass implications on the stability of the electroweak vacuum*, *Phys. Lett.* **B709** (2012) 222 [`1112.3022`].

[21] P. B. Arnold and S. Vokos, *Instability of hot electroweak theory: bounds on m(H) and M(t)*, *Phys. Rev.* **D44** (1991) 3620.

[22] J. A. Casas, J. R. Espinosa and M. Quiros, *Standard model stability bounds for new physics within LHC reach*, *Phys. Lett.* **B382** (1996) 374 [`hep-ph/9603227`].

[23] T. Hambye and K. Riesselmann, *Matching conditions and Higgs mass upper bounds revisited*, *Phys. Rev.* **D55** (1997) 7255 [`hep-ph/9610272`].

[24] H. B. Nielsen, *PREdicted the Higgs Mass*, *Bled Workshops Phys.* **13** (2012) 94 [`1212.5716`].

[25] M. Holthausen, K. S. Lim and M. Lindner, *Planck scale Boundary Conditions and the Higgs Mass*, *JHEP* **02** (2012) 037 [`1112.2415`].

[26] M. Gonderinger, Y. Li, H. Patel and M. J. Ramsey-Musolf, *Vacuum Stability, Perturbativity, and Scalar Singlet Dark Matter*, *JHEP* **01** (2010) 053 [`0910.3167`].

[27] S. Nie and M. Sher, *Vacuum stability bounds in the two Higgs doublet model*, *Phys. Lett.* **B449** (1999) 89 [`hep-ph/9811234`].

[28] G. Isidori, V. S. Rychkov, A. Strumia and N. Tetradis, *Gravitational corrections to standard model vacuum decay*, *Phys. Rev.* **D77** (2008) 025034 [`0712.0242`].

[29] J. R. Espinosa, G. F. Giudice and A. Riotto, *Cosmological implications of the Higgs mass measurement*, *JCAP* **0805** (2008) 002 [`0710.2484`].

[30] CMS collaboration, S. Chatrchyan et al., *Observation of a new boson at a mass of 125 GeV with the CMS experiment at the LHC*, *Phys. Lett.* **B716** (2012) 30 [`1207.7235`].

[31] ATLAS collaboration, G. Aad et al., *Observation of a new particle in the search for the Standard Model Higgs boson with the ATLAS detector at the LHC*, *Phys. Lett.* **B716** (2012) 1 [`1207.7214`].

[32] J. Elias-Miro, J. R. Espinosa, G. F. Giudice, G. Isidori, A. Riotto and A. Strumia, *Higgs mass implications on the stability of the electroweak vacuum, Phys. Lett.* **B709** (2012) 222 [1112.3022].

[33] G. Degrassi, S. Di Vita, J. Elias-Miro, J. R. Espinosa, G. F. Giudice, G. Isidori et al., *Higgs mass and vacuum stability in the Standard Model at NNLO, JHEP* **08** (2012) 098 [1205.6497].

[34] S. Alekhin, A. Djouadi and S. Moch, *The top quark and Higgs boson masses and the stability of the electroweak vacuum, Phys. Lett.* **B716** (2012) 214 [1207.0980].

[35] D. Buttazzo, G. Degrassi, P. P. Giardino, G. F. Giudice, F. Sala, A. Salvio et al., *Investigating the near-criticality of the Higgs boson, JHEP* **12** (2013) 089 [1307.3536].

[36] Y. Tang, *Vacuum Stability in the Standard Model, Mod. Phys. Lett.* **A28** (2013) 1330002 [1301.5812].

[37] A. Spencer-Smith, *Higgs Vacuum Stability in a Mass-Dependent Renormalisation Scheme,* 1405.1975.

[38] E. Gabrielli, M. Heikinheimo, K. Kannike, A. Racioppi, M. Raidal and C. Spethmann, *Towards Completing the Standard Model: Vacuum Stability, EWSB and Dark Matter, Phys. Rev.* **D89** (2014) 015017 [1309.6632].

[39] A. Eichhorn, M. Fairbairn, T. Markkanen and A. Rajantie, eds., *Proceedings, Higgs cosmology*, vol. A376, 2018.

[40] L. Di Luzio, G. Isidori and G. Ridolfi, *Stability of the electroweak ground state in the Standard Model and its extensions, Phys. Lett.* **B753** (2016) 150 [1509.05028].

[41] S. Chigusa, T. Moroi and Y. Shoji, *State-of-the-Art Calculation of the Decay Rate of Electroweak Vacuum in the Standard Model, Phys. Rev. Lett.* **119** (2017) 211801 [1707.09301].

[42] A. Datta and S. Raychaudhuri, *Vacuum Stability Constraints and LHC Searches for a Model with a Universal Extra Dimension, Phys. Rev.* **D87** (2013) 035018 [1207.0476].

[43] E. J. Chun, H. M. Lee and P. Sharma, *Vacuum Stability, Perturbativity, EWPD and Higgs-to-diphoton rate in Type II Seesaw Models, JHEP* **11** (2012) 106 [1209.1303].

[44] F. Bezrukov, M. Yu. Kalmykov, B. A. Kniehl and M. Shaposhnikov, *Higgs Boson Mass and New Physics, JHEP* **10** (2012) 140 [1205.2893].

[45] W. Rodejohann and H. Zhang, *Impact of massive neutrinos on the Higgs self-coupling and electroweak vacuum stability, JHEP* **06** (2012) 022 [1203.3825].

[46] C.-S. Chen and Y. Tang, *Vacuum stability, neutrinos, and dark matter, JHEP* **04** (2012) 019 [1202.5717].

[47] P. S. Bhupal Dev, D. K. Ghosh, N. Okada and I. Saha, *125 GeV Higgs Boson and the Type-II Seesaw Model, JHEP* **03** (2013) 150 [1301.3453].

[48] X.-G. He, H. Phoon, Y. Tang and G. Valencia, *Unitarity and vacuum stability constraints on the couplings of color octet scalars, JHEP* **05** (2013) 026 [1303.4848].

[49] V. Branchina and E. Messina, *Stability, Higgs Boson Mass and New Physics*, *Phys. Rev. Lett.* **111** (2013) 241801 [`1307.5193`].

[50] A. Kobakhidze and A. Spencer-Smith, *Neutrino Masses and Higgs Vacuum Stability*, *JHEP* **08** (2013) 036 [`1305.7283`].

[51] V. Branchina, E. Messina and A. Platania, *Top mass determination, Higgs inflation, and vacuum stability*, *JHEP* **09** (2014) 182 [`1407.4112`].

[52] A. Eichhorn, H. Gies, J. Jaeckel, T. Plehn, M. M. Scherer and R. Sondenheimer, *The Higgs Mass and the Scale of New Physics*, *JHEP* **04** (2015) 022 [`1501.02812`].

[53] V. Branchina, E. Messina and M. Sher, *Lifetime of the electroweak vacuum and sensitivity to Planck scale physics*, *Phys. Rev.* **D91** (2015) 013003 [`1408.5302`].

[54] V. Branchina and E. Messina, *Stability and UV completion of the Standard Model*, *EPL* **117** (2017) 61002 [`1507.08812`].

[55] E. Bentivegna, V. Branchina, F. Contino and D. Zappal, *Impact of New Physics on the EW vacuum stability in a curved spacetime background*, *JHEP* **12** (2017) 100 [`1708.01138`].

[56] J. Elias-Miro, J. R. Espinosa, G. F. Giudice, H. M. Lee and A. Strumia, *Stabilization of the Electroweak Vacuum by a Scalar Threshold Effect*, *JHEP* **06** (2012) 031 [`1203.0237`].

[57] M. Herranen, T. Markkanen, S. Nurmi and A. Rajantie, *Spacetime curvature and the Higgs stability during inflation*, *Phys. Rev. Lett.* **113** (2014) 211102 [`1407.3141`].

[58] V. Branchina, E. Messina and D. Zappala, *Impact of Gravity on Vacuum Stability*, *EPL* **116** (2016) 21001 [`1601.06963`].

[59] M. Kawasaki, K. Mukaida and T. T. Yanagida, *Simple cosmological solution to the Higgs field instability problem in chaotic inflation and the formation of primordial black holes*, *Phys. Rev.* **D94** (2016) 063509 [`1605.04974`].

[60] M. Fairbairn and R. Hogan, *Electroweak vacuum stability in light of bicep2*, *Phys. Rev. Lett.* **112** (2014) 201801.

[61] O. Lebedev and A. Westphal, *Metastable Electroweak Vacuum: Implications for Inflation*, *Phys. Lett.* **B719** (2013) 415 [`1210.6987`].

[62] A. Kobakhidze and A. Spencer-Smith, *Electroweak Vacuum (In)Stability in an Inflationary Universe*, *Phys. Lett.* **B722** (2013) 130 [`1301.2846`].

[63] A. Kobakhidze and A. Spencer-Smith, *The Higgs vacuum is unstable*, `1404.4709`.

[64] K. Bhattacharya, J. Chakrabortty, S. Das and T. Mondal, *Higgs vacuum stability and inflationary dynamics after BICEP2 and PLANCK dust polarisation data*, *JCAP* **1412** (2014) 001 [`1408.3966`].

[65] J. R. Espinosa, G. F. Giudice, E. Morgante, A. Riotto, L. Senatore, A. Strumia et al., *The cosmological higgstory of the vacuum instability*, *Journal of High Energy Physics* **2015** (2015) 174.

[66] J. Kearney, H. Yoo and K. M. Zurek, *Is a Higgs Vacuum Instability Fatal for High-Scale Inflation?*, Phys. Rev. **D91** (2015) 123537 [1503.05193].

[67] A. Hook, J. Kearney, B. Shakya and K. M. Zurek, *Probable or Improbable Universe? Correlating Electroweak Vacuum Instability with the Scale of Inflation*, JHEP **01** (2015) 061 [1404.5953].

[68] W. E. East, J. Kearney, B. Shakya, H. Yoo and K. M. Zurek, *Spacetime Dynamics of a Higgs Vacuum Instability During Inflation*, Phys. Rev. **D95** (2017) 023526 [1607.00381].

[69] T. Markkanen, S. Nurmi and A. Rajantie, *Do metric fluctuations affect the Higgs dynamics during inflation?*, JCAP **1712** (2017) 026 [1707.00866].

[70] T. Markkanen and A. Rajantie, *Massive scalar field evolution in de Sitter*, JHEP **01** (2017) 133 [1607.00334].

[71] B.-H. Lee, W. Lee and D. Ro, *Cosmological Implications of Fubini Type Instanton*, in *Proceedings, 2nd LeCosPA Symposium: Everything about Gravity, Celebrating the Centenary of Einstein's General Relativity (LeCosPA2015): Taipei, Taiwan, December 14-18, 2015*, pp. 483–489, 2017, DOI.

[72] K. Kamada, *Inflationary cosmology and the standard model Higgs with a small Hubble induced mass*, Phys. Lett. **B742** (2015) 126 [1409.5078].

[73] O. Czerwińska, Z. Lalak and Ł. Nakonieczny, *Stability of the effective potential of the gauge-less top-Higgs model in curved spacetime*, JHEP **11** (2015) 207 [1508.03297].

[74] A. Shkerin and S. Sibiryakov, *On stability of electroweak vacuum during inflation*, Phys. Lett. **B746** (2015) 257 [1503.02586].

[75] M. Herranen, T. Markkanen, S. Nurmi and A. Rajantie, *Spacetime curvature and Higgs stability after inflation*, Phys. Rev. Lett. **115** (2015) 241301 [1506.04065].

[76] C. Gross, O. Lebedev and M. Zatta, *Higgs-inflaton coupling from reheating and the metastable Universe*, Phys. Lett. **B753** (2016) 178 [1506.05106].

[77] K. Enqvist, M. Karciauskas, O. Lebedev, S. Rusak and M. Zatta, *Postinflationary vacuum instability and Higgs-inflaton couplings*, JCAP **1611** (2016) 025 [1608.08848].

[78] Y. Ema, K. Mukaida and K. Nakayama, *Fate of Electroweak Vacuum during Preheating*, JCAP **1610** (2016) 043 [1602.00483].

[79] K. Kohri and H. Matsui, *Higgs vacuum metastability in primordial inflation, preheating, and reheating*, Phys. Rev. **D94** (2016) 103509 [1602.02100].

[80] L. Delle Rose, C. Marzo and A. Urbano, *On the fate of the Standard Model at finite temperature*, JHEP **05** (2016) 050 [1507.06912].

[81] R. Gregory, I. G. Moss and B. Withers, *Black holes as bubble nucleation sites*, JHEP **03** (2014) 081 [1401.0017].

[82] P. Burda, R. Gregory and I. Moss, *Vacuum metastability with black holes*, JHEP **08** (2015) 114 [1503.07331].

[83] P. Burda, R. Gregory and I. Moss, *Gravity and the stability of the Higgs vacuum, Phys. Rev. Lett.* **115** (2015) 071303 [1501.04937].

[84] P. Burda, R. Gregory and I. G. Moss, *The fate of the higgs vacuum, Journal of High Energy Physics* **2016** (2016) 25.

[85] T. Markkanen, *Spacetime curvature and the Higgs stability during and after inflation: Gravity to the rescue?*, in *27th Rencontres de Blois on Particle Physics and Cosmology Blois, France, May 31-June 5, 2015*, 2015, 1509.05072, https://inspirehep.net/record/1393767/files/arXiv:1509.05072.pdf.

[86] M. Herranen, T. Markkanen, S. Nurmi and A. Rajantie, *Spacetime curvature and Higgs stability after inflation, Phys. Rev. Lett.* **115** (2015) 241301 [1506.04065].

[87] T. Markkanen, *Vacuum Stability in the Early Universe and the Backreaction of Classical Gravity, Phil. Trans. Roy. Soc. Lond.* **A376** (2018) 20170115 [1707.03415].

[88] A. Salvio, A. Strumia, N. Tetradis and A. Urbano, *On gravitational and thermal corrections to vacuum decay, JHEP* **09** (2016) 054 [1608.02555].

[89] D. G. Figueroa, A. Rajantie and F. Torrenti, *Higgs-curvature coupling and post-inflationary vacuum instability*, 1709.00398.

[90] O. Czerwiska, Z. Lalak, M. Lewicki and P. Olszewski, *The impact of non-minimally coupled gravity on vacuum stability, JHEP* **10** (2016) 004 [1606.07808].

[91] O. Czerwiska, Z. Lalak, M. Lewicki and P. Olszewski, *Non-minimally coupled gravity and vacuum stability, PoS* **CORFU2016** (2017) 064 [1701.05731].

[92] L. Di Luzio and L. Mihaila, *On the gauge dependence of the Standard Model vacuum instability scale, JHEP* **06** (2014) 079 [1404.7450].

[93] A. D. Plascencia and C. Tamarit, *Convexity, gauge-dependence and tunneling rates, JHEP* **10** (2016) 099 [1510.07613].

[94] A. V. Bednyakov, B. A. Kniehl, A. F. Pikelner and O. L. Veretin, *Stability of the Electroweak Vacuum: Gauge Independence and Advanced Precision, Phys. Rev. Lett.* **115** (2015) 201802 [1507.08833].

[95] J. R. Espinosa, M. Garny, T. Konstandin and A. Riotto, *Gauge-Independent Scales Related to the Standard Model Vacuum Instability, Phys. Rev.* **D95** (2017) 056004 [1608.06765].

[96] B. Garbrecht and P. Millington, *Green's function method for handling radiative effects on false vacuum decay, Phys. Rev. D* **91** (2015) 105021.

[97] S. Coleman and F. De Luccia, *Gravitational effects on and of vacuum decay, Phys. Rev. D* **21** (1980) 3305.

[98] S. Coleman, *Fate of the false vacuum: Semiclassical theory, Phys. Rev. D* **15** (1977) 2929.

[99] C. G. Callan and S. Coleman, *Fate of the false vacuum. ii. first quantum corrections, Phys. Rev. D* **16** (1977) 1762.

[100] V. A. Rubakov and S. M. Sibiryakov, *False vacuum decay in de Sitter space-time*, *Theor. Math. Phys.* **120** (1999) 1194 [`gr-qc/9905093`].

[101] A. R. Brown and E. J. Weinberg, *Thermal derivation of the Coleman-De Luccia tunneling prescription*, *Phys. Rev.* **D76** (2007) 064003 [`0706.1573`].

[102] D. J. Toms, *Renormalization of Interacting Scalar Field Theories in Curved Space-time*, *Phys. Rev.* **D26** (1982) 2713.

[103] D. J. Toms, *Gauged Yukawa model in curved spacetime*, `1805.01700`.

[104] D. J. Toms, *Effective action for the Yukawa model in curved spacetime*, *JHEP* **05** (2018) 139 [`1804.08350`].

[105] M. Atkins and X. Calmet, *Bounds on the Nonminimal Coupling of the Higgs Boson to Gravity*, *Phys. Rev. Lett.* **110** (2013) 051301 [`1211.0281`].

[106] S. W. Hawking and I. G. Moss, *Supercooled Phase Transitions in the Very Early Universe*, *Phys. Lett.* **110B** (1982) 35.

[107] A. A. Starobinsky and J. Yokoyama, *Equilibrium state of a self-interacting scalar field in the de sitter background*, *Phys. Rev. D* **50** (1994) 6357.

[108] L. G. Jensen and P. J. Steinhardt, *Bubble Nucleation for Flat Potential Barriers*, *Nucl. Phys.* **B317** (1989) 693.

[109] V. Balek and M. Demetrian, *Criterion for bubble formation in a de sitter universe*, *Phys. Rev. D* **69** (2004) 063518.

[110] J. C. Hackworth and E. J. Weinberg, *Oscillating bounce solutions and vacuum tunneling in de Sitter spacetime*, *Phys. Rev.* **D71** (2005) 044014 [`hep-th/0410142`].

[111] S. R. Coleman, *Quantum Tunneling and Negative Eigenvalues*, *Nucl. Phys.* **B298** (1988) 178.

[112] V. Balek and M. Demetrian, *Euclidean action for vacuum decay in a de Sitter universe*, *Phys. Rev.* **D71** (2005) 023512 [`gr-qc/0409001`].

[113] T. Tanaka and M. Sasaki, *False vacuum decay with gravity: Negative mode problem*, *Prog. Theor. Phys.* **88** (1992) 503.

[114] K.-M. Lee and E. J. Weinberg, *TUNNELING WITHOUT BARRIERS*, *Nucl. Phys.* **B267** (1986) 181.

[115] I. Affleck, *On Constrained Instantons*, *Nucl. Phys.* **B191** (1981) 429.

[116] A. Sürig, *Self-consistent treatment of bubble nucleation at the electroweak phase transition*, *Phys. Rev. D* **57** (1998) 5049.

[117] A. Andreassen, D. Farhi, W. Frost and M. D. Schwartz, *Precision decay rate calculations in quantum field theory*, *Phys. Rev.* **D95** (2017) 085011 [`1604.06090`].

[118] C. M. Bender, *Making sense of non-Hermitian Hamiltonians*, *Rept. Prog. Phys.* **70** (2007) 947 [`hep-th/0703096`].

[119] S. Coleman, V. Glaser and A. Martin, *Action minima among solutions to a class of euclidean scalar field equations*, *Communications in Mathematical Physics* **58** (1978) 211.

[120] S. Fubini, *A New Approach to Conformal Invariant Field Theories*, *Nuovo Cim.* **A34** (1976) 521.

[121] M. Visser, *How to Wick rotate generic curved spacetime*, `1702.05572`.

[122] R. Gregory, I. G. Moss and B. Withers, *Black holes as bubble nucleation sites*, *JHEP* **03** (2014) 081 [`1401.0017`].

[123] M. Spivak, *A comprehensive introduction to differential geometry*, no. v. 2 in A Comprehensive Introduction to Differential Geometry. Publish or Perish, inc., 1979.

[124] T. Willmore, *An Introduction to Differential Geometry*, Dover Books on Mathematics. Dover Publications, 2013.

[125] G. W. Gibbons and S. W. Hawking, *Cosmological Event Horizons, Thermodynamics, and Particle Creation*, *Phys. Rev.* **D15** (1977) 2738.

[126] M. Koehn, G. Lavrelashvili and J.-L. Lehners, *Towards a Solution of the Negative Mode Problem in Quantum Tunnelling with Gravity*, *Phys. Rev.* **D92** (2015) 023506 [`1504.04334`].

[127] B.-H. Lee, W. Lee, D. Ro and D.-h. Yeom, *Oscillating Fubini instantons in curved space*, *Phys. Rev.* **D91** (2015) 124044 [`1409.3935`].

[128] B. M. Project, H. Bateman, A. Erdélyi and U. S. O. of Naval Research, *Higher Transcendental Functions*, no. v. 2 in Bateman Manuscript Project California Institute of Technology. McGraw-Hill, 1953.

[129] M. A. Rubin and C. R. Ordez, *Eigenvalues and degeneracies for ndimensional tensor spherical harmonics*, *Journal of Mathematical Physics* **25** (1984) 2888 [`https://doi.org/10.1063/1.526034`].

[130] B. Simon, *Sturm Oscillation and Comparison Theorems*, *ArXiv Mathematics e-prints* (2003) [`math/0311049`].

[131] H. Lee and E. J. Weinberg, *Negative modes of Coleman-De Luccia bounces*, *Phys. Rev.* **D90** (2014) 124002 [`1408.6547`].

[132] G. Lavrelashvili, *The Number of negative modes of the oscillating bounces*, *Phys. Rev.* **D73** (2006) 083513 [`gr-qc/0602039`].

[133] K.-M. Lee, *Tunneling Without Barriers in Curved Space-time*, *Nucl. Phys.* **B282** (1987) 509.

[134] A. D. Linde, *Scalar Field Fluctuations in Expanding Universe and the New Inflationary Universe Scenario*, *Phys. Lett.* **116B** (1982) 335.

[135] B.-H. Lee, W. Lee, D. Ro and D.-H. Yeom, *Tunneling without a barrier: Fubini instantons in curved space*, in *Proceedings, 14th Marcel Grossmann Meeting on Recent Developments in Theoretical and Experimental General Relativity, Astrophysics, and Relativistic Field Theories (MG14) (In 4 Volumes): Rome, Italy, July 12-18, 2015*, vol. 3, pp. 2766–2768, 2017, DOI.

[136] S. Kanno, M. Sasaki and J. Soda, *Tunneling without barriers with gravity, Class. Quant. Grav.* **29** (2012) 075010 [1201.2272].

[137] J. Garriga and A. Megevand, *Decay of de Sitter vacua by thermal activation, Int. J. Theor. Phys.* **43** (2004) 883 [hep-th/0404097].

[138] A. Masoumi and E. J. Weinberg, *Bounces with O(3) x O(2) symmetry, Phys. Rev.* **D86** (2012) 104029 [1207.3717].

[139] I. M. Gelfand and A. M. Yaglom, *Integration in functional spaces and it applications in quantum physics, J. Math. Phys.* **1** (1960) 48.

[140] G. V. Dunne, *Functional determinants in quantum field theory, J. Phys.* **A41** (2008) 304006 [0711.1178].

[141] S. Coleman, *Aspects of Symmetry: Selected Erice Lectures*. Cambridge University Press, 1988.

[142] J. R. Espinosa, G. F. Giudice and A. Riotto, *Cosmological implications of the Higgs mass measurement, JCAP* **0805** (2008) 002 [0710.2484].

[143] S. Weinberg, *The Quantum Theory of Fields*, no. v. 2 in The Quantum Theory of Fields 3 Volume Hardback Set. Cambridge University Press, 1995.

[144] S. R. Coleman and E. J. Weinberg, *Radiative Corrections as the Origin of Spontaneous Symmetry Breaking, Phys. Rev.* **D7** (1973) 1888.

[145] M. Bando, T. Kugo, N. Maekawa and H. Nakano, *Improving the effective potential, Phys. Lett.* **B301** (1993) 83 [hep-ph/9210228].

[146] E. J. Weinberg, *Radiative corrections as the origin of spontaneous symmetry breaking*, Ph.D. thesis, Harvard U., 1973. hep-th/0507214.

[147] R. Jackiw, *Functional evaluation of the effective potential, Phys. Rev.* **D9** (1974) 1686.

[148] M. E. Peskin and D. V. Schroeder, *An Introduction to quantum field theory*. Addison-Wesley, Reading, USA, 1995.

[149] M. B. Einhorn and D. R. T. Jones, *A NEW RENORMALIZATION GROUP APPROACH TO MULTISCALE PROBLEMS, Nucl. Phys.* **B230** (1984) 261.

[150] C. Ford, *Multiscale renormalization group improvement of the effective potential, Phys. Rev.* **D50** (1994) 7531 [hep-th/9404085].

[151] C. Ford and C. Wiesendanger, *A Multiscale subtraction scheme and partial renormalization group equations in the O(N) symmetric phi**4 theory, Phys. Rev.* **D55** (1997) 2202 [hep-ph/9604392].

[152] M. Bando, T. Kugo, N. Maekawa and H. Nakano, *Improving the effective potential: Multimass scale case*, *Prog. Theor. Phys.* **90** (1993) 405 [`hep-ph/9210229`].

[153] E. Gildener and S. Weinberg, *Symmetry Breaking and Scalar Bosons*, *Phys. Rev.* **D13** (1976) 3333.

[154] L. Chataignier, T. Prokopec, M. G. Schmidt and B. Świeżewska, *Single-scale renormalisation group improvement of multi-scale effective potentials*, *Journal of High Energy Physics* **2018** (2018) 14.

[155] F. Loebbert, J. Miczajka and J. Plefka, *Consistent conformal extensions of the standard model*, *arXiv preprint arXiv:1805.09727* (2018) .

[156] C. Ford, D. R. T. Jones, P. W. Stephenson and M. B. Einhorn, *The Effective potential and the renormalization group*, *Nucl. Phys.* **B395** (1993) 17 [`hep-lat/9210033`].

[157] M. E. Machacek and M. T. Vaughn, *Two Loop Renormalization Group Equations in a General Quantum Field Theory. 1. Wave Function Renormalization*, *Nucl. Phys.* **B222** (1983) 83.

[158] M. E. Machacek and M. T. Vaughn, *Two Loop Renormalization Group Equations in a General Quantum Field Theory. 2. Yukawa Couplings*, *Nucl. Phys.* **B236** (1984) 221.

[159] M. E. Machacek and M. T. Vaughn, *Two Loop Renormalization Group Equations in a General Quantum Field Theory. 3. Scalar Quartic Couplings*, *Nucl. Phys.* **B249** (1985) 70.

[160] A. V. Bednyakov, A. F. Pikelner and V. N. Velizhanin, *Anomalous dimensions of gauge fields and gauge coupling beta-functions in the Standard Model at three loops*, *JHEP* **01** (2013) 017 [`1210.6873`].

[161] M. F. Zoller, *Standard Model beta-functions to three-loop order and vacuum stability*, in *17th International Moscow School of Physics and 42nd ITEP Winter School of Physics Moscow, Russia, February 11-18, 2014*, 2014, `1411.2843`, https://inspirehep.net/record/1327250/files/arXiv:1411.2843.pdf.

[162] D. V. Vassilevich, *Heat kernel expansion: User's manual*, *Phys. Rept.* **388** (2003) 279 [`hep-th/0306138`].

[163] M. Bounakis and I. G. Moss, *Gravitational corrections to Higgs potentials*, *JHEP* **04** (2018) 071 [`1710.02987`].

[164] I. Jack and L. Parker, *Proof of Summed Form of Proper Time Expansion for Propagator in Curved Space-time*, *Phys. Rev.* **D31** (1985) 2439.

[165] L. Parker and D. J. Toms, *New Form for the Coincidence Limit of the Feynman Propagator, or Heat Kernel, in Curved Space-time*, *Phys. Rev.* **D31** (1985) 953.

[166] L. C. Loveridge, *Physical and geometric interpretations of the Riemann tensor, Ricci tensor, and scalar curvature*, `gr-qc/0401099`.

[167] V. Miquel, *The volumes of small geodesic balls for a metric connection*, *Compositio Mathematica* **46** (1982) 121.

[168] C. Bender and S. Orszag, *Advanced Mathematical Methods for Scientists and Engineers I: Asymptotic Methods and Perturbation Theory*, Advanced Mathematical Methods for Scientists and Engineers. Springer, 1978.

[169] M. Abramowitz and I. Stegun, *Handbook of Mathematical Functions: With Formulas, Graphs, and Mathematical Tables*, Applied mathematics series. Dover Publications, 1965.

[170] A. Bohm, M. Gadella and G. B. Mainland, *Gamow vectors and decaying states*, *American Journal of Physics* **57** (1989) 1103 [https://doi.org/10.1119/1.15797].

[171] B. R. Holstein, *Understanding alpha decay*, *American Journal of Physics* **64** (1996) 1061 [https://doi.org/10.1119/1.18308].

Appendix A

Appendices

A.1 The False Vacuum State

Implicitly throughout this thesis, we have considered an object, the false vacuum state $|\phi_{\text{fv}}\rangle$, without defining it. Here we will discuss what this state is, because it will be crucial to understanding why the vacuum decays. We will discuss this in ordinary quantum mechanics, rather than quantum field theory, to avoid unnecessary complication brought about by the infinite number of degrees of freedom. Certainly it is not an eigenstate of the Hamiltonian: if it were, then it would be time independent and hence could not decay. Consequently, assigning it a meaningful energy is at first glance nonsense. However, it is meaningful to ask what happens to a wave-function initially confined to be around the false vacuum. Such a wave-function cannot be stationary, but that is what we want to describe - a decaying state. However, if the barrier is wide and tall, we might reasonably expect there to be a set of 'nearly bound' states that closely resemble bound-states, and decay only slowly.

To make this discussion more precise, consider ordinary quantum mechanics with the potential:

$$V(x) = \frac{1}{2}m\omega^2 x^2 + \frac{m^2\omega^3\lambda'}{4!\hbar}x^4. \tag{A.1}$$

The quantum theory of such a potential can be described by the path integral expression for the generating functional:

$$Z[x] = \int \mathcal{D}x \exp\left(-\int \mathrm{d}t\left[\frac{1}{2}\dot{x}^2 - V(x)\right]\right). \tag{A.2}$$

When the dimensionless interaction parameter $\lambda' = 0$, we don't have a problem defining the ground state of the theory. It is just the usual simple harmonic oscillator:

$$\psi_0(x) = \left(\frac{m\omega}{\pi\hbar}\right)^{\frac{1}{4}}\exp\left(-\frac{m\omega x^2}{2\hbar}\right). \tag{A.3}$$

Even with a small quartic term, $\lambda' \ll 0$, it is still possible to solve for the ground state perturbatively:

$$\tilde{\psi}_0(x) = \left(\frac{m\omega}{\pi\hbar}\right)^{\frac{1}{4}}\left[1 - \frac{\lambda'}{1536}H_4\left(\sqrt{\frac{m\omega}{\hbar}}x\right) - \frac{\lambda'}{24}H_2\left(\sqrt{\frac{m\omega}{\hbar}}x\right)\right]\exp\left(-\frac{m\omega x^2}{2\hbar}\right), \tag{A.4}$$

where $H_n(u)$ is a Hermite polynomial. This equation is valid only for:

$$x \ll \sqrt{\frac{12\hbar}{m\omega|\lambda'|}}, \tag{A.5}$$

since for x greater than this, the perturbation part of the potential is the same size or larger than the harmonic part. There is nothing peculiar about the $\lambda' \to 0^+$ limit. In fact, one might almost expect that the equation should remain valid for $\lambda' < 0$. There are two problems with this: (1) for $\lambda' < 0$ the potential in Eq. (A.1) is unbounded below, making the path integral in Eq. (A.2) undefined, and (2) the region in which we would like to fix the boundary conditions, $x \to \infty$, is beyond the range where perturbation theory applies. In fact, perturbation theory cannot tell us about tunnelling: more powerful non-perturbative techniques are needed.

The technique in question is the WKB approximation. This is a method of finding approximate (asymptotic) solutions to ordinary differential equations of the form:

$$\varepsilon^2 \frac{\mathrm{d}^2 y}{\mathrm{d}x^2} = Q(x)y. \tag{A.6}$$

An approximate solution is of the form [168]:

$$y(x) = \exp\left[\frac{1}{\varepsilon}\right] \sum_{n=0}^{\infty} \varepsilon^n S_n(x), \tag{A.7}$$

We apply this to the Schroedinger equation for energy E, $\psi(x,t) = y(x)e^{-\frac{i}{\hbar}Et}$ where $y(x)$ satisfies the Time-independent Schroedinger equation:

$$-\frac{\hbar^2}{2m}\frac{\mathrm{d}^2 y}{\mathrm{d}x^2} = (E - V(x))y. \tag{A.8}$$

Including only the first two terms of Eq. (A.7), this gives:

$$y(x) = \frac{1}{\left[\frac{1}{\hbar}\sqrt{2m(V(x)-E)}\right]^{\frac{1}{4}}} \left[C_+ \exp\left(\frac{1}{\hbar}\int_{x_0}^{x}\sqrt{2m(V(x)-E)}\mathrm{d}t\right)\right.$$
$$\left. + C_- \exp-\left(\frac{1}{\hbar}\int_{x_0}^{x}\sqrt{2m(V(x)-E)}\mathrm{d}t\right)\right], \tag{A.9}$$

which reproduces the familiar result that in regions where $E > V$, the solutions are oscillating plane waves, and in regions where $E < V$, the solutions are decaying exponentials. Note that Eq. (A.9) is not valid near the turning points of the potential at energy E. This can be dealt with using a different type of expansion in that region and patching together the solutions [168], but since we are mainly interested in the boundary conditions, this form will suffice.

If $\lambda' > 0$, then the result at large x is essentially what we expect - the solution decays exponentially. This is true even non-perturbatively, as Eq. (A.9) confirms (it is necessary to choose the decaying solution and apply the method of asymptotic matching to fix C_- - see [168]).

For $\lambda' < 0$, however, the opposite is true: both solutions become oscillating, and it is impossible to satisfy the $y(x) \to 0$ boundary condition. This is unsurprising: it is a reflection of the same problem recognised previously, that the path integral of Eq. (A.2) is ill-defined due to the potential being unbounded below. In any physical potential, however, we can always add higher order terms like αx^6 to the potential. So long as α is sufficiently small, these should not change the observable behaviour of states around the minimum at $x = 0$, however.

Physically, we can interpret the oscillating behaviour of the WKB solution at large x as plane waves exiting the false vacuum state after tunnelling through the barrier. Instead of the typical $\psi(x,t) \to 0$ boundary condition that is imposed in the $\lambda' > 0$ case, we can instead impose a plane-wave boundary condition at infinity. These are the so called Gamow boundary conditions [170, 171], and give rise to a complex energy, and hence tunnelling, since for large t:

$$|\psi_0(x,t)|^2 = |\psi_0(x,0)|^2 e^{-2\mathrm{Im}(E_0)t}, \tag{A.10}$$

156

where E_0 is the (complex) energy of the false vacuum state (ie, that with the smallest real part). However, this argument does not really illuminate what the false vacuum state ψ_0 actually is, if it is not an eigenstate of the Hamiltonian. Its status is in fact much like an excited state of an atom: it is an eigenstate of an unperturbed Hamiltonian, $\hat{H}_0$, but when extra terms (such as the coupling between electrons and the electromagnetic field), are added, it is no longer an eigenstate. However, because the extra terms, $\hat{H}_{\mathrm{pert}}$ are perturbatively small, much like the $\lambda' x^4$ term, the state is long lived and decays.

This can be made more precise in our potential by considering a WKB approximation for the wave function at energy E. Consider figure A.1. WKB approximations can be made in each of the three regions of the potential. The exception is near to the turning points, where the WKB approximation of Eq. (A.9) breaks down, since $E = V(a) = V(b)$. However, the transitions between these regions can be handled by using Airy functions as the solution to the Schroedinger equation in the vicinity of the turning points [168]:

$$
y_{\mathrm{Airya}}(x) \approx \alpha_a \mathrm{Ai}\left(\left(\frac{2mV'(a)}{\hbar^2}\right)^{\frac{1}{3}}(x-a)\right) + \beta_a \mathrm{Bi}\left(\left(\frac{2mV'(a)}{\hbar^2}\right)^{\frac{1}{3}}(x-a)\right).
$$

$$
y_{\mathrm{Airyb}}(x) \approx \alpha_b \mathrm{Ai}\left(\left(\frac{2m|V'(b)|}{\hbar^2}\right)^{\frac{1}{3}}(b-x)\right) + \beta_b \mathrm{Bi}\left(\left(\frac{2m|V'(x_0)|}{\hbar^2}\right)^{\frac{1}{3}}(b-x)\right). \tag{A.11}
$$

Following the example of calculating the decay rate of an alpha particle [171], the WKB approximations for the three regions are:

$$
y_I(x) \approx \frac{1}{\left[\frac{2m}{\hbar^2}(E-V(x))\right]^{\frac{1}{4}}}\left[C_{I+}\exp\left(+i\int_0^x \mathrm{d}x'\sqrt{\frac{2m}{\hbar^2}(E-V(x))}\right)\right.
$$
$$
\left. +C_{I-}\exp\left(-i\int_0^x \mathrm{d}x'\sqrt{\frac{2m}{\hbar^2}(E-V(x))}\right)\right], \tag{A.12}
$$

$$
y_{II}(x) \approx \frac{1}{\left[\frac{2m}{\hbar^2}(V(x)-E)\right]^{\frac{1}{4}}}\left[A\exp\left(+\int_a^x \mathrm{d}x'\sqrt{\frac{2m}{\hbar^2}(V(x)-E)}\right)\right.
$$
$$
\left. +B\exp\left(-\int_a^x \mathrm{d}x'\sqrt{\frac{2m}{\hbar^2}(V(x)-E)}\right)\right], \tag{A.13}
$$

$$
y_{III}(x) \approx \frac{1}{\left[\frac{2m}{\hbar^2}(E-V(x))\right]^{\frac{1}{4}}}\left[C_{III+}\exp\left(+i\int_b^x \mathrm{d}x'\sqrt{\frac{2m}{\hbar^2}(E-V(x))}\right)\right.
$$
$$
\left. +C_{III-}\exp\left(-i\int_b^x \mathrm{d}x'\sqrt{\frac{2m}{\hbar^2}(E-V(x))}\right)\right]. \tag{A.14}
$$

To keep things simple, we will assume that $y(0) = 0$, which requires $C_{I+} = -C_{I-}$ (that is, the potential is one sided). If we ultimately assume that the potential is not unbounded below due to the addition of higher order terms that don't affect this region of the potential, then the
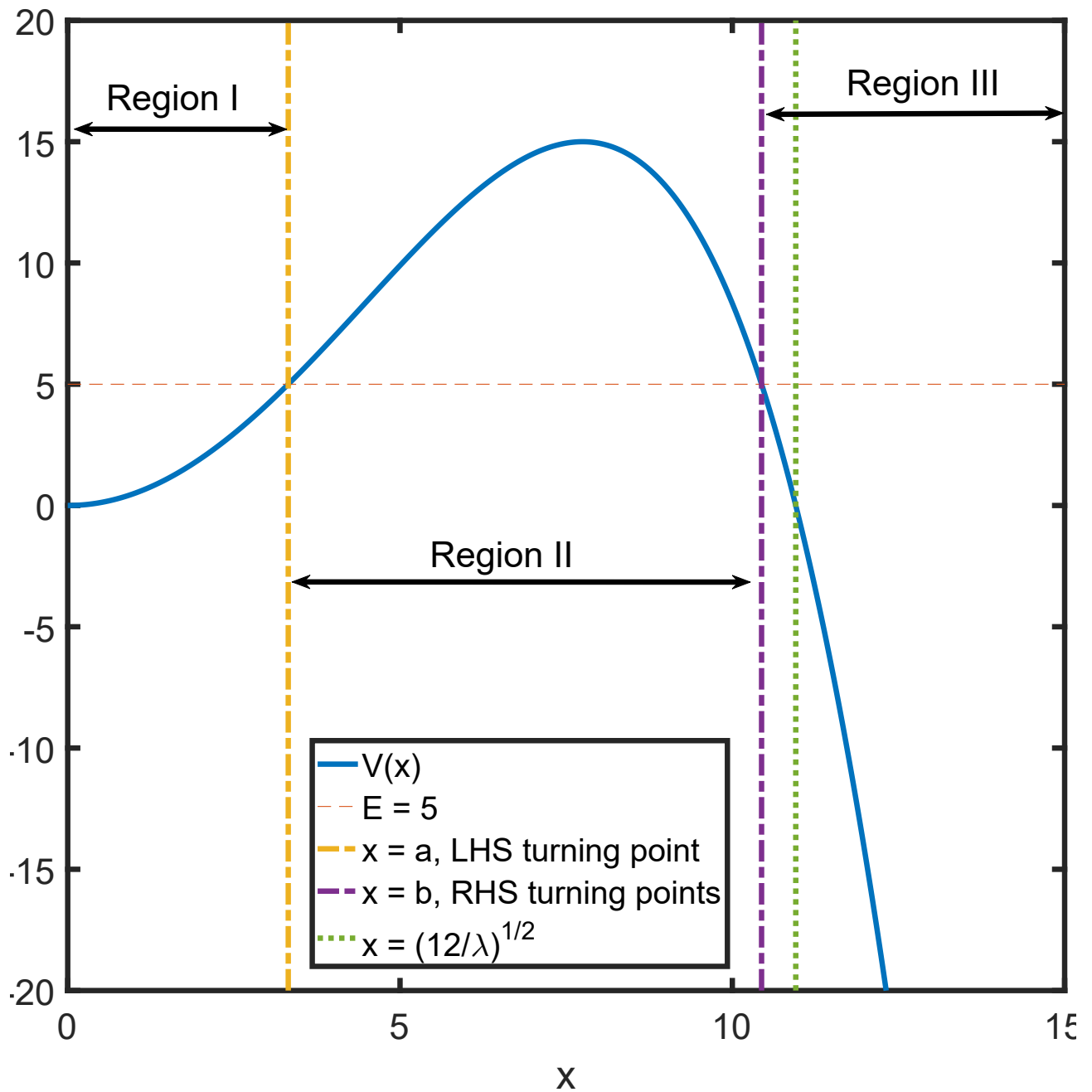
Figure A.1: Quartic potential of Eq. (A.1) with $m = \omega = \hbar = 1$ and $\lambda' = -0.1$. This can be splits into three regions, the false vacuum region (Region I, $x < a$), the barrier (Region II, $a < x < b$) and the true vacuum region (Region III, $x > b$).

wave function will be purely real and we can consider 'scattering states' of energy E:

$$y_I(x) \approx \frac{N}{\left[\frac{2m}{\hbar^2}(E - V(x))\right]^{\frac{1}{4}}} \sin\left(\int_0^x dx' \sqrt{\frac{2m}{\hbar^2}(E - V(x))}\right) \tag{A.15}$$

$$y_{II}(x) \approx \frac{N}{\left[\frac{2m}{\hbar^2}(V(x) - E)\right]^{\frac{1}{4}}} \left(A \exp\left(+\int_0^x dx' \sqrt{\frac{2m}{\hbar^2}(V(x) - E)}\right)\right.$$
$$\left. +B \exp\left(-\int_0^x dx' \sqrt{\frac{2m}{\hbar^2}(V(x) - E)}\right)\right), \tag{A.16}$$

$$y_{III}(x) \approx \frac{NC}{\left[\frac{2m}{\hbar^2}(E - V(x))\right]^{\frac{1}{4}}} \cos\left(\int_b^x dx' \sqrt{\frac{2m}{\hbar^2}(E - V(x))} + \phi + \frac{\pi}{4}\right), \tag{A.17}$$

where N is a normalisation constant. Relationships between the constants are bound by using the Airy-function approximation of Eq. (A.11). At the boundary between regions II and III, $y_I(x \to a)$ asymptotically matches Eq. (A.11) in the $x - a \to -\infty$ limit:

$$y_{\text{Airya}}(x \to -\infty) \sim \frac{1}{\sqrt{\pi}(a - x)^{\frac{1}{4}}} \left(\frac{2mV'(a)}{\hbar^2}\right)^{-\frac{1}{12}} \left[\alpha_a \sin\left(\frac{2}{3}\sqrt{\frac{2mV'(a)}{\hbar^2}}(a - x)^{3/2} + \frac{\pi}{4}\right)\right.$$
$$\left. +\beta_a \cos\left(\frac{2}{3}\sqrt{\frac{2mV'(a)}{\hbar^2}}(a - x)^{3/2} + \frac{\pi}{4}\right)\right] \tag{A.18}$$

While y_{II} matches the $x \to +\infty$ limit:

$$y_{\text{Airya}}(x \to +\infty) \sim \frac{1}{\sqrt{\pi}(x - a)^{\frac{1}{4}}} \left(\frac{2mV'(a)}{\hbar^2}\right)^{-\frac{1}{12}} \left[\frac{\alpha_a}{2} \exp\left(-\frac{2}{3}\sqrt{\frac{2mV'(a)}{\hbar^2}}(x - a)^{3/2}\right)\right.$$
$$\left. +\beta_a \exp\left(+\frac{2}{3}\sqrt{\frac{2mV'(a)}{\hbar^2}}(x - a)^{3/2}\right)\right], \tag{A.19}$$

and the results are analogous for $x = b$, taking into account that $V'(b)$ has the opposite sign:

$$y_{\text{Airyb}}(x \to -\infty) \sim \frac{1}{\sqrt{\pi}(b - x)^{\frac{1}{4}}} \left(\frac{2m|V'(b)|}{\hbar^2}\right)^{-\frac{1}{12}} \left[\frac{\alpha_b}{2} \exp\left[-\frac{2}{3}\left(\frac{2m|V'(b)|}{\hbar^2}\right)(b - x)^{\frac{3}{2}}\right]\right.$$
$$\left. +\beta_b \exp\left[\frac{2}{3}\left(\frac{2m|V'(b)|}{\hbar^2}\right)(b - x)^{\frac{3}{2}}\right]\right] \tag{A.20}$$

$$y_{\text{Airyb}}(x \to +\infty) \sim \frac{1}{\sqrt{\pi}(b - x)^{\frac{1}{4}}} \left(\frac{2m|V'(b)|}{\hbar^2}\right)^{-\frac{1}{12}} \left[\alpha_b \sin\left(\frac{2}{3}\left(\frac{2m|V'(b)|}{\hbar^2}\right)(b - x)^{\frac{3}{2}} + \frac{\pi}{4}\right)\right.$$
$$\left. +\beta_b \cos\left(\frac{2}{3}\left(\frac{2m|V'(b)|}{\hbar^2}\right)(b - x)^{\frac{3}{2}} + \frac{\pi}{4}\right)\right] \tag{A.21}$$

Near the relevant turning points, the WKB solutions take the form:

$$y_I(x \to a) \approx \frac{N}{(a-x)^{\frac{1}{4}}} \left(\frac{2mV'(a)}{\hbar^2}\right)^{-\frac{1}{4}} \left[\sin\left(K + \frac{\pi}{4}\right)\cos\left(\frac{2}{3}\left(\frac{2mV'(a)}{\hbar^2}\right)^{\frac{1}{2}}(a-x)^{\frac{3}{2}} + \frac{\pi}{4}\right)\right.$$

$$\left. - \cos\left(K + \frac{\pi}{4}\right)\sin\left(\frac{2}{3}\left(\frac{2mV'(a)}{\hbar^2}\right)^{\frac{1}{2}}(a-x)^{\frac{3}{2}} + \frac{\pi}{4}\right)\right] \tag{A.22}$$

$$y_{II}(x \to a) \approx \frac{N}{(x-a)^{\frac{1}{4}}} \left(\frac{2mV'(a)}{\hbar^2}\right)^{-\frac{1}{4}} \left[A\exp\left(+\frac{2}{3}\left(\frac{2mV'(a)}{\hbar^2}\right)^{\frac{1}{2}}(x-a)^{\frac{3}{2}}\right)\right.$$

$$\left. + B\exp\left(-\frac{2}{3}\left(\frac{2mV'(a)}{\hbar^2}\right)^{\frac{1}{2}}(x-a)^{\frac{3}{2}}\right)\right] \tag{A.23}$$

$$y_{II}(x \to b) \approx \frac{N}{(b-x)^{\frac{1}{4}}} \left(\frac{2m|V'(b)|}{\hbar^2}\right)^{-\frac{1}{4}} \left[A\exp\left(\sigma - \frac{2}{3}\left(\frac{2m|V'(b)|}{\hbar^2}\right)^{\frac{1}{2}}(b-x)^{\frac{3}{2}}\right)\right.$$

$$\left. + B\exp\left(-\sigma + \frac{2}{3}\left(\frac{2m|V'(a)|}{\hbar^2}\right)^{\frac{1}{2}}(b-x)^{\frac{3}{2}}\right)\right], \tag{A.24}$$

$$y_{III}(x \to b) \approx \frac{NC}{2(x-b)^{\frac{1}{4}}} \left(\frac{2m|V'(b)|}{\hbar^2}\right)^{-\frac{1}{4}} \left[\exp\left(i\left(\phi - \frac{\pi}{4}\right)\right)\exp\left(i\frac{2}{3}\left(\frac{2m|V'(b)|}{\hbar^2}\right)(x-b)^{\frac{3}{2}}\right)\right.$$

$$\left. + \exp\left(-i\left(\phi - \frac{\pi}{4}\right)\right)\exp\left(-i\frac{2}{3}\left(\frac{2m|V'(b)|}{\hbar^2}\right)(x-b)^{\frac{3}{2}}\right)\right] \tag{A.25}$$

where:

$$K = \int_0^a dx \sqrt{\frac{2m}{\hbar^2}(E - V(x))} \tag{A.26}$$

$$\sigma = \int_a^b dx \sqrt{\frac{2m}{\hbar^2}(V(x) - E)} \tag{A.27}$$

Matching the coefficients in these asymptotic expressions, we find:

$$A = = \sin\left(K - \frac{\pi}{4}\right) \tag{A.28}$$

$$B = -\frac{1}{2}\cos\left(Ka - \frac{\pi}{4}\right) \tag{A.29}$$

$$C = \sqrt{4A^2 e^{2\sigma} + B^2 e^{-2\sigma}} \tag{A.30}$$

$$\tan\phi = -\frac{Be^{-2\sigma}}{A}. \tag{A.31}$$

Equation (A.30) is crucial here. If σ is large, which is generally true for high, thick barriers, then it tells us that the wave function has exponentially suppressed support on the false vacuum side, $x \in (0, a)$, except for certain *resonant* energies, E_n, for which $A = 0$, in which case the true vacuum side has exponentially suppressed support. Another way of putting this is that the coefficient A describes solutions which grow exponentially in the barrier, which is not want we want for solutions starting in the false vacuum. WE now have a precise definition of what the low lying states in the false vacuum are - they are resonant states that have substantial support in the false vacuum, and are peaked around $E = E_0$ such that $A \approx 0$. In fact, it is easy to see that as $\sigma \to \infty$, these resonant states will become the bound states of the stabilised

vacuum. As an example, assume that the potential takes the form $\frac{1}{2}m\omega^2 x^2$ in the vicinity of the false vacuum. K is then easily computed to be:

$$K = \frac{\pi E}{2\hbar\omega}. \tag{A.32}$$

The energies satisfying $A = 0$ can be found by solving Eq. (A.28) and are:

$$E_n = \hbar\omega \left([2n+1] + \frac{1}{2}\right). \tag{A.33}$$

These are simply the Harmonic oscillator bound state energies, as we would expect. Note that only the odd states exist because we imposed the boundary condition $\psi(0,t) = 0$, which excludes the symmetric harmonic oscillator bound states. The only remaining question then, is why these states lead to exponential decay of the false vacuum. Again, following the example of [171] for alpha decay, we note that the normalisation constant N is essentially dominated by the true vacuum states, $N \approx \frac{1}{C}$. States near to a resonance have:

$$C \approx \sqrt{4 \left(\frac{\mathrm{d}A}{\mathrm{d}E}\bigg|_{E_{\text{res}}}\right)^2 (E - E_{\text{res}})^2 e^{2\sigma} + B(E_{\text{res}})e^{-2\sigma}}. \tag{A.34}$$

If y_E is such a state before normalisation, then the overlap of a state $\psi(x,0)$ initially confined to the region $x \in (0,a)$ with this state is:

$$c_E = \int_0^a \psi(x,0) \frac{y_E^*(x)}{C}, \tag{A.35}$$

So the time evolution is given by:

$$\psi(x,t) \approx \int_{-\infty}^{\infty} \mathrm{d}E\, e^{-i\frac{E}{\hbar}} \frac{1}{C^2} y_E(x) \left(\int_0^a \psi(y,0)y_E(y)\mathrm{d}y\right), \tag{A.36}$$

where we have ignored the states not close to a resonance, since these have exponentially suppressed overlap with $\psi(x,0)$. Although y_E and it's overlap with $\psi(x,0)$ also depend on E, we see that the $\frac{1}{C^2}$ factor gives a Breit-Wigner energy distribution. Expanding the solution $y_E(x) = y_{E_{\text{res}}}(x) + f(E - E_{\text{res}}, x)$ where $f(E - E_{\text{res}}, x)$ is some function vanishing at $f(0,x)$ (linear in $E - E_{\text{res}}$, in fact), we find:

$$\psi(x,t) = \int_{-\infty}^{\infty} \mathrm{d}E\, e^{-i\frac{Et}{\hbar}} \frac{y_{E_{\text{res}}}(x) \int_0^a y_{E_{\text{res}}}^*(y)\psi(y,0)\mathrm{d}y + F(E - E_{\text{res}}, x)}{4\left(\frac{\mathrm{d}A}{\mathrm{d}E}\big|_{E_{\text{res}}}\right)^2 (E - E_{\text{res}})^2 e^{2\sigma} + B(E_{\text{res}})e^{-2\sigma}}, \tag{A.37}$$

where F is some analytic function that depends on the potential and the shape of the nearly-bound states near to E_{res}. This integral can be done by standard contour integration methods, to give:

$$\psi(x,t) = e^{-i\frac{E_{\text{res}}t}{\hbar}} e^{-\Gamma t} G(x) \tag{A.38}$$

where:

$$\Gamma = \frac{B(E_{\text{res}})}{2\hbar A'(E_{\text{res}})} e^{-2\sigma} \tag{A.39}$$

$$G(x) = \frac{2\pi\hbar^2 A'(E_{\text{res}})e^{2\sigma} y_{E_{\text{res}}}(x) \int_0^a \mathrm{d}y\,\psi(y,0)y_{E_{\text{res}}}^*(y) \left[1 + F(-\frac{2\pi\hbar A'(E_{\text{res}})e^{2\sigma}}{B(E_{\text{res}})})\right]}{B(E_{\text{res}})} \tag{A.40}$$

161

Notice that an exponential decay has emerged from the Fourier transform of the Breit-Wigner distribution, despite the fact that there is no complex energy involved. It takes the WKB form:

$$\Gamma \propto \exp\left(-2\int_a^b \sqrt{\frac{2m}{\hbar^2}(V(x) - E_{\text{res}})}\right) \tag{A.41}$$

A.2 Perturbative Solution Near H_{crit}

Order by order then, the perturbative equations are:

$$a_1'' + a_1 + \frac{\sqrt{-V''(\phi_{\text{bar}})}\chi_{\text{max}}^{(0)}\chi_{\text{max}}^{(1)}}{\pi^2}\sin(x) = 0 \tag{A.42}$$

$$u_1'' + 3\cot(x)u_1' + 4u_1 - 3\frac{1}{\chi_{\text{max}}^{(0)}\sin(x)}\left[-\pi a_1(x)\cos(x) + \pi\sin(x)a_1'(x)\right]$$

$$+ \frac{4\sqrt{-V''(\phi_{\text{bar}})}\chi_{\text{max}}^{(1)}}{\pi}\cos(x) + \frac{4V^{(3)}(\phi_{\text{bar}})\Delta\phi_0^{(1)}}{V''(\phi_{\text{bar}})}\cos(x)^2 = 0 \tag{A.43}$$

The second order equations are:

$$a_2'' + a_2 + \frac{\sin(x)(-2\cos(x)^2 + \sin(x)^2)(\Delta\phi_0^{(0)})^2\chi_{\text{max}}^{(0)}}{3\pi M_{\text{P}}^2} - \frac{\chi_{\text{max}}^{(2)}}{\pi}\sin(x)$$

$$+ \frac{\sqrt{-V''(\phi_{\text{bar}})}\chi_{\text{max}}^{(1)}}{\pi}\left(a_1(x) + \frac{\chi_{\text{max}}^{(1)}}{\pi}\sin(x)\right)$$

$$- V''(\phi_{\text{bar}})\chi_{\text{max}}^{(0)}\frac{1}{4\pi^3}\left(\frac{4\pi^2}{\Lambda V''(\phi_{\text{bar}})} + (\chi_{\text{max}}^{(0)})^2 + \frac{4\pi\chi_{\text{max}}^{(2)}}{\sqrt{-V''(\phi_{\text{max}})}}\right)\sin(x) + \frac{\chi_{\text{max}}^{(2)}}{\pi}\sin(x) = 0 \tag{A.44}$$

$$u_2'' + 3\cot(x)u_2' + 4u_2 + \frac{2V^{(4)}(\phi_{\text{bar}})(\Delta\phi_0^{(0)})^2}{V''(\phi_{\text{bar}})}\cos^3(x) - \frac{V''(\phi_{\text{bar}})(\chi_{\text{max}}^{(1)})^2}{\pi^2}\cos(x)$$

$$+ \frac{4\sqrt{-V''(\phi_{\text{bar}})}\chi_{\text{max}}^{(2)}}{\pi} + \frac{4\sqrt{-V''(\phi_{\text{bar}})}\chi_{\text{max}}^{(1)}}{\pi}u_1(x)+$$

$$\frac{2V^{(3)}(\phi_{\text{bar}})\left(\pi\Delta\phi_0^{(2)}\cos^2(x) + \sqrt{-V''(\phi_{\text{bar}})}\Delta\phi_0^{(1)}\chi_{\text{max}}^{(1)}\cos^2(x) + 2\pi\Delta\phi_0^{(1)}\cos(x)u_1(x)\right)}{V''(\phi_{\text{bar}})\pi}$$

$$+ \frac{3}{(\chi_{\text{max}}^{(0)})\sin(x)}\left(-\pi^2\cot(x)a_1(x)^2 + \pi\chi_{\text{max}}^{(0)}\cos(x)a_2(x) - \pi\chi_{\text{max}}^{(1)}a_1(x)\cos(x)+\right.$$

$$\pi^2 a_1(x)a_1'(x) + \pi\chi_{\text{max}}^{(1)}\sin(x)a_1'(x) - \pi\chi_{\text{max}}^{(0)}\sin(x)a_2'(x) - \pi\chi_{\text{max}}^{(0)}\cot(x)a_1(x)u_1'(x)$$

$$\left.+\pi\chi_{\text{max}}^{(0)}a_1'(x)u_1'(x)\right) = 0. \tag{A.45}$$

We will also require third order perturbation equations:

$$
\begin{aligned}
& a_3'' + a_3 - \frac{\chi_{\max}^{(3)}}{\pi} \sin(x) \\
& - \frac{V^{(2)}(\phi_{\text{bar}})}{4\pi^2} \left(\left[a_1(x) + \frac{\chi_{\max}^{(1)}}{\pi} \sin(x) \right] \left[+ \frac{4\pi^2}{V^{(2)}(\phi_{\text{bar}})\Lambda} + (\chi_{\max}^{(1)})^2 + \frac{4\pi \chi_{\max}^{(2)}}{\sqrt{-V''(\phi_{\text{bar}})}} \right] \right. \\
& + \frac{4\pi \chi_{\max}^{(1)}}{\sqrt{-V''(\phi_{\text{bar}})}} \left[a_2(x) + \frac{\chi_{\max}^{(2)}}{\pi} \sin(x) \right] \\
& + \frac{\chi_{\max}^{(0)}}{\pi} \left[-\frac{4\pi \chi_{\max}^{(1)}}{\sqrt{-V''(\phi_{\text{bar}})}\Lambda} + 2\chi_{\max}^{(1)}\chi_{\max}^{(2)} + \frac{4\pi \chi_{\max}^{(3)}}{\sqrt{-V''(\phi_{\text{bar}})}} \right] \sin(x) \left. - \frac{4\pi \chi_{\max}^{(3)}}{V^{(2)}(\phi_{\text{bar}})} \sin(x) \right) \\
& + \frac{1}{3M_{\text{P}}^2} \left([-2\cos^2(x) + \sin^2(x)] \left[\frac{2}{\pi} \Delta\phi_0^{(1)} \Delta\phi_0^{(2)} \chi_{\max}^{(0)} + (\Delta\phi_0^{(1)})^2 \left\{ a_1(x) + \frac{\chi_{\max}^{(1)}}{\pi} \sin(x) \right\} \right] \right. \\
& + \sin(x) \frac{(\Delta\phi_0^{(1)})^2 \chi_{\max}^{(0)}}{\pi} \left[\frac{-2V^{(3)}(\phi_{\text{bar}})\Delta\phi_0^{(1)}}{3V^{(2)}(\phi_{\text{bar}})} \cos^3(x) - \frac{2\sqrt{-V''(\phi_{\text{bar}})}\chi_{\max}^{(1)}}{\pi} \cos^2(x) \right. \\
& \left. \left. - 4\cos(x)u_1(x) - 2\sin(x)u_1'(x) \right] \right) = 0 \quad\quad\quad\quad\quad\quad\quad (A.46)
\end{aligned}
$$

And the third order u_3 satisfies:

$$u_3'' + 3\cot(x)u_3' + 4u_3$$

$$+ \frac{4}{V^{(2)}(\phi_{\mathrm{bar}})\pi}\left(2\pi\frac{V^{(4)}(\phi_{\mathrm{bar}})}{6}\Delta\phi_0^{(1)}\Delta\phi_0^{(2)}\cos^3(x) + \sqrt{-V''(\phi_{\mathrm{bar}})}\frac{V^{(4)}(\phi_{\mathrm{bar}})}{6}(\Delta\phi_0^{(1)})^2\chi_{\mathrm{max}}^{(1)}\cos^3(x)\right.$$

$$\left.+3\pi\frac{V^{(4)}(\phi_{\mathrm{bar}})}{6}(\Delta\phi_0^{(1)})^2\cos^2(x)u_1(x)\right)$$

$$-\frac{1}{V^{(2)}(\phi_{\mathrm{bar}})\pi^2}\left(-2V^{(3)}(\phi_{\mathrm{bar}})\pi^2\Delta\phi_0^{(3)}\cos^2(x) - 2V^{(3)}(\phi_{\mathrm{bar}})\sqrt{-V''(\phi_{\mathrm{bar}})}\pi\Delta\phi_0^{(2)}\chi_{\mathrm{max}}^{(1)}\cos^2(x)\right.$$

$$+\frac{V^{(3)}(\phi_{\mathrm{bar}})}{2}V^{(2)}(\phi_{\mathrm{bar}})\Delta\phi_0^{(1)}(\chi_{\mathrm{max}}^{(1)})^2\cos^2(x) - 2V^{(3)}(\phi_{\mathrm{bar}})\sqrt{-V''(\phi_{\mathrm{bar}})}\pi\Delta\phi_0^{(1)}\chi_{\mathrm{max}}^{(2)}\cos^2(x)$$

$$-4V^{(3)}(\phi_{\mathrm{bar}})\pi^2\Delta\phi_0^{(2)}\cos(x)u_1(x) - 4V^{(3)}(\phi_{\mathrm{bar}})\sqrt{-V''(\phi_{\mathrm{bar}})}\pi\Delta\phi_0^{(1)}\chi_{\mathrm{max}}^{(1)}\cos(x)u_1(x)$$

$$\left.-2V^{(3)}(\phi_{\mathrm{bar}})\pi^2\Delta\phi_0^{(1)}u_1(x)^2 - 4V^{(3)}(\phi_{\mathrm{bar}})\pi^2\Delta\phi_0^{(1)}\cos(x)u_2(x)\right)$$

$$+\frac{1}{\pi^2}\left(-2V^{(2)}(\phi_{\mathrm{bar}})\chi_{\mathrm{max}}^{(1)}\chi_{\mathrm{max}}^{(2)}\cos(x) + 4\sqrt{-V''(\phi_{\mathrm{bar}})}\pi\chi_{\mathrm{max}}^{(3)} - V^{(2)}(\phi_{\mathrm{bar}})(\chi_{\mathrm{max}}^{(1)})^2u_1(x)\right.$$

$$\left.+4\sqrt{-V''(\phi_{\mathrm{bar}})}\pi\chi_{\mathrm{max}}^{(2)}u_1(x) + 4\sqrt{-V''(\phi_{\mathrm{bar}})}\pi\chi_{\mathrm{max}}^{(1)}u_2(x)\right)$$

$$+\frac{3}{(\chi_{\mathrm{max}}^{(0)})^2\sin^2(x)}\left(\pi^2a_1(x)^3\cot(x) - 2\pi^2\chi_{\mathrm{max}}^{(0)}a_1(x)a_2(x)\cos(x)\right.$$

$$+\pi(\chi_{\mathrm{max}}^{(0)})^2a_3(x)\cos(x)\sin(x) + 2\pi^2\chi_{\mathrm{max}}^{(1)}a_1(x)^2\cos(x)$$

$$-\pi\chi_{\mathrm{max}}^{(0)}\chi_{\mathrm{max}}^{(1)}a_2(x)\cos(x)\sin(x) + \pi(\chi_{\mathrm{max}}^{(1)})^2a_1(x)\cos(x)\sin(x)$$

$$-\pi\chi_{\mathrm{max}}^{(0)}\chi_{\mathrm{max}}^{(2)}a_1(x)\cos(x)\sin(x) - \pi^3a_1(x)^2a_1'(x)$$

$$+\pi^2\chi_{\mathrm{max}}^{(0)}a_2(x)a_1'(x)\sin(x) - 2\pi^2\chi_{\mathrm{max}}^{(1)}a_1(x)a_1'(x)\sin(x)$$

$$-\pi(\chi_{\mathrm{max}}^{(1)})^2a_1'(x)\sin^2(x) + \pi\chi_{\mathrm{max}}^{(0)}\chi_{\mathrm{max}}^{(2)}a_1'(x)\sin^2(x)$$

$$+\pi^2\chi_{\mathrm{max}}^{(0)}a_1(x)a_2'(x)\sin(x) + \pi\chi_{\mathrm{max}}^{(0)}\chi_{\mathrm{max}}^{(1)}a_2'(x)\sin^2(x)$$

$$+\pi^2\chi_{\mathrm{max}}^{(0)}a_1(x)^2u_1'(x)\cot(x)$$

$$-\pi(\chi_{\mathrm{max}}^{(0)})^2a_2(x)u_1'(x)\cos(x) + \pi\chi_{\mathrm{max}}^{(0)}\chi_{\mathrm{max}}^{(1)}a_1(x)u_1'(x)\cos(x)$$

$$-\pi^2\chi_{\mathrm{max}}^{(0)}a_1(x)a_1'(x)u_1'(x) - \pi\chi_{\mathrm{max}}^{(0)}\chi_{\mathrm{max}}^{(1)}a_1'(x)u_1'(x)\sin(x)$$

$$\pi(\chi_{\mathrm{max}}^{(0)})^2a_2'(x)u_1'(x)\sin(x) - \pi(\chi_{\mathrm{max}}^{(0)})^2a_1(x)u_2'(x)\cos(x)$$

$$\left.+\pi(\chi_{\mathrm{max}}^{(0)})^2a_1'(x)u_2'(x)\sin(x) - \pi(\chi_{\mathrm{max}}^{(0)})^2a_3'(x)\sin^2(x)\right) = 0 \tag{A.47}$$

To compute the action, first note that the expression for χ_{max} in Eq. (6.31) can be re-written as

$$\chi_{\mathrm{max}} = \frac{\pi}{H_{\mathrm{HMcrit}}}\left(1 + \frac{\epsilon^2}{2\Lambda}\right) - \frac{\pi\epsilon^2(\Delta\phi_0^{(1)})^2}{12M_{\mathrm{P}}^2\sqrt{-V^{(2)}(\phi_{\mathrm{bar}})}} + O(\epsilon^2)$$

$$= \frac{\pi}{H_{\mathrm{HM}}} - \frac{\pi\epsilon^2(\Delta\phi_0^{(1)})^2}{24M_{\mathrm{P}}^2 H_{\mathrm{HM}}} + O(\epsilon^2). \tag{A.48}$$

We define H_{HMcrit} to be the height of the potential (including V_0) when $H = H_{\mathrm{crit}}$:

$$H_{\mathrm{HMcrit}} \equiv \sqrt{-\frac{V^{(2)}(\phi_{\mathrm{bar}})}{4}} = \sqrt{\frac{V_{\mathrm{crit}}(\phi_{\mathrm{bar}})}{3M_{\mathrm{P}}^2}} = H_{\mathrm{HM}}\sqrt{1 + \frac{\epsilon^2}{\Lambda}}, \tag{A.49}$$

where V_{crit} is the height of the barrier when V_0 takes on the critical value. Since $V^{(2)}(\phi_{\text{bar}})$ is independent of V_0, and at the critical threshold $-V^{(2)}(\phi_{\text{bar}})/4 - V(\phi_{\text{bar}})/3M_{\text{P}}^2 \equiv 0$, it is most convenient to define H_{HMcrit} in terms of $V^{(2)}(\phi_{\text{bar}})$ (the first equality), but note it's interpretation in terms of the height of the barrier when at the critical threshold. The last equality uses the definition of ϵ in Eq. 6.9. The decay exponent can be placed in the form:

$$B = 2\pi^2 \frac{\chi_{\text{max}}}{\pi} \int_0^\pi \mathrm{d}x \left[a^3(x) \left(\frac{\dot{\phi}^2}{2} + V(\phi(x)) \right) - 3M_{\text{P}}^2 a(1 + \dot{a}^2) \right] - S_{\text{fv}}, \tag{A.50}$$

In the u variable, and making the change $x = \frac{\pi\chi}{\chi_{\text{max}}}$ this splits up as:

$$B = 2\pi^2 \left(\frac{\chi_{\text{max}}}{\pi} \right) \int_0^\pi \left[a^3 \epsilon^2 \Delta\tilde{\phi}^2 \left(\left(\frac{\pi}{\chi_{\text{max}}} \right)^2 \frac{u'(x)^2}{2} + \frac{V^{(2)}(\phi_{\text{bar}})}{2} u(x)^2 + \epsilon\Delta\tilde{\phi} \frac{V^{(3)}(\phi_{\text{bar}})}{6} u(x)^3 \right. \right.$$
$$\left. \left. + \epsilon^2 \Delta\tilde{\phi}^2 \frac{V^{(4)}(\phi_{\text{bar}})}{24} u(x)^4 \right) - 3M_{\text{P}}^2 a \left(1 + \left(\frac{\pi}{\chi_{\text{max}}} \right)^2 a'(x)^2 - H_{\text{HM}}^2 a^2 \right) \right] - S_{\text{fv}}, \tag{A.51}$$

where $\Delta\tilde{\phi} = \frac{\phi - \phi_{\text{max}}}{\epsilon} = \Delta\phi_0^{(1)} + O(\epsilon)$ and we have moved the V_{max} dependent term into the gravitational sector, since it doesn't couple directly to the field.

We must consider each piece in turn; the scalar sector of the action, and the gravitational sector, and devise a perturbative expression. As we will see, this results in an action that differs from the Hawking-Moss solution only at fourth order in ϵ, so we must nominally expand to fourth order in all solutions. However, it will soon become clear that only the second order contributions matter - those depending on u_3, a_3, u_4, a_4 etc... in fact vanish identically, so we will never need to know these solutions.

Starting with the gravitational action:

$$S_{\text{grav}} = -6\pi^2 M_{\text{P}}^2 \left(\frac{\chi_{\text{max}}}{\pi} \right) \int_0^\pi \mathrm{d}x\, a \left[1 + \left(\frac{\pi}{\chi_{\text{max}}} \right)^2 a'^2 - H_{\text{HM}}^2 a^2 \right]. \tag{A.52}$$

We will perturb to fourth order at constant χ_{max} and $\Delta\tilde{\phi}$ (which also depend on ϵ), in order to reduce clutter - expansions for χ_{max} and $\Delta\tilde{\phi}$ will be introduced as needed. We find:

$$S_{\text{grav}} = - 6\pi^2 M_{\text{P}}^2 \int_0^\pi \left(\frac{\chi_{\text{max}}}{\pi} \right) \left(a_0 \left[1 + \left(\frac{\chi_{\text{max}}}{\pi} \right)^{-2} a_0'^2 - H_{\text{HM}}^2 a_0^2 \right] \right.$$
$$+ \epsilon^2 \left[a_2 + \left(\frac{\chi_{\text{max}}}{\pi} \right)^{-2} \left\{ 2a_0' a_2' a_0 + a_2 a_0'^2 \right\} - H_{\text{HM}}^2 \left\{ 3a_0^2 a_2 \right\} \right]$$
$$+ \epsilon^3 \left[a_3 + \left(\frac{\chi_{\text{max}}}{\pi} \right)^{-2} \left\{ 2a_0 a_0' a_3' + a_0'^2 a_3 \right\} - H_{\text{HM}}^2 \left\{ 3a_0^2 a_3 \right\} \right]$$
$$\left. + \epsilon^4 \left[a_4 + \left(\frac{\chi_{\text{max}}}{\pi} \right)^{-2} \left\{ 2a_0 a_0' a_4' + a_0 a_2'^2 + 2a_2 a_2' a_0' + a_4 a_0'^2 \right\} - H_{\text{HM}}^2 \left\{ 3a_0^2 a_4 + 3a_0 a_2^2 \right\} \right] + O(\epsilon^5) \right). \tag{A.53}$$

Now, substitute in $a_0 = \left(\frac{\chi_{\text{max}}}{\pi} \right) \sin(x)$ and define:

$$\delta \equiv \left(1 - \left(\frac{\chi_{\text{max}} H_{\text{HM}}}{\pi} \right)^2 \right) = \frac{\epsilon^2 (\Delta\phi_0^{(1)})^2}{12M_{\text{P}}^2} + O(\epsilon^4). \tag{A.54}$$

Proceed order by order. The zeroth order contribution is:

$$S_{\text{grav}}^{(0)} = -6\pi^2 M_{\text{P}}^2 \left(\frac{\chi_{\max}}{\pi}\right)^2 \int_0^\pi dx \, \sin(x) \left[1 + \cos^2(x) - \sin^2(x) + \delta \sin^2(x)\right]$$

$$- \frac{6\pi^2 M_{\text{P}}^2}{H_{\text{HM}}^2}(1 - \delta) \left[\int_0^\pi dx \, 2\sin(x)\cos^2(x) + \delta \int_0^\pi dx \, \sin^3(x)\right]$$

$$- \frac{8\pi^2 M_{\text{P}}^2}{H_{\text{HM}}^2}(1 - \delta^2) = S_{\text{HM}} + \frac{8\pi^2 M_{\text{P}}^2}{H_{\text{HM}}^2}\delta^2 \tag{A.55}$$

Thus, the zeroth order term reproduces the Hawking-Moss action, plus a fourth-order residual arising from the change in $\chi_{\max}$. At second order we obtain:

$$S_{\text{grav}}^{(2)} = -6\pi^2 M_{\text{P}}^2 \left(\frac{\chi_{\max}}{\pi}\right) \epsilon^2 \int_0^\pi a_2 \left[1 - \frac{d}{dx}(2\sin(x)\cos(x)) + \cos^2(x) - (1-\delta)3\sin^2(x)\right]. \tag{A.56}$$

It is straightforward to verify that:

$$1 - \frac{d}{dx}(2\sin(x)\cos(x)) + \cos^2(x) - 3\sin^2(x) \equiv 0, \tag{A.57}$$

and in fact, this is a actually the equation of motion for a_0: the fact that this contribution vanishes is not accidental - it is a consequence of the fact that the lowest order fluctuations about the action of a stationary point give zero, since by definition the first functional derivative vanishes when the equations of motion are satisfied (note that since $a_1 = 0$, a_2 *is* the lowest order fluctuation here). This leaves only a residual term:

$$S_{\text{grav}}^{(2)} = -6\pi^2 M_{\text{P}}^2 \left(\frac{\chi_{\max}}{\pi}\right) \epsilon^2 \delta \int_0^\pi 3\sin^2(x) a_2(x) dx$$

$$= -18\pi^2 M_{\text{P}}^2 \left(\frac{\chi_{\max}}{\pi}\right)^2 \epsilon^2 \delta \frac{(\Delta\phi_0^{(1)})^2}{8M_{\text{P}}^2} \int_0^\pi \sin^5(x) dx$$

$$= -\frac{36\pi^2 (\Delta\phi_0^{(1)})^2}{15 H_{\text{HM}}^2} \epsilon^2 \delta + O(\epsilon^5)$$

$$= -\frac{3\pi^2 (\Delta\phi_0^{(1)})^4}{15 H_{\text{HM}}^2 M_{\text{P}}^2} \epsilon^4 + O(\epsilon^5). \tag{A.58}$$

In fact, exactly the same argument applies at third order in ϵ, since it has the same form as the second order contribution. However, the residual in that case is pushed to fifth order, which we neglect. Thus, only the fourth order term remains. Note that we can here apply the same trick to eliminate the a_4 dependent terms, leaving a sixth order residual, thus we obtain:

$$S_{\text{grav}}^{(4)} = -6\pi^2 M_{\text{P}}^2 \epsilon^4 \int_0^\pi dx \left[\left\{\sin(x) a_2'(x)^2 + 2a_2 a_2' \cos(x)\right\} - \left(\frac{\chi_{\max}}{\pi}\right)^2 H_{\text{HM}}^2 3\sin(x) a_2(x)^2\right]$$

$$= -\epsilon^4 \frac{6\pi^2 M_{\text{P}}^2}{H_{\text{HM}}^2} \frac{(\Delta\phi_0^{(1)})^4}{64 M_{\text{P}}^4} \int_0^\pi dx \left[\left\{9\sin^5(x)\cos^2(x) + 6\sin^5(x)\cos^2(x)\right\} - 3(1-\delta)\sin^7(x)\right]$$

$$= -\epsilon^4 \frac{6\pi^2 M_{\text{P}}^2}{H_{\text{HM}}^2} \frac{(\Delta\phi_0^{(1)})^4}{64 M_{\text{P}}^4} \left[15 \int_0^\pi \sin^5(x) dx - 18 \int_0^\pi \sin^7(x) dx\right] + O(\epsilon^6)$$

$$= \frac{3\pi^2 (\Delta\phi_0^{(1)})^4}{70 H_{\text{HM}}^2 M_{\text{P}}^2} \epsilon^4 + O(\epsilon^6). \tag{A.59}$$

Summing this with the residuals, we obtain:

$$S_{\text{grav}} = \frac{3\pi^2 (\Delta\phi_0^{(1)})^4}{70 H_{\text{HM}}^2 M_{\text{P}}^2}\epsilon^4 - \frac{3\pi^2 (\Delta\phi_0^{(1)})^4}{15 H_{\text{HM}}^2 M_{\text{P}}^2}\epsilon^4 + S_{\text{HM}} + \frac{8\pi^2 M_{\text{P}}^2}{H_{\text{HM}}^2}\delta^2$$

$$= S_{\text{HM}} + \frac{2\pi^2 (\Delta\phi_0^{(1)})^4 \epsilon^4}{15 H_{\text{HM}}^4}\left(-\frac{16 H_{\text{HM}}^2}{21 M_{\text{P}}^2}\right). \tag{A.60}$$

Next we compute the scalar part of the action:

$$S_{\text{scal}} = 2\pi^2 \left(\frac{\chi_{\max}}{\pi}\right) \int_0^\pi \left[a^3 \epsilon^2 \Delta\tilde{\phi}^2 \left(\left(\frac{\pi}{\chi_{\max}}\right)^2 \frac{u'(x)^2}{2} + \frac{V^{(2)}(\phi_{\text{bar}})}{2}u(x)^2 + \epsilon\Delta\tilde{\phi}\frac{V^{(3)}(\phi_{\text{bar}})}{6}u(x)^3\right.\right.$$

$$\left.\left.+\epsilon^2 \Delta\tilde{\phi}^2 \frac{V^{(4)}(\phi_{\text{bar}})}{24}u(x)^4\right)\right] \tag{A.61}$$

Using:

$$a^3 = a_0^3 + 3\epsilon^2 a_0^2 a_2 + O(\epsilon^3), \tag{A.62}$$
$$u^2 = u_0^2 + 2u_0 u_1 \epsilon + (2u_0 u_2 + u_1^2)\epsilon^2 + O(|epsilon^3|), \tag{A.63}$$
$$u^3 = u_0^3 + 3u_0^2 u_1 \epsilon + (3u_0^2 u_2 + 3u_0 u_1^2)\epsilon^2 + O(\epsilon^3), \tag{A.64}$$
$$u^4 = u_0^4 + 4u_0^3 u_1 \epsilon + (4u_0^3 u_2 + 6u_0^2 u_1^2)\epsilon^2 + O(\epsilon^3), \tag{A.65}$$

we find:

$$S_{\text{scal}} = 2\pi^2 \left(\frac{\chi_{\max}}{\pi}\right)\Delta\tilde{\phi}^2 \left(\epsilon^2 \int_0^\pi a_0^3 \left[\left(\frac{\chi_{\max}}{\pi}\right)^{-2}\frac{u_0'^2}{2} + \frac{V^{(2)}(\phi_{\text{bar}})}{2}u_0^2\right]\right.$$

$$+ \epsilon^3 \int_0^\pi a_0^3 \left[\left(\frac{\chi_{\max}}{\pi}\right)^{-2}u_0' u_1' + V^{(2)}(\phi_{\text{bar}})u_0 u_1 + \frac{V^{(3)}(\phi_{\text{bar}})}{6}\Delta\tilde{\phi}u_0^3\right]$$

$$\epsilon^4 \int_0^\pi \left[a_0^3\left\{\left(\frac{\chi_{\max}}{\pi}\right)^{-2}u_0' u_2' + \frac{1}{2}\left(\frac{\chi_{\max}}{\pi}\right)^{-2}u_1'^2 + V^{(2)}(\phi_{\text{bar}})\left(u_0 u_2 + \frac{1}{2}u_1^2\right)\right.\right.$$

$$\left.\left.+\frac{V^{(3)}(\phi_{\text{bar}})}{2}\Delta\tilde{\phi}u_0^2 u_1 + \frac{V^{(4)}(\phi_{\text{bar}})}{24}\Delta\tilde{\phi}^2 u_0^4\right\} + 3a_0^2 a_2\left\{\left(\frac{\chi_{\max}}{\pi}\right)^{-2}\frac{u_0'^2}{2} + \frac{V^{(2)}(\phi_{\text{bar}})}{2}u_0^2\right\}\right]\right). \tag{A.66}$$

To process this, define the operator:

$$\mathcal{D}\psi \equiv \frac{1}{\sin^3(x)}\frac{\mathrm{d}}{\mathrm{d}x}\left(\sin^3(x)\frac{\mathrm{d}\psi}{\mathrm{d}x}\right) + 4\psi. \tag{A.67}$$

The second order term gives:

$$S_{\text{scal}}^{(2)} = \frac{2\pi^2}{H_{\text{HM}}^4}(1-\delta)^2(\Delta\tilde{\phi})^2 \epsilon^2 \int_0^\pi \sin^3(x)\left[H_{\text{HMcrit}^2}\left(1 - \frac{2H_{\text{HMcrit}}\chi_{\max}^{(2)}\epsilon^2}{\pi}\right)\frac{u_0'^2}{2} + V^{(2)}(\phi_{\text{bar}})\frac{u_0^2}{2}\right]$$

$$= \frac{2\pi^2}{H_{\text{HM}}^4}(\Delta\tilde{\phi})^2 \epsilon^2 \int_0^\pi \sin^3(x)\left[H_{\text{HMcrit}}^2\frac{u_0'^2}{2} + V^{(2)}(\phi_{\text{bar}})\frac{u_0^2}{2}\right]$$

$$+ \frac{2\pi^2}{H_{\text{HM}}^4}(-2\delta)(\Delta\tilde{\phi})^2 \epsilon^2 \int_0^\pi \sin^3(x)\left[H_{\text{HMcrit}}^2\frac{u_0'^2}{2} + V^{(2)}(\phi_{\text{bar}})\frac{u_0^2}{2}\right]$$

$$+ \frac{2\pi^2}{H_{\text{HM}}^4}(\Delta\tilde{\phi})^2 \epsilon^2 \left(-\frac{2H_{\text{HMcrit}}^3 \chi_{\max}^{(2)}\epsilon^2}{\pi}\right)\int_0^\pi \sin^3(x)\left[\frac{u_0'^2}{2}\right] + O(\epsilon^5)$$

$$\tag{A.68}$$

Now use integration by parts, and that fact that:

$$\frac{V^{(2)}(\phi_{\text{bar}})}{H_{\text{HMcrit}}^2} + 4 \equiv 0, \tag{A.69}$$

to obtain:

$$
\begin{aligned}
S_{\text{scal}}^{(2)} = &-\frac{2\pi^2}{H_{\text{HM}}^4}(\Delta\tilde{\phi})^2\epsilon^2\frac{H_{\text{HMcrit}}^2}{2}\int_0^\pi \sin^3(x)u_0\mathcal{D}u_0 \\
&-\frac{2\pi^2}{H_{\text{HM}}^4}(-2\delta)(\Delta\tilde{\phi})^2\epsilon^2\frac{H_{\text{HMcrit}}^2}{2}\int_0^\pi \sin^3(x)u_0\mathcal{D}u_0 \\
&-\frac{2\pi^2}{H_{\text{HM}}^4}(\Delta\tilde{\phi})^2\epsilon^4\left(\frac{H_{\text{HMcrit}}^3\chi_{\text{max}}^{(2)}}{\pi}\right)\int_0^\pi \sin^5(x) + O(\epsilon^5)
\end{aligned}
\tag{A.70}
$$

However, $\mathcal{D}u_0 = 0$ by the definition of u_0, so we are left with a residual term:

$$S_{\text{scal}}^{(2)} = -\frac{2\pi^2(\Delta\tilde{\phi})^2\epsilon^4}{H_{\text{HM}}^4}\frac{16H_{\text{HMcrit}}^3\chi_{\text{max}}^{(2)}}{\pi}. \tag{A.71}$$

At third order:

$$
\begin{aligned}
S_{\text{scal}}^{(3)} =& 2\pi^2\left(\frac{\chi_{\text{max}}}{\pi}\right)\Delta\tilde{\phi}^2\epsilon^3\int_0^\pi a_0^3\left[\left(\frac{\chi_{\text{max}}}{\pi}\right)^{-2}u_0'u_1' + V^{(2)}(\phi_{\text{bar}})u_0u_1 + \frac{V^{(3)}(\phi_{\text{bar}})}{6}\Delta\tilde{\phi}u_0^3\right] \\
=& \frac{2\pi^2}{H_{\text{HM}}^4}\Delta\tilde{\phi}^2\epsilon^3\int_0^\pi \sin^3(x)\left[H_{\text{HMcrit}}^2u_0'u_1' + V^{(2)}(\phi_{\text{bar}})u_0u_1 + \frac{V^{(3)}(\phi_{\text{bar}})}{6}\Delta\tilde{\phi}u_0^3\right] + O(\epsilon^5) \\
=& -\frac{2\pi^2}{H_{\text{HM}}^4}(\Delta\tilde{\phi})^2\epsilon^3H_{\text{HMcrit}}^2\int_0^\pi \sin^3(x)\left[u_1\mathcal{D}u_0 + \frac{V^{(3)}(\phi_{\text{bar}})}{6}\Delta\tilde{\phi}\cos^3(x)\right] = 0.
\end{aligned}
\tag{A.72}
$$

The last line follows from applying integration by parts and vanishes because $\mathcal{D}u_0 = 0$ as before, and $\sin^3(x)\cos^3(x)$ is an odd function over the interval $[0,\pi]$. The only remaining terms (from changing χ_{max}) are fifth order, so we neglect them. The fourth order contribution is:

$$
\begin{aligned}
S_{\text{scal}}^{(4)} =& 2\pi^2\left(\frac{\chi_{\text{max}}}{\pi}\right)\Delta\tilde{\phi}^2\epsilon^4\int_0^\pi\left[a_0^3\left\{\left(\frac{\chi_{\text{max}}}{\pi}\right)^{-2}u_0'u_2' + \frac{1}{2}\left(\frac{\chi_{\text{max}}}{\pi}\right)^{-2}u_1'^2 + V^{(2)}(\phi_{\text{bar}})\left(u_0u_2 + \frac{1}{2}u_1^2\right)\right.\right. \\
&\left.\left.+\frac{V^{(3)}(\phi_{\text{bar}})}{2}\Delta\tilde{\phi}u_0^2u_1 + \frac{V^{(4)}(\phi_{\text{bar}})}{24}\Delta\tilde{\phi}^2u_0^4\right\} + 3a_0^2a_2\left\{\left(\frac{\chi_{\text{max}}}{\pi}\right)^{-2}\frac{u_0'^2}{2} + \frac{V^{(2)}(\phi_{\text{bar}})}{2}u_0^2\right\}\right].
\end{aligned}
\tag{A.73}
$$

The u_2 terms can be eliminated using the same trick used to eliminate the u_1 terms at third order, since this part is essentially the same, but produced $u_2\mathcal{D}u_0$ instead after integration by parts. A similar procedure can be applied to the $u_1^2, u_1'^2$ terms, however in that case, $\mathcal{D}u_1 \neq 0$, so this term does *not* vanish. We obtain:

$$
\begin{aligned}
S_{\text{scal}}^{(4)} =& 2\pi^2\left(\frac{\chi_{\text{max}}}{\pi}\right)\Delta\tilde{\phi}^2\epsilon^4\int_0^\pi\left[a_0^3\left\{-\frac{H_{\text{HMcrit}}^2}{2}u_1\mathcal{D}u_1\right.\right. \\
&\left.\left.+\frac{V^{(3)}(\phi_{\text{bar}})}{2}\Delta\tilde{\phi}u_0^2u_1 + \frac{V^{(4)}(\phi_{\text{bar}})}{24}\Delta\tilde{\phi}^2u_0^4\right\} + 3a_0^2a_2\left\{\left(\frac{\chi_{\text{max}}}{\pi}\right)^{-2}\frac{u_0'^2}{2} + \frac{V^{(2)}(\phi_{\text{bar}})}{2}u_0^2\right\}\right].
\end{aligned}
\tag{A.74}
$$

Note that we cannot get rid of the a_2 term in the same way, because this trick only works when the u_0^2, $u_0'^2$ terms are preceded by a_0^3, not $3a_0^2 a_2$. To proceed, we will need to compute each term. One trick that we can use is to decompose u_1 and u_0 into Gegenbauer Polynomials. The first few of these we will need are [128]:

$$C_0^{(3/2)}(u) = 1, \tag{A.75}$$

$$C_1^{(3/2)}(u) = 3u, \tag{A.76}$$

$$C_2^{(3/2)}(u) = -\frac{3}{2} + \frac{15}{2}u^2, \tag{A.77}$$

which gives:

$$u_0 = \frac{1}{3}C_1^{(3/2)}(\cos(x)) \tag{A.78}$$

$$u_1 = -\frac{V^{(3)}(\phi_{\mathrm{bar}})\Delta\phi_0^{(1)}}{6V^{(2)}(\phi_{\mathrm{bar}})}\left(\frac{9}{15}C_0^{(3/2)}(\cos(x)) - \frac{4}{15}C_2^{(3/2)}(\cos(x)) + \frac{1}{3}C_1^{(3/2)}(\cos(x))\right). \tag{A.79}$$

Gegenbauer polynomials satisfy the orthogonality relationship [128]:

$$\int_{-1}^{1}(1-u^2)C_n^{(3/2)}(u)C_m^{(3/2)}(u)\mathrm{d}u = \int_0^{\pi}\sin^3(x)C_n^{(3/2)}(\cos(x))C_m^{(3/2)}(\cos(x))\mathrm{d}x = \delta_{nm}\frac{(n+2)(n+1)}{\left(n+\frac{3}{2}\right)}, \tag{A.80}$$

and:

$$\frac{1}{\sin^3(x)}\frac{\mathrm{d}}{\mathrm{d}x}\left(\sin^3(x)\frac{\mathrm{d}C_n^{(3/2)}(\cos(x))}{\mathrm{d}x}\right) + n(n+3)C_n^{(3/2)}(\cos(x)) = 0. \tag{A.81}$$

Hence:

$$\mathcal{D}C_n^{(3/2)}(\cos(x)) = [4 - n(n+3)]C_n^{(3/2)}(\cos(x)). \tag{A.82}$$

Thus, we can show, using the orthogonality relationship:

$$\int_0^{\pi}\sin^3(x)u_1\mathcal{D}u_1 = \left(\frac{V^{(3)}(\phi_{\mathrm{bar}})\Delta\phi_0^{(1)}}{6V^{(2)}(\phi_{\mathrm{bar}})}\right)^2\int_0^{\pi}\mathrm{d}x\left[4\left(\frac{9}{15}C_0^{(3/2)}(\cos(x))^2 - 6\left(\frac{4}{15}\right)^2 C_2^{(3/2)}(\cos(x))^2\right)\right]$$

$$= \frac{48}{15\times 7}\left(\frac{V^{(3)}(\phi_{\mathrm{bar}})\Delta\phi_0^{(1)}}{6V^{(2)}(\phi_{\mathrm{bar}})}\right)^2. \tag{A.83}$$

Similarly:

$$u_0^2 = \frac{1}{15}\left(2C_2^{(3/2)}(\cos(x)) + 3C_0^{(3/2)}(\cos(x))\right), \tag{A.84}$$

so:

$$\int_0^{\pi}u_0^2 u_1\sin^3(x)\mathrm{d}x = -\frac{V^{(3)}(\phi_{\mathrm{bar}})\Delta\phi_0^{(1)}}{6V^{(2)}(\phi_{\mathrm{bar}})}\frac{1}{15}\left(\frac{27}{15}\int_0^{\pi}\sin^3(x)C_0^{(3/2)}(\cos(x))^2\mathrm{d}x - \right.$$

$$\left. \frac{8}{15}\int_0^{\pi}\sin^3(x)C_2^{(3/2)}(\cos(x))^2\mathrm{d}x\right)$$

$$= -\frac{V^{(3)}(\phi_{\mathrm{bar}})\Delta\phi_0^{(1)}}{6V^{(2)}(\phi_{\mathrm{bar}})}\frac{12}{15\times 21}, \tag{A.85}$$

while:

$$\int_0^{\pi}\mathrm{d}x\sin^3(x)u_0^4 = \int_0^{\pi}\sin^3(x)\cos^4(x)\mathrm{d}x = \frac{4}{35}. \tag{A.86}$$

169

Finally, we have the last term at fourth order, which we can evaluate by brute force rather than decomposition to Gegenbauer polynomials:

$$2\pi^2 \left(\frac{\chi_{\max}}{\pi}\right)(\Delta\tilde{\phi})^2\epsilon^4 \int_0^\pi 3a_0^2 a_2 \left\{\left(\frac{\chi_{\max}}{\pi}\right)^{-2}\frac{u_0'^2}{2} + V^{(2)}(\phi_{\rm bar})\frac{u_0^2}{2}\right\}$$

$$= 3\frac{2\pi^2}{H_{\rm HM}^4}(1-\delta)^2(\Delta\tilde{\phi})^2\epsilon^4\frac{(\Delta\phi_0^{(1)})^2}{8M_{\rm P}^2}\frac{H_{\rm HMcrit}^2}{2}\int_0^\pi \sin^5(x)\left\{\sin^2(x) - 4\cos^2(x)\right\}$$

$$= 3\frac{2\pi^2}{H_{\rm HM}^4}(\Delta\tilde{\phi})^2\epsilon^4\frac{(\Delta\phi_0^{(1)})^2}{8M_{\rm P}^2}\frac{48H_{\rm HMcrit}^2}{21\times 15} + O(\epsilon^5). \tag{A.87}$$

One thus obtains:

$$\begin{aligned}
S_{\rm scal}^{(4)} =& 3\frac{2\pi^2}{H_{\rm HM}^4}(\Delta\tilde{\phi})^2\epsilon^4\frac{(\Delta\phi_0^{(1)})^2}{8M_{\rm P}^2}\frac{48H_{\rm HMcrit}^2}{21\times 15} - \frac{2\pi^2}{H_{\rm HM}^4}(\Delta\tilde{\phi})^2\epsilon^4\frac{V^{(3)}(\phi_{\rm bar})}{2}\Delta\tilde{\phi}\frac{V^{(3)}(\phi_{\rm bar})\Delta\phi_0^{(1)}}{6V^{(2)}(\phi_{\rm bar})}\frac{12}{15\times 21}\\
&+\frac{2\pi^2}{H_{\rm HM}^4}(\Delta\tilde{\phi})^2\epsilon^4\frac{V^{(4)}(\phi_{\rm bar})}{24}(\Delta\tilde{\phi})^2\frac{4}{35} - \frac{2\pi^2}{H_{\rm HM}^4}(\Delta\tilde{\phi})^2\epsilon^4\frac{H_{\rm HM}^2}{2}\frac{48}{15\times 7}\left(\frac{V^{(3)}(\phi_{\rm bar})\Delta\phi_0^{(1)}}{6V^{(2)}(\phi_{\rm bar})}\right)^2\\
=& \frac{2\pi^2}{15H_{\rm HM}^4}(\Delta\tilde{\phi})^2\epsilon^4\left[\frac{(\Delta\phi_0^{(1)})^2}{21}\left(\frac{3}{2}V^{(4)}(\phi_{\rm bar}) - 2H_{\rm HM}^2\left(\frac{V^{(3)}(\phi_{\rm bar})}{V^{(2)}(\phi_{\rm bar})}\right)^2\right.\right.\\
&\left.\left.-\left(\frac{V^{(3)}(\phi_{\rm bar})}{V^{(2)}(\phi_{\rm bar})}\right)^2 V^{(2)}(\phi_{\rm bar}) + 18\frac{H_{\rm HMcrit}^2}{M_{\rm P}^2}\right)\right]\\
=& \frac{2\pi^2}{15H_{\rm HM}^4}(\Delta\tilde{\phi})^2\epsilon^4\left[\frac{(\Delta\phi_0^{(1)})^2 4H_{\rm HMcrit}^2}{21}\left(-\frac{3}{2}\frac{V^{(4)}(\phi_{\rm bar})}{V^{(2)}(\phi_{\rm bar})} + \frac{1}{2}\left(\frac{V^{(3)}(\phi_{\rm bar})}{V^{(2)}(\phi_{\rm bar})}\right)^2 + \frac{9}{2M_{\rm P}^2}\right)\right].
\end{aligned}\tag{A.88}$$

Now, using Eq. (6.33), we re-write this as:

$$S_{\rm scal}^{(4)} = \frac{2\pi^2}{15H_{\rm HM}^4}(\Delta\tilde{\phi})^2\epsilon^4\left[\frac{4H_{\rm HMcrit}^2}{\Lambda} + \frac{(\Delta\phi_0^{(1)})^2 2H_{\rm HMcrit}^2}{21M_{\rm P}^2}\right]. \tag{A.89}$$

We must add to this the residual term from Eq. (A.71) to obtain:

$$\begin{aligned}
S_{\rm scal} =& \frac{2\pi^2}{15H_{\rm HM}^4}(\Delta\tilde{\phi})^2\epsilon^4\left[\frac{4H_{\rm HMcrit}^2}{\Lambda} + \frac{(\Delta\phi_0^{(1)})^2 2H_{\rm HMcrit}^2}{21M_{\rm P}^2} - 16H_{\rm HM}^2\frac{\left(12M_{\rm P}^2 - \Lambda(\Delta\phi_0^{(1)})^2\right)}{24\Lambda M_{\rm P}^2}\right].\\
=& \frac{2\pi^2}{15H_{\rm HM}^4}(\Delta\tilde{\phi})^2\epsilon^4\left[-\frac{4H_{\rm HMcrit}^2}{\Lambda} + 16H_{\rm HMcrit}^2\frac{(\Delta\phi_0^{(1)})^2}{21M_{\rm P}^2} + O(\epsilon^2)\right].
\end{aligned}\tag{A.90}$$

Here we used the fact that $H_{\rm HM}^2$ and $H_{\rm HMcrit}^2$ differ by terms of order ϵ^2. Finally, we combine this with the gravitational part, Eq. (A.60), using this same trick to give:

$$\begin{aligned}
S =& S_{\rm HM} + \frac{2\pi^2(\Delta\tilde{\phi})^2\epsilon^4}{15H_{\rm HM}^4}\left[-\frac{4H_{\rm HMcrit}^2}{\Lambda}\right].\\
=& S_{\rm HM} + \frac{2\pi^2(\phi(0)-\phi_{\rm bar})^4}{15H_{\rm HM}^4}\left(-\frac{1}{14}\left[V^{(4)}(\phi_{\rm bar}) - \frac{(V^{(3)}(\phi_{\rm bar}))^2}{3V^{(2)}(\phi_{\rm bar})} - \frac{8V^{(2)}(\phi_{\rm bar})}{3M_{\rm P}^2}\right]\right).
\end{aligned}\tag{A.91}$$

A.2.1 Legendre Transforms

First a quick aside on Legendre transformations, as this has some relevance to the question of interpreting the effective action. The Legendre transformation, $f^*(p)$ of a function $f(x)$ is defined by:

$$f^*(p) = \sup_x(px - f(x)). \tag{A.92}$$

Since it is a maximum over the set of all x, then the derivative with respect to x vanishes and so we evaluate the RHS at the point $x^*(p)$ such that $f'(x^*) = p$. Visually, this is finding a point on the curve $f(x)$ whose gradient is p. It is easy to show that the Legendre transform preserves convexity of functions, since:

$$\frac{df^*}{dp} = x^*(p) + p\frac{dx^*}{dp} - f'(x^*)\frac{dx^*}{dp} = x^*(p) \tag{A.93}$$

$$\frac{d^2 f^*}{dp^2} = \frac{dx^*}{dp} = \frac{1}{f''(x^*(p))}. \tag{A.94}$$

Since $f''(x^*) > 0$ (i.e. because this is a maximum), then the Legendre transformation always produces a convex function. Also, the Legendre transform of a convex function is its own inverse since:

$$f^{**}(x) = \sup_p(xp - f^*(p)) \tag{A.95}$$

$$= xp^* - [p^*x^*(p^*) - f(x^*(p^*))] \tag{A.96}$$

$$= f(x). \tag{A.97}$$

The last line follows because by definition, $x = f^{*'}(p^*(x)) = x^*(p^*(x))$. However, note that the argument only works if the function is convex: if it is not, then the function $p^*(x)$, which is the inverse of $x^*(p)$, is not defined for x in some region of non-convexity, $x \in (a, b)$, since for any given p, no x in that range will maximise $px - f(x)$. Instead, $x^*(p)$ jumps from a to b at some point p_{cusp}. This causes $f^*(p)$ to acquire a cusp at p_{cusp} since $f^{*'}(p) = x^*(p)$. Note that since f^* is convex, then all $f^{*'}(p) < a$ for $p < p_{\text{cusp}}$ and $f^{*'}(p) > b$ for $p > p_{\text{cusp}}$, and there will be no points with derivatives on the range (a, b). This means that for $a < x < b$, $xp - f^*(p)$ is increasing for $p < p_{\text{cusp}}$ and decreasing for $p > p_{\text{cusp}}$. Hence, p_{cusp} will always maximise $xp - f^*(p)$ for $x \in (a, b)$, and the Legendre transformation of f^* should be evaluated there, that is:

$$f^{**}(x) = xp_{\text{cusp}} - f^*(p_{\text{cusp}}), \tag{A.98}$$

which describes a straight line. By definition, $f^*(p_{\text{cusp}}) = p_{\text{cusp}}a - f(a) = p_{\text{cusp}}b - f(b)$, so we can re-arrange this to obtain:

$$p_{\text{cusp}} = \frac{f(b) - f(a)}{b - a}, \tag{A.99}$$

$$f^*(p_{\text{cusp}}) = \frac{f(b)a - f(a)b}{b - a}. \tag{A.100}$$

This shows that the straight line is that passing through the points $(a, f(a))$ and $(b, f(b))$. It describes a 'convex hull' around the non-convex shape (see fig. A.2)
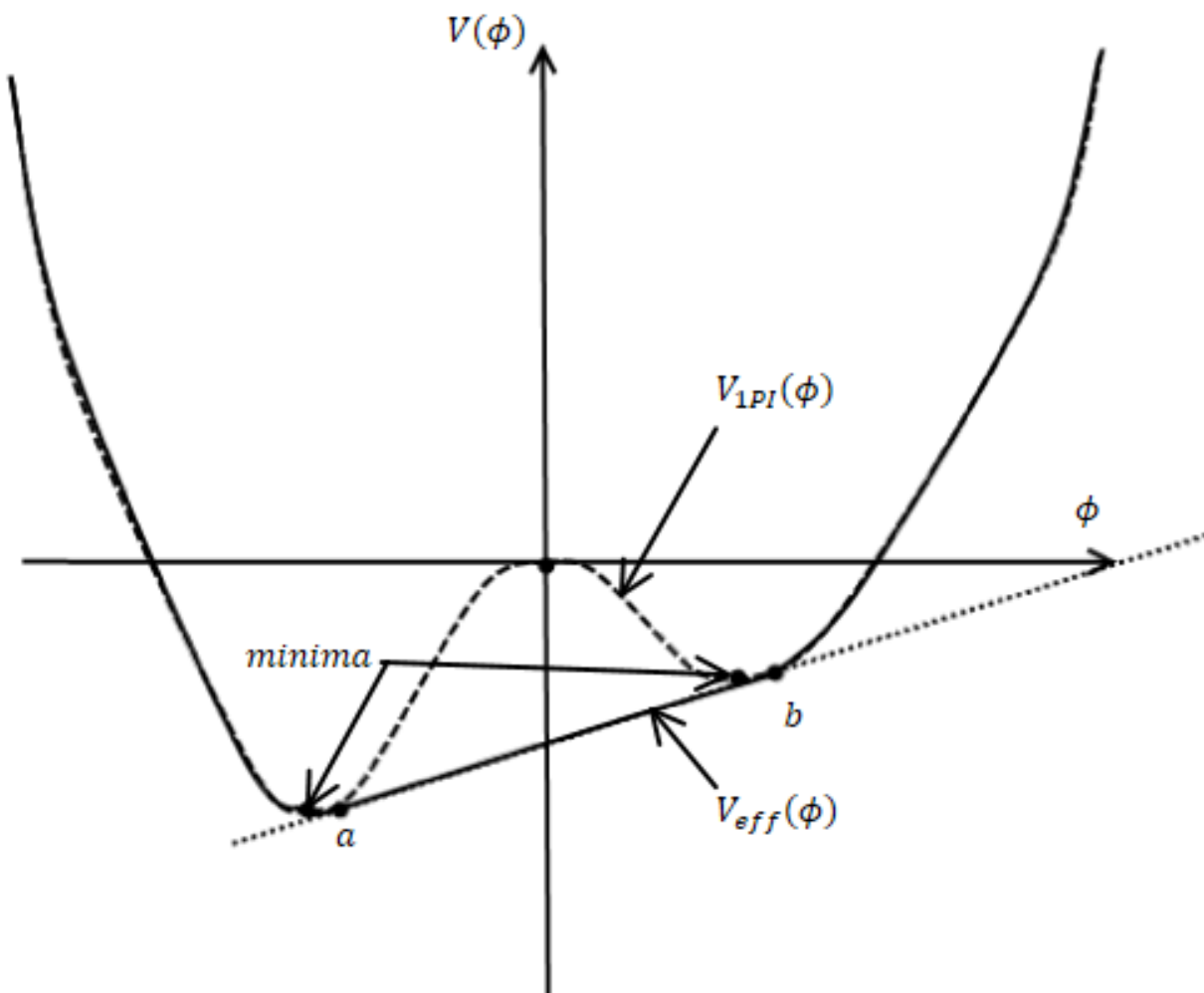
Figure A.2: Example of the double Legendre transformation of a non-convex function and the associated convex hull.